

STRATIGRAPHICAL, SEDIMENTOLOGICAL, GEOCHEMICAL AND
CYCLOSTRATIGRAPHICAL ANALYSES OF UPPER CRETACEOUS (UPPER
SANTONIAN- CAMPANIAN) PELAGIC SUCCESSIONS OF HAYMANA AND
MUDURNU-GÖYNÜK BASINS OF THE SAKARYA CONTINENT, TURKEY

A THESIS SUBMITTED TO
THE GRADUATE SCHOOL OF NATURAL AND APPLIED SCIENCES
OF
MIDDLE EAST TECHNICAL UNIVERSITY

BY
BAKHT ZAMIR AFRIDI

IN PARTIAL FULFILLMENT OF THE REQUIREMENTS
FOR
THE DEGREE OF MASTER OF SCIENCE
IN
GEOLOGICAL ENGINEERING

SEPTEMBER 2014

Approval of the thesis:

**STRATIGRAPHICAL, SEDIMENTOLOGICAL, GEOCHEMICAL AND
CYCLOSTRATIGRAPHICAL ANALYSES OF UPPER CRETACEOUS (UPPER
SANTONIAN- CAMPANIAN) PELAGIC SUCCESSIONS OF HAYMANA AND
MUDURNU-GÖYNÜK BASINS OF THE SAKARYA CONTINENT, TURKEY**

submitted by **BAKHT ZAMIR AFRIDI** in partial fulfillment of the requirements for
the degree of **Master of Science in Geological Engineering Department, Middle East
Technical University** by,

Prof. Dr. Canan Özgen _____
Dean, Graduate School of **Natural and Applied Sciences**

Prof. Dr. Erdin Bozkurt _____
Head of Department, **Geological Engineering**

Assist. Prof. Dr. İsmail Ömer Yılmaz _____
Supervisor, **Geological Engineering Dept., METU**

Examining Committee Members:

Prof. Dr. F. Bora Rojay _____
Geological Engineering Dept., METU

Assoc. Prof. Dr. İsmail Ömer Yılmaz _____
Geological Engineering Dept., METU

Prof. Dr. Faruk Ocakoğlu _____
Geological Engineering Dept., Eskişehir Osamangazi Üni.

Prof.Dr. Sevinç Özkan Altiner _____
Geological Engineering Dept., METU

Assist. Prof. Dr. Fatma Toksoy Köksal _____
Geological Engineering Dept., METU

Date: 09-04-2014

I hereby declare that all information in this document has been obtained and presented in accordance with academic rules and ethical conduct. I also declare that, as required by these rules and conduct, I have fully cited and referenced all material and results that are not original to this work.

Name, Last name : BAKHT ZAMIR AFRIDI

Signature : 

ABSTRACT

STRATIGRAPHICAL, SEDIMENTOLOGICAL, GEOCHEMICAL AND CYCLOSTRATIGRAPHICAL ANALYSES OF UPPER CRETACEOUS (UPPER SANTONIAN- CAMPANIAN) PELAGIC SUCCESSIONS OF HAYMANA AND MUDURNU-GÖYNÜK BASINS OF THE SAKARYA CONTINENT, TURKEY

Afridi, Bakht Zamir
M.S., Department of Geological Engineering
Supervisor: Assoc. Prof. Dr. İsmail Ömer Yılmaz
September 2014, 256 pages

The Upper Cretaceous (Upper Santonian-Campanian) successions were measured from two different basins of Turkey, Haymana basin and Mudurnu-Göynük basin. The measured Alagöz and Göynük sections are dominantly composed of red marly beds and fine grained siliciclastic green-gray beds with occasional interruption of fine grained turbiditic bedding. A variety of lithofacies are identified in the studied sections, including radiolarian packstone, silty marls, marls, mudstone, claystone, siltstone and fine grained quartzwacke sandstone. Abundant planktonic foraminifers and low presences of other microfossils are observed within the thin sections. The grains are mostly quartz with less percent of accessory minerals. The depositional environments are interpreted as oxic to suboxic deep marine environment with occasional interruption of turbiditic current and low contribution of organic matter. The low concentrations of P/Al and certain trace element ratio, suggests low nutrient supply and low primary productivity. The Alagöz Section is characterized by Fe-rich and Fe-poor lithologies, while Göynük lithologies possess Fe-poor character. The correlation coefficient of oxides and trace elements indicate terrigenous influx. The D* values and low Ti/A/ ratio suggest fluvial influence and also reflect transgressive condition. The ratios of oxides,

trace elements and Eu-anomalies represent mafic to felsic source rock for Alagöz Section and felsic source rock for Göynük Section. The ratio of trace elements and Ce-anomalies in the studied sections indicate oxic to dysoxic marine environmental conditions during the deposition. The high resolution cyclostratigraphy of the measured sections indicate centimeter to meter-scale cyclic bedding with few episodic cycles at different levels. The cyclic bedding may imply the collaboration of small-scale sea-level fluctuations and/or tectonic effect and changes in productivity.

Keywords: Upper Santonian-Campanian, Haymana Basin, Mudurnu-Göynük Basin, Sedimentology, Red beds and Green-gray beds, geochemical parameters, paleoceanographic changes and cyclostratigraphy.

ÖZ

Sakarya Kıtası'ndaki Haymana ve Mudurnu-Göynük Havzalarında Üst Kretase (Üst Santoniyen-Kampaniyen) Pelajik istiflerinin Stratigrafik, Sedimentolojik, Jeokimyasal
ve Devirsel Stratigrafik Analizleri

Afridi, Bakht Zamir
Yüksek Lisans, Jeoloji Mühendisliği Bölümü
Tez Yöneticisi: Yard.Doç. Dr. İsmail Ömer Yılmaz
Eylül 2014, 256 sayfa

Türkiye'deki iki farklı havzadan, Haymana Havzası ile Mudurnu-Göynük Havzası, Üst Kretase (Üst Santoniyen-Kampaniyen) yaşlı ardalanmalı kayaçlar ölçülmüştür. Ölçülmüş olan Alagöz ve Göynük kesimleri ağırlıklı olarak marnlı kırmızı ve ince taneli silisiklastik yeşil-gri tabakalardan oluşup ara katkılı ince taneli türbiditik tabakalar tanımlanmıştır. Radyolaryalı istiftaşı, siltli marn, camurtaş, kilitaşı ve ince taneli kuvarswake kumtaşını kapsayan farklı litofasiyesler tespit edilmiş ve incekesit örnekleri çıkarılarak incelenmiştir. Yoğun miktarda bulunan planktonik foraminiferler ile az miktarda diğer mikrofosiller de bu ince kesitlerde gözlemlenmiştir. Kayaçların çökelme ortamları zaman zaman türbiditik akıntılar ile kesilmiş derin denizel olarak tayin edilmiştir. Düşük P/Al konsantrasyonu ile belirgin iz element oranları, düşük besin kaynağı ve düşük ilksel produktivite'ye işaret etmektedir. Alagöz kesiti hem demirce zengin hem de demirce fakir litolojilerden oluşuyorken, Göynük kesiti demirce fakir litolojilerden oluşmaktadır. Oksitlerin korelasyon katsayıları ve iz elementler karasal kaynağa işaret etmektedir. D^* değerleri ve Ti/Al oranları ise flüviyal etki ve aynı zamanda transgresif koşullara işaret etmektedir. Oksitlerin oranları, iz elementler ve Eu-anomalileri Alagöz kesitinde mafik ile felsik arası, Göynük kesitinde ise felsik kökeni işaret etmektedir. İz elementler ve Ce-anomali oranlarına bakıldığından yapılan

kesitlerin çökelim ortamının oksijenli ile disoksik denizel koşullar arasında değiştiği gözlenmiştir. Kesitler üzerinde ölçülen yüksek çözünürlüklü devirsel stratigrafik çalışmalar sonucunda metre ve santimetre ölçekli devirsel tabakalar ve farklı seviyelerde ayriyeten gözlemlenen episodik döngüler belirlenmiştir. Döngüsel tabakaların varlığı küçük ölçekli deniz seviyesi değişimleri ve/veya tektonizma etkisive/veya üretim değişikliklerinin işbirliği olarak yorumlanabilir.

Anahtar kelimeler: Üst Santonyen-Kampaniyen, Haymana Havzası, Mudurnu-Göynük Havzası, Sedimentoloji, kırmızı tabakaları ve Yeşil-gri tabakaları, Jeokimyasal parametreler, eski okyanusal değişimler, ve Devirsel Stratigrafi.

To my beloved family.....

ACKNOWLEDGMENTS

I would like to express my sincere gratitude to Assoc. Prof. Dr. İsmail Ömer Yılmaz, my supervisor, for his patient guidance, enthusiastic encouragement, immense knowledge and useful critiques of this research work. His guidance helped me in all time of research and writing of this thesis. I could not have imagined having a better advisor and mentor for my M.S study.

Besides my supervisor, I would like to thank my committee members: Prof. Dr. F. Bora Rojay, Prof. Dr. Faruk Ocakoğlu, Prof.Dr. Sevinç Özkan Altiner and Assist. Prof. Dr. Fatma Toksoy Köksal, for their encouragement, insight comments, hard questions and providing me with a lot of suggestions to improve my research work. I also want to thank you for letting my defense be an enjoyable moments.

I am also grateful to Mr. Zafer Kaplan, for his remarkable assistance in preparation of thin sections for petrographic studies.

A special thanks to my family. Words cannot express how grateful I am to my parents, Dr. Khalid Zamir Afridi (Brother-in-law) and my elder sister (Mrs. Khalid Zamir Afridi) for all of the sacrifices that they have made on my behalf. Your prayer from me was what sustained me thus far. A bundle of thanks to my Uncles, Brothers, Sisters and Cousins whose unconditional love and support always encouraged me in every movement of my life. My sweet nephews and nieces, especially, are an endless source of great joy and love, no matter where they are around the world, they are always with me.

I wish to thank my best friend Ishfaq Bashir, for helping me get through the difficult times, and for all the emotional support, camaraderie, entertainment and care he provided.

I would like to extend my heartfelt thanks to all my friends (You know who you are), for their moral support, motivation and entertainment. I would never forget all the beautiful

moments, chats, trips and memories; I shared with some of my friends. I would like to thank Rıza Levent Kalaycıoğlu and Tuğrül Bülbül, for their help in the field and thesis. I express my sincere thanks to Faisal Baig, Syed Tanvir Shah, Saeed Ahmad Khan, Rizwan Aziz, Muhammad Saad Arshad and Islam Aslam for their good wishes and for all the fun we have had in the last two years.

TABLE OF CONTENTS

ABSTRACT.....	v
ÖZ.....	vii
ACKNOWLEDGEMENTS.....	x
TABLE OF CONTENTS.....	xiii
LIST OF TABLES.....	xviii
LIST OF FIGURES.....	xxii

CHAPTERS

1. INTRODUCTION.....	1
1.1 Purpose and scope.....	1
1.2 Geographic setting.....	2
1.3 Methods of study.....	3
1.4 Previous studies.....	7
1.4.1 Cretaceous Oceanic Red Beds.....	13
1.5 Regional Setting.....	14
1.5.1 Haymana-Polatlı Basin.....	15
1.5.2 Mudurnu-Göynük Basin.....	18
2. GENERAL STRATIGRAPHY.....	21
2.1 General stratigraphy of the Central Anatolia.....	21
2.2 Stratigraphy of Haymana-Polatlı Basin.....	22

2.2.1	Jurassic-lower Cretaceous Succession.....	25
2.2.2	Upper Cretaceous Formation.....	25
2.2.3	Paleogene Succession.....	27
2.2.4	Neogene.....	27
2.3	Stratigraphy of Mudurnu-Göynük Basin	28
2.3.1	Jurassic to Cretaceous Succession.....	28
2.3.2	Tertiary Succession.....	30
2.4	Quaternary Cover.....	31
2.5	Lithostratigraphy of the measured sections.....	31
2.5.1	Alagöz Measured Section.....	33
2.5.2	Göynük Measured Section.....	40
3.	SEDIMENTOLOGY.....	53
3.1	Sedimentological Studies.....	53
3.2	Microfacies of Alagöz Section	53
3.2.1	Red to pale green radiolarian packstone.....	53
3.2.2	Red silty marl.....	57
3.2.3	Greenish to gray mudstone.....	61
3.2.4	Greenish to gray claystone.....	61
3.2.5	Red siltstone.....	65
3.3	Sedimentary structure of the Alagöz stratigraphic section.....	66
3.4	Microfacies of Göynük section	71
3.4.1	Red to brownish marl.....	71
3.4.2	Greenish to gray mudstone.....	77

3.4.3	Greenish to gray claystone.....	77
3.4.4	Greenish to gray siltstone.....	82
3.4.5	Greenish to grayey fine quartzwacke sandstone.....	82
3.5	Sedimentary structure of the Göynük stratigraphic section.....	87
3.6	Petrography and results of point counting.....	89
3.6.1	Petrography and point counting of the Alagöz section.....	89
3.6.2	Petrography and point counting of the Göynük section....	99
3.7	Comparison graphic representation between Alagöz and Göynük sections.....	102
3.7.1	Quartz.....	115
3.7.2	Feldspar and Plagioclase.....	117
3.7.3	Mica.....	117
3.7.4	Glauconite and Heavy Minerals.....	119
3.7.5	Lithic clasts.....	119
3.7.6	Bioclasts.....	121
3.7.7	Heamatite and phosphate.....	121
3.7.8	Pyrite.....	123
3.7.9	Matrix/Clay.....	123
3.7.10	Total grains.....	125
3.8	Interpretation and depositional environment.....	126
4.	GEOCHEMICAL ANALYSIS.....	129
4.1	Introduction.....	129
4.2	Major oxides of the Alagöz and Göynük sections.....	129

4.2.1	Major oxides of red beds of the Alagöz and Göynük sections.....	135
4.2.2	Major oxides of green-gray beds of the Alagöz and Göynük sections.....	136
4.2.3	Vertical Distribution of the major oxides and their comparison.....	137
4.3	Trace element of the Alagöz and Göynük sections.....	139
4.3.1	Trace elements of the red beds of Alagöz and Göynük Sections.....	140
4.3.2	Trace element of the green-gray beds of Alagöz and Göynük Sections.....	141
4.4	Al-normalized major and trace elements of the Alagöz and Göynük sections.....	141
4.4.1	Vertical distribution of al-normalized major and trace elements of the Alagöz and Göynük sections.....	144
4.5	Rare earth elements of the Alagöz and Göynük sections.....	152
4.5.1	Vertical distribution of the rare earth elements of Alagöz and Göynük sections.....	153
4.5.2	REE-normalization of the Alagöz and Göynük sections...	153
4.6	Interpretation of geochemical data.....	158
4.6.1	Pearson's correlation coefficient of the Alagöz and Göynük sections.....	158
4.6.2	Geochemical classification of the samples from Alagöz and Göynük sections.....	161
4.6.3	Provenance studies of the Alagöz and Göynük sections....	163
4.6.4	Clastic influx and primary productivity in the Alagöz and	165

Göynük sections.....	
4.6.5 Geochemical approach to the tectonic setting of Alagöz and Göynük sections	168
4.6.6 Redox sensitive elements in the depositional environments of the Alagöz and Göynük sections.....	169
5. CYCLOSTRATIGRAPHY.....	179
5.1 Cyclostratigraphy.....	179
5.2 Cyclostratigraphy of the Alagöz Section.....	180
5.3 Cyclostratigraphy of Göynük Section.....	184
5.4 Interpretation	189
6. DISCUSSIONS AND RESULTS.....	191
7. CONCLUSIONS.....	197
REFERENCES.....	201
APPENDIX A.....	233
APPENDIX B.....	236
APPENDIX C.....	254

LIST OF TABLES

Table 2.1: Identification of color of the samples from the Alagöz Section	38
Table 2.2: Identification of color of the samples from the Göynük Section	48
Table 3.1: Folk's (1965) texture classification of fine-grained sedimentary rock	57
Table 3.2: Classifications of the Alagöz section based on compositional, grain size and texture parameters.....	58
Table 3.3: Classifications of the Alagöz section based on compositional, grain size and texture parameters.....	59
Table 3.4: Petrographic data and established/recognized Microfacies from Göynük Section samples	72
Table 3.5: Classifications of the Göynük section based on compositional, grain size and texture parameters.....	75
Table 3.6: Percent quantitative data of the Alagöz samples under microscope by using point counting method (unit as number of grains percent) (James Swift brand mechanical stage). (data display in graphic curve as Figures 3.29-3.30)	92
Table 3.7: Percent quantitative data of the Göynük samples under microscope by using point counting method (unit as number of grains percent) (James Swift brand mechanical stage). (data display in graphic curve as Figures 3.32-3.33).....	103
Table 3.8: Percent date Statistical description of red beds of the Alagöz Section from Table 3.6.	116
Table 3.9: Percent date statistical description of green to gray beds of the Alagöz Section from Table 3.6.....	116
Table 3.10: Percent date statistical description of red beds of Göynük Section from Table 3.7.	116

Table 3.11: Percent date statistical description of green to gray beds of the Göynük Section from Table 3.7	117
Table 4.1: Major element (wt.%) , REE (ppm) and normalized values of the red beds of Alagöz Section.	130
Table 4.2: Major element (wt.%) , REE (ppm) and normalized values of the green-gray beds of Alagöz Section.	130
Table 4.3: Trace element (ppm) concentration in the red beds of Alagöz Section....	130
Table 4.4: Trace element (ppm) concentration in the green-gray beds of Alagöz Section	131
Table 4.5: REE (ppm) concentration in the red beds of Alagöz Section.	131
Table 4.6: REE (ppm) concentration in the green-gray beds of Alagöz Section.....	131
Table 4.7: Major element (wt. %), REE (ppm) and normalized values of the red beds of Göynük Section.....	132
Table 4.8: Major element (wt.%), REE (ppm) and normalized values of the green-gray beds of Göynük Section.	132
Table 4.9: Trace element (ppm) concentration in the red beds of Göynük Section....	133
Table 4.10: Trace element (ppm) concentration in the green-gray beds of Göynük Section.	133
Table 4.11: REE (ppm) concentration in the red beds of Göynük Section.	134
Table 4.12: REE (ppm) concentration in the green-gray beds of Göynük Section....	134
Table 4.13: Pearson`s correlation coefficient of major element, REE and normalized values of the red beds of Alagöz Section.....	159
Table 4.14: Pearson`s correlation coefficient of major element, REE and normalized values of the green-gray beds of Alagöz Section.....	159

Table 4.15: Pearson's correlation coefficient of major element, REE and normalized values of the red beds of Göynük Section.	160
Table 4.16: Pearson's correlation coefficient of major element, REE and normalized values of the green-gray beds of Göynük Section.	160
Table 4.17: Range of La/Sc, Th/Co, Th/Sc ratios of the Alagöz and Göynük sections compared with felsic and mafic sediments origin ratio (¹ Cullers, 1994; 2002; ² Taylor and McLennan, 1985).....	167
Table 6.1: Correlation of the CORBs characteristic from different regions of the world (modified from Chen et al., 2007 and Hu et al., 2005)	195
Table A1:	233
Table A2:	234
Table B1:	236
Table B2:	236
Table B3:	237
Table B4:	237
Table B5:	238
Table B6:	238
Table B7:	239
Table B8:	239
Table B9:	240
Table B10:	240
Table B11:	241
Table B12:	241
Table B13:	242
Table B14:	242

Table B15:	243
Table B16:	243
Table B17:	244
Table B18:	244
Table B19:	245
Table B20:	245
Table B21:	247
Table B22:	247
Table B23:	248
Table B24:	248
Table B25:	250
Table B26:	251
Table B27:	252
Table B28:	253
Table C1:	254
Table C2:	254
Table C3:	255
Table C4:	255
Table C5:	256

LIST OF FIGURES

Figure 1.1: Satellite image showing the measured Alagöz Section in the Haymana Basin (Alagöz Section represented by green icon), Ankara and Mudurnu-Göynük Basin (Göynük Section represented by yellow icon), Bolu Provinces, Turkey. (red arrow represents North direction of the Google earth map).	4
Figure 1.2: Close view of the satellite image showing the measured Alagöz Section in the Haymana basin (green icon) and 39°45'19.73"N; 32°29'27.80"E geographic coordinate. (red arrow represents North direction of the Google earth map).	4
Figure 1.3: Close view of the satellite image showing the measured studied Göynük Section (yellow icon) and 40°23'44.50"N; 30°46'51.55"E geographic coordinate. (red arrow represents North direction of the Google earth map).	5
Figure 1.4: Showing regional tectonic of the Turkey and adjacent areas (modified from Okay and Tüysüz, 1999). (Note: rectangles represent studied sections; yellow-Göynük and pink-Alagöz sections and red arrow represents North direction map).	16
Figure 1.5: The regional tectonic and geological setting of the Haymana basin and subduction of the Neo-Tethyan Oceanic crust during the late Cretaceous to Middle Eocene (Koçyiğit et al., 1988 and 1991).	16
Figure 1.6: Representing schematic model for the tectonic divergent setting and depositional stratigraphy of the northern Sakarya Continental margin (Koçyiğit et al., 1991). a) Upto Aptian, b) Upto Cenomanian, and c) Upto Maastrichtian.	17
Figure 2.1: The generalized stratigraphy and correlation in the Haymana-Polatlı and adjacent areas (Modified from Ünalan et al., 1976) (Not to scale).	23
Figure 2.2: The generalized Cretaceous stratigraphy and correlation in the Mudurnu-Göynük Basin (Modified from Yılmaz, 2002) (Not to scale).	24

Figure 2.3: Composite Stratigraphic section of the Haymana basin and MS (red line) represent measured stratigraphic section near the Alagöz Village (Modified from Ünalan et al., 1976).	26
Figure 2.4: Composite Stratigraphic section of the Mudurnu-Göynük Basin and MS (red line) represents measured stratigraphic section in the Göynük Village (Modified from Altiner et al., 1991; Şener and Şengüler 1998).	29
Figure 2.5: The field photograph of the studied area representing sharp lower contact (pink line) with the Upper Jurassic-Lower Cretaceous sedimentary mélange and angular unconformity upper contact with the Tertiary strata (red line) SW dip direction (yellow line-measured section; black line-bedding).	34
Figure 2.6: The field photograph showing the Upper Santonian-Campanian red beds in the Alagöz section.	34
Figure 2.7: Measured stratigraphic section of the Alagöz Village in the Haymana Basin	35
Figure 2.8: Yellow dotted lines show calcite veins, perpendicular to bedding and conjugate symmetry in the field (red line representing bedding plane; Dipping in SW), in the Upper Santonian-Campanian Alagöz stratigraphic section.....	39
Figure 2.9: A) The Alagöz Section photomicrograph of sample ZR16 thin section, representing micro-borrow (PPL) (yellow line representing micro-borrow); B) The photograph of infilling-marl dendritic bioturbation pattern in Sample ZR0a.	39
Figure 2.10: The field photograph of measured stratigraphic section; A) 0-14 m and B) 14-28.75 m near the Göynük town, Bolu. SW dip direction (yellow line shows measured section; black lines for bedding; green line display contact with overlying Fine clastic turbiditic sequence; red line represents unconformable contact with volcanogenic turbiditic sequence).	42
Figure 2.11: Measured stratigraphic section of Göynük Village of the Göynük Basin..	43
Figure 2.12: The field photograph showing the Upper Santonian-Campanian red beds in the Göynük section.	49

Figure 2.13: The field photograph showing the Campanian greenish gray claystone and mudstone in the Göynük section.	49
Figure 2.14: Asymmetrical ripples in the GOZ38 (sandstone) of the Göynük section. A) GOZ38 with red dotted lines represents ripples and B) Sketch of A.....	50
Figure 2.15: Lamination in the samples of the Göynük section. A) Photo of GOZ49 and B) Sketch of A: C) Photo of GOZ51 and D) Sketch of C; red lines show lamination...	50
Figure 2.16: A) The field photograph of the Inoceramus fragment in the Göynük section. B) Photo showing iron nodule in the Göynük section.	51
Figure 3.1: Ternary mudstone compositional classification (for unconventional) diagram of the A) Diaz et al. (2012) and B) the Allix et al. (2010) used to plot the samples of Alagöz and Göynük sections, and their comparison with known unconventional reservoirs from USA.	54
Figure 3.2: A) Stow's (2005) classification and B) the Picard's (1971) classification based on relative proportions of grains size. (The samples of Alagöz and Göynük sections are represented by white and yellow circles, respectively).	55
Figure 3.3: Stow's compositional classification (2005) ternary diagram based on biogenic (carbonate and silica) and mud/clays: illustrate the Alagöz (white circles) and the Göynük sections samples (yellow circles).	56
Figure 3.4: Studied samples of the Göynük Section are plotted on the Folk's (1974) Sandstone classification ternary diagram based on relative proportions of grains size and presence of matrix.	56
Figure 3.5: Photomicrographs of red to pale green radiolarian packstone microfacies representing radiolarian sp. (R), calcareous radiolarian sp. (CR), siliceous radiolarian sp. (SR), sponge spicules (S), glauconite (G), pyrite (P) and matrix (M) (Sample no. ZR0b, (A) PPL, (B) XPL x4).	60
Figure 3.6: Photomicrographs of Red Silty Marl Microfacies having abundant silt-size quartz grains (Q) with pyrite (P) and iron rich matrix (Sample no. ZR04, PPL).	62

Figure 3.7: The field photograph showing the red beds of the Alagöz measured section	62
Figure 3.8: Photomicrographs of greenish to gray mudstone microfacies containing quartz (Q), mica (Mi), pyrite (P), calcite (Ct), radiolarian sp. (R), planktonic foraminifers and matrix and calcite filling fracture (F) (Sample no. ZR05, (A) XPL x4; ZR07, (B) PPL x4).	63
Figure 3.9: Photomicrographs of the greenish to gray mudstone microfacies containing quartz (Q), pyrite (P), hematite (He), planktonic foraminifers and matrix and yellow line shows bioturbation (Sample no. ZR07, (A) PPL x4; ZR21, (B) PPL x4).	64
Figure 3.10: The field photograph showing the greenish to gray mudstone and claystone of the Alagöz measured section.	65
Figure 3.11: Photomicrographs of the greenish to gray claystone microfacies representing quartz (Q), pyrite (P), planktonic foraminifers embedded in matrix (Sample no. ZR09, (A) PPL x4; ZR18, (B) PPL x4).....	67
Figure 3.12: Photomicrographs of the red siltstone facies containing quartz (Q), intra-clast of lime mudstone and iron rich matrix (He) (Sample no. ZR01 x2.5, (A) PPL; ZR04a, (B) PPL x2.5).	68
Figure 3.13: The field photograph showing transitional zone between the red beds and greenish to gray mudstone of the Alagöz measured section.....	69
Figure 3.14: The field photograph showing the medium dark gray mudstone with flaggy appearance of the Alagöz measured section.	69
Figure 3.15: Close view field photograph showing the greenish gray claystone of the Alagöz measured section.....	70
Figure 3.16: Close view field photograph showing the grayish red intra-clastic (lime mudstone fragment) bearing siltstone of the Alagöz measured section (sample no. ZR04a).	70

Figure 3.17: Photomicrographs of the red to brownish marl containing quartz (Q), pyrite (P), bivalve (Bv), phosphate (Ph), planktonic foraminifers and matrix and lamination of bioclasts represented by orange line (Sample no. GOZ6, (A) PPL x4; GOZ7, (B) PPL x2.5).	78
Figure 3.18: Photomicrographs of the greenish to gray mudstone microfacies representing quartz (Q), pyrite (P), inoceramus fragments (In), benthic foraminifers (Bn), planktonic foraminifers (Pf) and phosphate (Ph) (Sample no. GOZ13, (A) PPL x2.5; GOZ13, (B) PPL x4).	79
Figure 3.19: Photomicrographs of greenish gray to gray mudstone microfacies containing quartz (Q), pyrite (P), inoceramus fragments (In), plagioclase (Pg) and matrix (Sample no. GOZ17, (A) XPL with mica plate x4; (B) GOZ25, PPL x4).....	80
Figure 3.20: The field photograph showing the red to brownish marl microfacies of the Göynük Section.	81
Figure 3.21: The field photograph showing transitional zone between the red beds and the greenish to gray mudstone of the Göynük measured section.	81
Figure 3.22: Photomicrographs of greenish to gray claystone microfacies containing quartz (Q), pyrite (P), inoceramus fragments (In), planktonic foraminifers and matrix (Sample no. GOZ0, (A) PPL x4; GOZ10, (B) XPL x2.5).....	83
Figure 3.23: Photomicrographs of greenish to gray siltstone representing laminated siltstone and representing contact with greenish gray to gray Mudstone (Sample no. GOZ41, (A) PPL x2.5, GOZ45, (B) PPL x2.5).	84
Figure 3.24: The field photograph showing the greenish to gray mudstone, claystone and greenish yellow to grayey sandstone of the Göynük Section.	85
Figure 3.25: The field photograph showing the greenish gray to gray mudstone and greenish to gray siltstone of the Göynük Section.	85
Figure 3.26: The field photograph showing the Inoceramus in the greenish to gray mudstone of the Göynük measured section.	86

Figure 3.27: Photomicrographs of the greenish yellow to grayey fine sandstone showing quartz (Q), pyrite (P), plagioclase (Pg) and glauconite (G) (Sample no. GOZ28, (A) PPL x4) and (B) representing erosional contact (Sample no. GOZ49, (B) PPL x2.5).....	88
Figure 3.28: Graphic representation of quantitative data of the Alagöz samples under microscope by using point counting method (James Swift brand mechanical stage). ...	91
Figure 3.29: Representing Quartz-Bioclastic-Feldspar (10*)-Plagioclase (10*)-Glauconite (10*)-Lithic (10*)-Heavy minerals (10*) graphic curves of the Alagöz Stratigraphic Section petrographic studies. (Note: 10* represents 10 time increase).....	93
Figure 3.30: Representing Matrix-Total grains-Mica-Pyrite-Phosphate (10*) - Hematite graphic curves of the Alagöz Stratigraphic Section petrographic studies. (Note: 10* represents 10 time increase).....	96
Figure 3.31: Graphic representation of quantitative studied of the Göynük samples under microscope by using point counting method (James Swift brand mechanical stage).....	100
Figure 3.32: Representing Quartz-Bioclastic-Feldspar (10*)-Plagioclase (10*)-Glauconite (10*)-Lithic(10*)-Heavy minerals(10*) graphics curve of the Göynük stratigraphic section petrographic data. (Note: 10* represents 10 time increase).....	105
Figure 3.33: Representing Matrix-Total grains-Mica (2*)-Pyrite-Phosphate (10*) – Hematite (2*) graphic curves of the Göynük stratigraphic section petrographic data. (Note: 10* and 2* represents 10 and 2 time increase, respectively).	110
Figure 3.34: The graphic curves comparison of quartz, feldspar and plagioclase of Alagöz Section (black line) and Göynük Section (red line). (Red beds represented by red shaded area)	118
Figure 3.35: The graphic curves comparison of mica, glauconite and heavy minerals of the Alagöz Section (black line) and Göynük Section (red line) (red shade represents red beds). (Red beds represented by red shaded area)	120
Figure 3.36: The graphic curves comparison of lithic, bioclasts and heamitite of Alagöz Section (black line) and Göynük Section (red line). (Red beds represented by red shaded	

area)	122
Figure 3.37: The graphic curves comparison of pyrite, phosphate and matrix comparison graphic curves of Alagöz section (black line) and Göynük Section (red line). (Red beds represented by red shaded area)	124
Figure 3.38: The graphic curves comparison of total grains of Alagöz Section (black line) and Göynük Section (red line). (Red beds represented by red shaded area)	125
Figure 4.1: SiO_2 , Al_2O_3 , MgO , Fe_2O_3 , CaO , TiO_2 , Na_2O and K_2O wt.% geochemical data graphs of the Alagöz Section (black line) and Göynük Section (red line) and their relationship. (red shade represents red beds)	138
Figure 4.2: P_2O_3 , Cr_2O_3 and MnO wt.% geochemical data graphs of the Alagöz Section (black line) and Göynük Section (red line) and their relationship. (red Shade represents red beds)	140
Figure 4.3: PAAS-normalized trace elements of the Alagöz Section samples plot. PAAS (Taylor and McLennan, 1985) values are used for normalization. (A: Red Beds and B: Green-gray Beds)	142
Figure 4.4: PAAS-normalized trace elements of the Göynük Section samples plot. PAAS (Taylor and McLennan, 1985) values are used for normalization. (A: Red Beds and B: Green-gray Beds)	143
Figure 4.5: Graphic representation of Si/Al , Fe/Al , Mg/Al , Ca/Al and Na/Al of the Alagöz (black line) and Göynük (red line) sections. (red shade represents red beds) ..	145
Figure 4.6: Graphic representation of K/Al , Ti/Al , P/Al , Mn/Al and Cr/Al of the Alagöz (black line) and Göynük (red line) sections. (red shade represents red beds).....	147
Figure 4.7: Graphic representation of Sc/Al , Ba/Al , Co/Al , Nb/Al and Rb/Al of the Alagöz (black line) and Göynük (red line) sections. (red shade represents red beds)...	149
Figure 4.8: Graphic representation of Sr/Al Ta/Al , Th/Al , U/Al and V/Al of the Alagöz (black line) and Göynük (red line) sections. (red shade represents red beds)	150

Figure 4.9: Graphic representation of Zr/Al, Mo/Al Cu/Al, Pb/Al and Zn/Al of the Alagöz (black line) and Göynük (red line) sections. (red shade represents red beds)	151
Figure 4.10: Graphic representation of Ni/Al of the Alagöz (black line) and Göynük (red line) sections. (red shade represents red beds)	152
Figure 4.11: La, Ce, Nd and Pr geochemical data graph of the Alagöz Section. (red shade represents red beds)	154
Figure 4.12: Sm, Eu, Gd, Tb, Dy, Ho, Er, Tm, Yb and Lu geochemical data graphs of the Alagöz Section. (red shade represents red beds)	154
Figure 4.13: La, Ce, Nd and Pr geochemical data graph of the Göynük Section. (red shade represents red beds)	155
Figure 4.14: Sm, Eu, Gd, Tb, Dy, Ho, Er, Tm, Yb and Lu geochemical data graph of the Göynük Section. (red shade represents red beds)	155
Figure 4.15: PAAS-normalized REE of the Alagöz Section samples plot. PAAS (Taylor and McLennan, 1985) values are used for normalization. (A: Red beds and B: Green-gray beds)	156
Figure 4.16: PAAS-normalized REE of the Göynük Section samples plot. PAAS (Taylor and McLennan, 1985) values are used for normalization. (A: Red beds and B: Green-gray beds)	157
Figure 4.17: Log (Fe ₂ O ₃ /K ₂ O) vs Log (SiO ₂ /Al ₂ O ₃) graph of A) red beds and B) green-gray beds of the Alagöz Section by Herron (1988) for sandstone and shale classification.	162
Figure 4.18: Log (Fe ₂ O ₃ /K ₂ O) vs Log (SiO ₂ /Al ₂ O ₃) graph of A) red beds and B) green-gray beds of the Göynük Section by Herron (1988) for sandstone and shale classification.	162
Figure 4.19: Th/Co vs La/Sc graph of A) red beds and B) green-gray beds of the Alagöz Section. (terrigenous source from Cullers, 2002).	166

Figure 4.20: Th/Co vs La/Sc graph of A) red beds and B) green-gray beds of the Göynük Section. (terrigenous source from Cullers, 2002)	166
Figure 4.21: Log (K ₂ O/Na ₂ O) vs SiO ₂ graph of A) red beds and B) green-gray beds of the Alagöz Section. (sandstone-mudstone tectonic setting by Roser and Korsch, 1986)	170
Figure 4.22: Log (K ₂ O/Na ₂ O) Vs SiO ₂ graph of A) red beds and B) green-gray beds of the Göynük Section. (sandstone-mudstone tectonic setting by Roser and Korsch, 1986)	170
Figure 4.23: Ni/Co vs V/(V+Ni) graph of A) red beds and B) green-gray beds of the Alagöz Section for redox-sensitive cross plots (Hatch and Levenchal, 1992).	172
Figure 4.24: Ni/Co vs V/Cr graph of A) red beds and B) green-gray beds of the Alagöz Section for redox-sensitive cross plots (Jones and Manning, 1994).	172
Figure 4.25: Ni/Co vs V/(V+Ni) graph of A) red beds and B) green-gray beds of the Göynük Section for redox-sensitive cross plots (Hatch and Levenchal, 1992).	174
Figure 4.26: Ni/Co vs V/Cr graph of A) red beds and B) green-gray beds of Göynük Section for redox-sensitive cross plots (Jones and Manning, 1994).	174
Figure 4.27: Representing Ce anomalies along measured stratigraphic samples of the Alagöz Section to observe the redox sensitive marine condition. (red shade represents red beds: * PAAS- Taylor and McLennan, 1985)	175
Figure 4.28: Representing Ce anomalies along measured stratigraphic samples of the Göynük Section to observe the redox sensitive marine condition. (red shade represents red beds: * PAAS- Taylor and McLennan, 1985)	175
Figure 4.29: Ce-Anomaly vs Nd (ppm) graph of red beds of the Alagöz Section (Ce-anomaly vs Nd (ppm) graph of Wright et al., 1987).	176
Figure 4.30: Ce-Anomaly vs Nd (ppm) graph of green-gray beds of the Alagöz Section (Ce-anomaly vs Nd (ppm) graph of Wright et al., 1987).	176

Figure 4.31: Ce-Anomaly vs Nd (ppm) graph of red beds of the Göynük Section (Ce-anomaly vs Nd (ppm) graph of Wright et al., 1987)	177
Figure 4.32: Ce-Anomaly vs Nd (ppm) graph of green-gray beds of the Göynük Section (Ce-anomaly vs Nd (ppm) graph of Wright et al., 1987)	177
Figure 4.33: SiO ₂ vs Al ₂ O ₃ graph of A) red beds and B) green-gray beds of the Alagöz Section.	178
Figure 4.34: SiO ₂ vs Al ₂ O ₃ graph of A) red beds and B) green-gray beds of the Göynük Section.	178
Figure 5.1: Cyclostratigraphic framework in the Alagöz Stratigraphic Section.....	181
Figure 5.2: Cyclostratigraphic framework in the Göynük Stratigraphic Section.....	186

CHAPTER 1

INTRODUCTION

1.1 PURPOSE AND SCOPE

The Cretaceous period has a great importance in the geological science as many geological events occurred during this period. Therefore, this period has been focused worldwide for the paleoclimatology, global tectonics and especially global deep oceanic events (Oxic and Anoxic events). In the Cretaceous, Barremian, Aptian, Albian, Late Cenomanian-early Turonian and Coniacian-Santonian epochs are mostly characterized by Oceanic Anoxic Events while Berriasian-early Barremian, Cenomanian, Turonian, late Campanian-Maastrichtian epochs represents mostly Oceanic oxic events (Jenkyns, 1980; Yilmaz, 2008). The oceanic black shales and red beds were widespread in the paleoceanography and documented from several region of the world, including the North and South Atlantic Ocean, Pacific Ocean, Indian Ocean, Tethyan Realm and New Zealand (Chen et al., 2007). Several other studies have been carried out related to the origin and cause of the global oceanic events in the Valanginian, Aptian, Albian, Cenomanian/Turonian and late Santonian-Campanian stages from different parts of the world (Schlangar and Cita, 1982; Herbert and Fischer, 1986; Jenkyns and Clayton, 1986; Bralower et al., 1994; Herrle et al., 2003; Skelton et al., 2003; Erba, 2004; Coccioni et al., 2006; Yilmaz, 2008). The Cretaceous sediments have been examined for stable isotopes and geochemical analyses for special purposes (Weissert and Breheret, 1991; Menegatti et al., 1998; Jenkyns and Wilson, 1999; Stoll and Schrag, 2000; Price, 2003; Yilmaz et al., 2004a; Yilmaz, 2008; Hu et al., 2009). Sequence stratigraphic and cyclostratigraphic analyses has been carried out for the oceanic black shale and red beds to illuminate their mode of occurrences (Herbert and Fischer, 1986; Einsele et al., 1991; Claps and Masetti, 1994; Claps et al., 1995; House and Gale, 1995; Yilmaz et al., 2000, 2004a, and 2004b; Einsele, 2001; Yilmaz, 2002 and 2008; Hu et al., 2005; 2009).

The Cretaceous Oceanic black shale and Red beds have been documented from Central Anatolia and other parts of Turkey (Görür et al., 1993; Eren and Kidar, 1999; Eren and Taslı, 2002; Tüysüz, 1999, 2002 and 2003; Yılmaz, 2002 and 2008; Yurtsever et al., 2003; Yılmaz et al., 2004a, 2004b, 2010, 2012 and 2012; Yılmaz and Altiner, 2005b and 2006b).

This study deals with the Upper Cretaceous (Upper Santonian-Campanian) of the Haymana Basin and Mudurnu-Göynük Basin. The stratigraphic sections have been measured from sedimentary succession in the Alagöz village (Kocatepe Formation-Santonian age and Haymana Formation-Campanian age) and Göynük town (Değirmenözü Member-Santonian-Early Campanian age and Yenipazar Formation-Campanian-Maastrichtian age) for this study. The purpose of study is to determine the vertical changes in facies in the studied sections and interpret their depositional environment. The geochemical analyses have been carried out in order to understand the geochemical properties of the studied sections. The cyclostratigraphic study approaches to recognize centimeter to meter-scale cyclic bedding. This studied can be helpful for petroleum expects overview (Oxic and Anoxic event) and to establish the correlation with other stratigraphic successions.

1.2 GEOGRAPHIC SETTING

The Upper Santonian-Campanian stratigraphic sequences are studied from two different basins in the Central Anatolia of Turkey (Figure 1.1). These are present in Ankara province known as Haymana Basin and in Bolu province known as Mudurnu-Göynük Basin. Geographically, Haymana Basin lies in the south and southwest of Ankara and north of Tuz Gölü Basin, whereas Mudurnu-Göynük Basin is surrounded by Istanbul in the north and Ankara in the southeast. The geographic coordinates of the Haymana Basin and Mudurnu-Göynük Basin are 39°50'28.97"N-38°48'26.77"N; 32°4'15.30"E-33°28'18.43"E and 40°23'55.02"N-40°28'9.13"N; 30°47'11.20"E-31°12'35.91"E, approximately. Geologically, the areas are as if a sandwich between Intra-Pontide suture zone to the north and Izmir-Ankara-Erzincan suture zone to the south. These two suture

zones are formed as a result of closing Neo-Tethyan Ocean (Koçyiğit et al., 1991; Figure 1.4).

The Haymana Basin studied section is in the vicinity of the Alagöz village, located in the Ankara province in the Central Turkey and measured section is represented by 39°45'19.73"N; 32°29'27.80"E geographic coordinates (Figure 1.2). The studied section is about 35 km from the Ankara and easily accessible from the Ankara-Eskisehir road. It is surrounded by the Kırşehir Block, the Kütahya-Bolkardağı metamorphic rocks (originating from the Menderes-Taurus Platform) and some ophiolitic remnants of the Neo-Tethys oceanic crust (Aydemir, 2011).

The Mudurnu-Göynük Basin studied section is in the Göynük town, which is situated in the NW Turkey, within the province of Bolu, between Istanbul and Ankara. The geographic coordinates of the measured stratigraphic column are 40°23'44.50"N; 30°46'51.55"E (Figure 1.3). The Göynük Section can be easily accessible from Göynük town as it is about 550 m from the main market of the town and is exposed to road side section. It is a part of the Mesozoic-Tertiary basin extending between the metamorphics of Eskisehir-Bilecik in the south and the old basement rocks of Bolu Paleozoic Massif in the north.

1.3 METHODS OF STUDY

The study has been carried out in the exposed Upper Santonian-Campanian outcrops near the Alagöz village in the Haymana basin and in the Göynük town in the Mudurnu-Göynük basin.

In the Haymana basin and Mudurnu-Göynük basin, two different basins, the stratigraphic sections were measured using centimeter tape. 1900 and 2875 cm thick stratigraphic sections from bottom to top were selected for this study in the Alagöz village and Göynük town, respectively. A total of 24 samples were collected from the Alagöz Section and 56 samples from the Göynük Section. The collected samples were disoriented and mostly the intervals between the samples were ranging from 10cm, 50



Figure 1.1: Satellite image showing the measured Alagöz Section in the Haymana Basin (Alagöz Section represented by green icon), Ankara and Mudurnu-Göynük Basin (Göynük Section represented by yellow icon), Bolu Provinces, Turkey. (red arrow represents North direction of the Google earth map).



Figure 1.2: Close view of the satellite image showing the measured Alagöz Section in the Haymana basin (green icon) and 39°45'19.73"N; 32°29'27.80"E geographic coordinate. (red arrow represents North direction of the Google earth map).

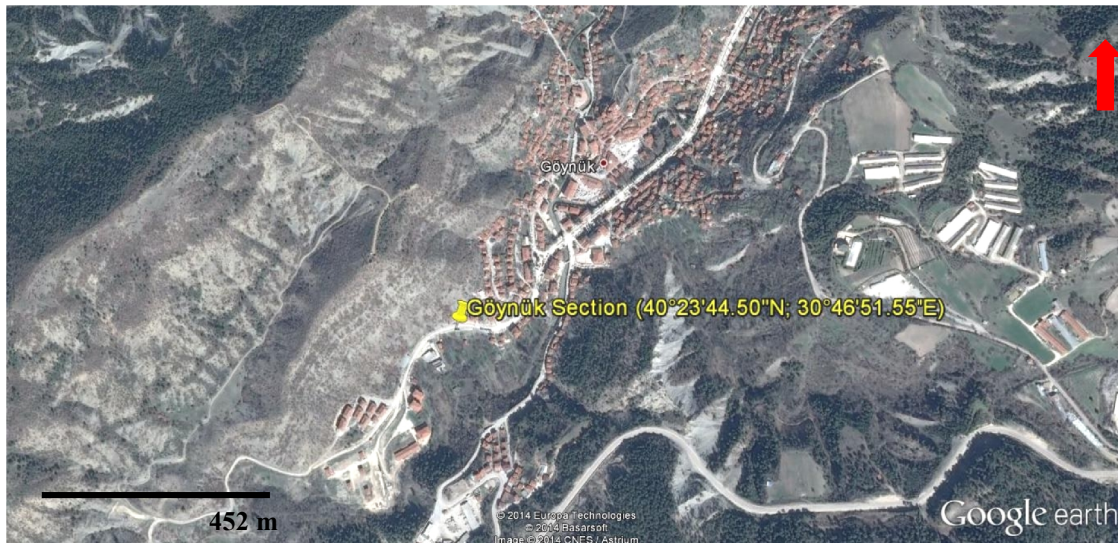


Figure 1.3: Close view of the satellite image showing the measured studied Göynük Section (yellow icon) and 40°23'44.50"N; 30°46'51.55"E geographic coordinate. (red arrow represents North direction of the Google earth map).

cm, 70 cm and 100 cm. The measured stratigraphic log was drawn on the note book along with description of observed sedimentary structures. The rock colours have been assigned by using colour codes of the geological rock color chart of Geological Society of America (GSA), 2009.

In laboratory, the collected samples were separated for further detailed analyses such as microscopic studies, geochemical and cyclostratigraphic analyses.

For microscopic studies, a total of 80 thin sections were prepared and studied under polarized microscope for the microfacies analyses. These thin sections were also used for quantitative analysis by using James Swift electro-mechanical stage that is mounted to microscopic stage. This point-counter was used for determination of content in terms of numbers as well as in percentage. 7500-8500 average points were counted per thin section. These microscopic details were used for interpretation of sedimentology and depositional environments.

The studied sections are classified from different perspectives and parameters which are based on the mineralogical composition, relative grain size proportion and textural and

structural parameters (Tables 3.2 and 3.4). The mineralogical composition of the studied sections have been classified by using Diaz et al. (2012) mudstone classification (Figure 3.1), Allix's et al. (2010) shale classification (Figure 3.1) and Stow's (2005) classification (Figure 3.3). The Diaz et al. (2012) mudstone classification and Allix's et al. (2010) shale classification are based on the three end members Quartz/ Feldspars-Clay-Carbonate constitutes and also used for the comparison with other unconventional reservoirs. Stow's (2005) classification characterized the calcareous-siliceous and clay proportions. Dunham's (1962) and Folk's (1962) classification is used to describe limestones. Stow's (2005) siliciclastic (Figure 3.2) and Picard (1971) triangular classifications (Figure 3.2) are used to determined the grain size proportion in individual samples and to approach the unconventional reservoir characteristic of the samples and classification. The textural classification of the studied sections are determined by using Folk's (1965) textural classification table for fine-grained sedimentary rocks. It is based on the relative percentage of grains size within the fine-grained rocks and their outcrop appearances (Table 3.1). Folk's (1965) sandstone classification (Figure 3.4) is used to define the mineralogy, textural maturity and matrix proportion in the sandstone.

Geochemical analysis has been carried out for 77 samples from the Alagöz and Göynük sections to obtained major oxides, trace elements, rare earth elements and refractory elements data. The obtained geochemical data of the studied samples are examined to interpret the geochemical parameters and their characteristic features. The geochemical analyses have been carried out in the Acme Labs of Vancouver, Canada. In the Acme Lab, SPECTRO Ciros Vision and ELAN 9000 devices are used for ICP-Emission Spectrometry and ICP-Mass Spectrometry analyses, respectively. The major oxides and few trace elements are detected from samples by using the ICP-Emission Spectroscopy analyzer and then treated by lithium borate fusion and disintegrated in the nitric acid. At 1000°C, Loss of ignition (LOI) has been observed by the difference in the weight loss of the sample after ignition. The other trace elements and rare earth elements (REE) are determined by applying the ICP-Mass Spectroscopic processes. These are followed by lithium borate and decomposed in the nitric acid. The precious and base metals are obtained from the dissolved Aqua regia and analyzed by ICP-Mass Spectroscopy. Five

grams of sample is required for geochemical data processes. The detection limits of the major oxides in ICP-ES are 0.01 (wt. %) for SiO₂, Al₂O₃, CaO, MgO, Na₂O, K₂O, TiO₂, P₂O₅, MnO; 0.04 (wt. %) for Fe₂O₃ and 0.002 (wt. %) for Cr₂O₃. The trace element detection limits are 1 (ppm) for Sc, Ba, Zn; 0.1 (ppm) for Y, Nb, Rb, Ta, U, Zr, Mo, Cu, Pb, Ni, Cd; 0.2 (ppm) for Co, Th; 0.5 (ppm) for Sr, As and 8 (ppm) for V. The rare earth element detection limits are 0.1 ppm for La, Ce; 0.02 (ppm) for Pr, Eu, Ho; 0.3 (ppm) for Nd; 0.05 (ppm) for Sm, Gd, Dy, Yb; 0.01 ppm for Tb, Tm, Lu and 0.03 (ppm) for Er. The rare earth elements are normalized by using Post-Archaen Australian Shale (PAAS) of Taylor and McLennan (1985). The PAAS-normalization is used to interpret the sediments characteristic.

1.4 PREVIOUS WORK

The Central Anatolian block of the Turkey have been carried out the numerous researches in different aspects since 1900's. This region has greater prospect for the geologists as it shows certain characteristics for hydrocarbon and coal resources. It has also great importance in the history of tectonic evolution of the Tethyan oceans.

In early 1900's, the Haymana-Polatlı basin has been first studied for detailed geological frame work and establishment of regional stratigraphy by Chaput (1932, 1935a, 1935b and 1936). His early research is related to the Triassic-Eocene successions, including radiolarite, shales, limestone and flysch deposits. During his research, he came out with occurrence of Upper Cretaceous-Eocene succession in the region along with randomly distributed outcrops of flysch deposits. He also interpreted the tectonic deformation in the basin and pointed out that these were occurred during Tertiary epoch.

Lokman and Lahn (1946), Lahn (1949) and Egeran and Lahn (1951) explained the tectono-stratigraphy and regional structural geology of the Central Anatolian block. Lokman and Lahn (1946) enlightened that orogenic processes evolved in the Haymana-Polatlı region before Early Cretaceous and their tectonic movement correlated with the Late Mesozoic-Eocene Alpine-orogeny.

In early 1960's, the Mudurnu-Göynük basin has been studied for basin analysis and stratigraphic characteristic (Abdüsseleamoğlu, 1959; Türkünal, 1960). The region has been assigned with stratigraphic succession from Pre-Devonian to recent deposits and designed a geological map to a scale of 1:100,000. It has been noticed that the Late Cretaceous in the Mudurnu region is composed of alternating carbonates and turbiditic facies and the early Cretaceous were mainly characterized by carbonates in the southern part of the Mudurnu area (Abdüsseleamoğlu, 1959). The east-north-east to west-south-west trending orogenic belt in the northwestern Central Anatolia region is divided into two zones, named as Sillon and Cordilleres by Türkünal (1960). The Sillon zone composed of Cretaceous clayey, globotruncana bearing variegated limestone, volcanic and flyschoidal deposits. This zone included Mudurnu basin, Vakıfaktaş basin, Şıhlar village basin and Köstebekçayı basin. The Cordilleres zone comprises of lower Cretaceous marly limestone and includes Tavşat Mountain, Nallıhan Mountain, Sarıçal Mountain and Çal Mountain. These sedimentary succession zones are correlated and examined to know the paleogeography and tectonics of the northwestern Anatolia, Turkey.

Since 1960's, the Central Anatolia was focused for hydrocarbon potentials and exploration (Rigo de Rigni and Cortesini, 1959; Reckamp and Özbey, 1960; Schmidt, 1960; Akarsu, 1971; Arıkan, 1975; Şenalp and Gökçen, 1978; Ünalan and Yüksel, 1985; Görür and Tüysüz, 2001; Gülbay and Kormaz, 2008; Sarı and Geze, 2008; Yılmaz, 2008; Yılmaz et al., 2010, 2012 and 2012; Aliyev et al., 2009 and Çimen et al., 2013). The Haymana-Polatlı basin has been investigated for the hydrocarbon prospect and exploration by Druitt and Rackamp (1959), Şenalp and Gökçen (1978), Coşkun et al. (1990), Grovel et al. (2000), Aydemir and Ateş (2006), Acer et al. (2007) and Aydemir (2011). During their studies, they observed oil-bearing clastic rocks and interpreted these clastic rocks as submarine fan channel fill deposits. Coşkun et al. (1990) studied the petroleum system of the Haymana basin and identified the source rocks and reservoir units. According to his research, the Upper Cretaceous shales in the Haymana basin act as source rock, where the Upper Cretaceous turbiditic sequence and clastic sediments of the Tertiary signify as reservoir succession in the Haymana basin.

Acer et al. (2007) examined the Upper Cretaceous shales for organic characteristic, thermal maturity and depositional environment of the Tuz Gölü basin of Turkey. The Haymana and Tuz Gölü basins are interpreted as a single basin because both have similar stratigraphy and depositional environment (Arikan, 1975; Ünalan et al., 1976; Acer et al., 2007). This study suggested that the basin has a capability of oil and gas accumulation. The seismic, gravity and aeromagnetic survey of the region has been conducted for structural studies and indicates that the basin has probability of the hydrocarbon accumulations (Aydemir and Ateş, 2006; Aydemir, 2011). Turgay and Kurtulus (2000) investigated the subsurface lithology of the Haymana-Polatlı basin for petroleum prospect by using seismic stratigraphy and correlated with the stratigraphy of Ünalan et al. (1976).

In 1961, Erol studied the Cenomanian-Turonian limestone and Turonian-Santonian limestone of the Haymana region which are underlain by the Senonian flyschoidal deposits. According to his studies, this change in the condition of environment and facies leads to the indication of Sub-Hercynian (Paleozoic mountain belt) tectonic movements.

The sedimentological and mineralogical properties of the Cretaceous succession of the Haymana region has been studied by Norman (1973), Gökçen (1977) and Gökçen and Kelling (1983). The mix siliciclastic strata of the Cretaceous-Paleogene in the Haymana region have been investigated for the provenance studies, mineralogical composition, sedimentation and facies recognition (Norman et al., 1980; Gökçen and Kelling, 1983).

Çetin et al. (1986) examined the Upper Cretaceous-Eocene succession by studying sedimentological and petrographic characteristic and concluded that the source rocks of the clastics in the Haymana region are magmatic and metamorphic rocks. He also interpreted the presence of fore-arc depositional environment in the region. Later, Demirel and Şahbaz (1994) investigated the Haymana basin and concluded that the basin represents fore-arc model and their clastics were derived from the Kirşehir Massif and/or subduction regime lithologies.

Fourquin (1975), Toker (1975), Altınlı (1977) and Saner (1980a and 1980b) worked on the general stratigraphy and tectono-stratigraphy in the northwestern Anatolia. Saner (1980a) performed the geophysical survey in the Western Pontide. During his survey, he explained the geological structures and geotectonic features of the upper Cretaceous region and correlated with the Russian, Carpathian and Caucasus region. He illustrates the tectonic movement in the northwestern region and basin formation adjacent to the western Pontide. Later, Saner (1980b) worked out on the Mudurnu-Göynük basin and established the Jurassic-Quaternary stratigraphy of the region.

Sirel (1975) worked out on the paleontology and lithostratigraphy of the Haymana region and established planktonic biozones in the Cretaceous and Paleocene period. Ünalan et al. (1976) described the detailed litho-stratigraphy and depositional environment from Cretaceous to Tertiary in the Haymana basin and prepared a geological map of the region at the scale of 1:25,000 for about 2800 km² area. Another geological map and stratigraphic succession units of the southern Haymana region has been prepared by Gökçen (1976).

Toker (1975, 1977 and 1980), examined the calcareous nannoplanktonic and planktonic foraminifera in the Cretaceous strata in the Haymana. He explained the paleobathmetry based on the presence of nannoplanktonic and planktonic foraminifers and their correlation. The detailed paleontological study, taxonomy of the benthic foraminifers and stratigraphical description of the Cretaceous units in the Haymana region were also studied by Özkan-Altiner and Özcan (1997), Özcan and Özkan-Altiner (1997, 1999 and 2001), Özcan et al. (2001) and Özcan (2002).

The tectonic evolution of Tethys and tectono-stratigraphic frame work of Turkey has been studied by Şengör and Yılmaz (1981), Görür (1981), Koçyiğit (1991), Koçyiğit et al. (1991); Rojay and Süzen (1997); Görür et al. (1984 and 1998); Çemen et al. (1999); Okay and Tüysüz (1999); Kaymakçı (2000); Okay et al. (2001); Rojay et al. (2001 and 2004) and Koçyiğit and Altiner (2002).

Şengör and Yılmaz (1981) described the Tethyan evolution of Turkey by plate tectonic

models. The formation of Haymana-Polatlı basin is related with the continental collision which causes the closing of the Neo-Tethyan ocean during the late Cretaceous-Tertiary period (Şengör and Yılmaz, 1981; Görür, 1981; Görür et al., 1984, 1998; Koçyiğit, 1991; Rojay and Süzen, 1997). The Haymana-Polatlı basin was interpreted as fore-arc accretionary complex basin. The occurrence of Tertiary calc-alkaline volcanism on the former Sakarya Continent and ophiolitic basement indicates the subduction of the Neo-Tethyan oceanic crust under the Sakarya continental crust and formation of fore-arc accretionary complex. The tectonic deformations in the Haymana-Polatlı basin continuing after collision until Paleocene were also recorded. According to Okay and Tüysüz (1999) and Okay (2001), the Haymana-Polatlı basin indicates foreland feature as well as fore-arc setting characteristics.

Yılmaz (1981) carried out the detailed tectonic studies on the southern margin of the Sakarya Continent. During his studies, he observed that the southern margin of the Sakarya Continent indicates different features from the north side of the Sakarya River in terms of time, environment and deposition. Tectonically, he divided the southern margin of the Sakarya Continent into three units; 1) Granitic rocks, 2) ophiolitic complex and equivalent metamorphosed rocks, 3) dynamic metamorphosed rocks.

The other region of study is in the northwestern region of the Central Anatolia, known as Mudurnu Trough (Altiner et al., 1989). This margin of the former Sakarya Continent Altiner et al., 1989) has been first studied by Arabu (1934/1935), Erk (1942) and Aygen (1956) in terms of lithostratigraphy.

The tectono-stratigraphy and regional geology of the northwestern Anatolia has been investigated by Koçyiğit et al. (1988 and 1991). They represented the structural development model of the northern margin of the Sakarya Continent and concluded it as divergent margin during late Triassic-Aptian. They also figured out the volcanic activity before Callovian and after Pliensbachian. Sedimentologically and tectonically, they divided the area into four tectonic features as 1) Biga-Bursa-Bilecik carbonate platform, 2) Mudurnu Trough, 3) Aktaş-Sakinindoruk High and 4) Doğu Trough.

Altiner (1991), Altiner et al. (1991), Altiner and Özkan (1991), Özkan (1993a and 1993b), Özkan-Altiner (1996, 1999) and Rojay and Altiner (1998) worked on the biostratigraphy and biozones in the northwestern Anatolia of Turkey. The Rosso-Ammonitico facies have been observed in the Jurassic-lower Cretaceous successions of the northwestern Anatolia and the Hettangian-Aptian tectonic evolution of the region has been established (Altiner et al., 1991). The Callovian-Aptian chronostratigraphic subdivision has been carried out established by using the biostratigraphy of benthic foraminifers and calpionellids in the southern part of the northwestern Anatolia and established Jurassic-lower Cretaceous biostratigraphy (Altiner et al., 1991).

Çiner (1992) and Çiner et al. (1993a, 1993b, 1996a and 1996b) carried out sequence stratigraphy and sedimentological research on three formations of the Eocene epoch; including carbonate platform of the Çayraz Formation, braided to deltaic Beldede Formation and turbiditic Yamak Formation. The Haymana-Polatlı basin has also been investigated for the sequence stratigraphy and cyclostratigraphy studies (Huseynov, 2007; Aghayev, 2008). These studies performed on the Upper Cretaceous clastics and Eocene carbonates sequences in order to document the sequence and parasequences. The Upper Cretaceous clastic deposit of the Haymana basin has been studied by Hüseynov (2007) to understand the sequence stratigraphic characteristic and deposition of the Haymana basin.

Later, Okay and Tüysüz (1999) described the Tethyan sutures of Turkey and studied the stratigraphy of the western central regime of the Sakarya Continent. He observed continental to shallow marine clastic sediments with interbedded Rosso-Ammonitico facies horizons (Altiner et al., 1991) of the lower Jurassic to lower Cretaceous, pelagic carbonates of the Upper Jurassic-Lower Cretaceous and volcanogenic-turbiditic sedimentary succession of the Upper Cretaceous-Paleocene.

In late 1990's and 2000's, Altiner et al. (1998 and 1999), Yılmaz and Altiner (2001), Yılmaz (2002), Yılmaz and Altiner (2005a, 2005b, 2006a; 2006b), Ocakoğlu et al., 2007, Yılmaz (2008), Yılmaz et al. (2010, 2012 and 2012) and Hu et al. (2012) have carried out detailed studies on the sequence stratigraphy, cyclostratigraphy,

sedimentological, geochemical and sedimentary geochemistry analysis of Cretaceous pelagic successions and determined the records of the Cretaceous oceanic oxic and oceanic anoxic events in the basin and also established the correlation with global oceanographic event charts. Açıkalın (2011) has carried out research on the provenance and climatic studies of Campanian-Maastrichtian boundary. In which she interpreted mafic to felsic origin of sediments and indicated rising in sea level in Campanian and falling in the sea level at Campanian-Maastrichtian boundary.

The oil shales have been examined from the northwestern Anatolian region and are related to Tertiary epoch (Görür and Tüysüz, 2001; Gülbay and Korkmaz, 2008; Sarı and Geze, 2008; Aliyev et al., 2009; Çimen et al., 2013). Recently, Yılmaz (2008), Yılmaz et al. (2010, 2012 and 2012) has worked on the records of oceanic anoxic events of the lower Cretaceous of the northwestern Anatolia and determined their organic characteristic, depositional environment, TOC values and stable isotope analysis.

1.4.1 CRETACEOUS OCEANIC RED BEDS

Cretaceous Oceanic Red Beds (CORBs) have been known for last 150 years. The Šturm (1860) and Gümbel (1861) were the first pioneer to discover the oceanic red beds from Púchov beds in the Carpathians and Nierental Beds in the Eastern Alps. In the recent years, global distribution of CORBs was studied by UNESCO: IGCP projects 463 and 494. Chen et al. (2005), Hu et al., (2005), Wei and Wang (2005) and Wang et al., (2009) have studied the distribution, lithostratigraphy, palaeoenvironmental condition and age of the Tethyan CORBs. They interpreted that the CORBS are red to brown to pinkish colour shale, marlstone, mudstone, limestone and/or chert and deposited under oxic condition in the deep marine environment during Late Cretaceous.

The CROB are recorded from different parts of the world including Europe, Tethyan realm, the Caribbean, New Zealand, the Atlantic ocean, the Pacific ocean and the Indian ocean and ranging from early to late Cretaceous (Hu et al., 2005 and 2006a; Chen et al., 2007). Tethyan CORB are extended from the Himalayas to Caucasus, Jordan, Turkey,

the Carpathians, Alps and Apennines, Spain to central North Atlantic and the Caribbean (Hu et al., 2005). Sedimentologically, these are mainly composed of red to brown to pinkish to occasionally green-gray shale, marlstone, mudstone, pelagic carbonate, hemipelagic and/or chert with sometime intercalation of fine grained siliciclastic turbidites and deposited in variety of oceanic setting from continental slope to deep marine basin (Hu et al., 2005 and 2006a; Wagreich and Krenmayr, 2005; Wang et al., 2005; Chen et al., 2007). The occurrence of CORBs are due to changes in redox condition from anoxic to oxic environment, accompanied by low sedimentation rate, change in climate, tectonic and circulation at the ocean bottom (Hu et al., 2009).

1.5 REGIONAL SETTING

The Upper Santonian-Campanian sections have been studied in two different regimes in the former Sakarya Continent of Central Pontide which is bordered by three major Tethyan sutures as Intra-Pontide suture in the north, Izmir-Ankara Erzincan suture in the south and Kırşehir block in the southeast (Okay and Tüysüz, 1999; Şengör and Yılmaz, 1981; Figure 1.4). These sutures indicate the closing of the Tethyan Ocean during early Tertiary, when Tethyan oceanic crust is subducted beneath the Eurasian plate (Okay and Tüysüz, 1999; Yalınız et al., 2000).

Turkey represents a complex juxtaposed regional geological setting that is the combination of continental and oceanic crust and show lateral tectonic continuity setting with Alpine-Himalayan orogeny (Ketin, 1966; Şengör and Yılmaz, 1981; Görür and Tüysüz, 2001; Moix et al., 2008; Lefebvre, 2013; Figure 1.4). The East-West trending Pontide or the three zones are the blocks of the Laurasian Supercontinent which are consisting of metamorphosed basement of the Paleozoic rock overlain by Mesozoic-Cenozoic sedimentary successions (Şengör and Yılmaz, 1981). The Kırşehir block, Menderes-Taurus Platform and Arabian Platform are the remnant of the Gondwana Supercontinent (Görür and Tüysüz, 2001).

In the regional tectonic frame of Turkey, the Alagöz and Göynük sections represent two different setting on the Sakarya continental margins. The Alagöz section is developed on the Haymana-Polatlı accretionary complex fore-arc basin of the Neo-Tethyan Ocean in the south of the Sakarya Continent (Koçyiğit et al., 1988; Koçyiğit, 1991; Figure 1.5). The Göynük section lies on the divergent margin setting along the northern margin of the Sakarya Continent that was formed during late-Triassic-Aptian period and is known as Mudurnu Trough (Şengör and Yılmaz, 1981; Şengör et al., 1984; Koçyiğit, 1987 and 1989; Koçyiğit et al., 1988 and 1991; Figure 1.6).

1.5.1 HAYMANA-POLATLI BASIN

The geological position of the Haymana-Polatlı basin is in the Central Anatolia, about 70 km southwest of Ankara. It is the fore-arc basin that was developed over the accretionary prism of the subducted Neo-Tethys crust during the late Cretaceous-Eocene time. The collision resulted in the formation of the Izmir-Ankara suture along the convergent boundary (Figure 1.5). This convergence occurred between the Sakarya Continent in the north and the Gondwana in the south (Fourquin, 1975; Şengör and Yılmaz, 1981; Görür et al., 1984; Koçyiğit et al., 1988; Koçyiğit, 1991). The northward subduction of the Neo-Tethys under the Sakarya Continent has been indicated by appearance of calc-alkaline Galatean volcanic arc in the Sakarya Continent during the Tertiary period (Fourquin, 1975; Şengör and Yılmaz, 1981). The Haymana basin lies over the ophiolitic mélange and Central Anatolian Crystalline Complex (Görür et al., 1984, Koçyiğit et al., 1988; Koçyiğit, 1991). It indicates that the Haymana-Polatlı basin is an accretionary type fore-arc basin (Dickinson and Seely, 1979; Koçyiğit et al., 1988; Koçyiğit, 1991).

According to Koçyiğit (1991), the tectonic collision continued in the Haymana-Polatlı Basin until late Pliocene period, even after the closure of the northern Neo-Tethys and caused strong deformation in the deposited sedimentary succession.

This sedimentary basin contains approx. 5 km thick sedimentary succession of the Upper Cretaceous-Middle Eocene that are comprised of clastic turbidites in the middle

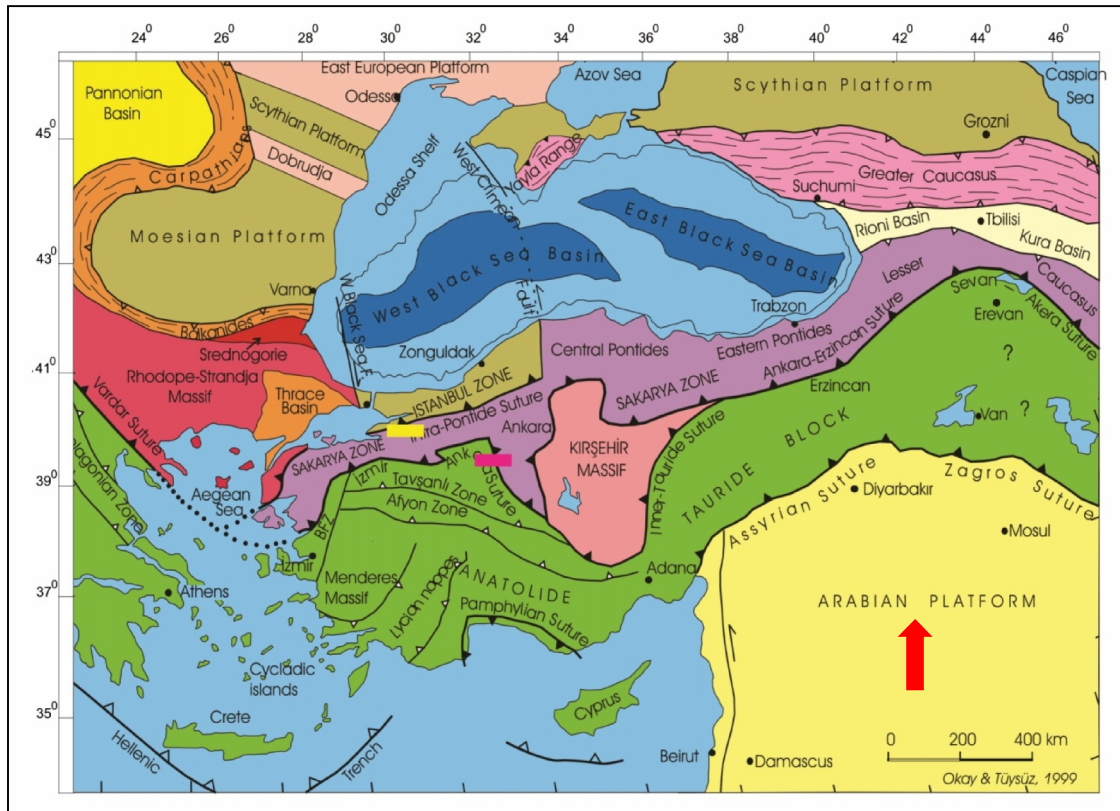


Figure 1.4: Showing regional tectonic of the Turkey and adjacent areas (modified from Okay and Tüysüz, 1999). (Note: rectangles represent studied sections; yellow-Göynük and pink-Alagöz sections and red arrow represents North direction map).

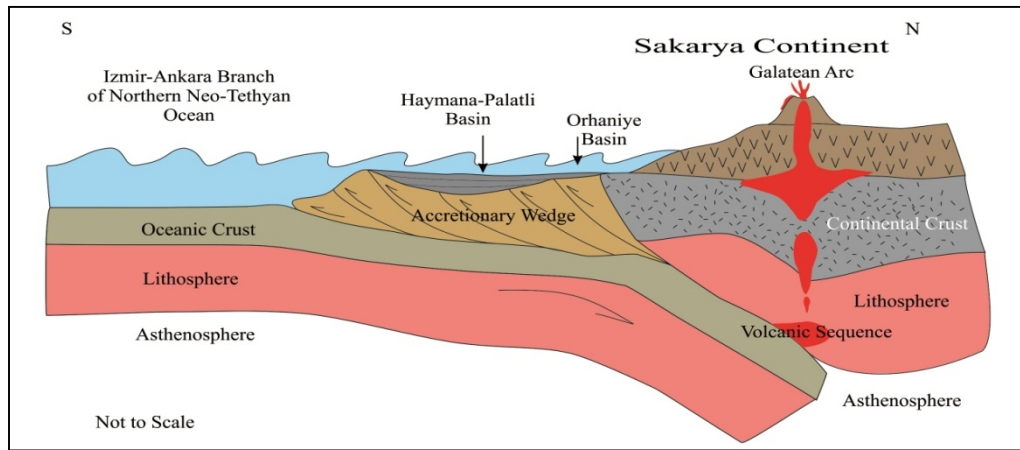


Figure 1.5: The regional tectonic and geological setting of the Haymana basin and subduction of the Neo-Tethyan Oceanic crust during the late Cretaceous to Middle Eocene (Koçyiğit et al., 1988 and 1991).

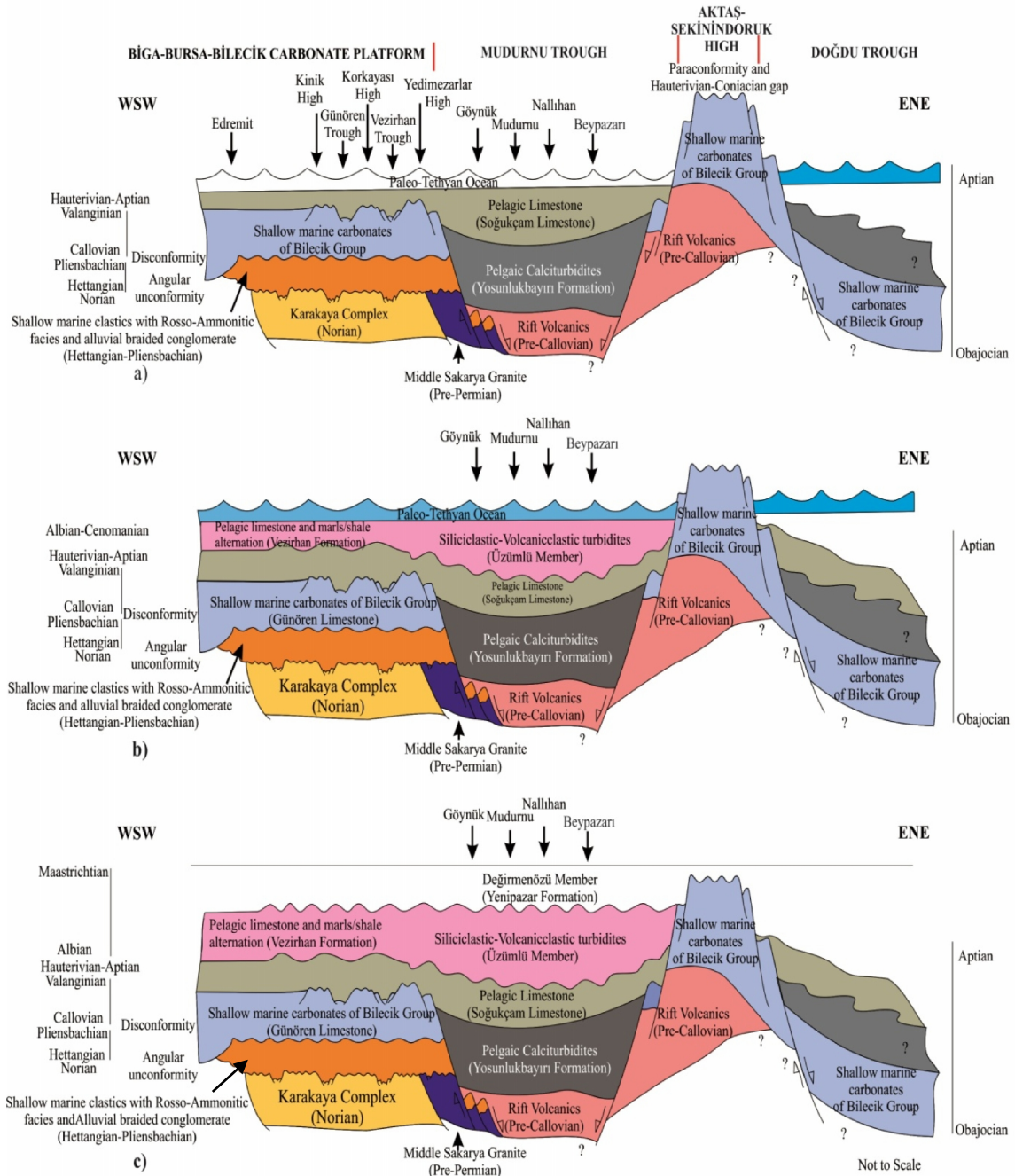


Figure 1.6: Representing schematic model for the tectonic divergent setting and depositional stratigraphy of the northern Sakarya Continental margin (Koçyiğit et al., 1991). a) Upto Aptian, b) Upto Cenomanian, and c) Upto Maastrichtian.

of the basin and the pelagic carbonates passes to continental red beds toward the uplifted basin margin (Yüksel, 1970; Görür, 1981; Çiner, 1992; Figure 2.3). The Eocene successions are thrusted by Cretaceous Ophiolitic mélange nappes (Ünalan et al., 1976; Görür, 1981; Görür et al., 1984).

1.5.2 MUDURNU-GÖYNÜK BASIN

The Sakarya Continent has been characterized by Paleozoic metamorphic basement and overlying Mesozoic and Cenozoic sedimentary succession. Geologically, the Mudurnu-Göynük basin is located in the south of the Intra-Pontide suture and in north of the Sakarya Continent. Tectonically, it is interpreted as developed on the rifting margin of the northern Sakarya Continent during the Lower Triassic-Aptian interval. The sedimentary filling in the Mudurnu-Göynük basin comprises of Mesozoic-Cenozoic succession (Figure 2.4). This rifting basin in the northern Sakarya Continental margin is also known as Mudurnu Trough (Koçyiğit, 1987; 1989; Figure 1.6).

The Upper Jurassic to Cretaceous sequences are identified by alternating shelf carbonates and pelagic, cherts, volcanics and volcano-clastics, and followed by slope to basinal upper Cretaceous deposits (Altiner, 1991; Altiner et al., 1991).

The rifting begins in the Toarcian-Bathonian and appearance of rift basin, known as the Mudurnu Basin (Koçyiğit et al., 1991). During the early Callovian-Tithonian, carbonates are deposited in the Mudurnu basin which is intruded by rift volcanics (Koçyiğit et al., 1991). The uplifting of the Aktas-Sekinidoruk area happened during the Jurassic-Early Cretaceous period and represents horst structure. This paleohigh caused division in the Mudurnu rift basin and resulted in the formation of two new sub-basins named as Mudurnu Trough and Doğu Trough. These troughs are characterized by thick pelagic deposits and turbidites (Koçyiğit et al., 1991; Figure 1.6). Later in the Valanginian-Early Hauterivian, the Mudurnu and Doğu troughs were exposed as a result of extension (Koçyiğit et al., 1991). Towards the Sakarya Continent, divergent margin was characterized by broad Biga-Bilecik carbonate platform (Koçyiğit et al., 1991).

The two stratigraphic sections of the Upper Santonian-Campanian age are measured from the Haymana-Polatlı Basin near the Alagöz village (Alagöz Section) and other one is from the Mudurnu Trough in the Göynük town (Göynük Section).

CHAPTER 2

STRATIGRAPHY

2.1 GENERAL STRATIGRAPHY OF THE CENTRAL ANATOLIA

The general stratigraphy of the Central Anatolia is ranging from Paleozoic to Quaternary deposits. In the Alagöz and Göynük studied areas, the oldest rock is represented by the upper Triassic Karakaya Complex (Ünalan et al., 1976; Koçyiğit et al., 1988, 1991; Koçyiğit, 1991), where as the youngest rock in both regions is represented by Pliocene which is covered by Quaternary alluvial and talus breccias deposits.

In the Sakarya Continent of the Central Anatolian Block, the basement is composed of several volcanic-volcanosedimentary and low to high grade metamorphosed rocks of the subducted-accretion complexes (Tekeli, 1981; Şengör et al., 1984; Tüysüz and Yiğitbaş, 1994). The crystalline basement of the Sakarya Continent is divided into three units i.e Variscan metamorphic, Paleozoic Granitioids and Karakaya complex (Okay, 2008). The Variscan metamorphic units are characterized as high grade metamorphic rocks and are determined as Carboniferous (Okay et al., 2006; Okay, 2008). In the Pulur region in the east of the Sakarya Continent, it is overlain by Upper Carboniferous molasses (Göncüoğlu, 2010). The small outcrops of the Paleozoic Granitioids are exposed randomly in different areas of the Sakarya Continent. These are unconformably lying on the Jurassic-Eocene sequences (Delaloye and Bingöl, 2000; Okay et al., 2002, 2006; Topuz et al., 2007).

The Karakaya Complex, the lower portion comprised of alternation of metabasite, marble and phyllite and the lower-mid Triassic age assigned to unit. The upper portion is known as the Nilüfer meta-volcanics sequence. This unit composed of high pressure-low temperature metamorphosed mafic to ultramafic rocks (Okay, 1986; Okay et al., 1991). These are considered as greenschist facies metamorphism. However, in some places it

shows even high pressure mineral assemblages such as blueschist and eclogite metamorphic facies (Okay and Monié, 1997). The metamorphism in the Nilüfer units occurred in the upper Triassic (Okay et al., 2002). The flysch-type deposits are overlying the Karakaya Complex. These are composed of olistostromes and are characterized by Carboniferous-Permian age neritic limestone blocks and radiolarian chert along with clastic and volcanic rocks. The upper Triassic age has been assigned to this unit.

The overlain successions on the Karakaya Complex are varying in different regions. In the western zone of the Sakarya Continent, the Karakaya Complex is unconformable overlain by lower Jurassic fluvial to shallow marine sandstone, shale and conglomerate with Ammonitic rosso horizons (Altiner et al., 1991). In the eastern part, upper contact is characterized as unconformably overlain by volcanoclastic with the intercalation of sandstone (Koçyiğit, 1991; Koçyiğit et al., 1991; Okay and Tüysüz, 1999; Okay, 2008; Göncüoğlu, 2010). In the Mudurnu-Göynük, the middle Jurassic succession is lying above the Karakaya Complex. In the Ankara region, the middle Jurassic-lower Cretaceous ophiolitic mélange of the Ankara group shows angular unconformity relation with the Karakaya Complex (Ünalan et al., 1976; Koçyiğit, 1991).

In the Haymana region, the general stratigraphy has been introduced by Yüksel (1970), Ünalan et al. (1976), Görür (1981) and Çiner (1992) (Figure 2.1). In the Mudurnu-Göynük region, stratigraphic framework of the area has been represented by Fourquin (1975), Toker (1975), Altınlı (1977), Saner (1980a), Altiner et al. (1991), Koçyiğit et al. (1991), Okay and Tüysüz (1999), Yılmaz (2002) and Okay (2008) (Figure 2.2).

2.2 STRATIGRAPHY OF HAYMANA-POLATLI BASIN

The Haymana-Polatlı Basin comprised of about 5 km thick marine and terrestrial deposits of Upper Cretaceous to Eocene (Koçyiğit, 1991; Figure 2.3).

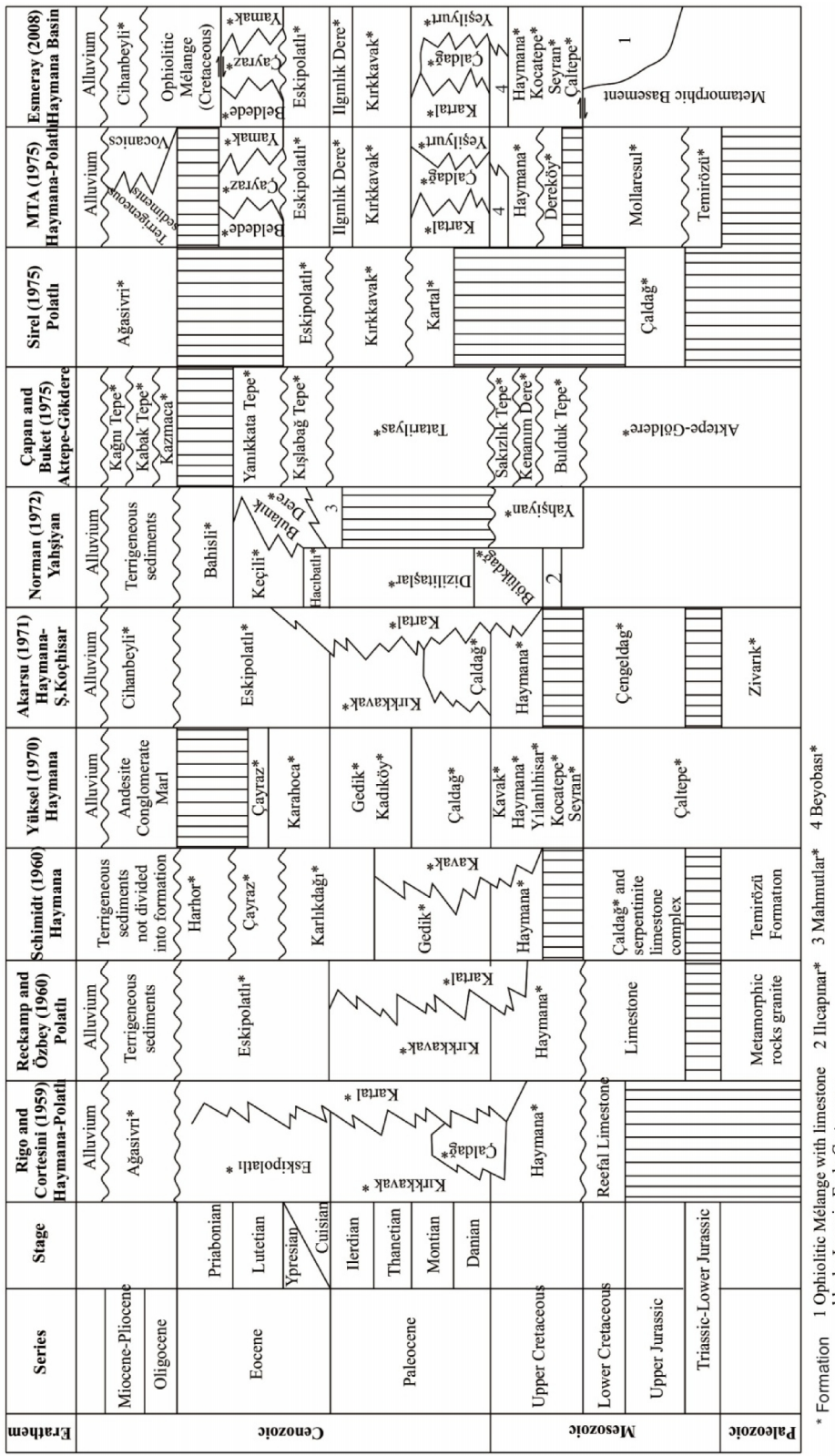


Figure 2.1: The generalized stratigraphy and correlation in the Haymana-Polatlı and adjacent areas (Modified from Ünalan et al., 1976) (Not to scale).

Epoch	Lower Cretaceous		Upper Cretaceous		Yosunluköy'in Formation	Soğukgöz Formación	Soğukgöz Formación	Yenipazar Formación	Yenipazar Formación	Kuru (1996)	Yilmaz (2002)
	Fourquin (1975)	Toker (1975)	Altınlı (1977)	Saner (1980b)							
Maastrichtian				Taraklı Formation							
Campanian				Seben Formation							
Santonian		?									
Turonian		?									
Cenomanian				Calcaires pélagiques marneux rouges	Bozkaya Formation	Nardin Formation					
Albian											
Aptian											
Barremian											
Hauterivian											
Valanginian											
Berriasian											

Not to scale

Figure 2.2: The generalized Cretaceous stratigraphy and correlation in the Mudurnu-Göynük Basin (Modified from Yilmaz, 2002) (Not to scale).

2.2.1 JURASSIC-LOWER CRETACEOUS SUCCESSION

The oldest rock of the region is the Upper Triassic Karakaya Complex of the Sakarya Continent, underlying the middle Jurassic-lower Cretaceous Ankara Mélange (Norman, 1975; Ünalan et al., 1976; Norman et al., 1980; Şengör and Yılmaz, 1981; Görür et al., 1984; Koçyiğit, 1991; Rojay, 2013).

In the northern Turkey, the Ankara Group is exposed in discontinuous packages in the region (Koçyiğit, 1987). The Ankara Group comprised of conglomerate, shallow marine clastics with intercalation of Rosso Ammonitico horizons, carbonates and sedimentary mélange. The sedimentary mélange is considered as the Damlaağaçdere Formation. The Late Hettangian to Early Campanian age has been given to the Ankara Group. It shows angular unconformity with the Karakaya Complex. The upper contact of the Ankara Group with Anatolian Complex ophiolitic mélange interpreted faulted tectonic contact (Koçyiğit et al., 1988; Koçyiğit, 1991).

2.2.2 UPPER CRETACEOUS SUCCESSION

In the Haymana Basin, the Upper Cretaceous rocks have been documented and are formalized as Çaltepe, Seyran, Kocatepe, Haymana and Beyobası formations. The Çaltepe Formation is composed of thick bedded limestone. It has been noticed that limestone blocks is embedded in the ophiolitic mélange matrix (Ünalan et al., 1976). It shows conformable contact with the underlying ophiolitic mélange and unconformable with the above Turonian-Coniacian Seyran Formation, which consists of limestone, shale, siltstone and breccias (Yüksel, 1970). The unconformable overlying Kocatepe Formation of Santonian age is mainly composed of reddish to pinkish, thin to medium bedded limestone with occasional interbedded shales (Yüksel, 1970). In the Early Campanian to Maastrichtian Haymana Formation represents mudstone, shale, turbiditic sandstone with alternating olistostromes, conglomerate and debris flow deposits (Ünalan et al., 1976). The upper contact of the formation is transitional with the Late Maastrichtian Beyobası Formation and Paleocene Yeşilyurt Formation (Ünalan et al., 1976). The Beyobası Formation is predominantly composed of sandstone,

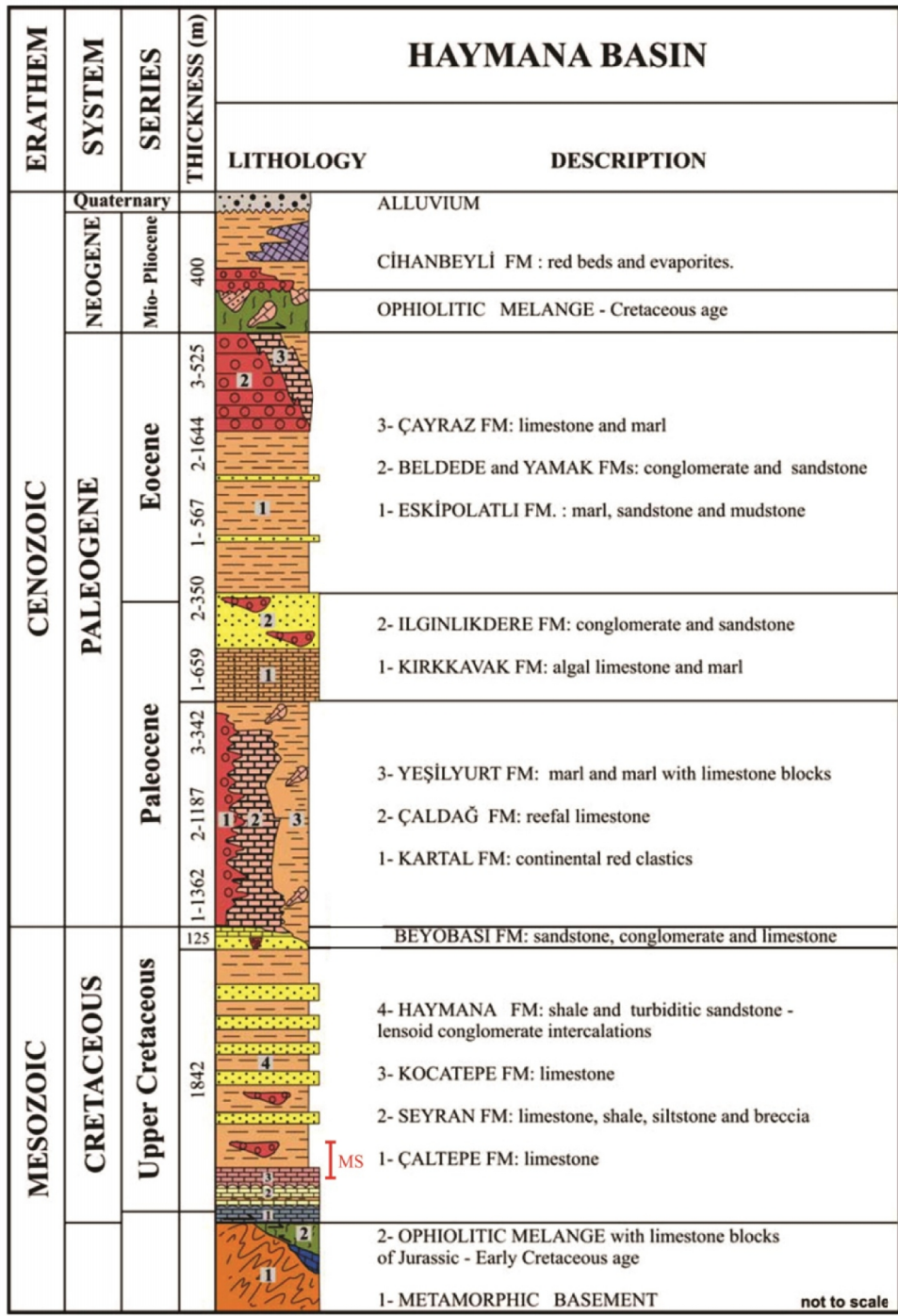


Figure 2.3: Composite Stratigraphic section of the Haymana basin and MS (red line) represent measured stratigraphic section near the Alagöz Village (Modified from Ünalan et al., 1976).

conglomerates, conglomeratic limestone and sandy marls (Ünalan et al., 1976; Esmeray, 2008).

2.2.3 PALEOGENE SUCCESSION

In the Paleogene period, during Early Paleocene epoch, the transitional environment observed in the Haymana-Polatlı basin as shifting from deep sea turbidites to the red beds (Okay et al., 2001). In Lower Paleocene, facies varies from continental clastics in the northwest to shallow marine limestone and pelagic shales in the southeast. In the Upper Paleocene, deposition of shallow marine limestone and marls are deposited and characterized by transgressive phase in the sea-level. In Eocene time, there is an onset of regressive phase in the sea-level and deposition of turbiditic sequence (Ünalan et al., 1976). The Paleocene formation such as Kartal Formation, Çaldağ Formation and Yeşilyurt Formation are characterized by basin margin to the central part of the basins. The Kartal Formation is characterized by the continental red beds and the Çaldağ Formation having reefal limestone. Both are interpreted as shallow marine environment. The Yeşilyurt Formation indicates deep marine and comprises of shale, marl and intercalation of limestone (Görür and Derman, 1978). The Upper Paleocene is characterized by algal limestone-marls of the Kırkkavak Formation and conglomerate-sandstone of the İlginlikdere Formation and is overlain by Eocene turbiditic sequence (Ünalan et al., 1976).

In the Early to Middle Eocene, the occurrence of short period turbiditic and deltaic sequences suggests the onset of the regression in the Haymana-Polatlı basin. These are represented by the Eskipolatlı Formation, Beldede Formation (deltaic) and Yamak Formation and followed by Upper Eocene shallow marine nummulitic limestone of the Çayraz Formation (Çiner et al., 1996a; 1996b).

2.2.4 NEOGENE

The Neogene deposits are represented by the Cihanbeyli Formation. It consists of red

terrestrial conglomerates, marl, sandstone, evaporates and tuffs. It aged Miocene-Pliocene. It is overlying unconformable Cretaceous ophiolitic mélange nappe and Lutetian deposits (Ünalan et al., 1976; Görür, 1981; Görür et al., 1984).

2.3 STRATIGRAPHY OF MUDURNU-GÖYNÜK BASIN

The Mudurnu-Göynük Basin characterizes the Upper Triassic-Eocene stratigraphic successions. The Late Triassic Karakaya Complex has been documented as the oldest rock in the region, which are overlain by Jurassic-lower Cretaceous units (Koçyiğit et al., 1991; Altiner et al., 1991) (Figure 2.4).

2.3.1 JURASSIC TO CRETACEOUS SUCCESSION

The Jurassic to Lower Cretaceous strata have been formalized as Kabalar Group by Altiner et al. (1991). This group includes Mudurnu Formation, Kurcalikdere Formation, Yosunlukbayırı Formation and Soğukçam limestone. According to Saner (1980b), the Mudurnu Formation in the Middle Jurassic consists of volcanogenic sediments. Altiner et al. (1991) interpreted that the Mudurnu Formation comprises of marine deposits and equivalent to Dogger. The Bojocian-Callovian age has been assigned to the formation (Saner, 1980b; Altiner et al., 1991). The Mudurnu Formation displays transition zone is known as Kurcalikdere Formation and represents Callovian-Kimmeridgian age. The Kurcalikdere Formation composed of olistostromes of reefal fragments, tuffaceous, siliceous and basaltic level and pelagic mudstones. The upper contact of the Yosunlukbayırı Formation is conformable with the Soğukçam Limestone and composed of argillaceous limestone and packstone with intercalation of mudstone. The formation is dated as Tithonian-Late Valanginian age (Altiner et al., 1991).

In the Barremian-Aptian of Lower Cretaceous, transgressive condition has been observed in the Mudurnu Trough which is indicated by the Soğukçam Limestone as it is composed of slope/basin pelagic carbonate and intercalation of black shale/mudstone (Altiner, 1991; Altiner et al., 1991; Yılmaz, 2008; Yılmaz et al., 2012). The Soğukçam

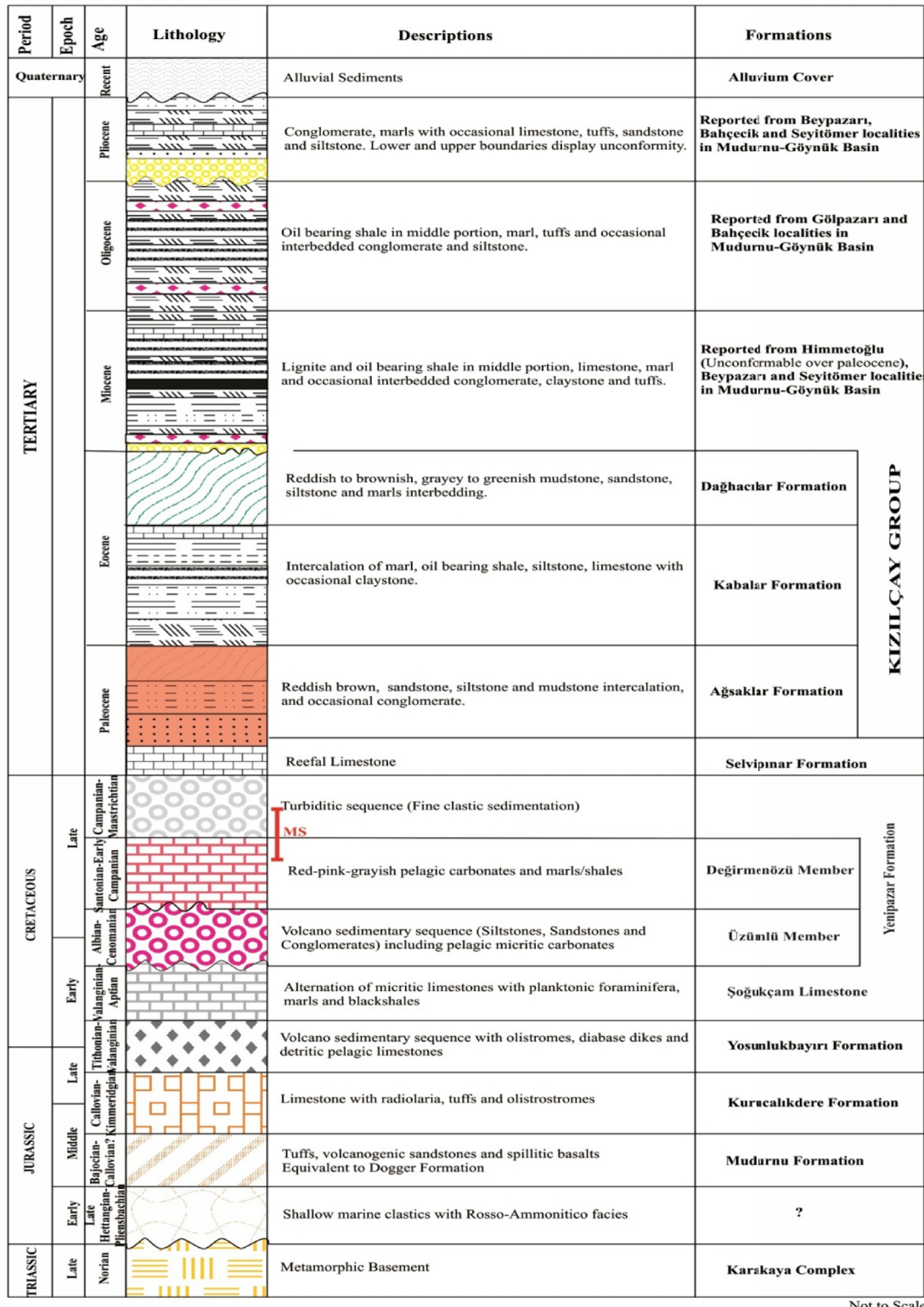


Figure 2.4: Composite Stratigraphic section of the Mudurnu-Göynük Basin and MS (red line) represents measured stratigraphic section in the Göynük Village (Modified from Altner et al., 1991; Şener and Şengüler 1998).

Limestone is unconformably overlain by the Albian-Cenomanian Üzümlü member of the lower part of Yenipazar Formation. It consists of volcano-turbidite/turbidites, pelagic carbonates and intercalation of grey-black shales. It is followed by unconformity with the Santonian-Campanian red-pink pelagic carbonate and marls of the Değirmenözü member of the upper part of Yenipazar Formation (Timur and Aksay, 2002; Yılmaz, 2008). In the Mudurnu-Göynük basin, the Soğukçam Limestone and Yenipazar Formation have disconformity boundary with Neptunian Dykes (Yılmaz, 2008).

2.3.2 TERTIARY SUCCESSION

The Tertiary deposits are reported from Bolu-Bahçecik basin in Turkey. In the Beypazarı, the Paleocene-Eocene is comprised of red color clastic deposits with the Hatıldağ oil shale. It represents unconformable lower contact with the Paleozoic metamorphic basement. In Hımmetoğlu Halitdağ and Gölpaşarı areas, it overlies unconformably the Jurassic-Lower Cretaceous succession (Gülbay and Korkmaz, 2008). The Miocene successions consist of oil shales with intercalation of lignite, claystone and limestones. The lower and upper boundaries represent unconformable relation with the Paleogene and Pliocene strata. The Oligocene units are documented from the Gölpaşarı and Bahçecik villages. These are composed of marls, tuffs and oil shales. In the Bahçecik areas, it shows unconformable boundary with the Pliocene Conglomerate (Figure 2.4).

In the Dağhacılar Village in the Mudurnu-Göynük Basin, the Paleocene-Eocene successions are characterized by the Selvipınar Formation and Kızılıçay Group. The Lower Paleocene Selvipınar Formation represents reefal limestone. It displays transitional lower contact with the Upper Cretaceous Taraklı Formation, consisting of marl, shale and sandstone. It has conformable upper contact with the Kızılıçay Group. The Kızılıçay Group includes middle Paleocene Ağsaklar Formation, Upper Paleocene Kabalar Formation and Eocene Dağhacılar Formation. The Ağsaklar Formation displays reddish brown-gray conglomerate, siltstone, sandstone and mudstone lithological alternation. It is conformably overlain by the Kabalar Formation. The Kabalar

Formation comprised of marls, mudstone, shale, siltstone, limestone bedding and occasional claystone. The middle portion characterizes oil-shale. The formation interprets shallow marine environment. The Eocene Dağhacilar Formation indicates reddish to brownish, gray to greenish mudstone, sandstone, siltstone and marl. The Eocene formation has conformable lower contact and unconformable contact with Quaternary deposits (Altiner et al., 1991; Şener and Şengüler, 1998; Çimen et al., 2013; Figure 2.4).

2.4 QUATERNARY COVER

In the Haymana-Polatlı Basin, the Mudurnu-Göynük Basin and the surrounding areas, Quaternary deposits are resting unconformably over the Tertiary, Mesozoic and Paleozoic succession. In the Göynük studied area, the upper Cretaceous and Tertiary stratigraphic successions are unconformable overlain by alluvial cone and Talus breccias of the Quaternary deposits. In the Alagöz studied area, the Quaternary deposits are unconformably resting over the Miocene-Pliocene successions.

2.5 LITHOSTRATIGRAPHY OF THE MEASURED SECTIONS

Two stratigraphic units from Upper Santonian to Campanian age have been measured near the Alagöz village in the SW Ankara and just in SW Göynük town in the Bolu province. These vertical measured sections have been identified Kocatepe Formation (Santonian) and Haymana Formation (Campanian) in the Haymana basin and Değirmenözü Member (Santonian-Early Campanian) and Yenipazar Formation (Campanian) in the Mudurnu-Göynük Basin from previous studies. These formations are characterized by alternation of siliciclastic and calcareous pelagic deposits. It is regressively overlain by volcanogenic beds/turbiditic succession of Maastrichtian-Paleocene age (Yüksel, 1970; Ünalan et al., 1976; Altiner et al., 1991; Yılmaz, 2002; 2008).

The Kocatepe Formation was named by Yüksel (1970). In the type section, the formation is mainly composed of reddish to pinkish, thin to medium bedded limestone with occasional interbedded shales. It is unconformably overlying the Seyran Formation and conformable with the Haymana Formation. The Santonian age is inferred to Kocatepe Formation by documented globotruncanids including *Dicarinella asymmetrica*, *Dicarinella concavata*, *Marginotruncana coronata* and *Muricohedbergella flandriini* in the formation (Hüseyinov, 2007).

The type locality of the Haymana Formation is near the Haymana town. The Haymana Formation comprised of mudstone, shale, turbiditic sandstone with alternating olistostromes, conglomerate and debris flow deposits (Yüksel, 1970; Ünalan et al., 1976; Hüseyinov, 2007). The planktonic foraminifers were documented from the formation and dated as early to middle Campanian (Ünalan et al., 1976; Hüseyinov, 2007).

The Yenipazar Formation is further divided into members i.e. the Üzümlü Member and Değirmenözü Member (Altiner et al., 1991). The Yenipazar Formation is lying unconformable above the Soğukçam Limestone and also represents unconformable upper contact with Quaternary deposits in the Mudurnu-Göynük Basin. The Üzümlü Member of the Yenipazar Formation is composed of volcano-turbidite/turbidites, pelagic carbonates and intercalation of grey-black shales. It is interpreted as continental slope to toe depositional environment with interference of turbiditic current (Yılmaz, 2008). Değirmenözü Member and Yenipazar Formation mainly consist of brown-pink and grayish pelagic limestone, green to grayey mudstone, marl and fine grained turbiditic sequence, respectively. These are unconformably overlain by volcanogenic bed. The Santonian-Campanian age has been given to the Değirmenözü Member and Yenipazar Formation (Altiner et al., 1991; Yılmaz, 2002).

For the detail studies of microfacies, micropaleontology and depositional environment, a total of 77 samples have been collected from the field along the measured stratigraphic Sections, which are analyzed to determine the vertical variation in the facies. Out of 77 samples, 24 samples belong to the Alagöz Section and remaining 53 to the Göynük

Section. The field studies and microscopic analysis are used to describe the lateral and vertical changes in the facies and depositional setting.

2.5.1 ALAGÖZ MEASURED SECTION

The locality of the Alagöz stratigraphic section lies in the NE of the Alagöz village, southwest of Ankara ($39^{\circ}45'19.73''N$; $32^{\circ}29'27.80''E$). The total measured stratigraphic section was about 1900 cm thick (Figures 2.5 and 2.6) and a total of 24 samples were collected.

The Alagöz measured section is started as thin bedded red limestone from the bottom and is classified as radiolarian limestone. By using geological rock color chart, it is divided into two stratigraphic units, based on the color differences (Table 2.1). These are categorized as 1) Red beds and 2) Alternating green to gray mudstone-claystone. The red beds are 425 cm thick at the lower portion. It comprises of thin to medium bedded, red, radiolaria bearing limestone, silty marls and occasionally interbedded siltstone (Figure 2.7). It is followed by cyclic alternation of greenish to gray mudstone and claystone (Figures 2.6 and 2.8). The boundary between red beds and green-gray beds are observed as transitional and characterized as changing the marine environment from oxic to dysoxic condition.

In the field studies, the units represent very thin to thin bedding with shaly to flaggy appearances (Figures 2.6 and 2.8). The micro-bioturbation is observed in sample ZR01 to ZR04, ZR06, ZR14, ZR16 and ZR 21 (Figure 2.9 A). Other sedimentary structures are calcite veins and purple-reddish marl infilling dendritic pattern in single sample (Figure 2.9 B). Calcite veins are present in the form of conjugate sets (Figure 2.8) which suggests multi-direction post-depositional tectonic stresses.

Fossils observed during the field study and/or in the thin sections are dominantly planktonic foraminifers, benthic foraminifers, radiolaria, sponge spicules, bivalve and single echinoids.

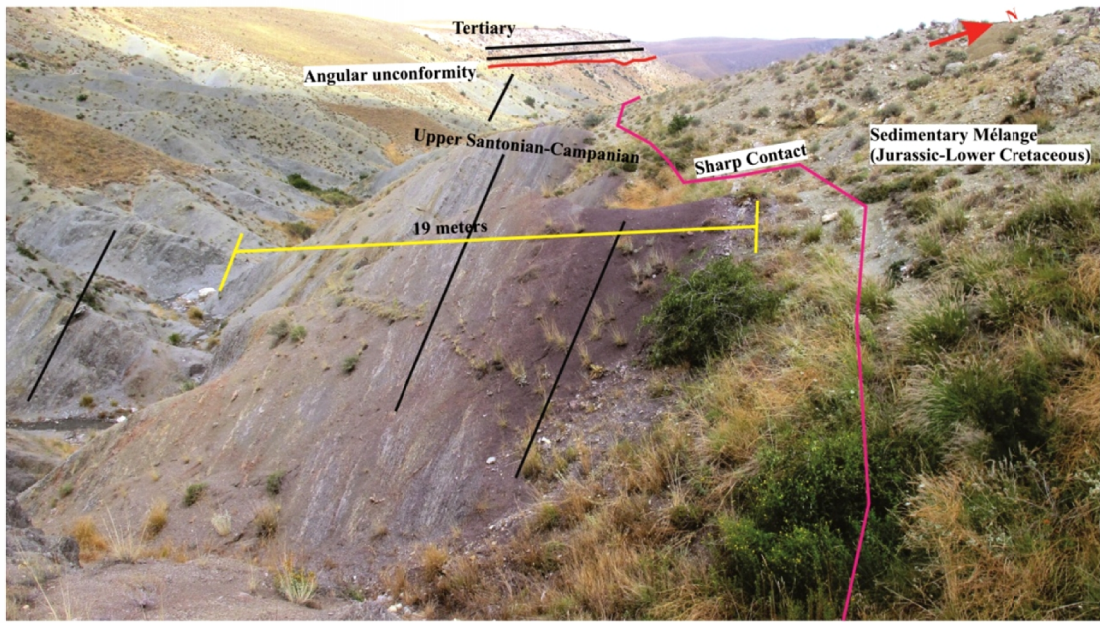


Figure 2.5: The field photograph of the studied area representing sharp lower contact (pink line) with the Upper Jurassic-Lower Cretaceous sedimentary mélange and angular unconformity upper contact with the Tertiary strata (red line) SW dip direction (yellow line-measured section; black line-bedding).



Figure 2.6: The field photograph showing the Upper Santonian-Campanian red beds in the Alagöz section.

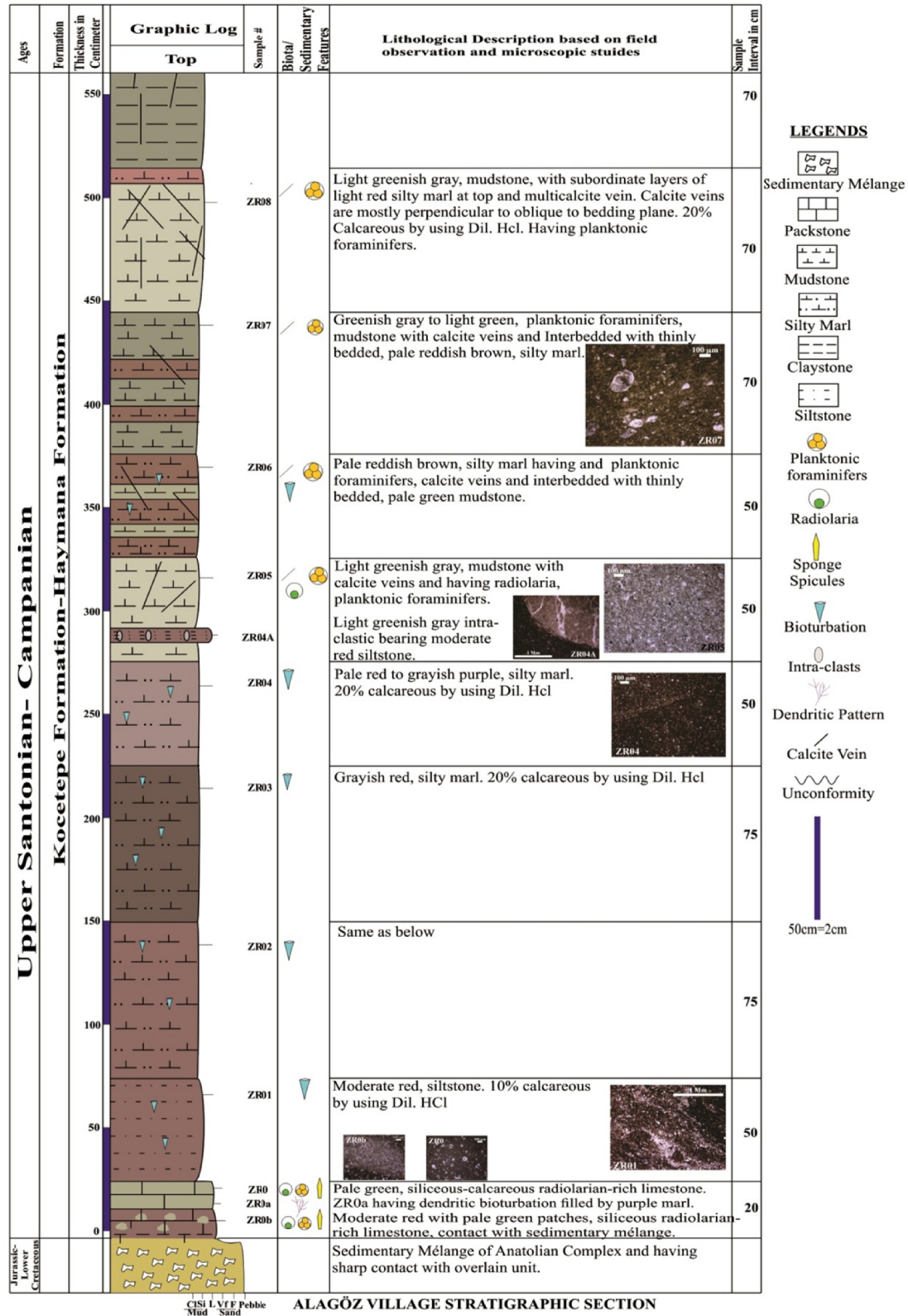
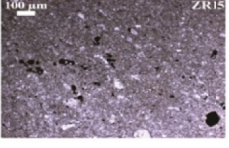
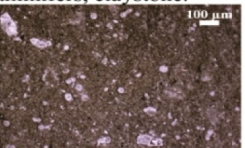
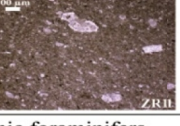
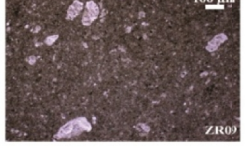


Figure 2.7: Measured stratigraphic section of the Alagöz Village in the Haymana Basin (0-565 cm).

Ages	Formation	Graphic Log		Sample #	Biofa/ Sedimentary Features	Lithological Description based on field observation and microscopic studies		Sample Interval in cm
		Thickness in Centimeter	Top					
		1100		ZR15	⊕	Medium dark gray, planktonic foraminifers, claystone.		120
		1050						
		1000		ZR14	▼	Medium dark gray, planktonic foraminifers, claystone.		70
		950						
		900		ZR13	⊕	Greenish gray, claystone with intensive calcite veins (conjugate form) and having planktonic foraminifers.		70
		850		ZR12	⊕	Light gray to pale green, claystone bearing planktonic foraminifers with intensive calcite veins (forming conjugate network).		110
		800		ZR11	⊕	Brownish on weather whereas greenish gray on fresh surface, mudstone. Bearing planktonic foraminifers.		54
		750		ZR10	⊕	Greenish gray, claystone bearing planktonic foraminifers, with intensive calcite vein. Calcite veins are mostly perpendicular to oblique to bedding plane.		70
		700		ZR09	⊕	Greenish gray, claystone, with calcite vein. Calcite veins are mostly perpendicular to oblique to bedding plane and Having planktonic foraminifers.		70
		650						
		600						
		550						

CISI L VTF Pebble
Mud Sand

Figure 2.7: Continued (565-1105 cm).

AgeS	Formation	Thickness in Centimeter	Graphic Log		Sample #	Biota/ Sedimentary Features	Lithological Description based on field observation and microscopic studies	Sample Interval in cm
			Top					
Upper Santonian- Campanian	Haymana Formation	1650						
		1600			ZR20		Medium dark gray, mudstone and having planktonic foraminifers. Occurrence one set type of calcite veins (Perpendicular to slightly oblique).	
		1550						140
		1500						
		1450			ZR19		Greenish gray, planktonic foraminifers, claystone with calcite veins (Conjugate form).	
		1400						100
		1350			ZR18		Greenish gray, planktonic foraminifers, claystone with calcite veins (Conjugate form).	
		1300						100
		1250			ZR17		Medium light gray, mudstone with calcite veins and having planktonic foraminifers. 3 cm thick calcite vein observed.	
		1200						85
		1150			ZR16		Medium gray, planktonic foraminifers, claystone with calcite veins.	
		1100						100

C/Si L V/F Pebble
Mud Sand

Figure 2.7: Continued (1070-1650 cm).

ALAGÖZ VILLAGE STRATIGRAPHIC SECTION

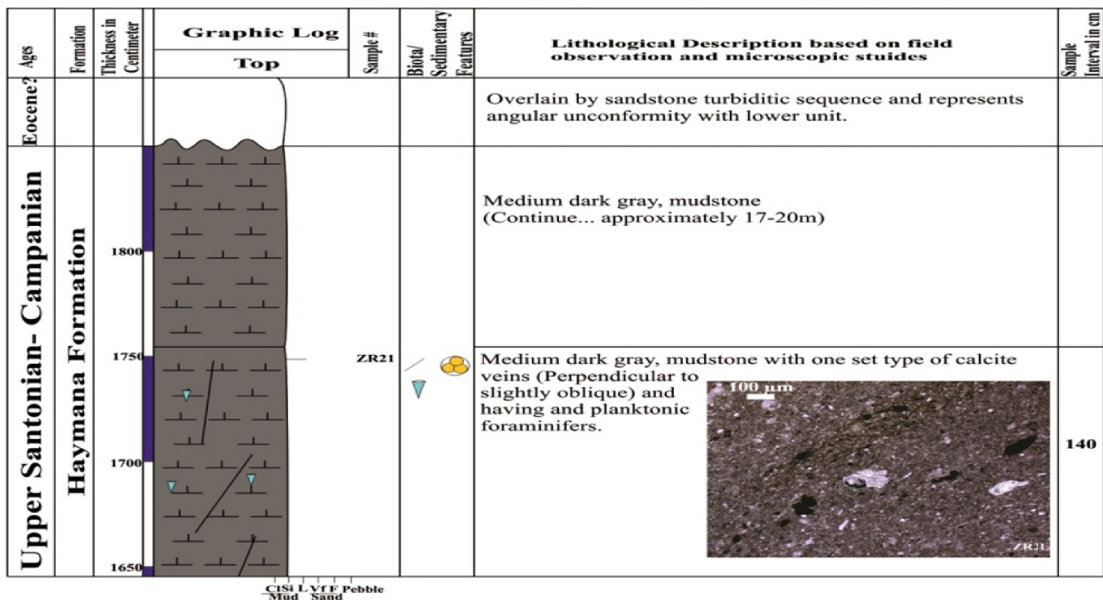


Figure 2.7: Continued (1595-1900 cm).

Table 2.1: Identification of color of the samples from the Alagöz Section.

Alagöz Section samples color name and their color codes				
No.	Sample	Rock and their outcrop color	Color Name (Munsell Color Book) (GSA, 2009)	Geological Color Chart Code (Munsell Color Book) (GSA*, 2009)
1.	ZR0b	Moderate Red Packstone/Radiolarian Rich Packstone/Siliceous Mudstone	Moderate Red	5R 4/6
2.	ZR0	Pale green Packstone/Mixed Radiolarian Rich Packstone/Mixed Sil-Cal Mudstone	Pale green to Light Greenish Gray	5G 7/2 – 5GY 8/1
3.	ZR01	Red Siltstone	Moderate Red	5R 4/6
4.	ZR02	Red Silty Marl	Moderate Red	5R 4/6
5.	ZR03	Red Silty Marl	Dusky Red	5R 3/4
6.	ZR04	Red Silty Marl	Dusky Red	5R 3/4
7.	ZR04a	Greenish Gray Intra-clastic bearing Red Siltstone	Grayish Red	5R 4/2
8.	ZR05	Greenish Gray Mudstone	Pale green to Grayish green	10G 6/2 – 10G 4/2
9.	ZR06	Reddish Silty Marl	Pale Reddish Brown	10R 5/4
10.	ZR07	Greenish Gray Mudstone	Light Olive Gray	5Y 6/1
11.	ZR08	Greenish Gray Mudstone	Light Greenish Gray to Light Gray	5GY 8/1 – N7
12.	ZR09	Greenish Gray Claystone	Medium Gray	N5
13.	ZR10	Greenish Gray Claystone	Greenish Gray	5G 6/1
14.	ZR11	Greenish Gray Mudstone	Medium Gray	N5
15.	ZR12	Light Gray to Pale Green Claystone	Medium Bluish Gray	5B 5/1
16.	ZR13	Greenish Gray Claystone	Greenish Gray	5GY 6/1
17.	ZR14	Medium Dark Gray Claystone	Medium Dark Gray	N4
18.	ZR15	Medium Dark Gray Claystone	Medium Dark Gray	N4
19.	ZR16	Medium Gray Claystone	Medium Gray	N5
20.	ZR17	Medium Light Gray Mudstone	Medium Light Gray	N6
21.	ZR18	Greenish Gray Claystone	Greenish Gray	5GY 6/1
22.	ZR19	Greenish Grey Claystone	Greenish Gray	5G 6/1
23.	ZR20	Medium Dark Gray Mudstone	Medium Dark Gray	N4
24.	ZR21	Medium Dark Gray Mudstone	Medium Dark Gray	N4

*Geological Society of America Rock-Color Chart Committee, 2009



Figure 2.8: Yellow dotted lines show calcite veins, perpendicular to bedding and conjugate symmetry in the field (red line representing bedding plane; Dipping in SW), in the Upper Santonian-Campanian Alagöz stratigraphic section.

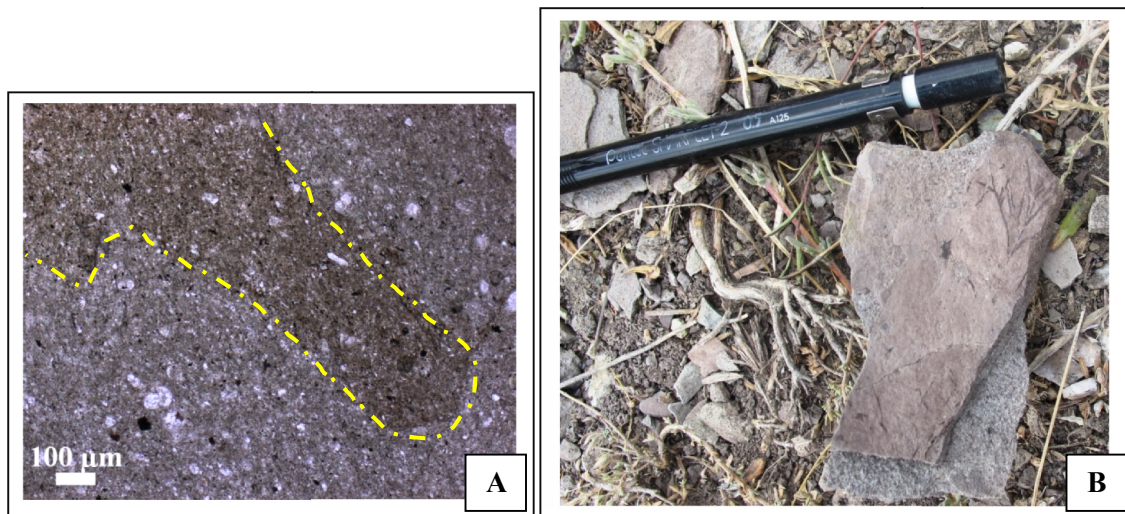


Figure 2.9: **A)** The Alagöz Section photomicrograph of sample ZR16 thin section, representing micro-borrow (PPL) (yellow line representing micro-borrow); **B)** The photograph of infilling-marl dendritic bioturbation pattern in Sample ZR0a.

In the studied area, the measured stratigraphic section has sharp lower contact with upper Jurassic-lower Cretaceous succession. The upper contact represents angular unconformity with Tertiary succession (Figure 2.5). The planktonic biota and lithological features in the studied section interpret deep marine environment. 300 to 400 cm intervals in the studied stratigraphic section indicate the changes from oxic to dysoxic/anoxic depositional condition (Figure 2.7).

2.5.2 GÖYNÜK MEASURED SECTION

The other measured section, stratigraphically equivalent to the Alagöz Section, is exposed near the Göynük town, Bolu Province ($40^{\circ}23'44.50''N$; $30^{\circ}46'51.55''E$). A total of 2875 cm thick stratigraphic section was measured for the detail study. 53 numbers of samples were collected along the stratigraphic section and vertical changes in the beds were recorded (Figures 2.10, 2.11).

During the field work, two broad color contrasts. Later, these were marked as red beds and green-gray beds (Table 2.2 and Figures 2.12, 2.13). The measured section begins with greenish claystone interbedded with the red marls. The red to brownish interval is about 740 cm thick.

These are composed of thin to medium, red to brownish marls. The strata overlying the red beds are characterized as greenish, grayey, very thin to medium, mudstone and claystone with occasionally interbedded greenish to greenish gray, yellowish, thin to medium bedded, siltstone and sandstone. Towards the top, there is increase in siltstone and sandstone intervals that indicates the invasion of sandy turbiditic deposits in the upper portion and is followed by volcanogenic beds (Figure 2.10).

The beds in the Göynük Section are characterized by shaly to flaggy features (Figures 2.10, 2.12, 2.13). Micro-borrows have been observed under microscope studies at different stratigraphic levels (samples GOZ1, GOZ3, GOZ4-6, GOZ11, GOZ30, GOZ33 and GOZ41). Parallel-cross laminations and asymmetrical ripple structures are documented in sandstone at different stratigraphic levels (Figure 2.14). Parallel

laminations are also observed in siltstone and mudstone (Figure 2.15). Calcite veins and iron nodules (Figure 2.16 B) are present but are generally rare.

Average abundance of macro- and micro- fossils has been observed in the field and thin sections. The recognized biota in the studied section includes inoceramus fragments (Figure 2.16 A), planktonic foraminifers, benthic foraminifers, bivalve and radiolaria.

The base of the measured section in the studied area is unexposed. Near Göynük town, it has been interpreted as conformable contact with underlying succession (Figure 2.4). The measured section is capped by volcanogenic beds of the Campanian-Maastrichtian of Yenipazar Formation (Figure 2.10). An interval of 720 to 750 cm indicates changes in redox-condition in the studied stratigraphic section (Figure 2.11).

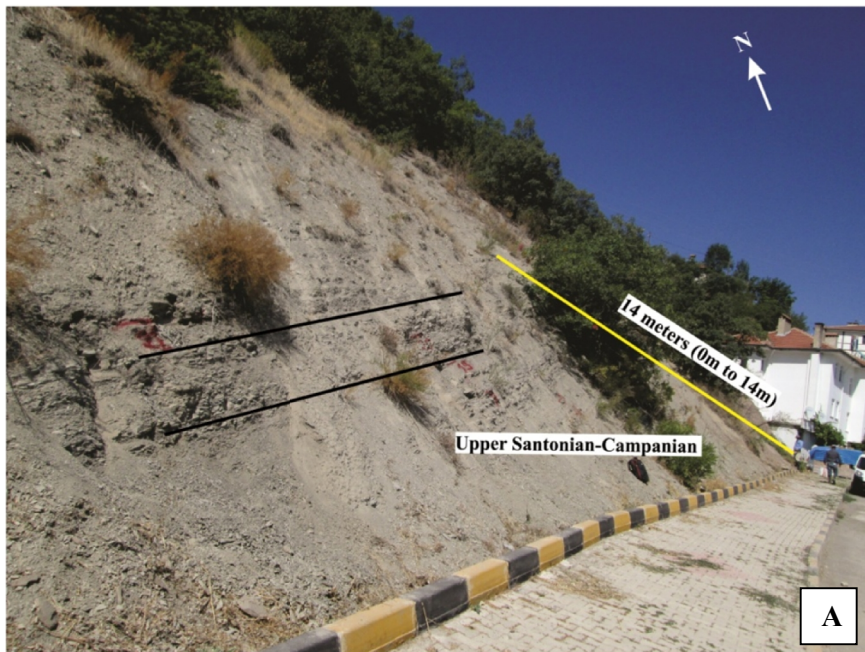
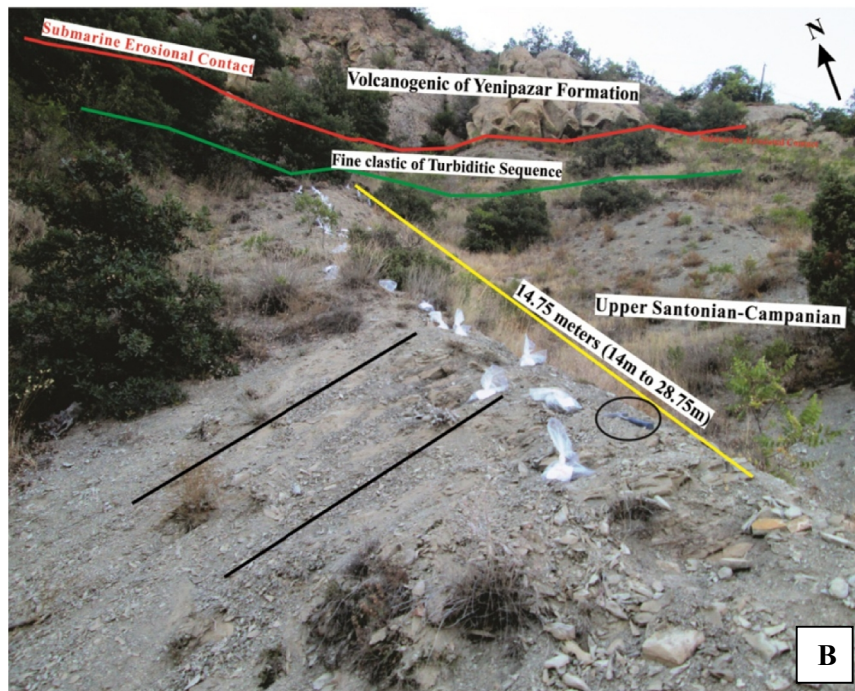


Figure 2.10: The field photograph of measured stratigraphic section; **A)** 0-14 m and **B)** 14-28.75 m near the Göynük town, Bolu. SW dip direction (yellow line shows measured section; black lines for bedding; green line display contact with overlying Fine clastic turbiditic sequence; red line represents unconformable contact with volcanogenic turbiditic sequence).

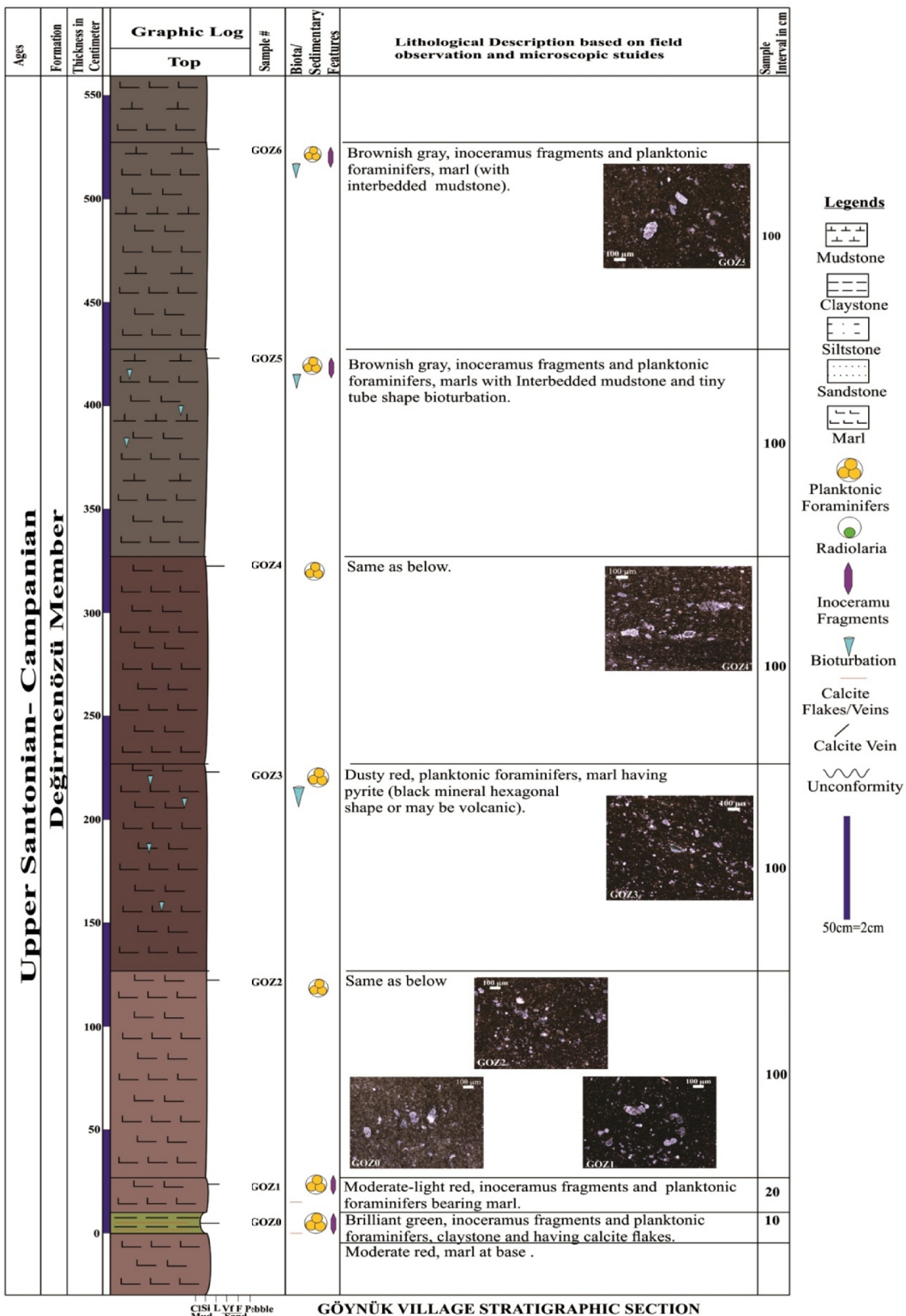


Figure 2.11: Measured stratigraphic section of Göynük Village of the Göynük Basin (0-560 cm).

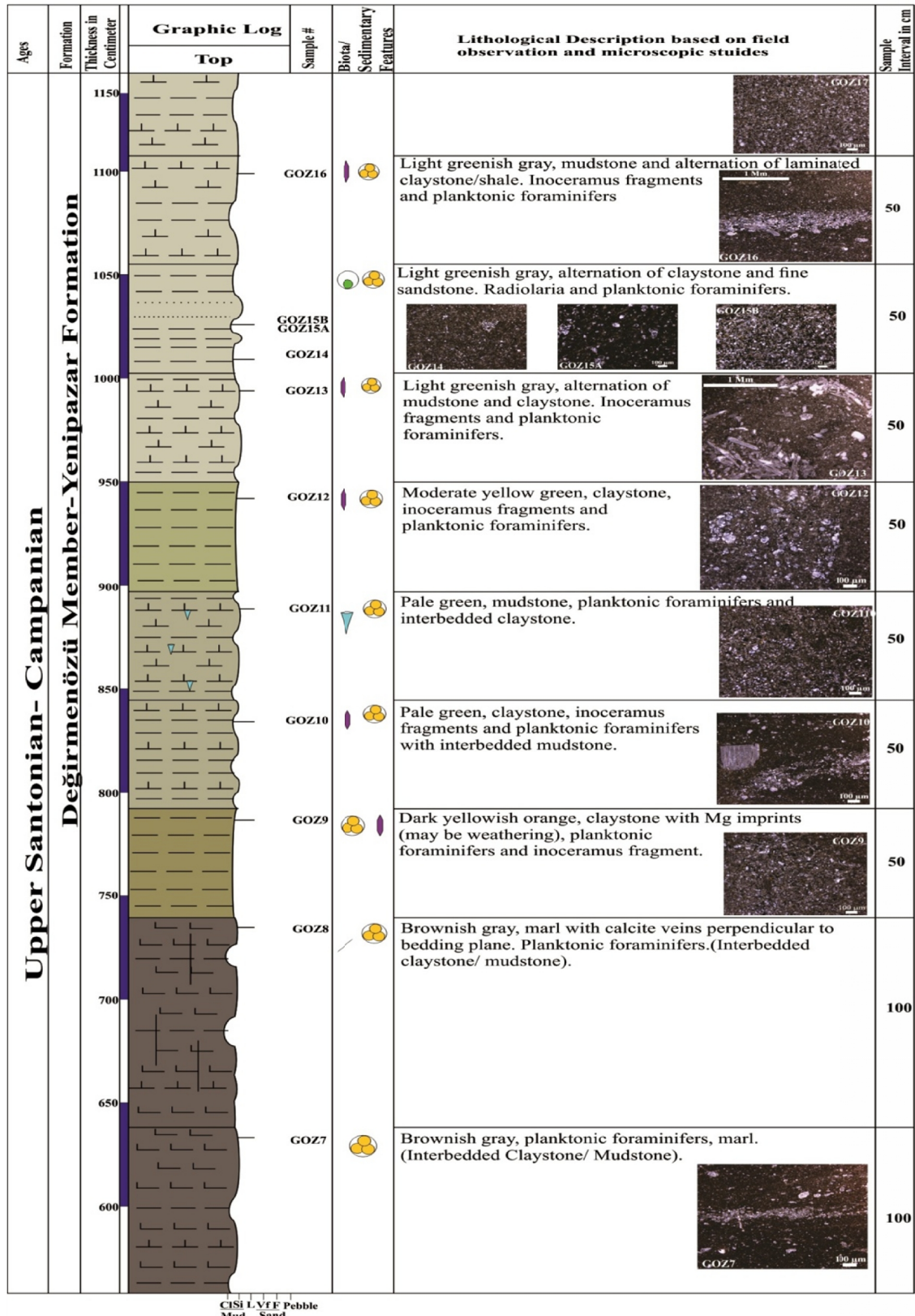


Figure 2.11: Continued (560-1160 cm).

Age	Formation	Thickness in Centimeter	Graphic Log		Sample#	Biota/ Sedimentary Features	Lithological Description based on field observation and microscopic studies		Sample Interval in cm
			Top						
Upper Santonian- Campanian Yenipazar Formation		1750		GOZ28		Greenish gray, mudstone and having Planktonic foraminifers. Green, fine grained Sandstone with small scale Ripple.		50	
		1700		GOZ27					
		1650		GOZ26		Pale green, claystone. Inoceramus fragments and planktonic foraminifers.		50	
		1600		GOZ25		Pale green, mudstone. Planktonic foraminifers.		50	
		1550		GOZ24		Pale green, claystone and having planktonic foraminifers.		50	
		1500		GOZ23		Light green, claystone and having planktonic foraminifers.		50	
		1450		GOZ22		Light green, claystone and having planktonic foraminifers.		50	
		1400		GOZ21		Light green, mudstone. Inoceramus fragments and planktonic foraminifers.		50	
		1350		GOZ20		Light green, mudstone and thinly bedded claystone alternation. Inoceramus fragments and planktonic foraminifers		50	
		1300		GOZ19		Pale green, mudstone with intercalation of occasional bedded siltstone. Planktonic foraminifers		50	
		1250		GOZ18		Light greenish gray, mudstone and alternation of claystone. Inoceramus fragments and planktonic foraminifers.		50	
		1200		GOZ17		Greenish gray, alternation of mudstone and claystone.		50	

Figure 2.11: Continued (1160-1760 cm).

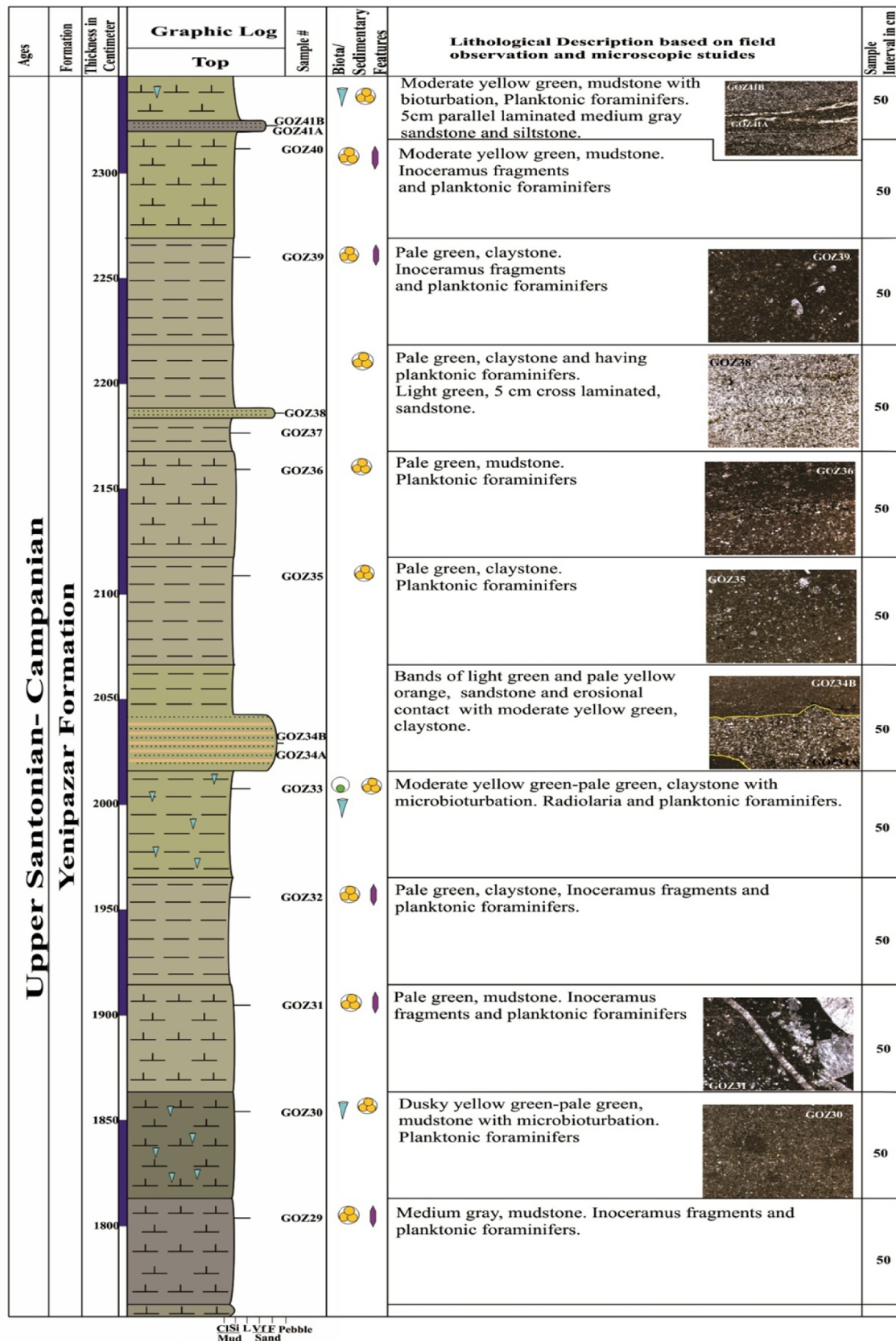


Figure 2.11: Continued (1760-2350 cm).

GÖYNÜK VILLAGE STRATIGRAPHIC SECTION

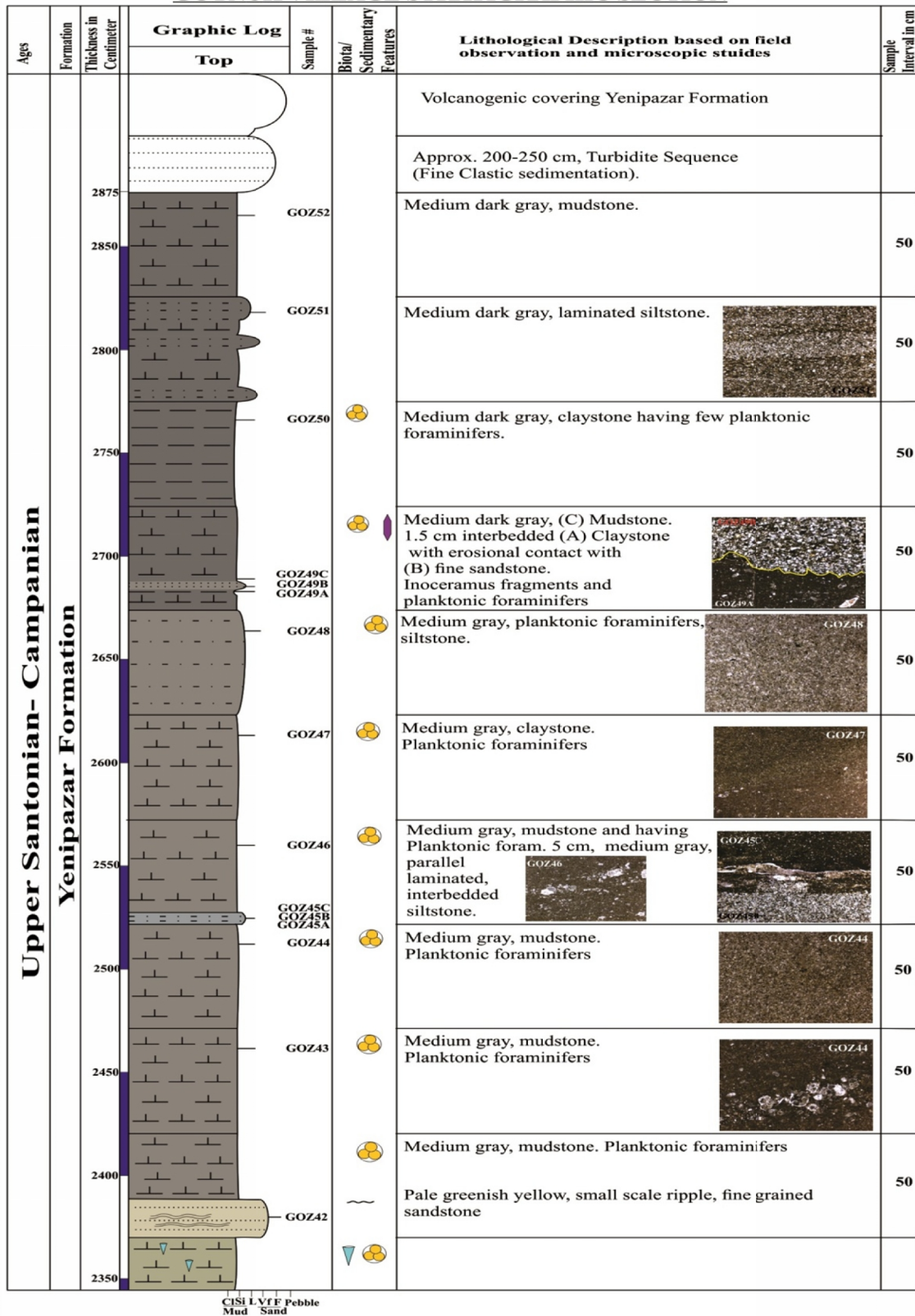


Figure 2.11: Continued (2345-2875 cm).

Table 2.2: Identification of color of the samples from the Göynük Section.

Göynük Section samples color name and their color codes				
No.	Sample	Rock and their outcrop color	Color Name (Munsell Color Book) (GSA*, 2009)	Geological Color Chart Code (Munsell Color Book) (GSA*, 2009)
1.	GOZ-0	Greenish Claystone	Brilliant Green	5G 6/6
2.	GOZ-1	Red Marl	Light Red	5R 6/6
3.	GOZ-2	Red Marl	Moderate Red	5R 5/4
4.	GOZ-3	Red Marl	Dusky Red	5R 3/4
5.	GOZ-4	Red Marl	Dusky Red	5R 3/4
6.	GOZ-5	Brownish Marl	Brownish Gray	5YR 4/1
7.	GOZ-6	Brownish Marl	Brownish Gray	5YR 4/1
8.	GOZ-7	Brownish Marl	Brownish Gray	5YR 4/1
9.	GOZ-8	Brownish Marl	Brownish Gray	5YR 4/1
10.	GOZ-9	Yellowish Claystone	Dark Yellowish Orange	10YR 6/6
11.	GOZ-10	Greenish Claystone	Pale Green	5G 7/2
12.	GOZ-11	Greenish Mudstone	Pale Green to Grayish Yellow Green	5G 7/2 – 5GY 7/2
13.	GOZ-12	Greenish Claystone	Light Greenish Gray	5GY 8/1
14.	GOZ-13	Greenish Gray Mudstone	Light Greenish Gray	5GY 8/1
15.	GOZ-14	Greenish Gray Claystone	Light Greenish Gray	5GY 8/1
16.	GOZ-15A	Greenish Gray Claystone	Light Greenish Gray	5GY 8/1
	GOZ-15B	Fine Sandstone /Greenish Gray Quartzwacke	Light Greenish Gray	5GY 8/1
17.	GOZ-16	Greenish Gray laminated Mudstone	Light Greenish Gray to Grayish Yellow Green	5GY 8/1 – 5GY 7/2
18.	GOZ-17	Greenish Gray Mudstone	Greenish Gray	5G 6/1
19.	GOZ-18	Greenish Gray Mudstone	Light Greenish Gray	5GY 8/1
20.	GOZ-19	Greenish Siltstone	Pale Green	5G 7/2
21.	GOZ-20	Greenish Mudstone	Light Green	5G 7/4
22.	GOZ-21	Greenish Mudstone	Light Green	5G 7/4
23.	GOZ-22	Greenish Claystone	Light Green	5G 7/4
24.	GOZ-23	Greenish Claystone	Light Green	5G 7/4
25.	GOZ-24	Greenish Claystone	Pale Green	5G 7/2
26.	GOZ-25	Greenish Mudstone	Pale Green	5G 7/2
27.	GOZ-26	Greenish Claystone	Pale Green	5G 7/2
28.	GOZ-27	Greenish Gray Mudstone	Greenish Gray	5GY 6/1
29.	GOZ-28	Fine Sandstone /Greenish Gray Quartz-wacke	Greenish Gray	5G 6/1
30.	GOZ-29	Gray Mudstone	Medium Gray to Moderate Yellow Green	N5 – 5GY 7/4
31.	GOZ-30	Greenish Mudstone	Pale Green	5G 7/2
32.	GOZ-31	Greenish Mudstone	Pale Green	5G 7/2
33.	GOZ-32	Greenish Claystone	Pale Green	5G 7/2
34.	GOZ-33	Greenish Claystone	Pale Green	5G 7/2
35.	GOZ-34a	Fine Sandstone/ Greenish Quartz-wacke	Light Green to Pale Yellow Orange	5G 7/4 – 10YR 8/6
	GOZ-34b	Greenish Claystone	Light Green to Pale Yellow Orange	5G 7/4 – 10YR 8/6
36.	GOZ-35	Greenish Claystone	Pale Green	5G 7/2
37.	GOZ-36	Greenish laminated Mudstone	Pale Green	5G 7/2
38.	GOZ-37	Greenish Claystone	Pale Green	5G 7/2
39.	GOZ-38	Fine Sandstone /Greenish Quartz-wacke	Pale Green	5G 7/2
40.	GOZ-39	Greenish Claystone	Pale Green	5G 7/2
41.	GOZ-40	Greenish Mudstone	Moderate Yellow Green	5GY 7/4
42.	GOZ-41 (Lower)a	Gray Siltstone	Medium Gray	N5
	GOZ-41 (Upper)b	Fine Sandstone /Gray Quartz-wacke	Medium Gray	N5
43.	GOZ-42	Fine Sandstone/Greenish Quartz-wacke	Moderate Greenish Yellow to Pale Yellowish Orange	10Y 7/4 – 10YR 8/6
44.	GOZ-43	Light Gray Mudstone	Medium Gray	N5
45.	GOZ-44	Light Gray Mudstone	Medium Gray	N5
	GOZ-45 (Lower)a	Light Gray Mudstone	Medium Gray	N5
46.	GOZ-45 (Middle)b	Light Gray Siltstone	Medium Gray	N5
	GOZ-45 (Upper)c	Light Gray Mudstone	Medium Gray	N5
47.	GOZ-46	Light Gray Mudstone	Medium Gray	N5
48.	GOZ-47	Light Gray Mudstone	Medium Gray	N5
49.	GOZ-48	Light Gray Siltstone	Medium Gray	N5
	GOZ-49 (Lower)a	Light Gray Claystone	Medium Gray	N5
50.	GOZ-49 (Middle)b	Fine Sandstone / Light Gray Quartz-wacke	Medium Gray	N5
	GOZ-49 (Upper)c	Light Gray Mudstone	Medium Gray	N5
51.	GOZ-50	Gray Claystone	Medium Dark Gray	N4
52.	GOZ-51	Gray Siltstone	Medium Dark Gray	N4
53.	GOZ-52	Gray Mudstone	Medium Dark Gray	N4

*Geological Society of America Rock-Color Chart Committee, 2009.



Figure 2.12: The field photograph showing the Upper Santonian-Campanian red beds in the Göynük section.



Figure 2.13: The field photograph showing the Campanian greenish gray claystone and mudstone in the Göynük section.

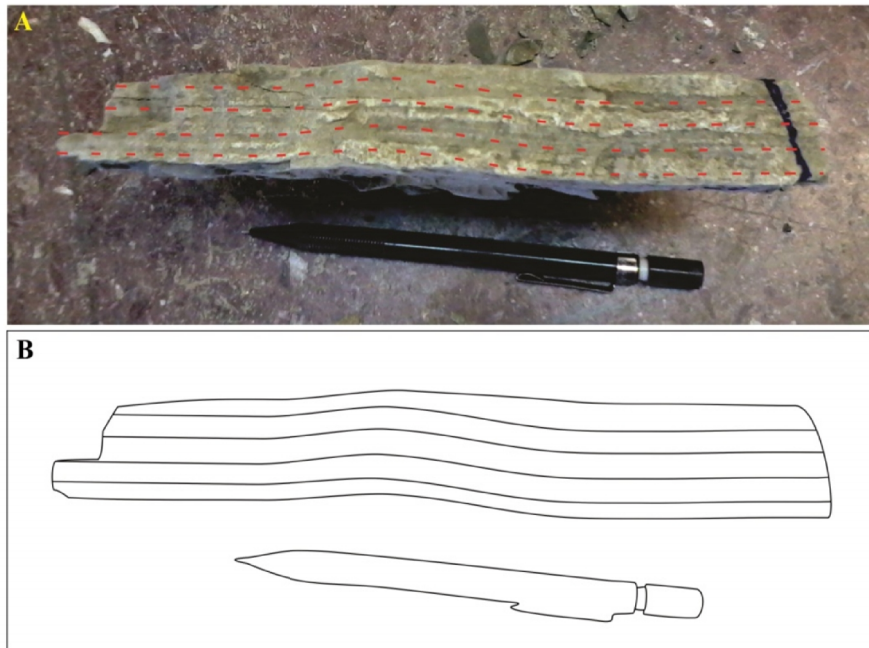


Figure 2.14: Asymmetrical ripples in the GOZ38 (sandstone) of the Göynük section. A) GOZ38 with red dotted lines represents ripples and B) Sketch of A.

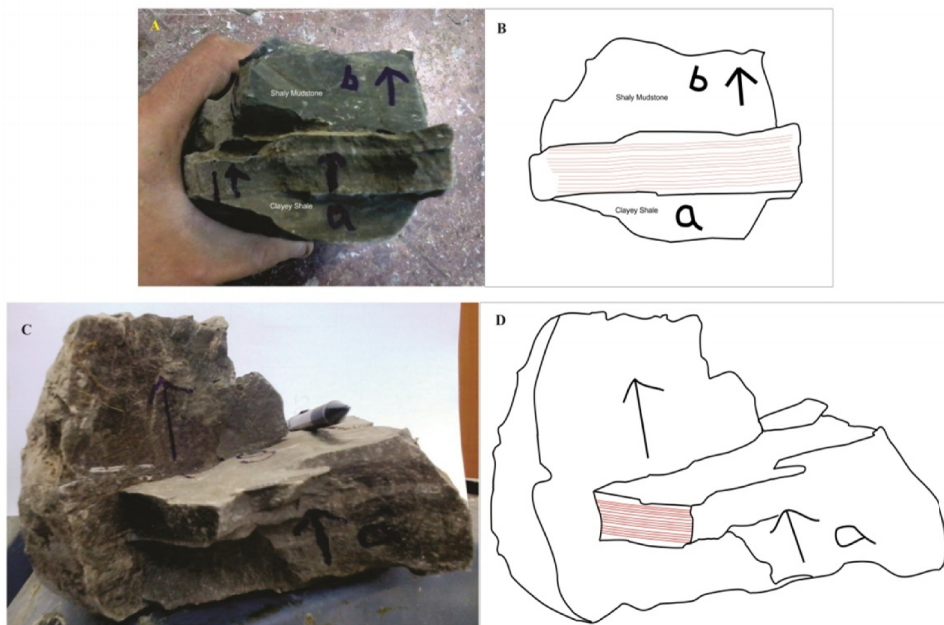


Figure 2.15: Lamination in the samples of the Göynük section. A) Photo of GOZ49 and B) Sketch of A: C) Photo of GOZ51 and D) Sketch of C; red lines show lamination.



A



B

Figure 2.16: **A)** The field photograph of the Inoceramus fragment in the Göynük section. **B)** Photo showing iron nodule in the Göynük section.

CHAPTER 3

SEDIMENTOLOGY

3.1 SEDIMENTOLOGICAL STUDIES

The sedimentological analysis is based on the field observations and microscopic studies. These studies include sedimentary structure, fossil recognitions, petrographic analysis and point counting measurement of the samples and are used to classify and interpret the Alagöz and Göynük sections (Figures 3.1-3.4; Table 3.1). A total of five different microfacies are established in each measured sections.

3.2 MICROFACIES OF ALAGÖZ SECTION

In the Alagöz stratigraphic section, five microfacies are recognized on basis of outcrop and microscopic studies (Tables 3.2-3.3). These are as following;

3.2.1 RED TO PALE GREEN RADIOLARIAN PACKSTONE

Radiolarian packstone microfacies show moderate red (5R 4/6), pale green to light greenish gray (5R 7/2-5GY 8/1) color, purple marl infilling dendritic bioturbation pattern (Figure 2.9 B) and thin to medium bedded in the field (Figures 3.7). It is composed of abundant siliceous radiolaria, calcited radiolaria, sponge spicules with few planktonic foraminifers and embedded in the lime mud matrix (Figure 3.5 A, 3.5 B). The opal/silicification is observed in the form of patches that represents replacement of lime mud matrix during diagenesis. The sponge spicules are mostly monaxon and triaxon form. The other accessory minerals are quartz, mica, glauconite, biotite, lithic fragments (calcite and volcanogenic glass), pyrite and rare phosphate. The quartz grains are silt size to few sand sizes and angular to sub-angular grains shape.

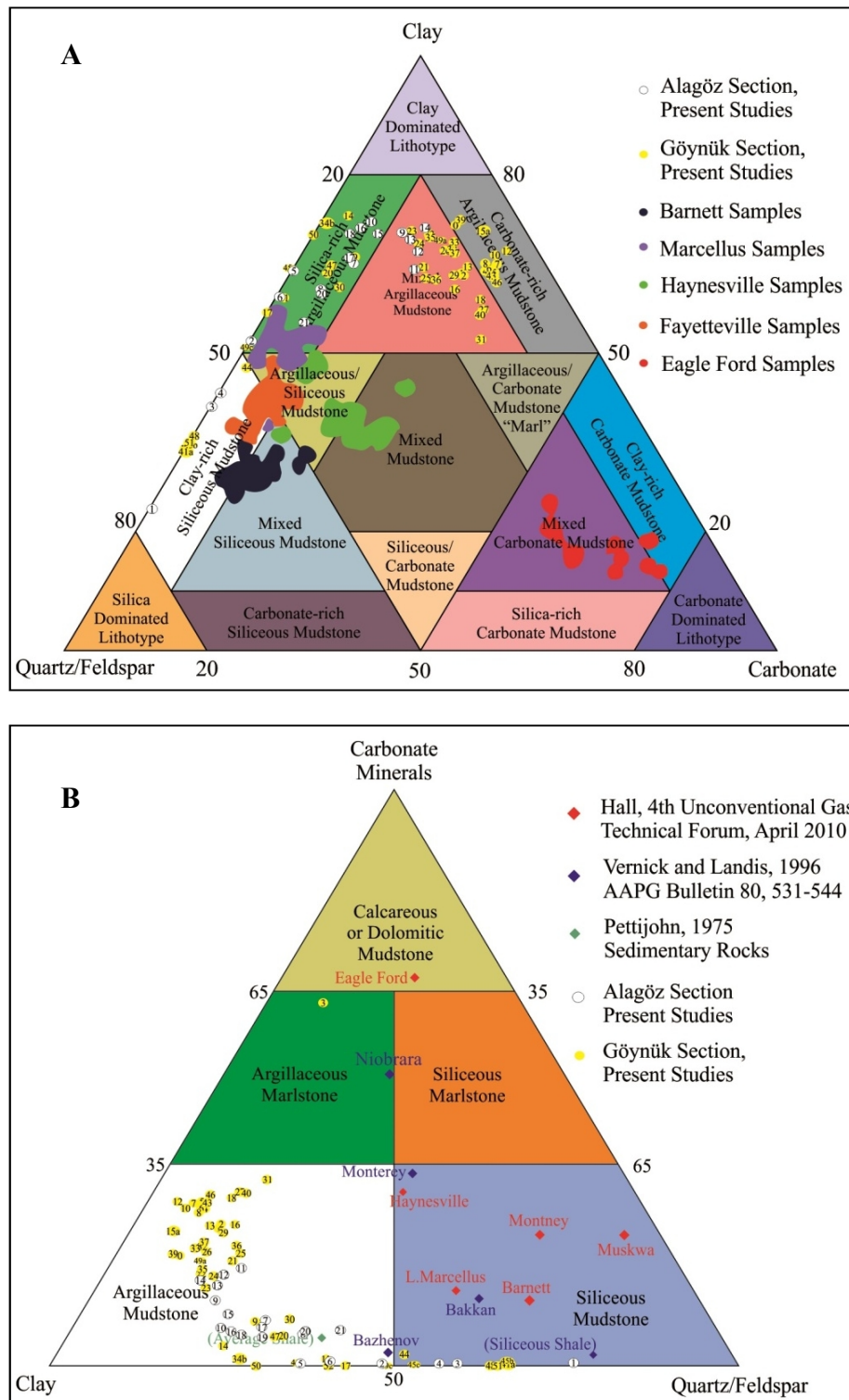


Figure 3.1: Ternary mudstone compositional classification (for unconventional) diagram of the **A)** Diaz et al. (2012) and **B)** the Allix et al. (2010) used to plot the samples of Alagöz and Göynük sections, and their comparison with known unconventional reservoirs from USA.

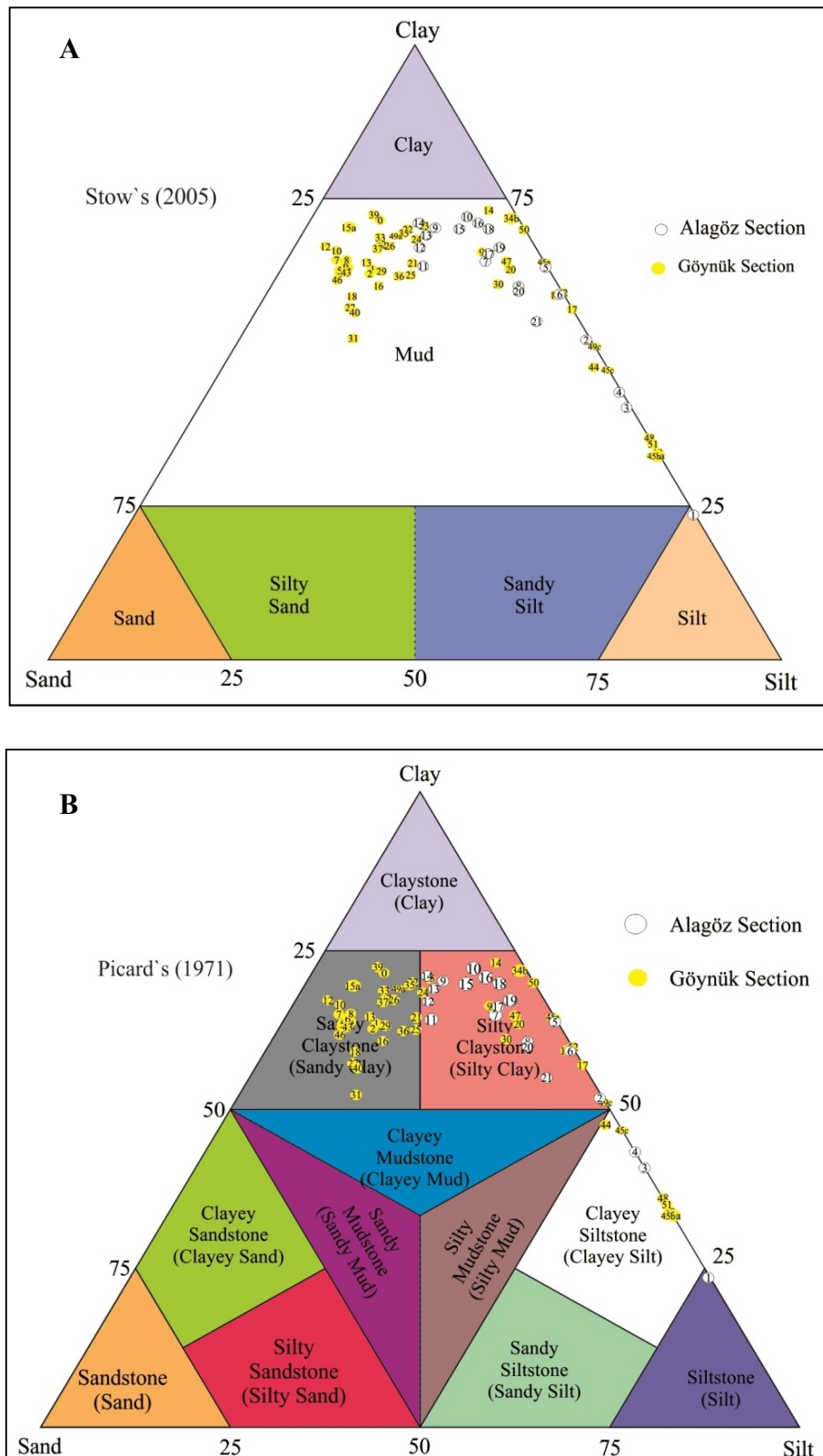


Figure 3.2: **A)** Stow's (2005) classification and **B)** the Picard's (1971) classification based on relative proportions of grains size. (The samples of Alagöz and Göynük sections are represented by white and yellow circles, respectively).

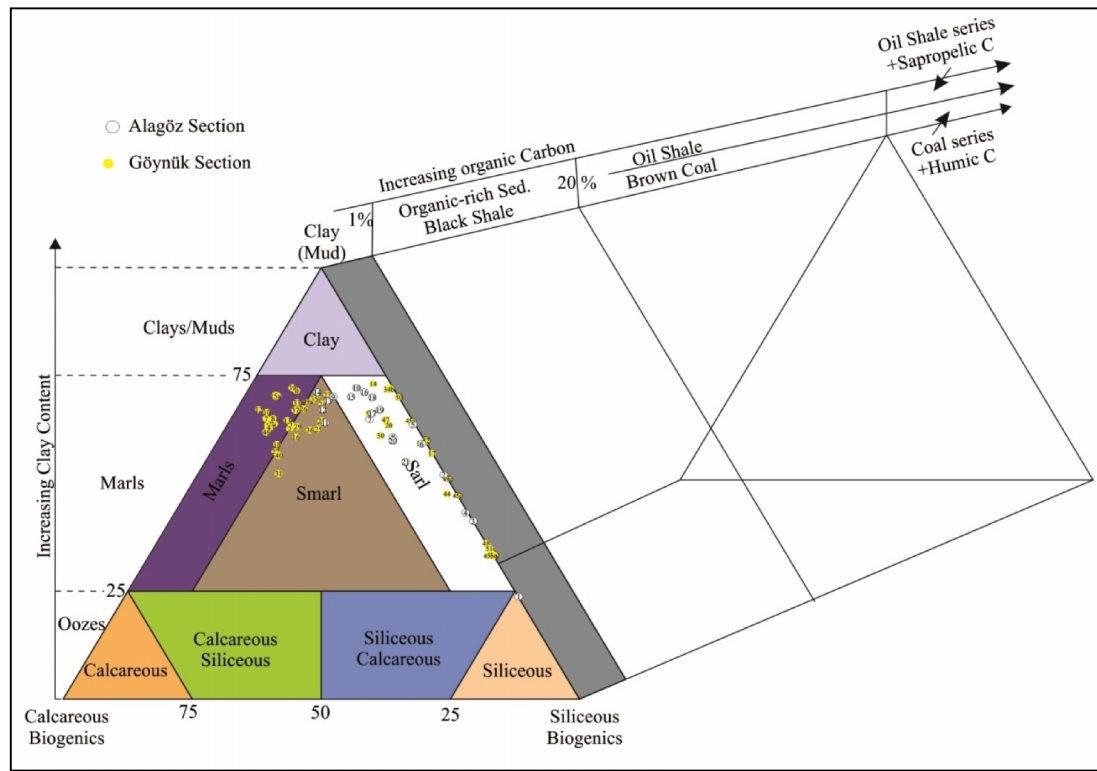


Figure 3.3: Stow's compositional classification (2005) ternary diagram based on biogenic (carbonate and silica) and mud/clays: illustrate the Alagöz (white circles) and the Göynük sections samples (yellow circles).

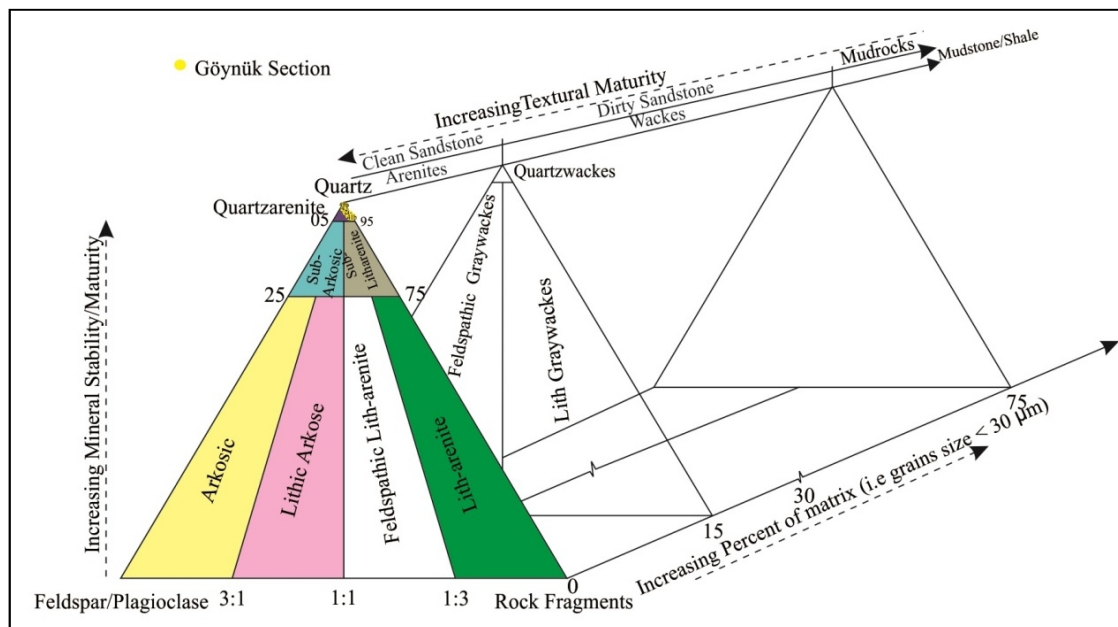


Figure 3.4: Studied samples of the Göynük Section are plotted on the Folk's (1974) Sandstone classification ternary diagram based on relative proportions of grains size and presence of matrix.

***Table 3.1:** Folk's (1965) texture classification of fine-grained sedimentary rock.

Mud-rock division based upon texture and structure			
Grain size of mud fraction	Soft	Indurated, Non-fissile	Indurated, Fissile
>66 % Silt	Silt	Siltstone	Silt-Shale
33-66 % (Sub-equal silt and clay)	Mud	Mudstone	Mud-Shale
>66 % Clay	Clay	Claystone	Clay-Shale

The Dunham's (1962) and Folk's (1962) carbonate classifications are used to classify the limestone lithofacies. According to their combined classification, a limestone consists of a ratio of 3:4 of bioclasts and 1:4 of micrite, afterwards it is defined as bioclastic packstone. The point counting analysis and visual observation of the limestone facies indicate high proportion of bioclasts (more than 65 %) and low amount of micrite, which interprets radiolarian packstone microfacies. This microfacies is similar to SMF1 of Wilson's (1975) SMF Model. This microfacies is confined to the basinal portion of the measured stratigraphic section (Figure 2.7).

3.2.2 RED SILTY MARL

Marl is classified as a fine grained sedimentary rock type which has relatively soft/loose sediment, containing 35-65% carbonate and 65-35% clay, and fizzing property when treated with dilute HCl (Pettijohn, 1975 and Potter et al., 2005). In the studied section, the marl facies has been identified with relatively high proportion of silt size quartz grains (average around 45-50%) and interbedded with siltstone. The facies is classified as silty marl and confined to the red beds (Figure 2.7).

The silty marl is documented as moderate red (5R 4/6), dusky red/grayish red (5R 3/4), pale reddish brown (10G 5/4) color and very thin to thin bedded in the field (Figure 3.7) and with a fizzing character by applying diluted HCl. It consists of predominantly quartz grains and matrix (Figure 3.6). The feldspar, plagioclase, mica, lithic fragments

Table 3.2: Petrographic data and established/recognized Microfacies from Alagöz Section samples.

Sample No.	Quartz	Feldspar(F)/Plagioclase(P)	Mica	Glauconite	Heavy minerals	Lithic-clasts (Volcano-genic* /Rock Fragment^)	Bioclasts (Ra/Pf/InS/B/Bi/E/Uf)	Other (P-OM^/He/Ph)	Matrix (Lm/Cl/Op)	Nomenclature (Texture/Compositional)
ZR0b	0.6	-	0.05	0.02	0.01	-	51.24Ra/0.5Pf/15.34S=67.08	0.6P/0.05Ph=0.65	24.15Lm/7.42Op=31.57	Moderate Red Packstone/Radiolarian Rich Packstone/Siliceous Mudstone
ZR0	0.3	-	0.02	0.01	-	0.01*/0.03^=0.04	52.2Ra/16.73S/0.5Pf/0.01B=70.24	0.4P/0.1Ph=0.50	24.18Lm/4.71Op=28.89	Pale green Packstone/Mixed Radiolarian Rich Packstone/Mixed Sil-Cal Mudstone
ZR01	72.81	0.1P	1.9	0.01	0.01	0.01*/0.1^=0.11	0.03Pf	2.0P	23.03Cl	Red Siltstone
ZR02	45.25	0.01F/0.05P=0.06	1.6	0.02	0.01	0.02*/0.02^=0.04	-	2.0P/0.04Ph=2.04	50.97Cl	Red Silty Marl
ZR03	54.98	0.01F/0.06P=0.07	2	0.01	0.01	0.02*/0.05^=0.07	-	1.7P/1.1He=2.80	40.06Cl	Red Silty Marl
ZR04	51.69	0.01F/0.01P=0.02	2	0.02	-	0.01*/0.03^=0.04	-	3.88P=3.88	42.35Cl	Red Silty Marl
ZR04a	36.22	0.03P	1.5	0.01	0.01	0.01*/39.63^=39.64	-	0.8P/1.0He=1.8	20.79Cl	Greenish Gray Intra-clastic bearing Red Siltstone
ZR05	33.65	0.01P	1	0.02	-	0.02*/0.02^=0.04	0.2Ra/0.01Pf/0.01B=0.22	3.9P	61.16Cl	Greenish Gray Mudstone
ZR06	37.68	0.01P	0.7	0.03	0.01	0.05^	0.24Pf	2.83P/1.55He=4.38	56.9Cl	Reddish Silty Marl
ZR07	25.94	0.01F	0.01	-	-	-	7.92 Pf	2.0P/0.6He=2.6	63.49Cl	Greenish Gray Mudstone
ZR08	32.53	-	0.7	0.01	0.01	-	5.40 Pf/0.01Bi=5.41	1.9P	59.44Cl	Greenish Gray Mudstone
ZR09	17.18	-	0.04	0.01	-	-	11.90 Pf/0.01B=11.91	2.3P	68.56Cl	Greenish Gray Claystone
ZR10	19.87	-	0.02	0.03	-	-	6.48 Pf/0.02B=6.5	3.1P/2.5He=5.6	67.98Cl	Greenish Gray Claystone
ZR11	18.3	-	0.01	-	-	-	16.99 Pf/0.01Bi=17	1.0P/1.1He=2.1	62.59Cl	Greenish Gray Mudstone
ZR12	16.7	-	-	-	-	-	15.49 Pf/0.01B=15.5	1.4P	66.4Cl	Light Gray to Pale Green Claystone
ZR13	17.2	-	-	-	-	-	13.5 Pf	0.6P	68.7Cl	Greenish Gray Claystone
ZR14	13.3	-	-	-	-	-	14.7 Pf	1.9P	70.1Cl	Medium Dark Gray Claystone
ZR15	20.48	-	0.02	0.02	-	-	8.39/0.01B=8.4	2.6P/0.6He=3.2	67.88Cl	Medium Dark Gray Claystone
ZR16	21.94	-	-	0.02	-	-	6.14 Pf	2.3P	69.6Cl	Medium Gray Claystone
ZR17	26.12	-	0.1	0.01	0.02	-	6.89 Pf/0.01B=6.9	1.6P	65.25Cl	Medium Light Gray Mudstone
ZR18	24.6	-	0.05	-	-	-	4.4 Pf	3.6P	67.35Cl	Greenish Gray Claystone
ZR19	27.3	-	0.05	-	-	-	4.39 Pf/0.01B=4.4	2.1P/0.3He=2.4	65.85Cl	Greenish Grey Claystone
ZR20	32.66	-	0.03	-	-	0.04^	5.59 Pf/0.01E=5.6	3.7P	57.97Cl	Medium Dark Gray Mudstone
ZR21	37.3	-	-	-	-	-	6.0 Pf	3.5P	53.2Cl	Medium Dark Gray Mudstone

Ra=Radiolaria, S=Sponge Spicule, In=Inceramus, Pf=Planktonic Fossil, P=Pyrite, Om=Organic matter, Ph=Phosphate, Lm=Lime Mud, Cl=Clay, Op=Opal/Silica, E=Echinoid, B=Benthic Foram, Bi=Bivalve

Table 3.3: Classifications of the Alagöz section based on compositional, grain size and texture parameters.

Sample No.	Alagöz Section Classification						This Studied (Texture and/or Compositional)
	Compositional Classification			Grains Size Classification		Texture Classification*	
	Diaz's (2012) Mudstone (Unconventional)	Stow's (2005) (Biogenic +Clay/Mud)	Allix's (2010) Shale	Stow's (2005) Silic-Clastic	Picard's (1971)	Folk's (1965)	
ZR0b	Packstone (Dunham's Classification 1962)/ Siliceous Radiolarian Packstone (Folk's 1962 and Dunham's 1962 Classification)						Packstone/Radiolarian Rich Packstone/Siliceous Mudstone
ZR0	Packstone (Dunham's Classification 1962)/ Siliceous-calcareous Radiolarian Packstone (Folk's 1962 and Dunham's 1962 Classification)						Packstone/Mixed Radiolarian Rich Packstone/Mixed Sil-Cal Mudstone
ZR01	Clay-rich Siliceous Mudstone	Siliceous	Siliceous Mudstone	Silt	Siltstone	Silt-Shale	Siltstone
ZR02	Silica-rich Argillaceous Mudstone	Sarl	Argillaceous Mudstone	Mud	Silty-Claystone	Mud-Shale	Silty Marl
ZR03	Clay-rich Siliceous Mudstone	Sarl	Siliceous Mudstone	Mud	Clayey-Siltstone	Mud-Shale	Silty Marl
ZR04	Clay-rich Siliceous Mudstone	Sarl	Siliceous Mudstone	Mud	Clayey-Siltstone	Mud-Shale	Silty Marl
ZR04a	Intraclastic-rich Siliceous Mudstone	Sarl	Siliceous Marlstone	Mud	Intra/Sandy-Siltstone	Silt-Shale	Intra-clastic bearing Siltstone
ZR05	Silica-rich Argillaceous Mudstone	Sarl	Argillaceous Mudstone	Mud	Silty-Claystone	Mud-Shale	Mudstone
ZR06	Silica-rich Argillaceous Mudstone	Sarl	Argillaceous Mudstone	Mud	Silty-Claystone	Mud-Shale	Silty Marl
ZR07	Silica-rich Argillaceous Mudstone	Sarl	Argillaceous Mudstone	Mud	Silty-Claystone	Mud-Shale	Mudstone
ZR08	Silica-rich Argillaceous Mudstone	Sarl	Argillaceous Mudstone	Mud	Silty-Claystone	Mud-Shale	Mudstone
ZR09	Mixed Argillaceous Mudstone	Sarl	Argillaceous Mudstone	Mud	Silty-Claystone	Clay-Shale	Claystone
ZR10	Silica-rich Argillaceous Mudstone	Sarl	Argillaceous Mudstone	Mud	Silty-Claystone	Clay-Shale	Claystone
ZR11	Mixed Argillaceous Mudstone	Smarl	Argillaceous Mudstone	Mud	Silty-Claystone	Mud-Shale	Mudstone
ZR12	Mixed Argillaceous Mudstone	Smarl	Argillaceous Mudstone	Mud	Silty-Claystone	Clay-Shale	Claystone
ZR13	Mixed Argillaceous Mudstone	Smarl	Argillaceous Mudstone	Mud	Silty-Claystone	Clay-Shale	Claystone
ZR14	Mixed Argillaceous Mudstone	Smarl	Argillaceous Mudstone	Mud	Silty-Claystone	Clay-Shale	Claystone
ZR15	Silica-rich Argillaceous Mudstone	Sarl	Argillaceous Mudstone	Mud	Silty-Claystone	Clay-Shale	Claystone
ZR16	Silica-rich Argillaceous Mudstone	Sarl	Argillaceous Mudstone	Mud	Silty-Claystone	Clay-Shale	Claystone
ZR17	Silica-rich Argillaceous Mudstone	Sarl	Argillaceous Mudstone	Mud	Silty-Claystone	Mud-Shale	Mudstone
ZR18	Silica-rich Argillaceous Mudstone	Sarl	Argillaceous Mudstone	Mud	Silty-Claystone	Clay-Shale	Claystone
ZR19	Silica-rich Argillaceous Mudstone	Sarl	Argillaceous Mudstone	Mud	Silty-Claystone	Clay-Shale	Claystone
ZR20	Silica-rich Argillaceous Mudstone	Sarl	Argillaceous Mudstone	Mud	Silty-Claystone	Mud-Shale	Mudstone
ZR21	Silica-rich Argillaceous Mudstone	Sarl	Argillaceous Mudstone	Mud	Silty-Claystone	Mud-Shale	Mudstone

* Based on grains size of mud fraction, nonfissile/fissile and soft.

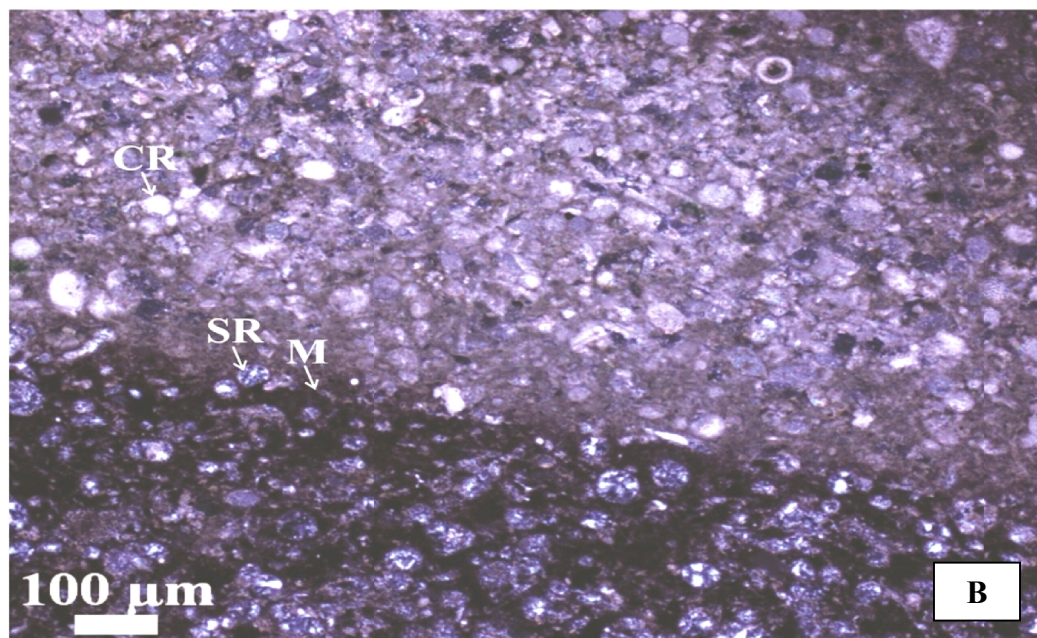
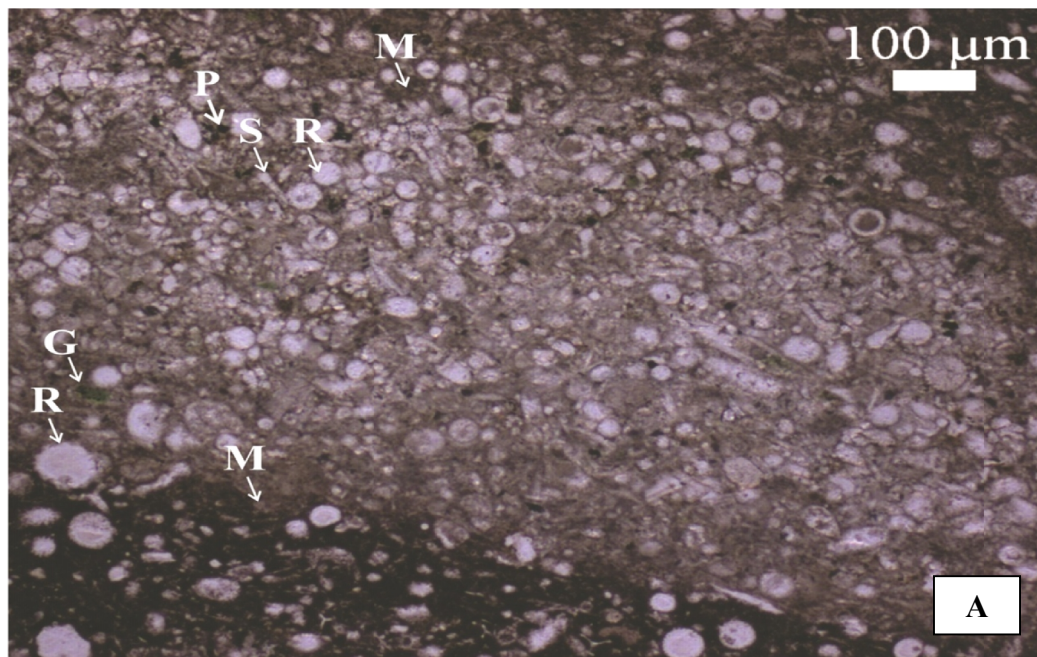


Figure 3.5: Photomicrographs of red to pale green radiolarian packstone microfacies representing radiolarian sp. (R), calcareous radiolarian sp. (CR), siliceous radiolarian sp. (SR), sponge spicules (S), glauconite (G), pyrite (P) and matrix (M) (Sample no. ZR0b, **(A)** PPL, **(B)** XPL x4).

(volcanogenic glass, chert, and calcite), blue tourmaline, pyrite and iron oxides are observed in minor amounts. Planktonic foraminifers are present but very limited in numbers. The observed micro-bioturbations in the microfacies indicate oxic condition during the deposition of sediments.

3.2.3 GREENISH TO GRAY MUDSTONE

The mudstone facies are documented from the green-gray intervals in the measured stratigraphic section. In the field, it is characterized by pale green (10G 6/2), light greenish gray (5GY 8/1), greenish gray (10G 4/2), light olive gray (N7), medium gray (N5), medium dark gray (N4) color, very thin to thin bedded and flaggy appearance (Figure 3.10). It is comprised of silt size to a few very fine sand size and angular to sub-angular quartz grains, bioclasts and matrix (Figure 3.8 A, 3.8 B, 3.9 A) with association of trace amount of feldspar, mica, glauconite, lithic clasts, biotite, blue tourmaline, pyrite and hematite. The fossil includes abundant planktonic foraminifers, bivalve, benthic foraminifers and echinoids. Infilling micro-borrows and pyrite infilling chamber of planktonic forams have been noticed (Figure 3.9 B).

According to Folk's classification (1965) and Pettijohn (1975), mudstone are the sedimentary rock which is relatively harder than shale, massive bedded and composed of sub-equal mixture of silt and clay size materials. This facies contains 50-65% clayey matrix and the remaining consists of silt and very fine grains clasts and bioclasts. Thus, it is classified as mudstone microfacies. This microfacies dominates in the middle and upper top unit of the measured stratigraphic section (Figure 2.7).

3.2.4 GREENISH TO GRAY CLAYSTONE

Claystone is another very fine grained sedimentary rock which contains more than 66% percent clayey matrix (Folk, 1965; Pettijohn, 1975). The claystones are dominated in the middle portion of the measured stratigraphic section. This facies interbedded with

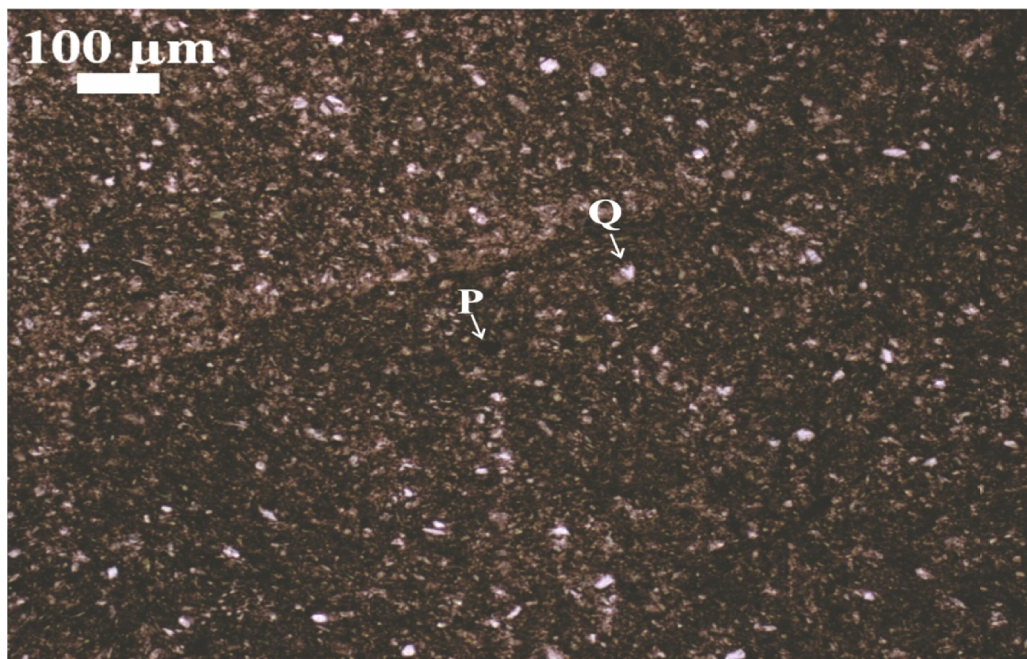


Figure 3.6: Photomicrographs of Red Silty Marl Microfacies having abundant silt-size quartz grains (Q) with pyrite (P) and iron rich matrix (Sample no. ZR04, PPL).

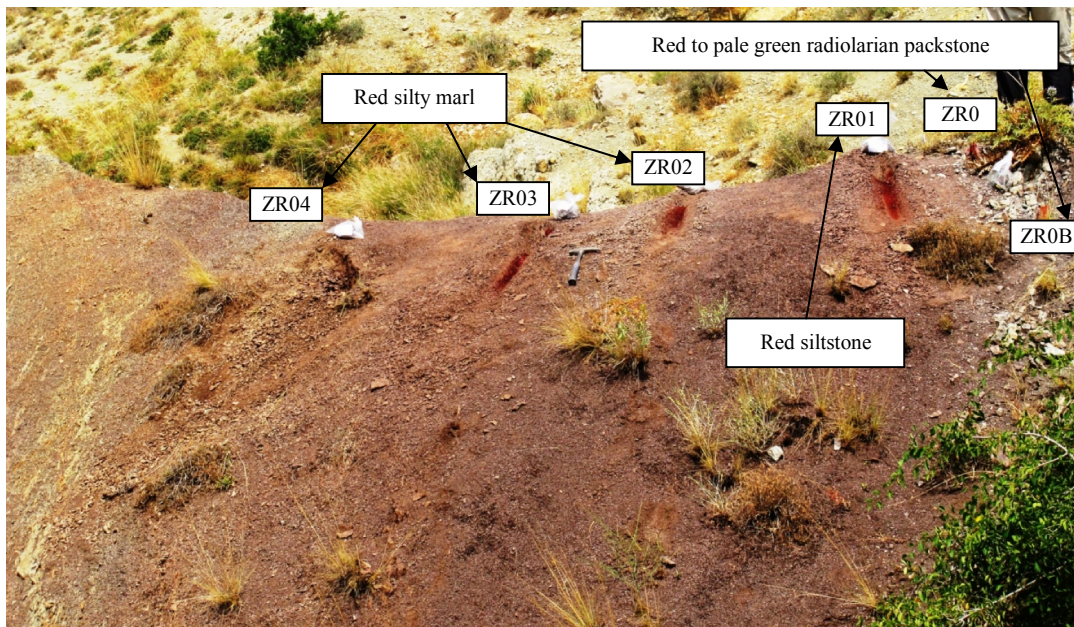


Figure 3.7: The field photograph showing the red beds of the Alagöz measured section.

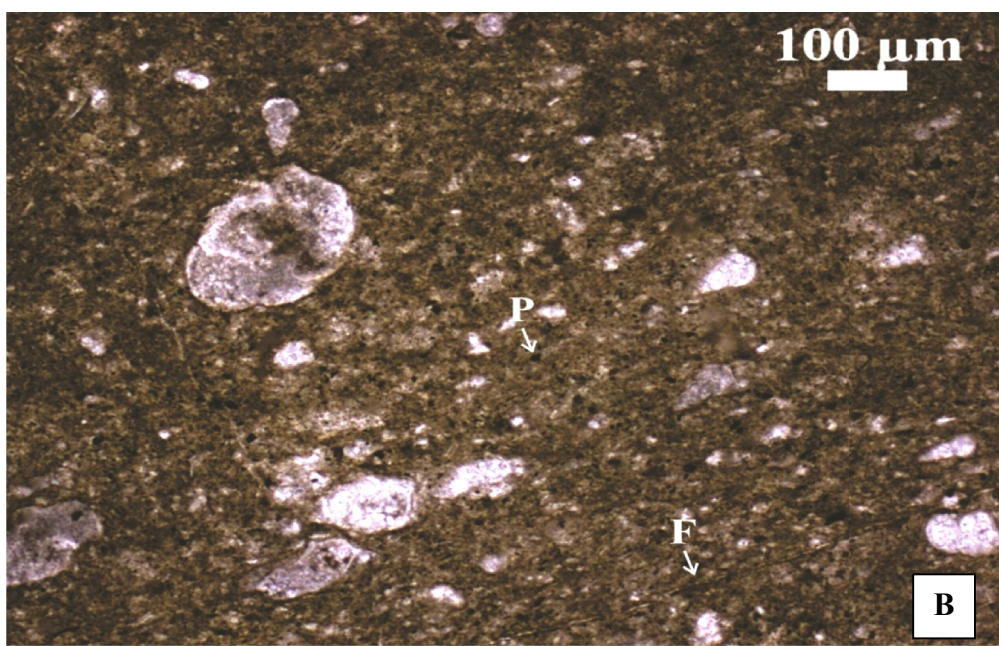
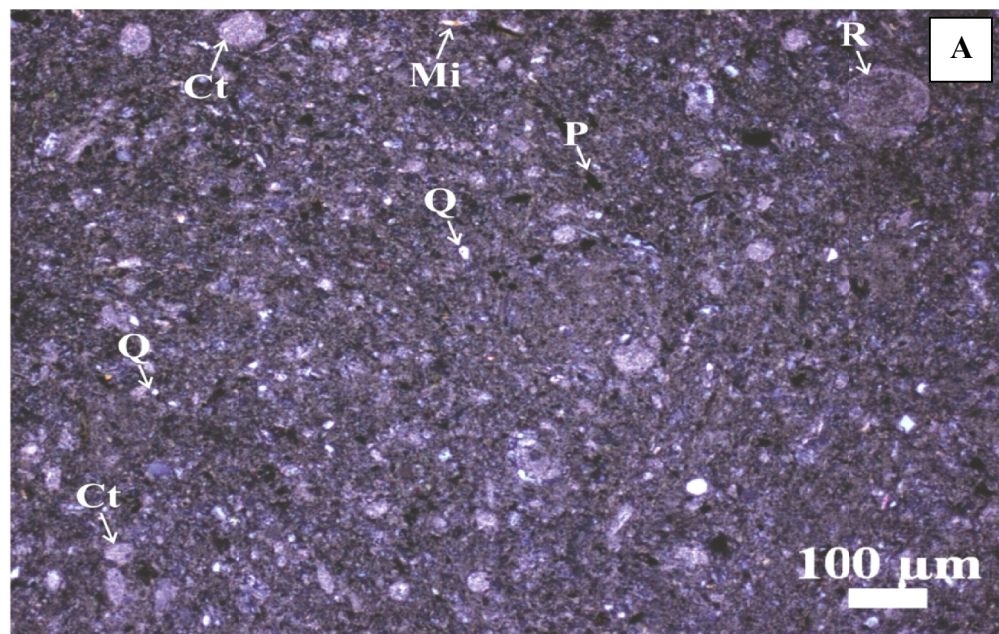


Figure 3.8: Photomicrographs of greenish to gray mudstone microfacies containing quartz (Q), mica (Mi), pyrite (P), calcite (Ct), radiolarian sp. (R), planktonic foraminifers and matrix and calcite filling fracture (F) (Sample no. ZR05, **(A)** XPL x4; ZR07, **(B)** PPL x4).

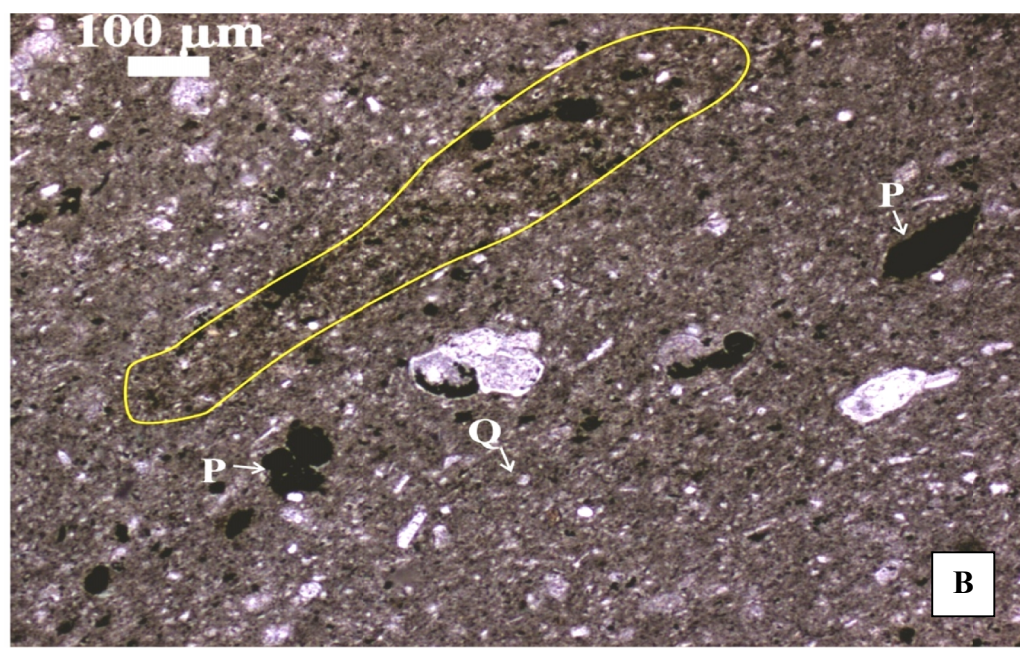
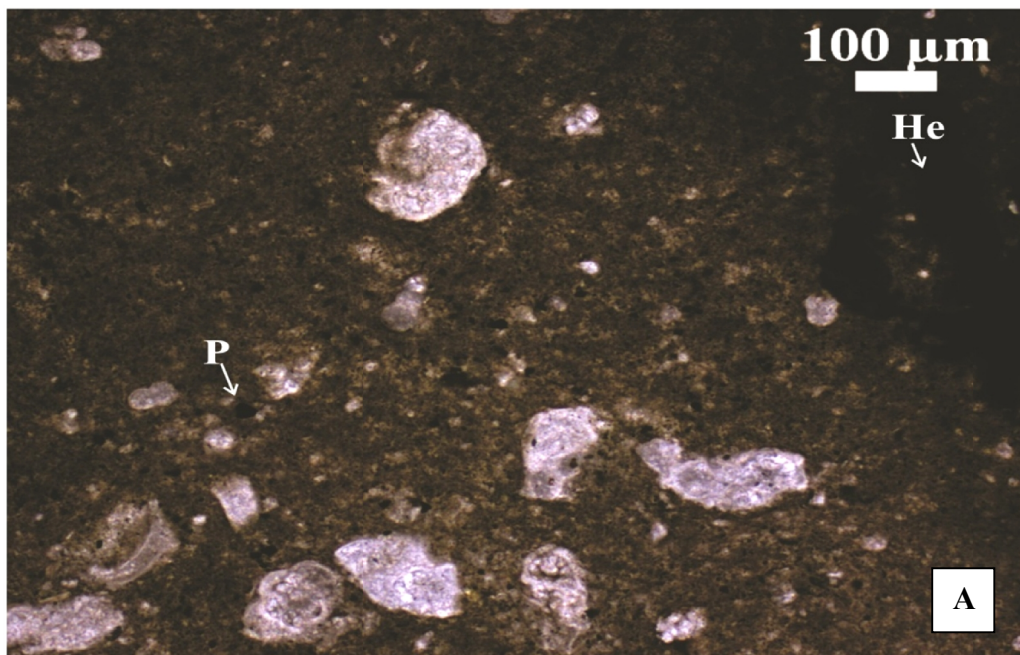


Figure 3.9: Photomicrographs of the greenish to gray mudstone microfacies containing quartz (Q), pyrite (P), hematite (He), planktonic foraminifers and matrix and yellow line shows bioturbation (Sample no. ZR07, (A) PPL x4; ZR21, (B) PPL x4).

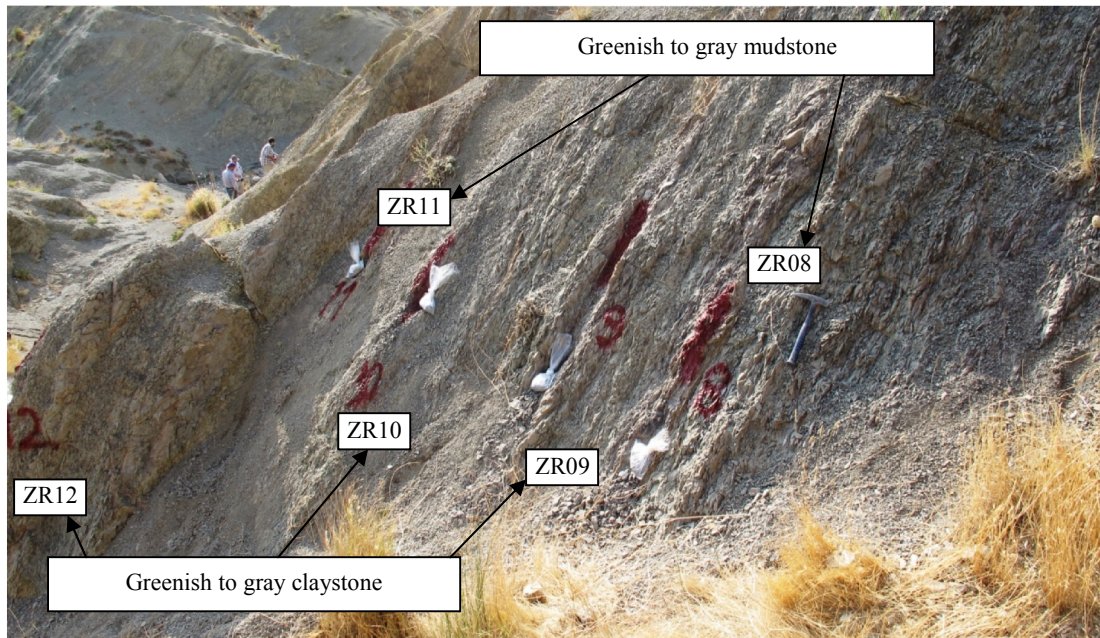


Figure 3.10: The field photograph showing the greenish to gray mudstone and claystone of the Alagöz measured section.

mudstone microfacies (Figure 2.7). The claystone facies are medium gray (N5), greenish gray (5G 6/1-5GY 6/1), medium bluish gray (5B 5/1), medium dark gray (N4) and flaggy to very thin bedded with generally characterized as fissility (Figure 3.10). It is consisting of silt-size, angular to sub-angular quartz, bioclasts along with trace amount of mica, glauconite, iron oxides which are embedded in the clayey matrix (Figure 3.11 A, 3.11 B). Pyrite and pyritization in the chambers of fossil has been observed.

Planktonic foraminifers, rare benthic foraminifers, bivalve and few neomorphosed fossils are recognized. The infilling micro-burrow has not very commonly been observed in the facies. The middle unit of measured stratigraphic section is characterized by this microfacies (Figure 2.7).

3.2.5 RED SILTSTONE

In the fine clastic rocks, the siltstone is defined as hard rock composed of around 66

percent of silt size quartz grains and accessory minerals (Folk, 1965; Pettijohn, 1975). In the studied area, Siltstone lithofacies represents moderate red (5R 4/6) to grayish red (5R 4/2), thin bedded and occasionally bearing lime mudstone of grains (Figure 3.7). It is comprised of silt and very fine sand sizes, angular to sub-angular quartz grains with association of lithic fragments of lime mudstone, chert, volcanogenic glass and calcite (Figure 3.12 A, 3.12 B). The accessory minerals are plagioclase, mica, pyroxene, glauconite, pyrite and iron oxides. Proportionally, it represents more than or equal to 66% silts-size to very fine sand size quartz grain and other minerals. This lithofacies is confined to lower unit of measured stratigraphic section (Figure 2.7).

3.3 SEDIMENTARY STRUCTURE IN THE ALAGÖZ STRATIGRAPHIC SECTION

Sedimentary structures in the Alagöz stratigraphic section that have been observed in field and microscopic level are as below;

I. BEDDING AND LAMINATION

The bedding of the Alagöz section are very thin to medium bedded with shaly (fissility feature) to flaggy characteristics (Figures 3.10, 3.13, 3.15). Limestone units in the studied section represent thin to medium bedding.

II. BIOTURBATION

Bioturbation is determined mostly at microscopic level. In the field, it has been noticed in lower unit which shows dentritic pattern infilling structures in the marls (Figure 2.9 B). They are frequently present in red beds and rarely in the greenish gray beds. The infilling materials in micro-burrows comprises of dark color mud with some silt-size quartz grains (Figure 3.9 B).

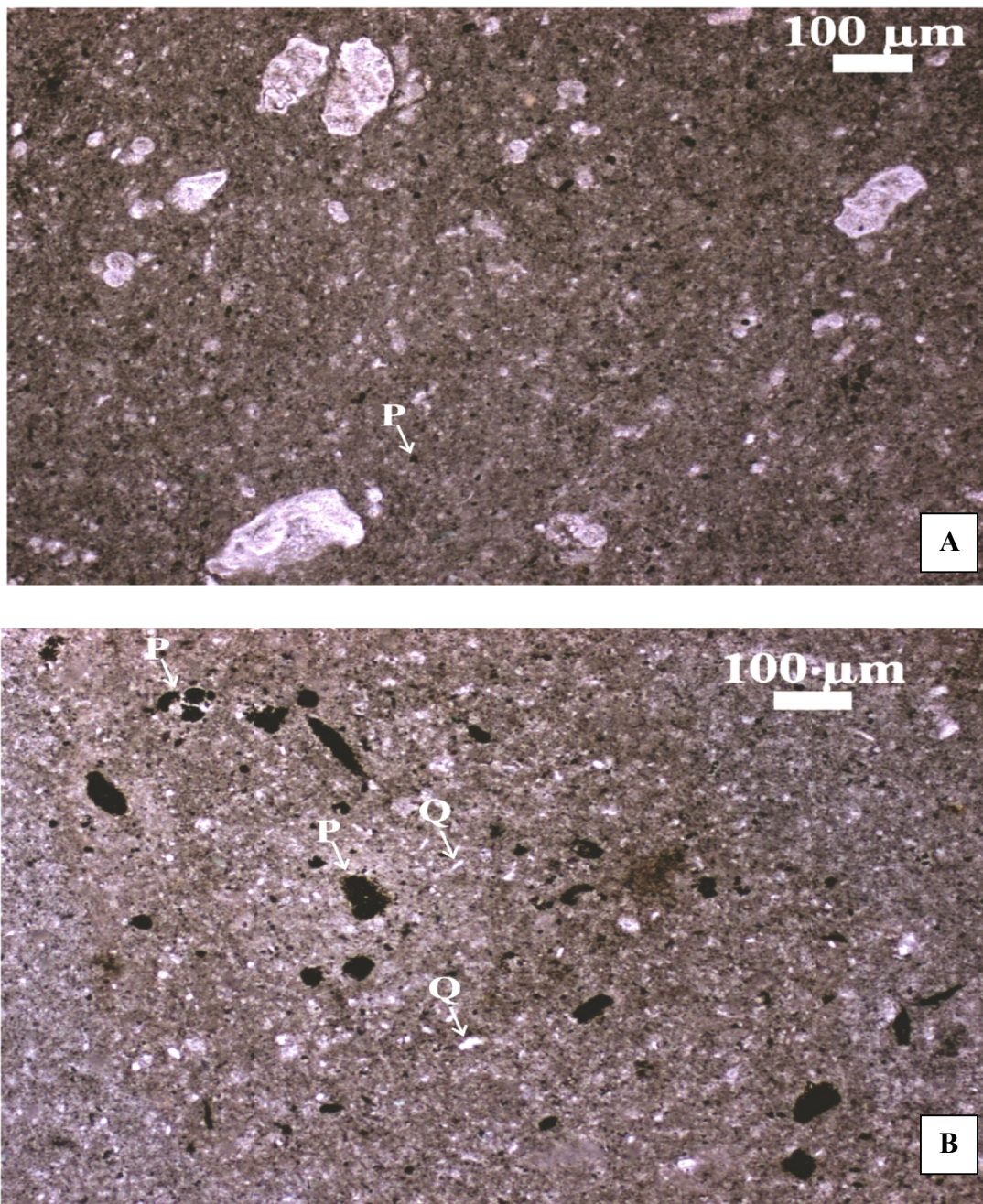


Figure 3.11: Photomicrographs of the greenish to gray claystone microfacies representing quartz (Q), pyrite (P), planktonic foraminifers embedded in matrix (Sample no. ZR09, (A) PPL x4; ZR18, (B) PPL x4).

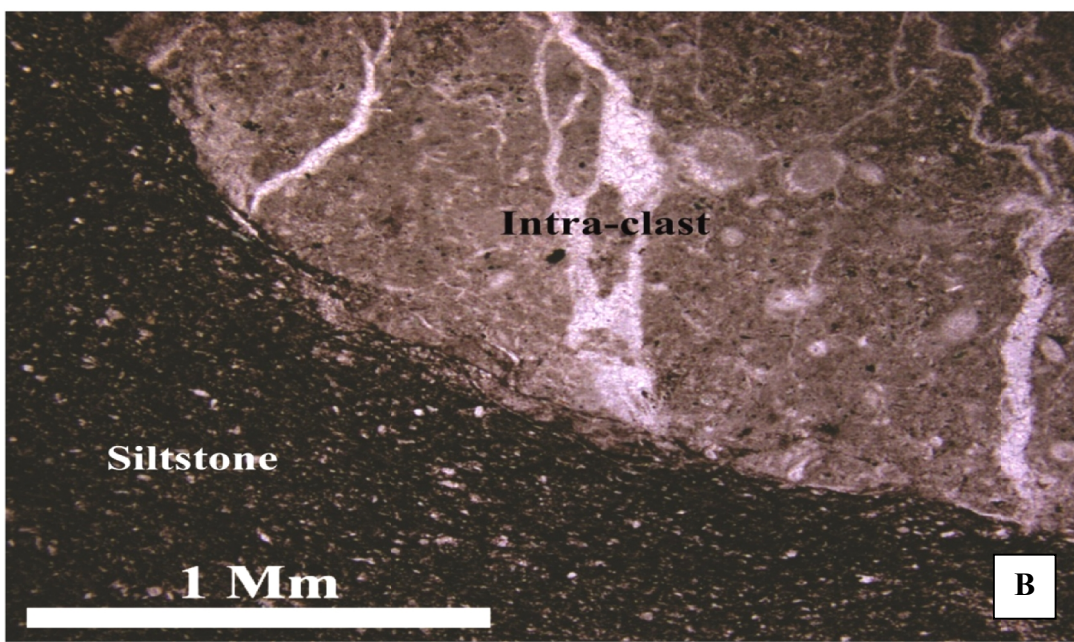
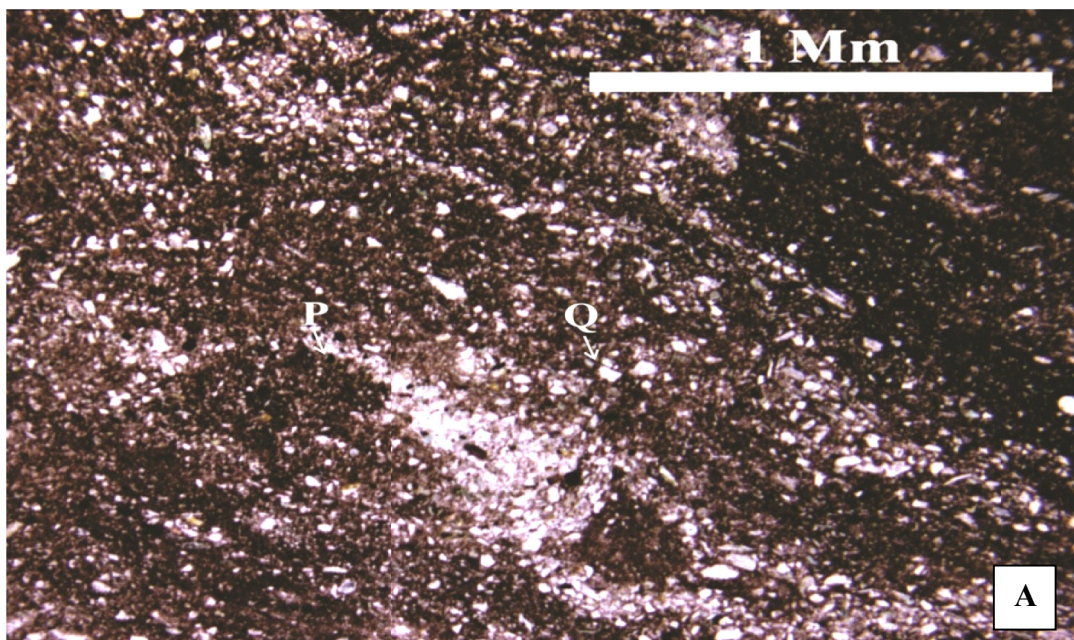


Figure 3.12: Photomicrographs of the red siltstone facies containing quartz (Q), intra-clast of lime mudstone and iron rich matrix (He) (Sample no. ZR01 x2.5, **(A)** PPL; ZR04a, **(B)** PPL x2.5).

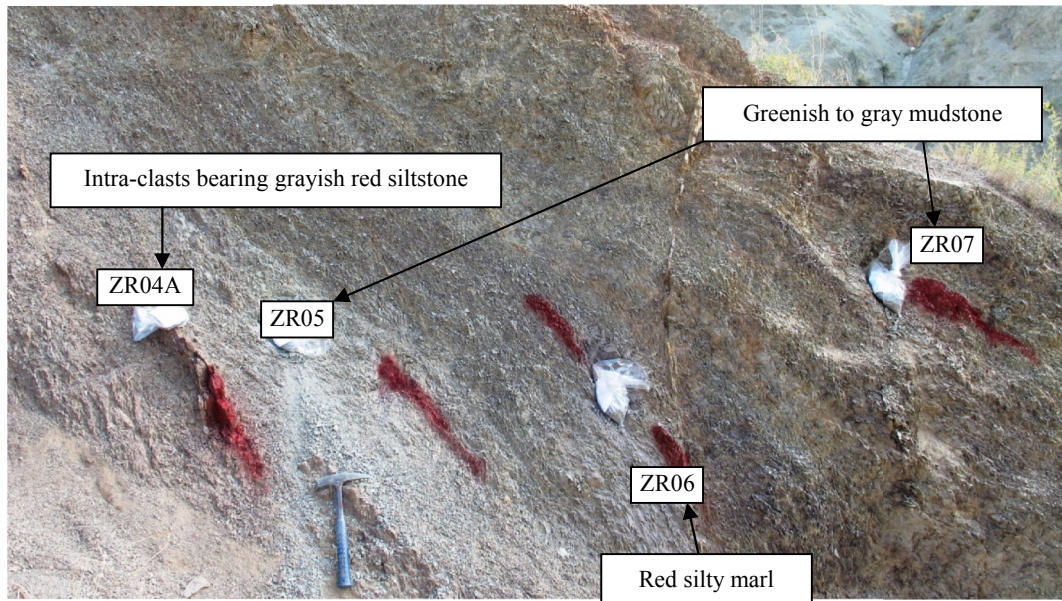


Figure 3.13: The field photograph showing transitional zone between the red beds and greenish to gray mudstone of the Alagöz measured section.



Figure 3.14: The field photograph showing the medium dark gray mudstone with flaggy appearance of the Alagöz measured section.



Figure 3.15: Close view field photograph showing the greenish gray claystone of the Alagöz measured section.



Figure 3.16: Close view field photograph showing the grayish red intra-clastic (lime mudstone fragment) bearing siltstone of the Alagöz measured section (sample no. ZR04a).

3.4 MICROFACIES OF GÖYNÜK SECTION

According to the field observation and microscopic analysis, a total of five microfacies are recognized in the Göynük measured stratigraphic section. The microfacies are described as below (Tables 3.4-3.5);

3.4.1 RED TO BROWNISH MARL

The Göynük Section Marl microfacies are light red (5R 6/6), moderate red (5R 5/4), dusky red (5R ¾), brownish gray (5YR 4/1) and thin to medium bedded with flaggy character (Figures 3.20-3.21). In the contrast to the Alagöz Section, it comprises of abundant planktonic foraminifers along with few inoceramus fragments, rare bivalve and benthic foraminifers (Figures 3.17 A, 3.17 B) and association of minor amount of silt size quartz grains. Other accessory minerals are feldspar, plagioclase, mica, glauconite, green and brown biotite, lithic-clasts (volcanogenic, calcite fragments) and a few phosphatic minerals. Pyrite is observed randomly within the iron rich matrix.

According to Stow (2005), the facies will be characterized as marl i.e. soft and composed of more than 25% calcareous biogenic clasts and less than 12.5% siliceous biogenic clasts/siliciclastic grains following which, it is categorized as marl microfacies. Some fossils chambers are infiltrated by iron oxides, pyrite and silica. Laminations are due to the concentrated layers of fossils within the matrix (Figure 3.17 B). Micro-bioturbation are present however not very common in the microfacies. These micro-burrows suggest oxic condition in deep marine environment. This microfacies is restricted to lower portion of measured stratigraphic section (Figure 2.11).

3.4.2 GREENISH TO GRAY MUDSTONE

Mudstone microfacies has been observed throughout the green-gray beds of the measured stratigraphic section (Figure 2.11). Mudstone beddings represent pale green to grayish yellow green (5G 7/2-5GY 7/2), light greenish gray (5GY 8/1), grayish yellow

Table 3.4: Petrographic data and established/recognized microfacies from Göynük Section samples.

Sample No.	Quartz	Feldspar (F)/ Plagioclase (P)	Mica	Glauconite	Heavy minerals	Lithic-clasts (Volcano-genic* /Rock Fragment^)	Bioclasts (Ra/Pf/In/S/B/Bi/E)	Other (P-OM^/He/Ph)	Matrix (Lm/Cl/ Op/G)	Nomenclature (Texture/Compositional)
GOZ-0	9.5	-	0.06	-	-	0.02^	18.50 Pf/0.03In/0.01B=18.54	0.2P^/0.02Ph=0.22	71.66Cl	Pale green Claystone
GOZ-1	12.5	-	0.07	0.01	0.01	0.02^	23.90 Pf/0.07In/0.01Bf=23.98	0.2P^/0.01Ph=0.21	63.20Cl	Red Marl
GOZ-2	12.4	0.02F	0.07	0.01	0.02	0.01*/0.02^=0.03	24.50 Pf/0.01Bi=24.51	0.43P^/0.17He/0.02Ph=0.62	62.32Cl	Red Marl
GOZ-3	8.1	0.02P	0.09	-	0.01	0.02*	28.52 Pf/0.02B/0.02Bi=28.56	0.35P^/0.38He/0.02Ph=0.75	62.45Cl	Red Marl
GOZ-4	9.09	-	0.2	-	-	-	26.80 Pf/0.01B/0.01Bi=26.82	0.65P^/0.2He/0.15Ph=1.0	62.89Cl	Red Marl
GOZ-5	8.08	-	0.05	0.06	-	0.03*	27.90 Pf/0.05In/0.01B=27.96	0.6P^/0.2He/0.18Ph=0.98	62.84Cl	Brownish Marl
GOZ-6	8.2	-	0.03	0.05	-	0.02*/0.02^=0.04	27.08 Pf/0.05In/0.03B=27.16	0.5P^/0.2He/0.06Ph=0.76	63.76Cl	Brownish Marl
GOZ-7	6.72	0.02P	0.3	-	-	0.03^	27.80 Pf/0.01B=27.81	0.4P^/0.6He/0.08Ph=1.08	64.04Cl	Brownish Marl
GOZ-8	8.4	0.03P	0.3	-	-	0.06^	25.83 Pf/0.02B/0.01Bi=25.86	1.1P^/0.6He^/0.3Ph=2.0	63.35Cl	Brownish Marl
GOZ-9	25.36	0.05P	0.3	0.08	-	0.02*/0.04^=0.06	7.30 Pf/0.2In/0.04B=7.54	0.32P^/0.55He/0.03Ph=0.9	65.71Cl	Yellowish Claystone
GOZ-10	6.1	-	0.3	-	-	0.01*/0.06^=0.07	21.1 Pf/5.9In/0.01Bi=27.01	0.6P^/0.05Ph=0.65	65.87Cl	Greenish Claystone
GOZ-11	37.76	0.08P	0.6	-	0.01	0.03*/0.03^=0.06	1.1 Pf	3.3P^/2.1He/0.05Ph=5.45	54.94Cl	Greenish Mudstone
GOZ-12	4.3	-	0.06	-	0.02	-	27.60 Pf/0.5In/0.02B=28.12	1.0P^/0.06Ph=1.06	66.44Cl	Greenish Claystone
GOZ-13	10.72	0.03P	-	-	-	0.03^	22.90 Pf/0.5In/0.01B=23.41	1.9P^/0.4He/0.04Ph=2.33	62.94Cl	Greenish Gray Mudstone
GOZ-14	22.8	0.02F/0.06P=0.08	1	-	-	0.01*/0.04^=0.04	3.30 Pf/0.04B=3.34	0.9P^/0.3He/0.05Ph=1.25	71.49Cl	Greenish Gray Claystone
GOZ-15A	5.8	-	0.04	-	-	-	7.6Ra/14.1 Pf=21.7	1.2P^	71.26Cl	Greenish Gray Claystone
GOZ-15B	61.23	1.8P	2	0.4	0.07	0.03^	-	1.7P^/1.6He/0.06Ph=3.36	31.11Cl	Fine Sandstone /Greenish Gray Quartz-wacke
GOZ-16	14.5	0.03P	0.3	-	-	0.02^	20.90 Pf/3.2In/0.02B/0.01Bi=24.13	0.9P^/0.07Ph=0.97	60.05Cl	Greenish Gray laminated Mudstone
GOZ-17	41.25	0.2P	1.5	-	0.02	0.05^	0.1 Pf	2.35P^/0.6He/0.1Ph = 3.05	53.83Cl	Greenish Gray Mudstone

Ra=Radiolaria, S=Sponge Spicule, In=Inceramus, Pf=Planktonic Fossil, Uf=Unidentified Fossil, P=Pyrite, Om=Organic matter, Ph=Phosphate, Lm=Lime Mud, Cl=Clay, Op=Opal/Silica, E=Echinoid, B=Benthic Foraminifer, Bi=Bivalve

Table 3.4: Continued.

GOZ-18	11.45	0.05P	0.1	-	-	0.03^	26.40 Pf/1.5In/0.02B=27.92	3.1P^/0.1Ph=3.2	57.25Cl	Greenish Gray Mudstone
GOZ-19	63.35	0.1P	1.2	-	0.01	0.02^	-	2.4P^/0.6He=3.0	32.29Cl	Greenish Siltstone
GOZ-20	29.72	0.08P	0.2	0.08	-	0.02*	4.80 Pf/0.1In/0.03B=4.93	4.0P^/0.5He=4.5	60.47Cl	Greenish Mudstone
GOZ-21	16.82	0.04P	-	-	0.01	0.01*/0.02^=0.03	17.30 Pf/0.3In/0.01B=17.61	2.5P^/0.4He/0.02Ph=2.92	62.57Cl	Greenish Mudstone
GOZ-22	13.17	0.01F/0.03P=0.04	0.1	-	-	-	15.10 Pf/0.01B=15.11	5.1P^/0.08Ph=5.18	66.40Cl	Greenish Claystone
GOZ-23	15.5	-	0.05	-	-	-	13.11 Pf/0.01B=13.12	2.2P^/0.1Ph=2.3	69.03Cl	Greenish Claystone
GOZ-24	15.35	-	0.1	-	-	0.02^	1510 Pf/0.01B=15.11	2.9P^/0.4He/0.05Ph=3.35	66.07Cl	Greenish Claystone
GOZ-25	17.54	-	0.1	-	-	0.02*/0.05^=0.07	18.70 Pf/0.03B=18.73	1.9P^/0.7He/0.02Ph=2.62	60.94Cl	Greenish Mudstone
GOZ-26	12.56	-	0.1	0.01	-	0.04^	19.10 Pf/0.3In=19.4	1.9P^/0.1Ph=2.0	65.89Cl	Greenish Claystone
GOZ-27	12.34	-	-	-	-	-	29.8 Pf/0.01B=29.81	1.3P^/0.1Ph=1.4	56.45Cl	Greenish Gray Mudstone
GOZ-28	66.18	0.06F/0.1P =0.16	1.5	0.5	0.05	0.04*/0.06^=0.1	0.09 Pf/0.01B=0.1	7.1P^/0.3He/0.03Ph=7.43	23.98Cl	Fine Sandstone /Greenish Gray Quartz-wacke
GOZ-29	13.53	-	0.1	0.04	0.02	0.03^	21.63 Pf/1.0In=22.63	0.8P^/0.1He/0.04Ph=0.94	62.71Cl	Light Gray Mudstone
GOZ-30	29.1	0.04P	0.1	-	-	-	7.62 Pf/0.01B=7.63	4.8P^/0.21He=5.01	58.12Cl	Greenish Mudstone
GOZ-31	15.1	0.01F/0.05P=0.06	0.1	-	-	0.01*/0.02^=0.03	19.70 Pf/12.1In=31.8	1.1P^/0.22Ph=1.32	51.59Cl	Greenish Mudstone
GOZ-32	11.5	0.01F/0.05P=0.06	0.04	0.05	-	-	19.52 Pf/0.5In/0.03B=20.05	1.5P^/0.18Ph=1.68	66.62Cl	Greenish Claystone
GOZ-33	10.64	-	0.08	-	-	-	0.35Rat/19.32 Pf/0.03B=19.7	2.8P^/0.1Ph=2.9	66.78Cl	Greenish Claystone
GOZ-34a	66.2	0.06F/0.25P=0.31	1.5	0.02	0.3	0.01*/0.06^=0.07	0.06 Pf	6.9P^/0.2He/0.06Ph=7.16	24.38Cl	Fine Sandstone/ Greenish Quartz-wacke
GOZ-34b	26.3	0.07P	0.2	-	-	0.01*/0.01^=0.02	0.9 Pf	2.3P^/0.08Ph=2.38	70.13Cl	Greenish Claystone
GOZ-35	13.34	-	0.05	0.02	-	-	16.10 Pf/0.02B=16.12	3.1P^/0.04Ph=3.14	67.33Cl	Greenish Claystone
GOZ-36	15.87	0.02F/0.05P=0.07	0.1	-	0.07	0.04^	20.20 Pf/0.02B=20.22	3.4P^/0.05Ph=3.45	59.98Cl	Greenish laminated Mudstone

Ra=Radiolaria, S=Sponge Spicule, In=Inceramus, Pf=Planktonic Fossil, Uf=Unidentified Fossil, P=Pyrite, Om=Organic matter, Ph=Phosphate, Lm=Lime Mud, Cl=Clay, Op=Opal/Silica, E=Echinoid, B=Benthic Foraminifer, Bi=Bivalve

Table 3.4: Continued.

GOZ-37	11.35	-	0.1	-	-	-	21.10 Pf/0.03B=21.13	1.3P^/0.06Ph=1.36	66.06Cl	Greenish Claystone
GOZ-38	69.9	0.04F/0.15P=0.19	0.5	0.06	0.1	0.03*/0.05^=0.08	0.02 Pf	5.1P^	24.05Cl	Fine Sandstone /Greenish Quartz-wacke
GOZ-39	7.9	-	-	-	-	0.01^	3.1Gt/9.4Gr/0.4In/5.9Pf=18.8 0	2.9P^/0.06Ph=2.96	70.33Cl	Greenish Claystone
GOZ-40	13.4	0.03P	-	-	-	-	8.5Gt/16.2Gr/0.9In/4.4Pf=29. 9	0.4P^/0.02Ph=0.42	56.25Cl	Greenish Mudstone
GOZ-41 (Lower)a	63.65	0.06P	0.1	0.02	-	0.05^	-	2.2P^	32.92Cl	Gray Siltstone
GOZ-41 (Upper)b	58.98	0.08P	1.9	0.07	0.3	0.02*/0.07^=0.09	-	6.1P^/0.04Ph=6.14	32.44Cl	Fine Sandstone /Gray Quartz-wacke
GOZ-42	60.95	0.7P	0.5	0.06	0.3	0.03*/0.04^=0.07	0.02 Pf	7.1P^/0.1Ph=7.2	30.20Cl	Fine Sandstone/Greenish Quartz-wacke
GOZ-43	8.48	0.04P	0.1	-	-	0.02^	27.90 Pf/0.02B=27.92	0.9P^/0.09Ph=0.99	62.45Cl	Light Gray Mudstone
GOZ-44	47.55	0.05P	0.3	-	-	-	1.6 Pf	5.25P^	44.22Cl	Light Gray Mudstone
GOZ-45 (Lower)a	33.95	0.02P	0.2	0.06	0.01	-	-	4.1P^	61.66Cl	Light Gray Mudstone
GOZ-45 (Middle)b	60.82	0.12P	0.2	0.08	0.04	-	0.38 Pf	5.9P^	32.46Cl	Light Gray Siltstone
GOZ-45 (Upper)c	49.3	0.08P	0.1	0.08	0.02	-	-	5.9P^	44.52Cl	Light Gray Mudstone
GOZ-46	8.27	0.03P	0.1	-	-	0.01*	29 Pf/0.05In=29.05	1.7P^/0.14Ph=1.84	60.70Cl	Light Gray Mudstone
GOZ-47	33.15	-	0.5	-	-	0.02^	4.99 Pf	1.0P^/0.7He/0.08Ph= 1.78	58.56Cl	Light Gray Mudstone
GOZ-48	60.21	0.04P	0.4	-	-	0.02^	0.07 Pf	8.5P^	32.76Cl	Light Gray Siltstone
GOZ-49 (Lower)a	12.6	0.02P	-	-	-	0.01*	18.10 Pf/0.08In/0.01B=18.19	0.7P^	68.49Cl	Light Gray Claystone
GOZ-49 (Middle)b	63.65	0.05P	1	0.4	0.1	-	-	4.5P^/0.04Ph=4.54	29.26Cl	Fine Sandstone/Greenish Quartz-wacke
GOZ-49 (Upper)c	47.5	-	0.2	0.07	-	-	0.03 Pf	2.1P^	50.1Cl	Light Gray Mudstone
GOZ-50	28.7	-	0.1	-	-	-	0.12 Pf	5.1P^/0.08Ph=5.78	65.90Cl	Gray Claystone
GOZ-51	60.37	0.08P	0.5	0.02	0.02	-	-	5.7P^	32.31Cl	Gray Siltstone
GOZ-52	38.2	0.06P	-	0.07	-	-	-	5.1P^	56.57Cl	Gray Mudstone

Ra=Radiolaria, S=Sponge Spicule, In=Inceramus, Pf=Planktonic Fossil, Uf=Unidentified Fossil, P=Pyrite, Om=Organic matter, Ph=Phosphate, Lm=Lime Mud, Cl=Clay, Op=Opal/Silica, E=Echinoid, B=Benthic Foraminifer, Bi=Bivalve

Table 3.5: Classifications of the Göynük section based on compositional, grain size and texture parameters.

Göynük Section Classification							
Sample	Compositional Classification			Grains Size Classification		Texture Classification	This Studied (Texture and/or Compositional)
	Diaz's (2012) Mudstone (Unconventional)	Stow's (2005) (Biogenic +Clay/Mud)	Allix's (2010) Shale	Stow's (2005) Silic-Clastic	Picard's (1971)	Folk's (1965)	
GOZ-0	Carbonate-rich Argillaceous Mudstone	Marl	Argillaceous Mudstone	Mud	Bio/Sandy-Claystone	Clay-Shale	Claystone
GOZ-1	Mixed Argillaceous Mudstone	Marl	Argillaceous Mudstone	Mud	Bio/Sandy-Claystone	Mud-Shale	Marl
GOZ-2	Mixed Argillaceous Mudstone	Marl	Argillaceous Mudstone	Mud	Bio/Sandy-Claystone	Mud-Shale	Marl
GOZ-3	Carbonate-rich Argillaceous Mudstone	Marl	Argillaceous Marlstone	Mud	Bio/Sandy-Claystone	Mud-Shale	Marl
GOZ-4	Carbonate-rich Argillaceous Mudstone	Marl	Argillaceous Mudstone	Mud	Bio/Sandy-Claystone	Mud-Shale	Marl
GOZ-5	Carbonate-rich Argillaceous Mudstone	Marl	Argillaceous Mudstone	Mud	Bio/Sandy-Claystone	Mud-Shale	Marl
GOZ-6	Carbonate-rich Argillaceous Mudstone	Marl	Argillaceous Mudstone	Mud	Bio/Sandy-Claystone	Mud-Shale	Marl
GOZ-7	Carbonate-rich Argillaceous Mudstone	Marl	Argillaceous Mudstone	Mud	Bio/Sandy-Claystone	Mud-Shale	Marl
GOZ-8	Carbonate-rich Argillaceous Mudstone	Marl	Argillaceous Mudstone	Mud	Bio/Sandy-Claystone	Mud-Shale	Marl
GOZ-9	Silica-rich Argillaceous Mudstone	Sarl	Argillaceous Mudstone	Mud	Silty-Claystone	Clay-Shale	Claystone
GOZ-10	Carbonate-rich Argillaceous Mudstone	Marl	Argillaceous Mudstone	Mud	Bio/Sandy-Claystone	Clay-Shale	Claystone
GOZ-11	Silica-rich Argillaceous Mudstone	Sarl	Argillaceous Mudstone	Mud	Silty-Claystone	Mud-Shale	Mudstone
GOZ-12	Carbonate-rich Argillaceous Mudstone	Marl	Argillaceous Mudstone	Mud	Bio/Sandy-Claystone	Clay-Shale	Claystone
GOZ-13	Mixed Argillaceous Mudstone	Marl	Argillaceous Mudstone	Mud	Bio/Sandy-Claystone	Mud-Shale	Mudstone
GOZ-14	Silica-rich Argillaceous Mudstone	Sarl	Argillaceous Mudstone	Mud	Silty-Claystone	Clay-Shale	Claystone
GOZ-15A	Carbonate-rich Argillaceous Mudstone	Marl	Argillaceous Mudstone	Mud	Bio/Sandy-Claystone	Clay-Shale	Claystone
GOZ-15B	Fine Sandstone/Quartz-wacke (Folk's 1974)						
GOZ-16	Mixed Argillaceous Mudstone	Smarl	Argillaceous Mudstone	Mud	Bio/Sandy-Claystone	Mud-Shale	Mudstone
GOZ-17	Silica-rich Argillaceous Mudstone	Sarl	Argillaceous Mudstone	Mud	Silty-Claystone	Mud-Shale	Mudstone
GOZ-18	Mixed Argillaceous Mudstone	Marl	Argillaceous Mudstone	Mud	Bio/Sandy-Claystone	Mud-Shale	Mudstone
GOZ-19	Clay-rich Argillaceous Mudstone	Sarl	Siliceous Mudstone	Mud	Clayey-Siltstone	Silt-Shale	Siltstone
GOZ-20	Silica-rich Argillaceous Mudstone	Sarl	Argillaceous Mudstone	Mud	Silty-Claystone	Mud-Shale	Mudstone
GOZ-21	Mixed Argillaceous Mudstone	Smarl	Argillaceous Mudstone	Mud	Bio/Sandy-Claystone	Mud-Shale	Mudstone
GOZ-22	Mixed Argillaceous Mudstone	Smarl	Argillaceous Mudstone	Mud	Bio/Sandy-Claystone	Clay-Shale	Claystone
GOZ-23	Mixed Argillaceous Mudstone	Smarl	Argillaceous Mudstone	Mud	Silty-Claystone	Clay-Shale	Claystone
GOZ-24	Mixed Argillaceous Mudstone	Smarl	Argillaceous Mudstone	Mud	Silty-Claystone	Clay-Shale	Claystone
GOZ-25	Mixed Argillaceous Mudstone	Smarl	Argillaceous Mudstone	Mud	Bio/Sandy-Claystone	Mud-Shale	Mudstone
GOZ-26	Mixed Argillaceous Mudstone	Smarl	Argillaceous Mudstone	Mud	Bio/Sandy-Claystone	Clay-Shale	Claystone
GOZ-27	Mixed Argillaceous Mudstone	Smarl	Argillaceous Mudstone	Mud	Bio/Sandy-Claystone	Mud-Shale	Mudstone
GOZ-28	Fine Sandstone/Quartz-wacke (Folk's 1974)						
GOZ-29	Mixed Argillaceous Mudstone	Smarl	Argillaceous Mudstone	Mud	Bio/Sandy-Claystone	Mud-Shale	Mudstone
GOZ-30	Silica-rich Argillaceous Mudstone	Sarl	Argillaceous Mudstone	Mud	Silty-Claystone	Mud-Shale	Mudstone
GOZ-31	Mixed Argillaceous Mudstone	Smarl	Argillaceous Mudstone	Mud	Bio/Sandy-Claystone	Mud-Shale	Mudstone
GOZ-32	Mixed Argillaceous Mudstone	Marl	Argillaceous Mudstone	Mud	Bio/Sandy-Claystone	Clay-Shale	Claystone
GOZ-33	Mixed Argillaceous Mudstone	Marl	Argillaceous Mudstone	Mud	Bio/Sandy-Claystone	Clay-Shale	Claystone

Table 3.5: Continued.

GOZ-34 a	Fine Sandstone/Quartz-wacke (Folk's 1974)						
GOZ-34 b	Silica-rich Argillaceous Mudstone	Sarl	Argillaceous Mudstone	Mud	Silty-Claystone	Clay-Shale	Claystone
GOZ-35	Mixed Argillaceous Mudstone	Smarl	Argillaceous Mudstone	Mud	Bio/Sandy-Claystone	Clay-Shale	Claystone
GOZ-36	Mixed Argillaceous Mudstone	Smarl	Argillaceous Mudstone	Mud	Bio/Sandy-Claystone	Mud-Shale	Mudstone
GOZ-37	Mixed Argillaceous Mudstone	Marl	Argillaceous Mudstone	Mud	Bio/Sandy-Claystone	Clay-Shale	Claystone
GOZ-38	Fine Sandstone/Quartz-wacke (Folk's 1974)						
GOZ-39	Carbonate-rich Argillaceous Mudstone	Marl	Argillaceous Mudstone	Mud	Bio/Sandy-Claystone	Clay-Shale	Claystone
GOZ-40	Mixed Argillaceous Mudstone	Smarl	Argillaceous Mudstone	Mud	Bio/Sandy-Claystone	Mud-Shale	Mudstone
GOZ-41 (Lower) a	Clay-rich Siliceous Mudstone	Sarl	Siliceous Mudstone	Mud	Clayey-Siltstone	Silt-Shale	Siltstone
GOZ-41 (Upper) b	Fine Sandstone/Quartz-wacke (Folk's 1974)						
GOZ-42	Fine Sandstone/Quartz-wacke (Folk's 1974)						
GOZ-43	Carbonate-rich Argillaceous Mudstone	Marl	Argillaceous Mudstone	Mud	Bio/Sandy-Claystone	Mud-Shale	Mudstone
GOZ-44	Clay-rich Siliceous Mudstone	Sarl	Siliceous Mudstone	Mud	Clayey-Siltstone	Mud-Shale	Mudstone
GOZ-45 (Lower) a	Silica-rich Argillaceous Mudstone	Sarl	Argillaceous Mudstone	Mud	Silty-Claystone	Mud-Shale	Mudstone
GOZ-45 (Middle)b	Clay-rich Siliceous Mudstone	Sarl	Siliceous Mudstone	Mud	Clayey-Siltstone	Silt-Shale	Siltstone
GOZ-45 (Upper) c	Clay-rich Siliceous Mudstone	Sarl	Siliceous Mudstone	Mud	Clayey-Siltstone	Mud-Shale	Mudstone
GOZ-46	Carbonate-rich Argillaceous Mudstone	Marl	Argillaceous Mudstone	Mud	Bio/Sandy-Claystone	Mud-Shale	Mudstone
GOZ-47	Silica-rich Argillaceous Mudstone	Sarl	Argillaceous Mudstone	Mud	Silty-Claystone	Mud-Shale	Mudstone
GOZ-48	Silica-rich Argillaceous Mudstone	Sarl	Argillaceous Mudstone	Mud	Silty-Claystone	Mud-Shale	Siltstone
GOZ-49 (Lower) a	Mixed Argillaceous Mudstone	Smarl	Argillaceous Mudstone	Mud	Bio/Sandy-Claystone	Clay-Shale	Light Gray Claystone
GOZ-49 (Middle)b	Fine Sandstone/Quartz-wacke (Folk's 1974)						
GOZ-49 (Upper)c	Clay-rich Siliceous Mudstone	Sarl	Argillaceous Mudstone	Mud	Silty-Claystone	Mud-Shale	Mudstone
GOZ-50	Silica-rich Argillaceous Mudstone	Sarl	Argillaceous Mudstone	Mud	Silty-Claystone	Clay-Shale	Claystone
GOZ-51	Clay-rich Siliceous Mudstone	Sarl	Siliceous Mudstone	Mud	Clayey-Siltstone	Silt-Shale	Siltstone
GOZ-52	Silica-rich Argillaceous Mudstone	Sarl	Argillaceous Mudstone	Mud	Silty-Claystone	Mud-Shale	Mudstone

* Based on grains size of mud fraction, nonfissile/fissile and soft.

green (5G 6/1), light green (5G 7/4), moderate yellow green (5GY 7/4), medium gray to medium dark gray (N5-N4) color, flaggy features and thin to thick bedded with intercalation of claystone/marl (Figures 3.21, 3.24, 3.25), which contains abundant bioclasts and silt-size quartz grains. The observed trace minerals are plagioclase, mica, glauconite, pyrite, phosphate, heavy minerals (biotite, chlorite, pyroxene, zircon and monazite) and lithic-clasts (bio-mudstone, shale, calcite and volcanogenic) which are embedded in the matrix (Figures 3.18 A, 3.18 B, 3.19 A, 3.19 B). The point count analysis and visual observation indicates mudstone facies, by comparing with Folk's (1965) and Pettijohn's (1975) mudrock definition.

The identified fossils are planktonic foraminifers, inoceramus fragments (Figures 3.26, 3.18 A), bivalve, benthic foraminifers and neomorphosed fossils. Microbioturbation and laminations have been noticed during microscopic studies. The infilling material in microbioturbation consists of dark mud and silt size quartz grains. The laminations are identified as alternating layers of concentrated planktonic foraminifers (Figure 3.18 A), bivalve, benthic foraminifers and dark matrix. Iron oxides have been observed in the chamber of the fossils and patches within the matrix.

3.4.3 GREENISH TO GRAY CLAYSTONE

Claystone facies contains more than 66% clayey matrix which distinguishes it from mudstone (Folk, 1965; Potter et al., 2005). In the studied area, claystone is differentiated by brilliant green (5G 6/6), pale green (5G 7/2), dark yellowish orange (5GY 8/1), light green (5G 7/4), medium gray to medium dark gray (N5-N4), soft, very thinly bedded to thin bedded and display fissility to flaggy nature (Figure 3.24). It is interbedded with mudstone and red marl throughout the studied section.

Microscopic studies indicated that it is comprised of predominantly clayey matrix (more than 66 %) and relatively low proportion of planktonic foraminifers (Figures 3.22 A, 3.22 B). Inoceramus fragment, calcareous radiolaria, benthic foraminifers and bivalve are also present but few in number. Along with bioclasts, other grains are silt to few

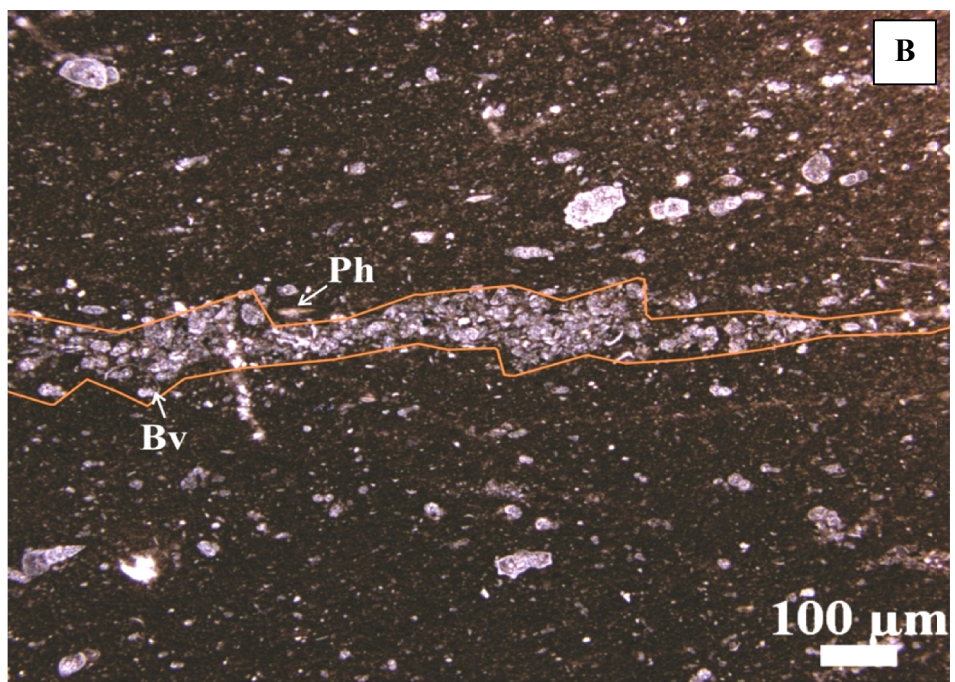
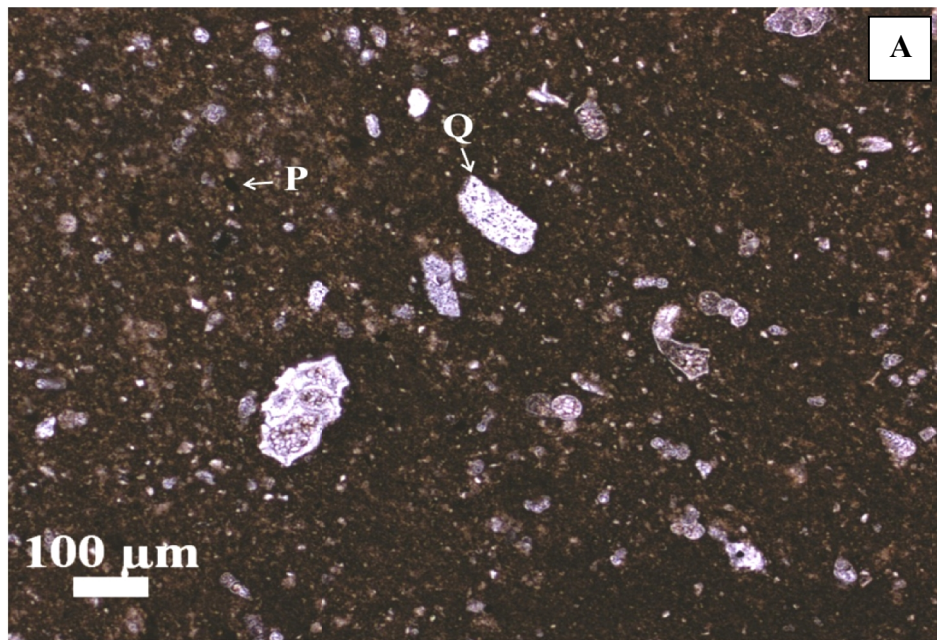


Figure 3.17: Photomicrographs of the red to brownish marl containing quartz (Q), pyrite (P), bivalve (Bv), phosphate (Ph), planktonic foraminifers and matrix and lamination of bioclasts represented by orange line (Sample no. GOZ6, **(A)** PPL x4; GOZ7, **(B)** PPL x2.5).

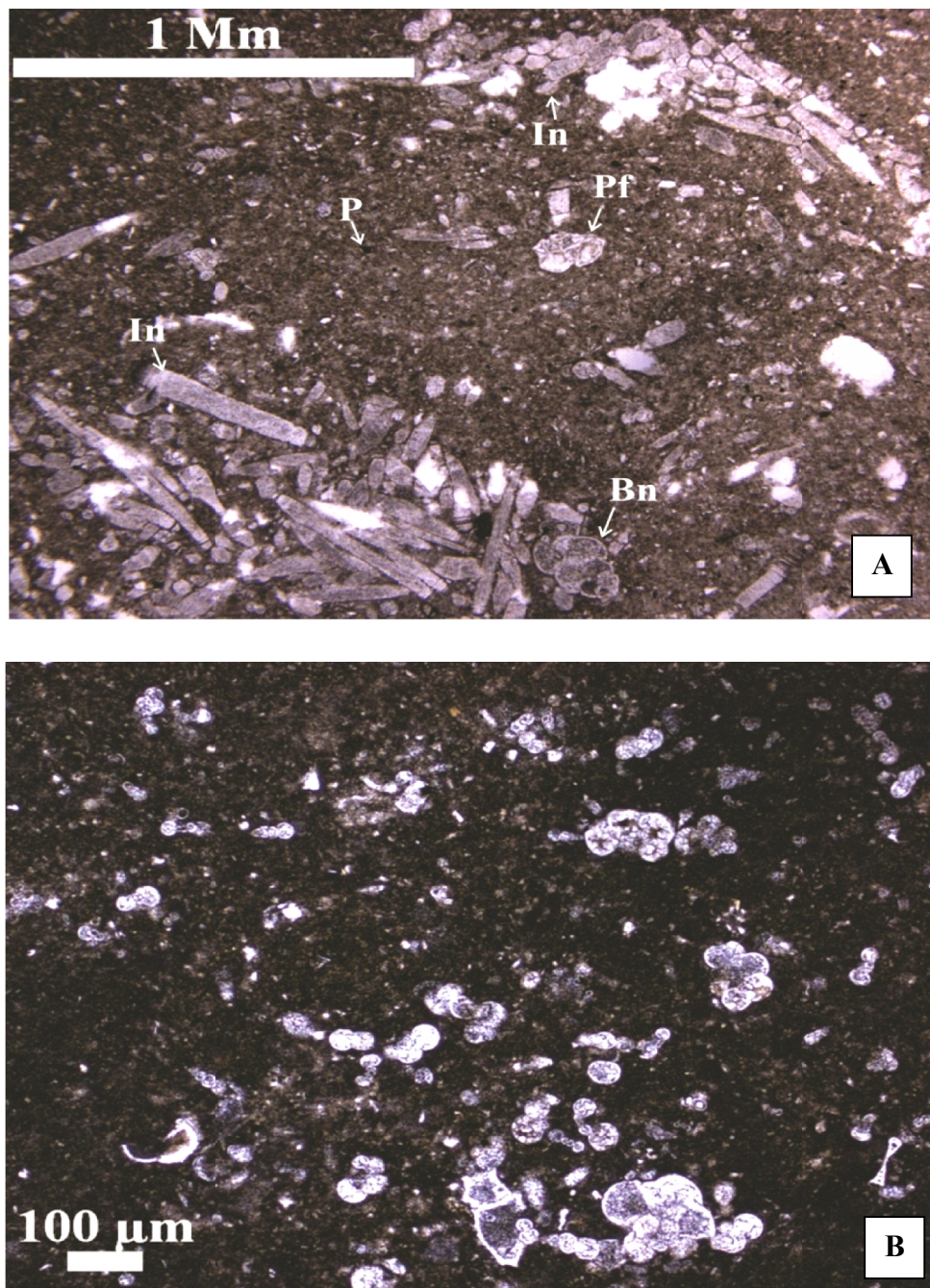


Figure 3.18: Photomicrographs of the greenish to gray mudstone microfacies representing quartz (Q), pyrite (P), inoceramus fragments (In), benthic foraminifers (Bn), planktonic foraminifers (Pf) and phosphate (Ph) (Sample no. GOZ13, **(A)** PPL x2.5; GOZ13, **(B)** PPL x4).

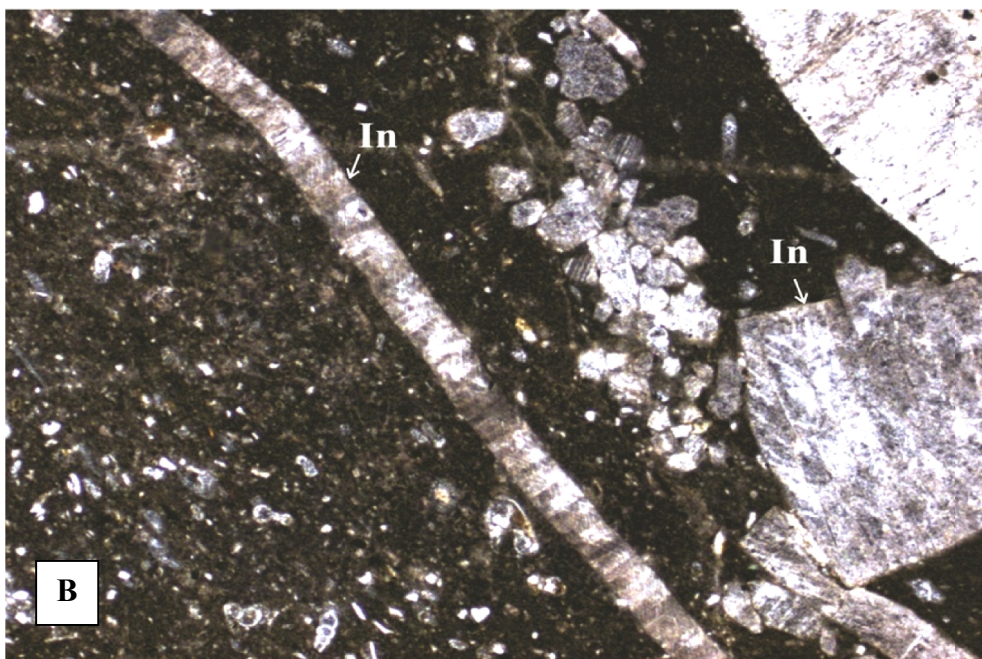
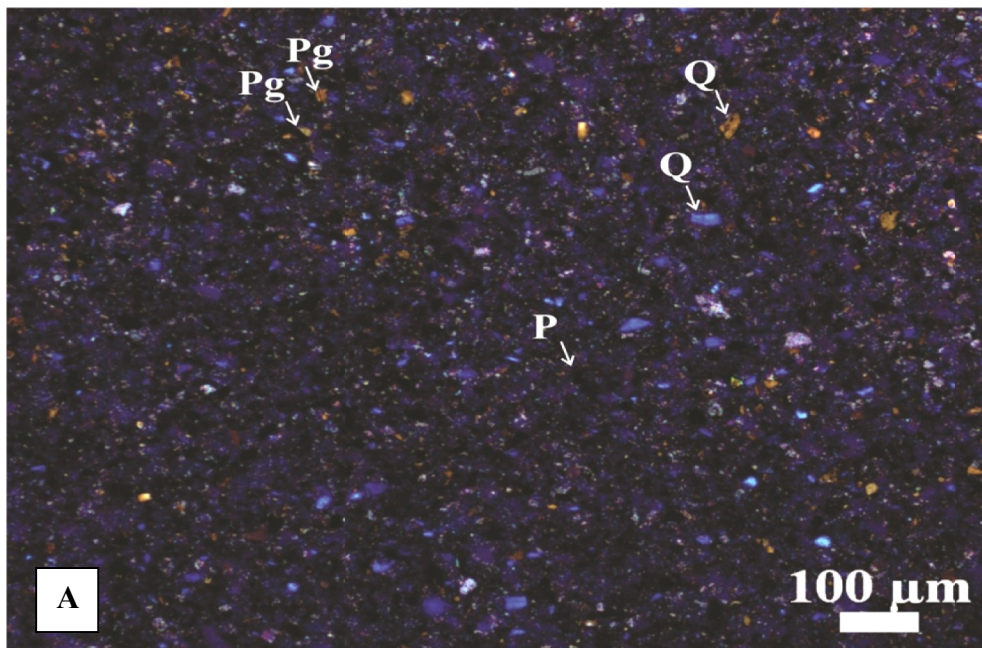


Figure 3.19: Photomicrographs of greenish gray to gray mudstone microfacies containing quartz (Q), pyrite (P), inoceramus fragments (In), plagioclase (Pg) and matrix (Sample no. GOZ17, **(A)** XPL with mica plate x4; **(B)** GOZ25, PPL x4).



Figure 3.20: The field photograph showing the red to brownish marl microfacies of the Göynük Section.

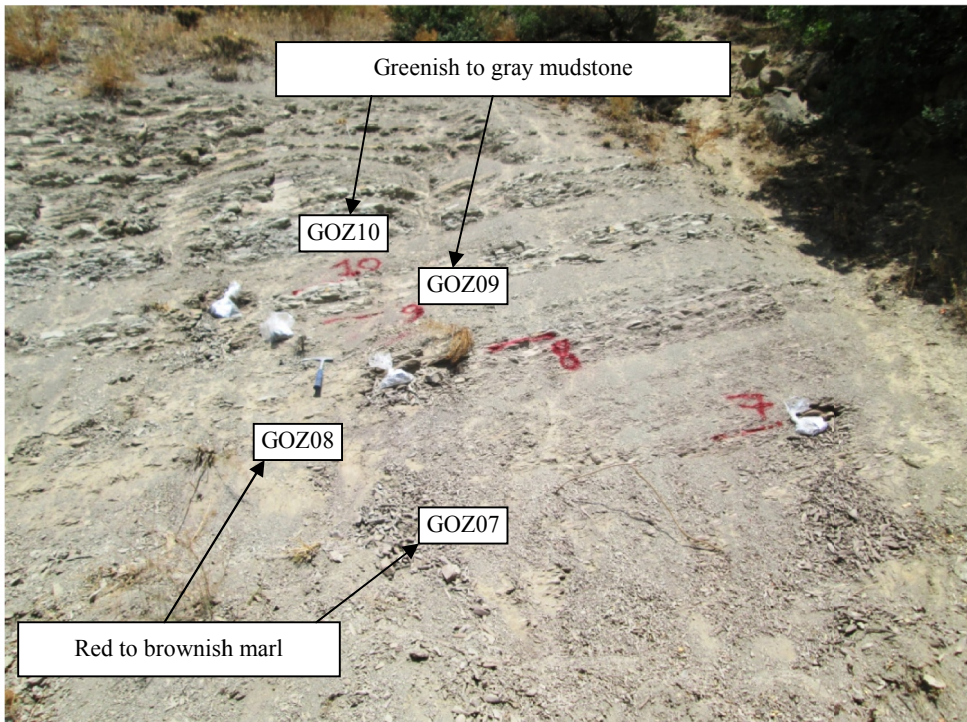


Figure 3.21: The field photograph showing transitional zone between the red beds and the greenish to gray mudstone of the Göynük measured section.

sand size, angular to sub-angular quartz grains and association of trace amount of feldspar, plagioclase, mica, glauconite, blue tourmaline, lithics of volcanogenic and mudstone and shale. Pyrite and phosphate are randomly discriminated throughout the thin sections. Iron oxides infiltrate the few fossils chambers and also observed in matrix in the form of patches. This microfacies represents mostly middle portion of the measured stratigraphic section (Figure 2.11).

3.4.4 GREENISH TO GRAY SILTSTONE

According to Folk (1965) and Pettijohn (1975), siltstone is applied for fine sedimentary rock, which is hard and containing more than 66% silt size quartz grains. The siltstone lithofacies has been observed in the green-gray strata at different stratigraphic levels in the studied section. This lithofacies has been distinguished in the field as laminated (Figure 2.15 C, 2.15 D), thin bedded, hard with pale green (5G 7/2), medium gray to medium dark gray (N5-N4) color (Figures 2.11, 3.25). It is composed of high proportion of silt-size, few sand sizes, angular to sub-angular quartz grains and minor amount of plagioclase, mica, volcanogenic clasts, shale and mudstone clasts, heavy minerals (biotite, chlorite, monazite and zircon), glauconite and rare planktonic foraminifers (Figures 3.23 A, 3.23 B). Pyrite is randomly distributed with a relatively high percentage.

Microbioturbation has been rarely observed, which are in-filled by dark muddy materials. The observed laminae in the lithofacies have been identified as parallel lamina between the alternating layers of high concentration of quartz and matrix (Figure 3.23 A).

3.4.5 GREENISH TO GRAYEY FINE QUARTZWACKE SANDSTONE

Sandstone lithofacies are the coarse grained sedimentary rock as compared to siltstone and mudrock. It is classified with three end member i.e. feldspar-plagioclase member, quartz member and rock fragment member (Folk, 1974). According to Folk's

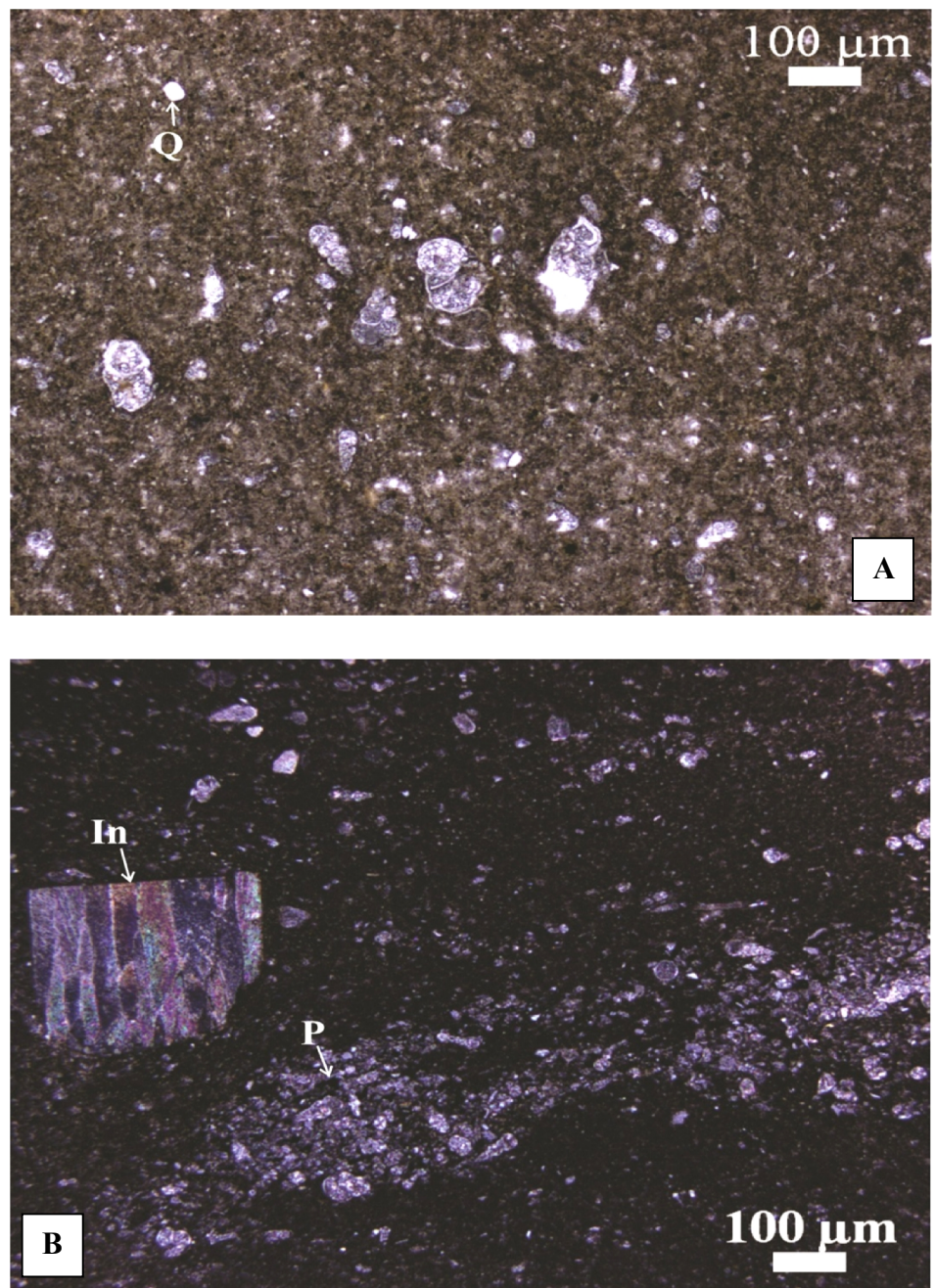


Figure 3.22: Photomicrographs of greenish to gray claystone microfacies containing quartz (Q), pyrite (P), inoceramus fragments (In), planktonic foraminifers and matrix (Sample no. GOZ0, **(A)** PPL x4; GOZ10, **(B)** XPL x2.5).

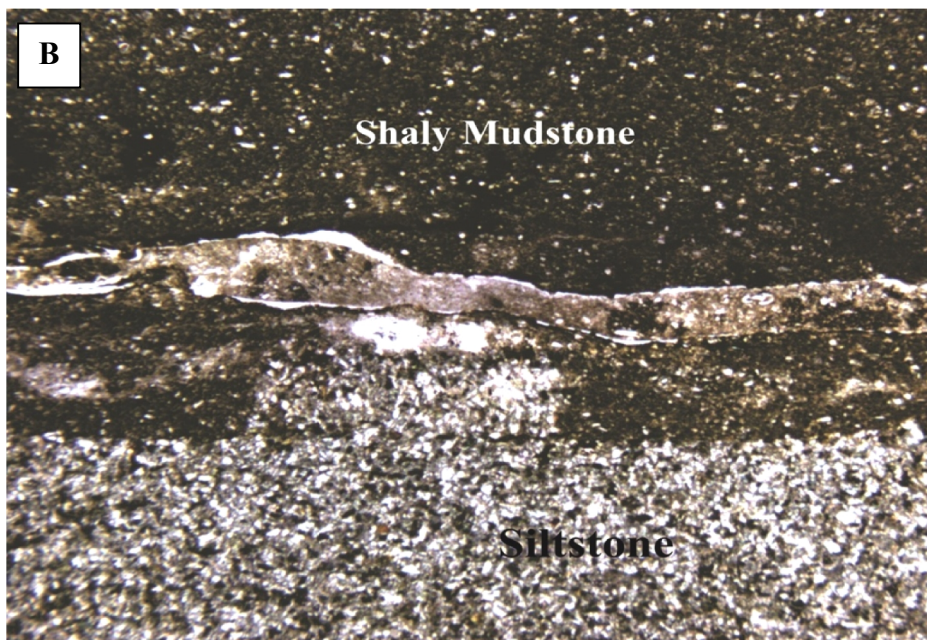
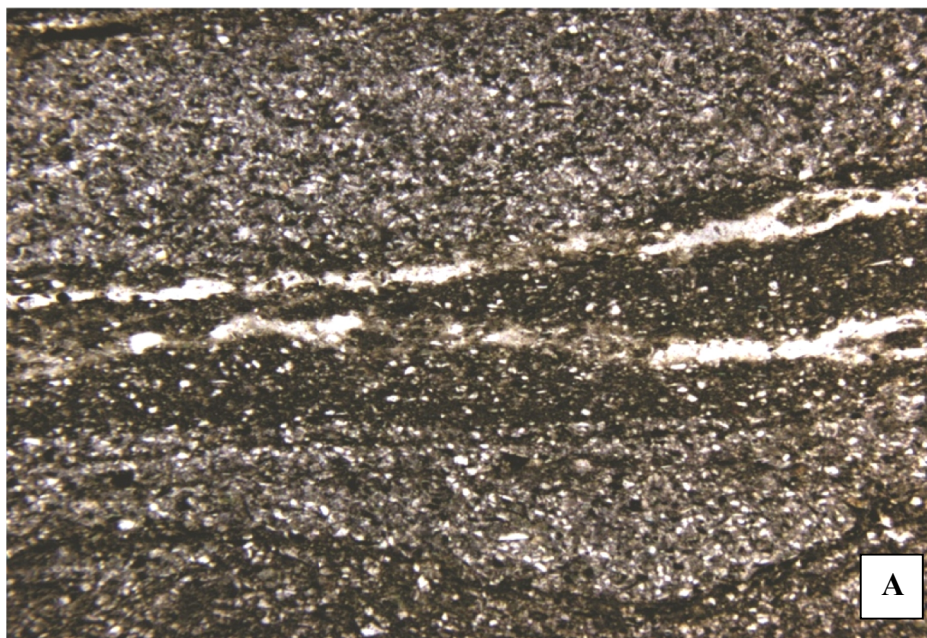


Figure 3.23: Photomicrographs of greenish to gray siltstone representing laminated siltstone and representing contact with greenish gray to gray Mudstone (Sample no. GOZ41, **(A)** PPL x2.5, GOZ45, **(B)** PPL x2.5).

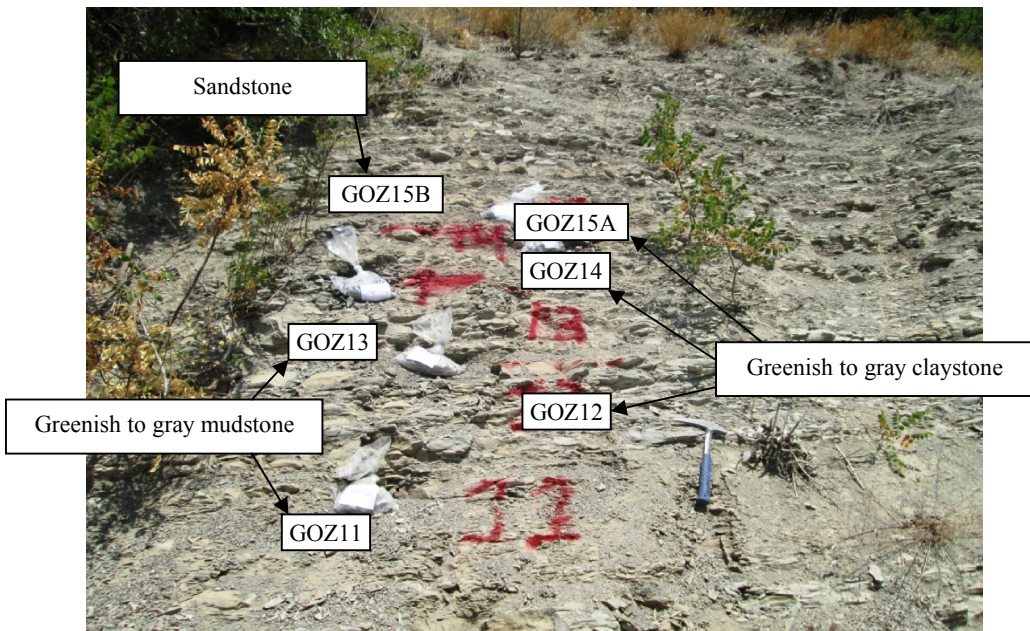


Figure 3.24: The field photograph showing the greenish to gray mudstone, claystone and greenish yellow to grayey sandstone of the Göynük Section.

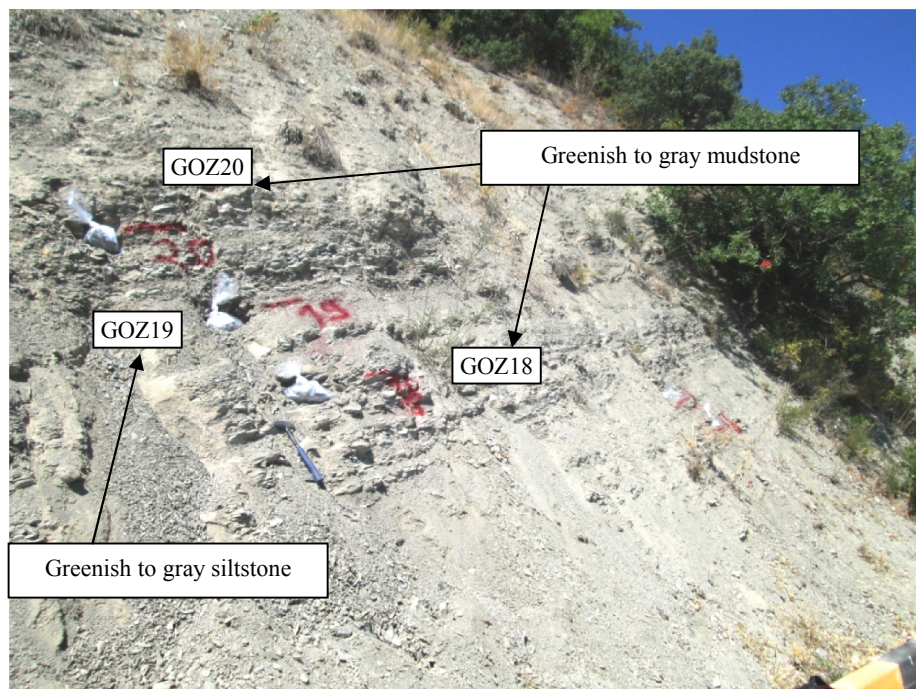


Figure 3.25: The field photograph showing the greenish gray to gray mudstone and greenish to gray siltstone of the Göynük Section.



Figure 3.26: The field photograph showing the Inoceramus in the greenish to gray mudstone of the Göynük measured section.

classification (1974), the matrix-dominated sandstone are classified as greywackes or dirty sandstone. The studied sandstone lithologies in the measured stratigraphic section are matrix-dominated and high proportion of quartz grains. Therefore, it is named as quartzwacke sandstone lithofacies.

In the field, this lithofacies has been distinguished by their sand grain size texture, parallel to cross laminated (Figures 2.14, 2.15 A, 2.15 B), thin to medium bedded with asymmetrical ripple structure and having light greenish gray (5GY 8/1), greenish gray (5G 6/1), light green (5G 7/4), pale yellow orange (10YR 8/6), pale green (5G 7/2), moderate greenish yellow to pale yellowish orange (10Y 7/4-10YR 8/6) and medium gray (N5) (Figures 2.14 and 3.24). This lithofacies consists of predominantly quartz grains which are coarse silt to fine sand size, angular to sub rounded texture and embedded in clayey matrix (Figures 3.27 A, 3.27 B). Other associated grains are feldspar, plagioclase, mica, lithic fragments (including shale, mudstone, volcanogenic, calcitic) and glauconite. The accessory minerals are comprised of blue tourmaline, biotite, chlorite, rutile, zircon, monazite, and hornblende. There is discriminately

distribution of pyrite with subordinate phosphate and hematite. This lithofacies represents generally well sorted to moderately sorting texture. This lithofacies form periodically within middle and upper portion of the measured stratigraphic section (Figure 2.11).

3.5 SEDIMENTARY STRUCTURE OF THE GÖYNÜK STRATIGRAPHIC SECTION

Different sedimentary structures have been observed at the outcrop and microscopic level in the Göynük section. These are tabulated as below;

I. BEDDING AND LAMINATION

In the outcrop, the Göynük Section along the road side represents very thin to medium bedded. The mudstone and claystone lithologies also indicate shaly (fissility) features to flaggy character (Figures 3.24, 3.25). The sandstone represents parallel to cross laminations and asymmetrical ripple marks (Figure 2.14). Occasional parallel laminations have been observed in the marl, mudstone and siltstone (Figures 2.14, 2.15, 3.23 A). Generally, the laminations in the marls and mudstone are due to alternations of concentrated bands of bioclasts and the dark matrix.

II. BIOTURBATION

Small-scale micro burrows have been noticed during the microscopic analysis of the Göynük samples. These are mostly observed in the red beds and occasionally in the green-gray beds. Microbioturbation are restricted to marls, mudstone and rarely noticed in claystone and siltstone. The identified infilling materials in the micro-burrows are silt size quartz grains embedded in the dark matrix. These are related with the development of oxic horizons at different level during the sediment deposits.

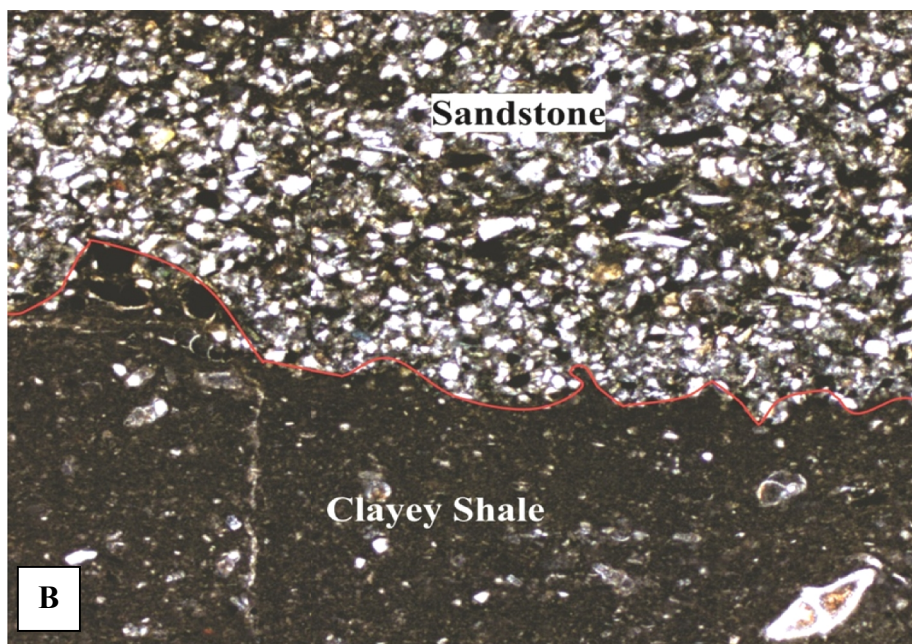
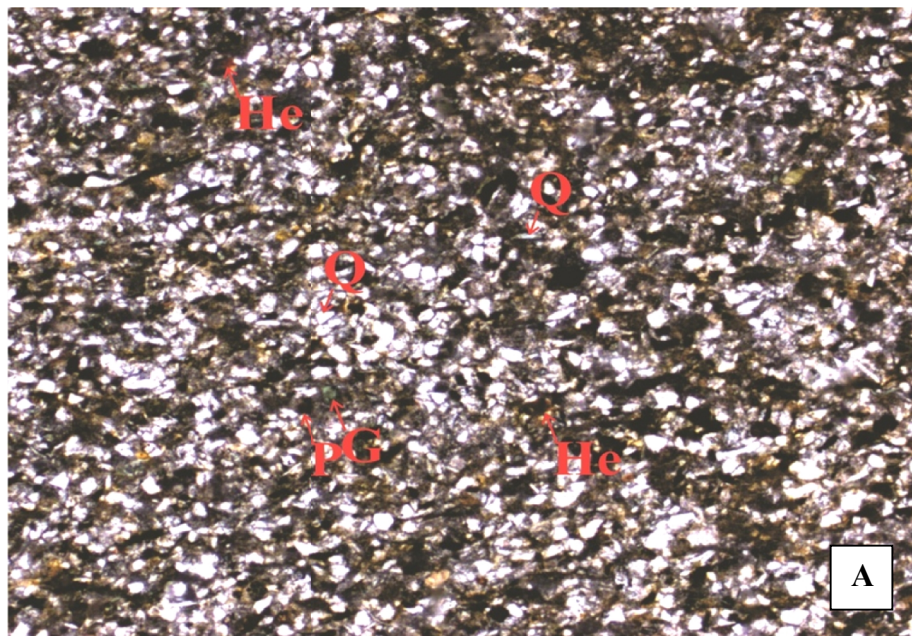


Figure 3.27: Photomicrographs of the greenish yellow to grayey fine sandstone showing quartz (Q), pyrite (P), plagioclase (Pg) and glauconite (G) (Sample no. GOZ28, **(A)** PPL x4) and **(B)** representing erosional contact (Sample no. GOZ49, **(B)** PPL x2.5).

3.6 PETROGRAPHY AND RESULTS OF POINT COUNTING

Petrography and results of point counting method have been carried out to determine the microfacies, changes in their composition and relative changes in constitutes percentage and quantity of the microfacies and even in the same microfacies at different stratigraphic level.

During the petrographic studies, different mineral grains (quartz, feldspar, plagioclase, mica, glauconite, heavy minerals), lithic-clasts, bioclasts, pyrite, hematite, phosphate and matrix have been identified and counted in each thin section as quantitatively (number of counted grains in the thin section) and percentage by using point counting machine. These are represented in the form of point counting quantitative measurement (Figures 3.28, 3.31; Tables A1, A2), percentage measurement (Tables 3.6, 3.7), measured stratigraphic thickness versus percent point counting graphs (Figures 3.29-3.30; 3.32-3.33) and their percentage point counting graphs comparison with one another of the studied sections.

3.6.1 PETROGRAPHY AND POINT COUNTING OF THE ALAGÖZ SECTION

The petrography and point counting analysis have been carried out on the basis of increase or decrease in the quartz, bioclasts and matrix/clay at certain levels of measured stratigraphic section along with other trace amount of minerals. The measured stratigraphic section is divided into different intervals on the basis of changes in the quartz, bioclasts, matrix and total grains which are illustrated below;

Between 0 to 20 cm interval: The base of the measured section is characterized by high proportion of bioclasts with trace amount of terrigenous influx to the basin (Figure 3.29). While glauconite and pyrite grains are decreasing and an increase has been observed in the phosphate and lithics (Figures 3.29, 3.30). The matrix shows decreasing trend (Figure 3.30). Overall, it represents low terrigenous input to oceans as it is

deposited in the bathyal environment with high concentration of fossil under calm condition.

Between 20 to 70 cm interval: Between 20 to 70 cm thick interval of the succession, there is sudden increase in the terrigenous grains (quartz, plagioclase, mica, lithics, heavy minerals and pyrite) which also affects the bio-diversity. There is also a decrease in glauconitic and phosphatic curves (Figures 3.29-3.30).

Between 70 to 700 cm interval: This interval generally shows steadily decreasing pattern in the quartz toward the top while very low fluctuation in the bioclasts setting (Figure 3.29). The accessory minerals display some fluctuation peaks but their linear trend shows decreasing pattern (Figures 3.29-3.30).

At 130 cm level, there is a decrease in the terrigenous input including quartz, lithics, plagioclase and mica (Figures 3.29-3.30). The glauconite and phosphate turn toward the positive side due to rise in the sea level. The heavy mineral and feldspar show some crest which may be derived from the nearby rework sediments or volcanic activity. At 280 cm region, lithics show strong changes in the curve line along with plagioclase and heavy minerals (Figure 3.29). As a result, total grains switched from 60 percent to 80 percent and in the matrix from 40 percent to 20 percent (Figure 3.30). This event also affected the glauconite percent as the condition agitated.

Between 700 to 950 cm interval: According to the quartz-bioclasts and total grains-matrix graphs represent relatively uniform proportion without any change or sharp peak (Figures 3.29-3.30). Other minerals approach to zero except pyrite. Pyrite mineral represents an increasing linear trend. However, in between, it shows gradual depletion in the percent and then followed by increasing climax in the curve line (Figure 3.30).

Between 950 to 1750 cm interval: After 950 cm, the quartz grains are shifting to increasing trend (Figure 3.29). Due to increase in the sedimentation rate, it affects the glauconitic curve that gradually moves toward the left. The pyritic line continues their increasing trend toward top with some variation (Figure 3.30). The trace amount of heavy mineral apex at 1250 cm and vanishes towards the top. Mica curve shows small

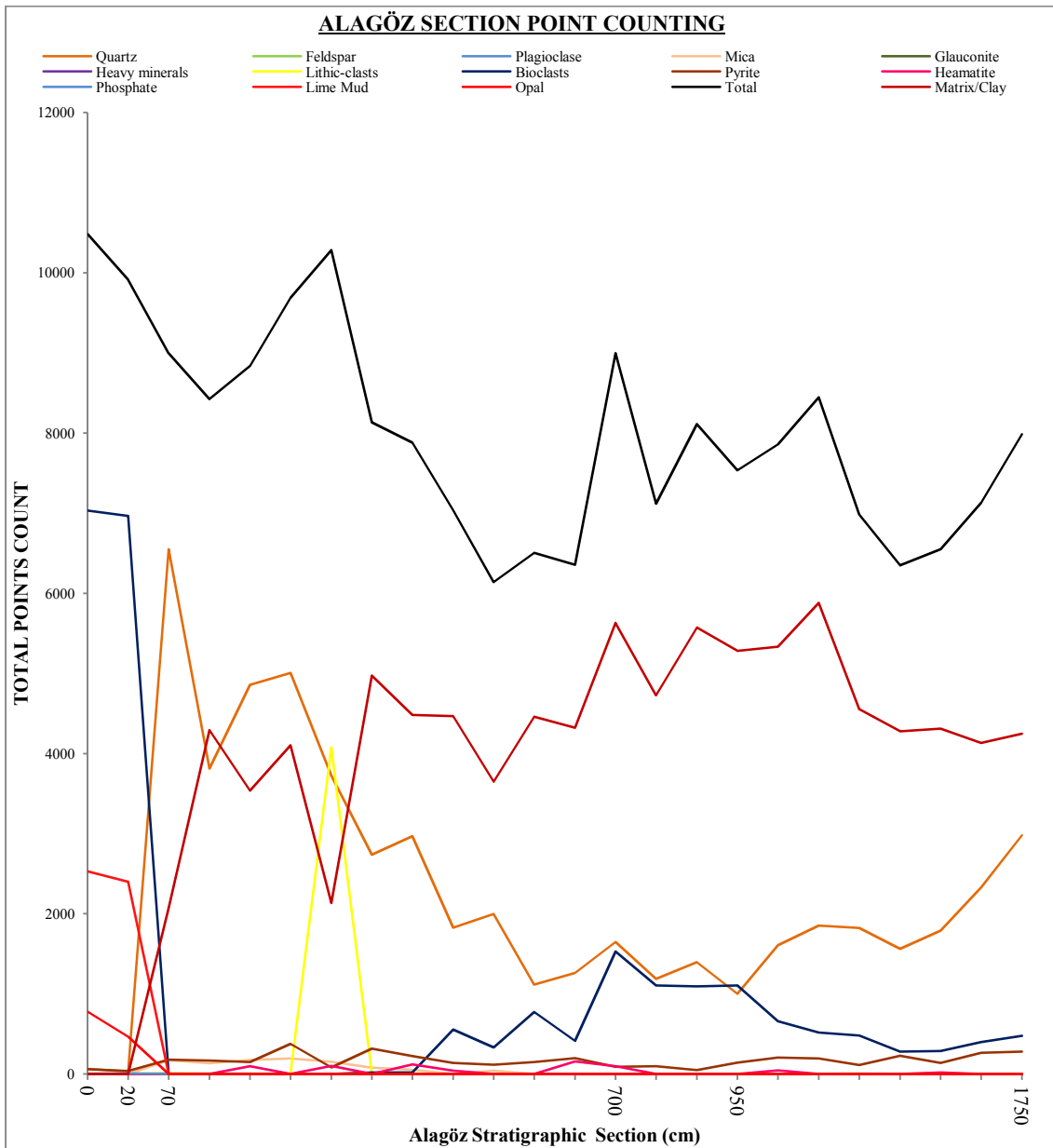


Figure 3.28: Graphic representation of quantitative data of the Alagöz samples under microscope by using point counting method (James Swift brand mechanical stage).

variation and suggests steadily increase in the sedimentation influx (Figure 3.30). At 1600 cm, strong evaluations of feldspar and diminished towards the top (Figures 3.29-3.30). The total grains curve coming closer to the matrix line curve after 950 cm toward the top. A total shift of positive 15% (from 30 % to 45 %) in the total grains curve was observed (Figure 3.30).

Table 3.6: Percent quantitative data of the Alagöz samples under microscope by using point counting method (unit as number of grains percent) (James Swift brand mechanical stage). (data display in graphic curve as Figures 3.29-3.30).

Sample No	Alagöz Section Point Counting in Percent													Total	
	Quartz	Feldspar	Plagioclase	Mica	Glaucite	Heavy Minerals	Lithics	Biotacts	Pyrite	Hematite	Phosphate	Matrix/Clay			
												Lime Mud	Matrix /Clay	Opal	
ZR0b	0.6	0	0	0.05	0.02	0.01	0.02	67.08	0.6	0	0.05	24.15	0	7.42	100
ZR0	0.3	0	0	0.02	0.01	0	0.04	70.24	0.4	0	0.1	24.18	0	4.71	100
ZR01	72.81	0	0.1	1.9	0.01	0.01	0.11	0.03	2	0	0	0	23.03	0	100
ZR02	45.25	0.01	0.05	1.6	0.02	0.01	0.05	0	2	0	0.04	0	50.97	0	100
ZR03	54.98	0.01	0.06	2	0.01	0.01	0.07	0	1.7	1.1	0	0	40.06	0	100
ZR04	51.69	0.01	0.01	2	0.02	0	0.04	0	3.88	0	0	0	42.35	0	100
ZR04a	36.22	0	0.03	1.5	0.01	0.01	39.64	0	0.8	1	0	0	20.79	0	100
ZR05	33.65	0	0.01	1	0.02	0	0.04	0.22	3.9	0	0	0	61.16	0	100
ZR06	37.68	0	0.01	0.7	0.03	0.01	0.05	0.24	2.83	1.55	0	0	56.9	0	100
ZR07	25.94	0.01	0	0.01	0	0	0.03	7.92	2	0.6	0	0	63.49	0	100
ZR08	32.53	0	0	0.7	0.01	0.01	0	5.41	1.9	0	0	0	59.44	0	100
ZR09	17.18	0	0	0.04	0.01	0	0	11.91	2.3	0	0	0	68.56	0	100
ZR10	19.87	0	0	0.02	0.03	0	0	6.5	3.1	2.5	0	0	67.98	0	100
ZR11	18.3	0	0	0.01	0	0	0	17	1	1.1	0	0	62.59	0	100
ZR12	16.7	0	0	0	0	0	0	15.5	1.4	0	0	0	66.4	0	100
ZR13	17.2	0	0	0	0	0	0	13.5	0.6	0	0	0	68.7	0	100
ZR14	13.3	0	0	0	0	0	0	14.7	1.9	0	0	0	70.1	0	100
ZR15	20.48	0	0	0.02	0.02	0	0	8.4	2.6	0.6	0	0	67.88	0	100
ZR16	21.94	0	0	0	0.02	0	0	6.14	2.3	0	0	0	69.6	0	100
ZR17	26.12	0	0	0.1	0.01	0.02	0	6.9	1.6	0	0	0	65.25	0	100
ZR18	24.6	0	0	0.05	0	0	0	4.4	3.6	0	0	0	67.35	0	100
ZR19	27.3	0	0	0.05	0	0	0	4.4	2.1	0.3	0	0	65.85	0	100
ZR20	32.66	0	0	0.03	0	0	0.04	5.6	3.7	0	0	0	57.97	0	100
ZR21	37.3	0	0	0	0	0	0	6	3.5	0	0	0	53.2	0	100

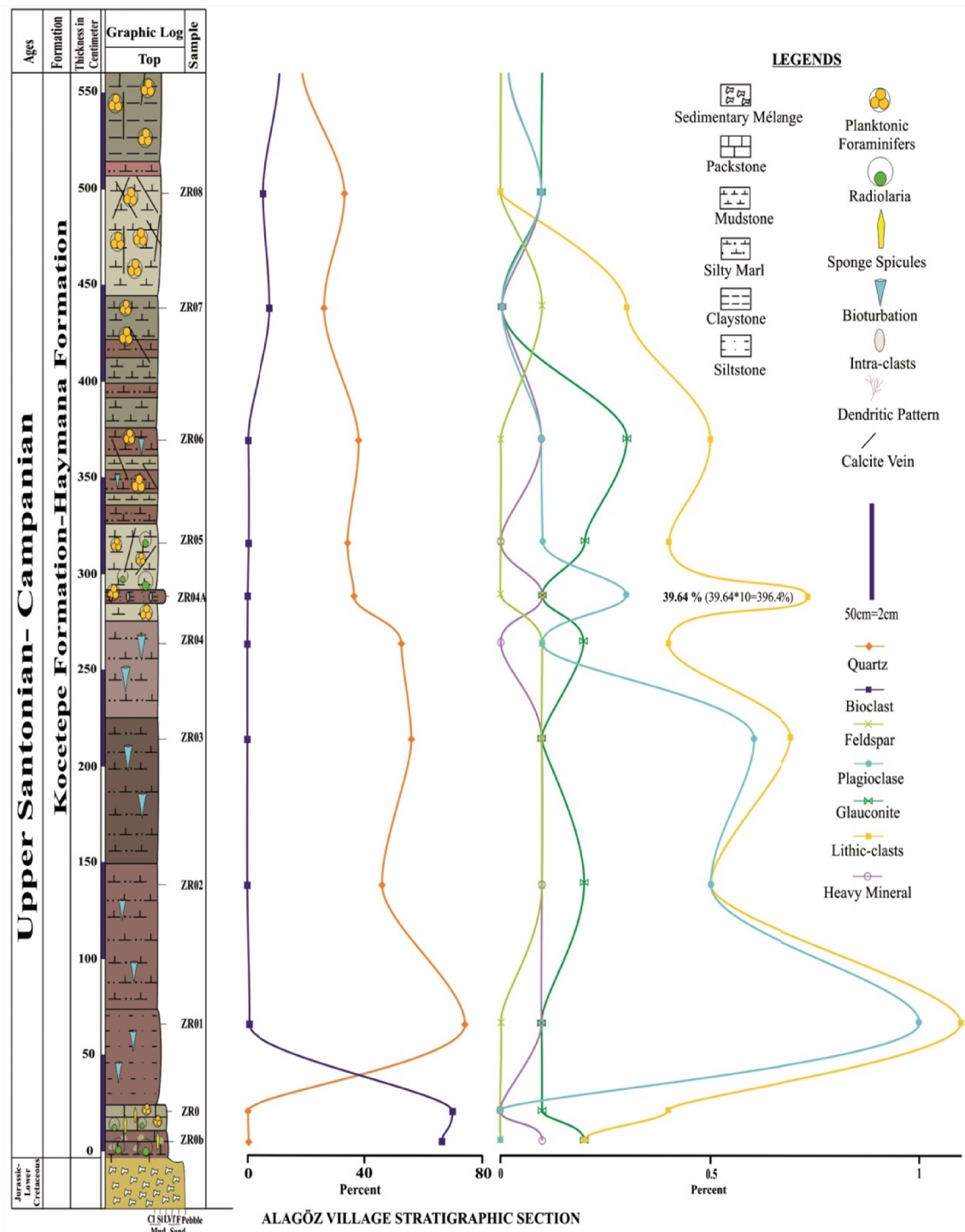


Figure 3.29: Representing Quartz-Bioclastic-Feldspar (10*)-Plagioclase (10*)-Glauconite (10*)-Lithic (10*)-Heavy minerals (10*) graphic curves of the Alagöz Stratigraphic Section petrographic studies. (Note: 10* represents 10 time increase).

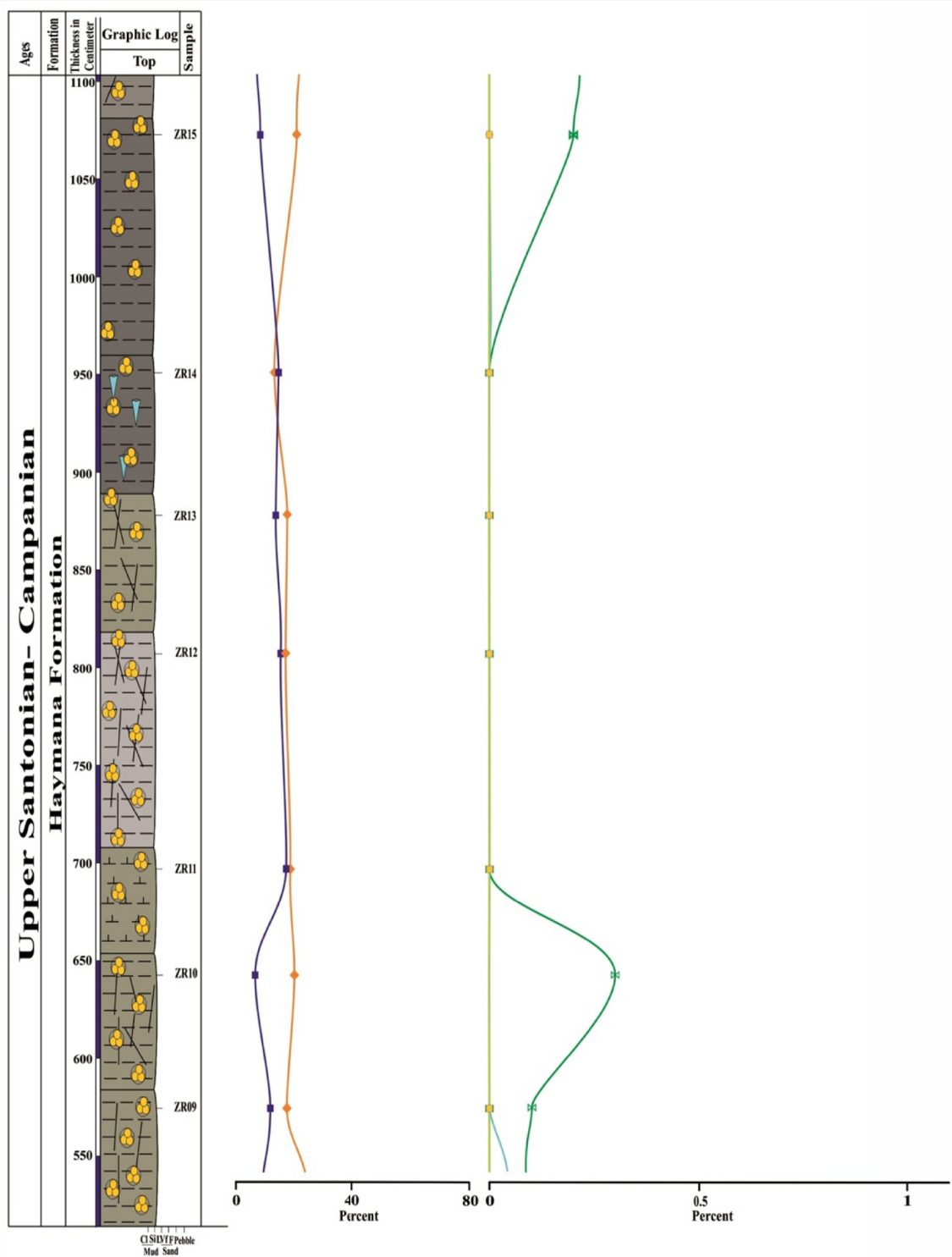


Figure 3.29: Continued.

ALAGÖZ VILLAGE STRATIGRAPHIC SECTION

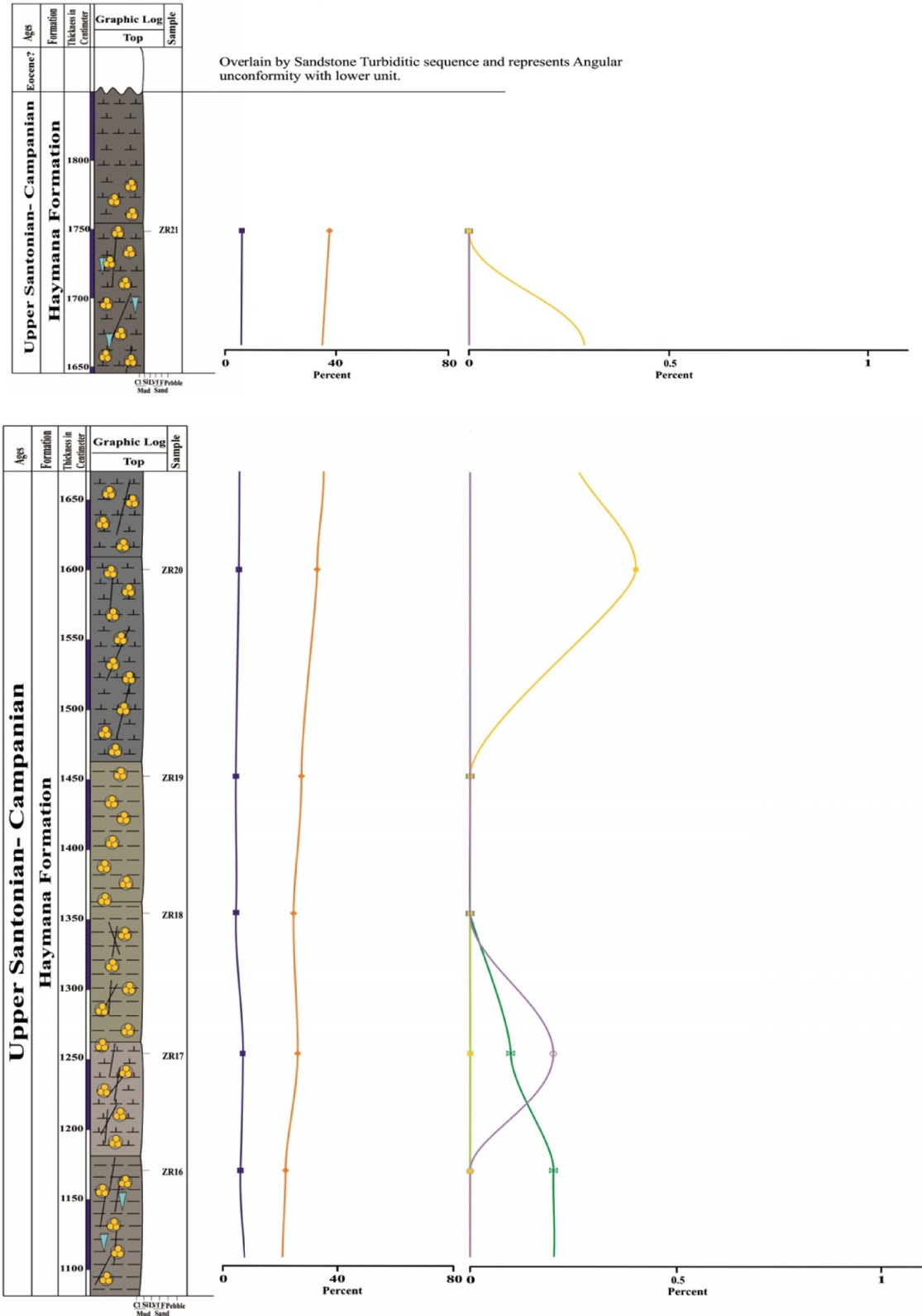


Figure 3.29: Continued.

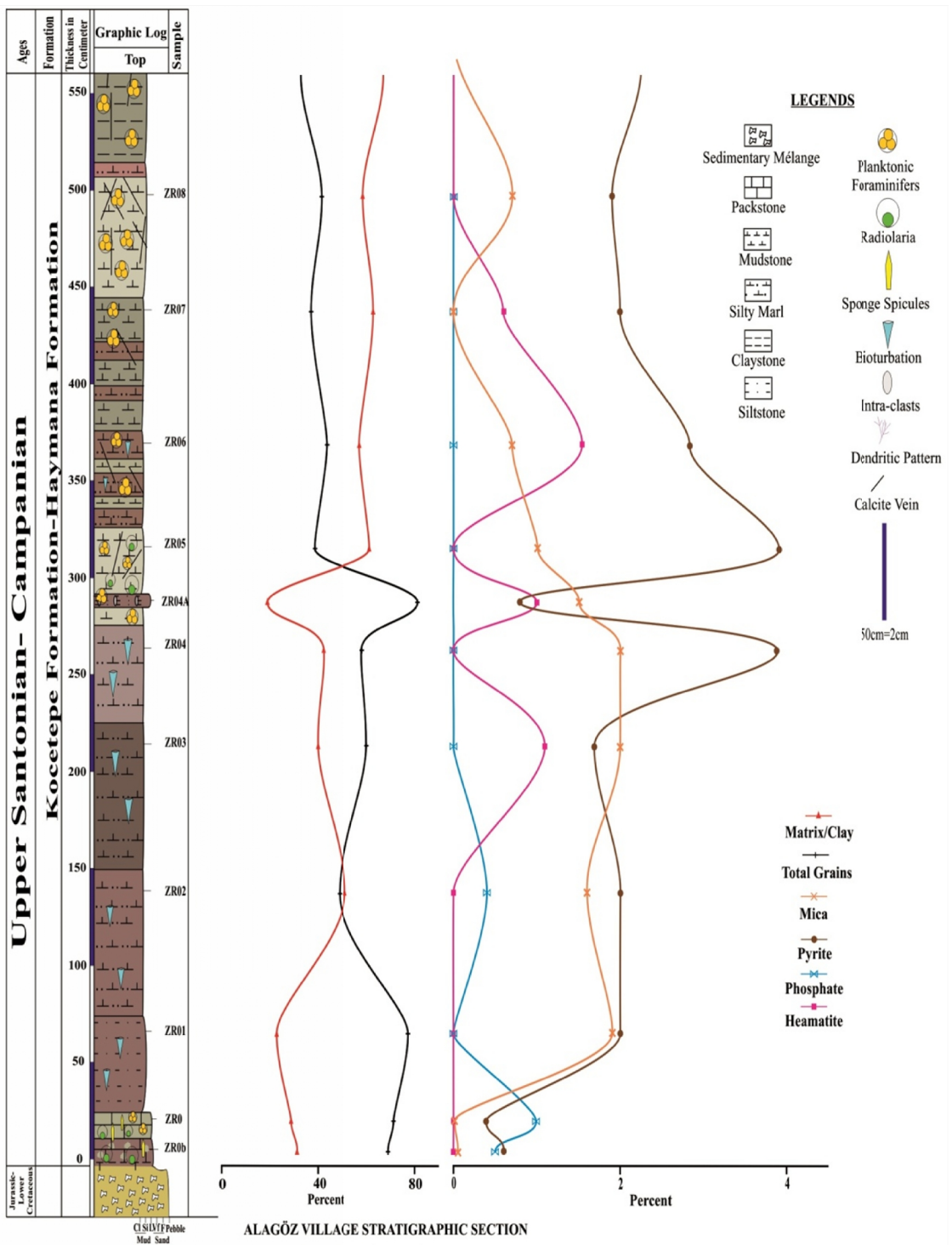


Figure 3.30: Representing Matrix-Total grains-Mica-Pyrite-Phosphate (10*) - Hematite graphic curves of the Alagöz Stratigraphic Section petrographic studies. (Note: 10* represents 10 time increase).

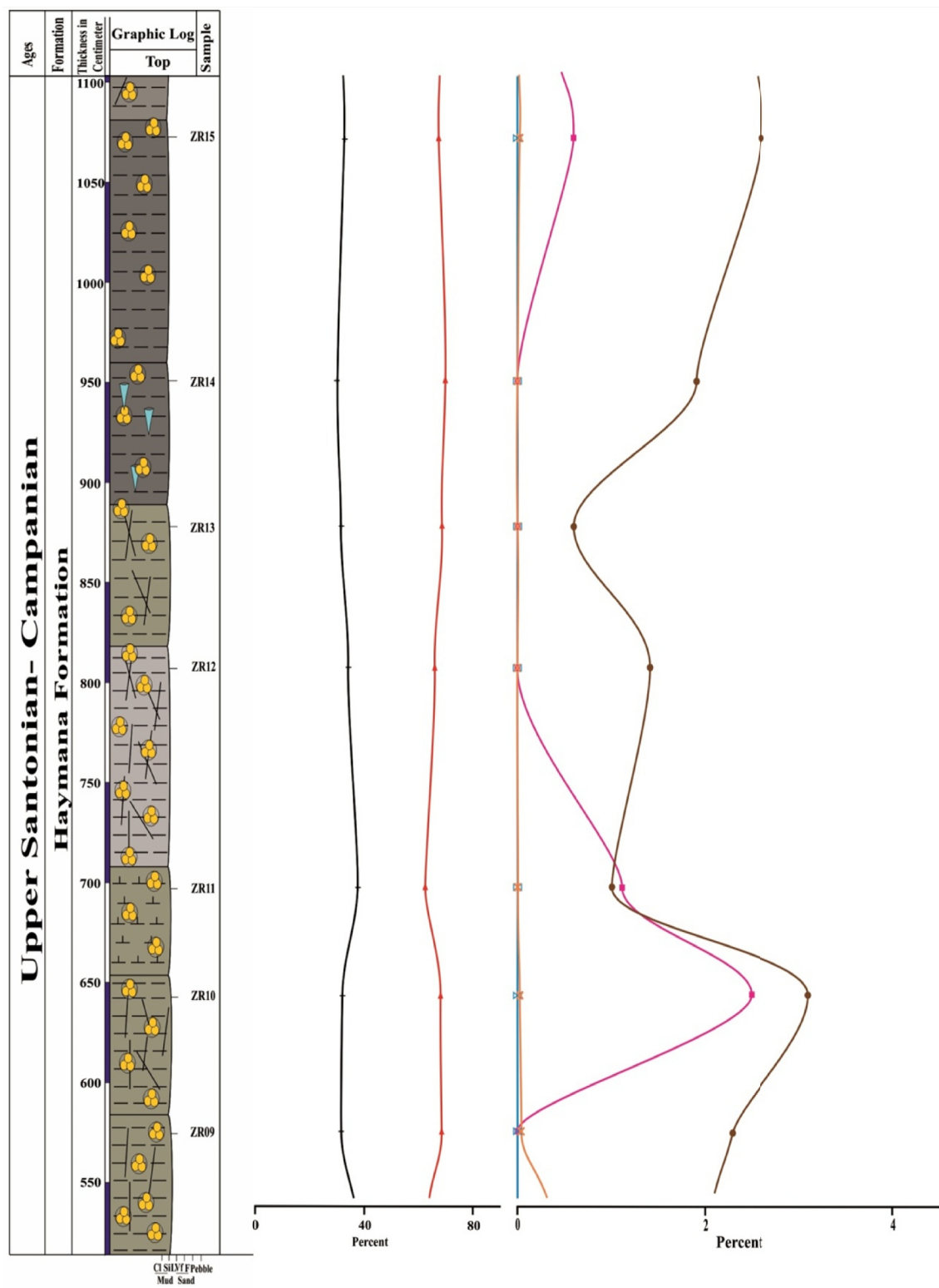


Figure 3.30: Continued.

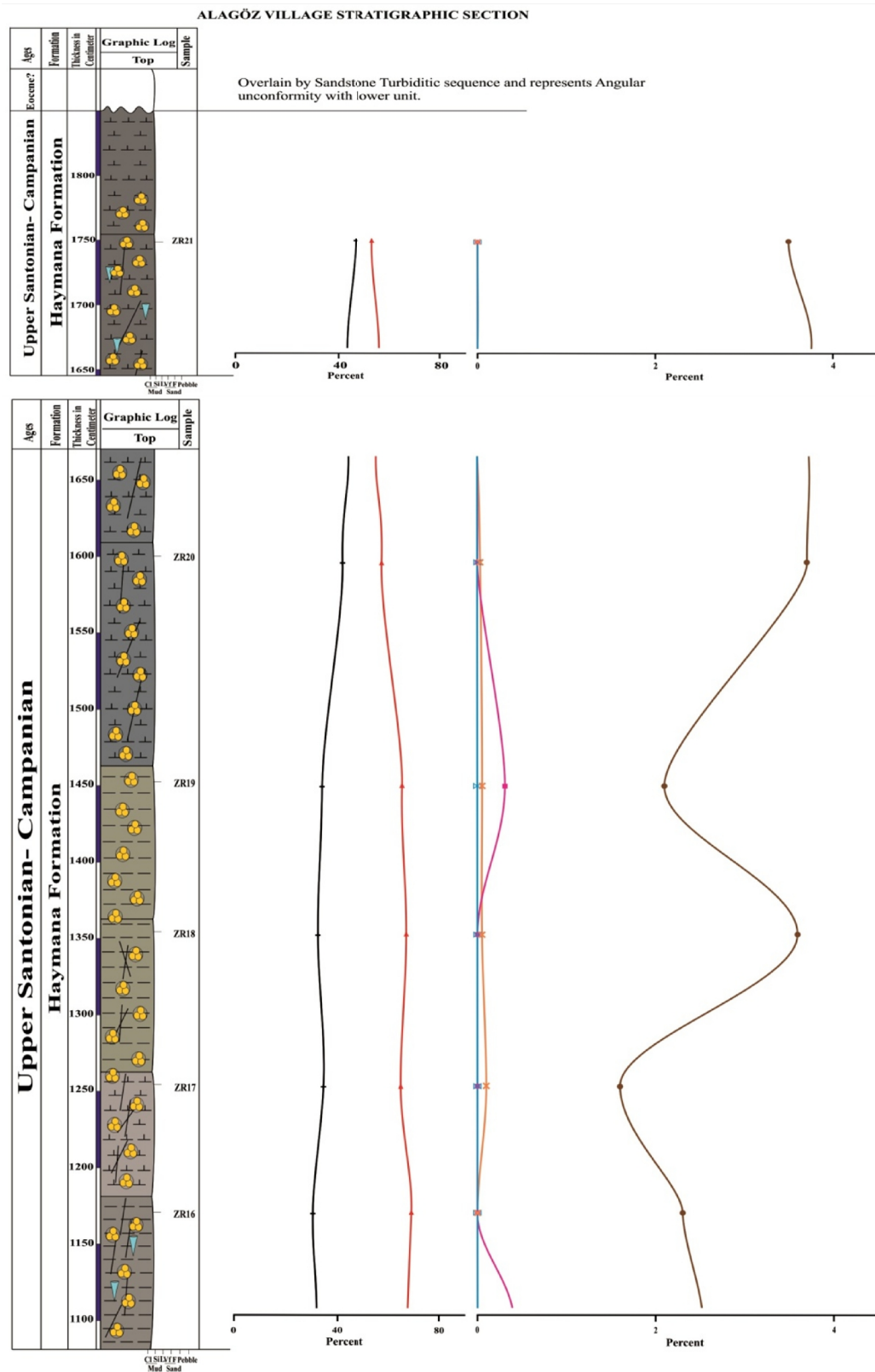


Figure 3.30: Continued.

3.6.2 PETROGRAPHY AND POINT COUNTING OF THE GÖYNÜK SECTION

Petrographic studies and point counting of the Göynük Section have been used in order to explain and determine the terrigenous content, bio-diversity and matrix quantification along the measured stratigraphic section at different levels. On the basis of the changes in the quartz, bioclasts, matrix and total grains content in the lithologies, it has been divided into different stratigraphic intervals along the vertical section which are mentioned below;

Between 0 to 750 cm interval: At the very base of measured section, there is a slight increase in the bioclastic curve and followed by almost uniform trend toward the top (Figure 3.32). The terrigenous influx has gradually increased to certain levels of measured stratigraphic and then slightly depleted at 225 cm and remained uniform afterwards. Glauconite trend revealed ascending graph except a collapse at 225 cm and die out near 625 cm (Figure 3.32).

Pyrite curve represents uniform trend but shows minor deviation at 740 cm. The phosphate demonstrated increasing deflection from 225 cm to 525 cm and then at 740 cm. The mica line displays minor fluctuation but uniform trend after 625 cm (Figure 3.33). Plagioclase represents initially increasing pulse at 225 cm and shrinks afterwards. At 525 cm, another ascending pulse of plagioclase curve occurred and gradually elongated toward the top (Figure 3.32). Lithics curve shows uniform proportion except zero value at 325 cm and then followed by increasing proportion (Figure 3.32). The total grains curve represents increasing curvature while decreasing in the matrix curve. However, after 10 cm, there is inconsequential increasing and decreasing deflection observed in the graphic curves of total grains and matrix (Figure 3.33).

Between 750 to 1400 cm interval: During 750cm to 1400 cm, frequent variation in the inclination of graphic lines of quartz and bioclasts and forms twisting pattern (Figure 3.32).

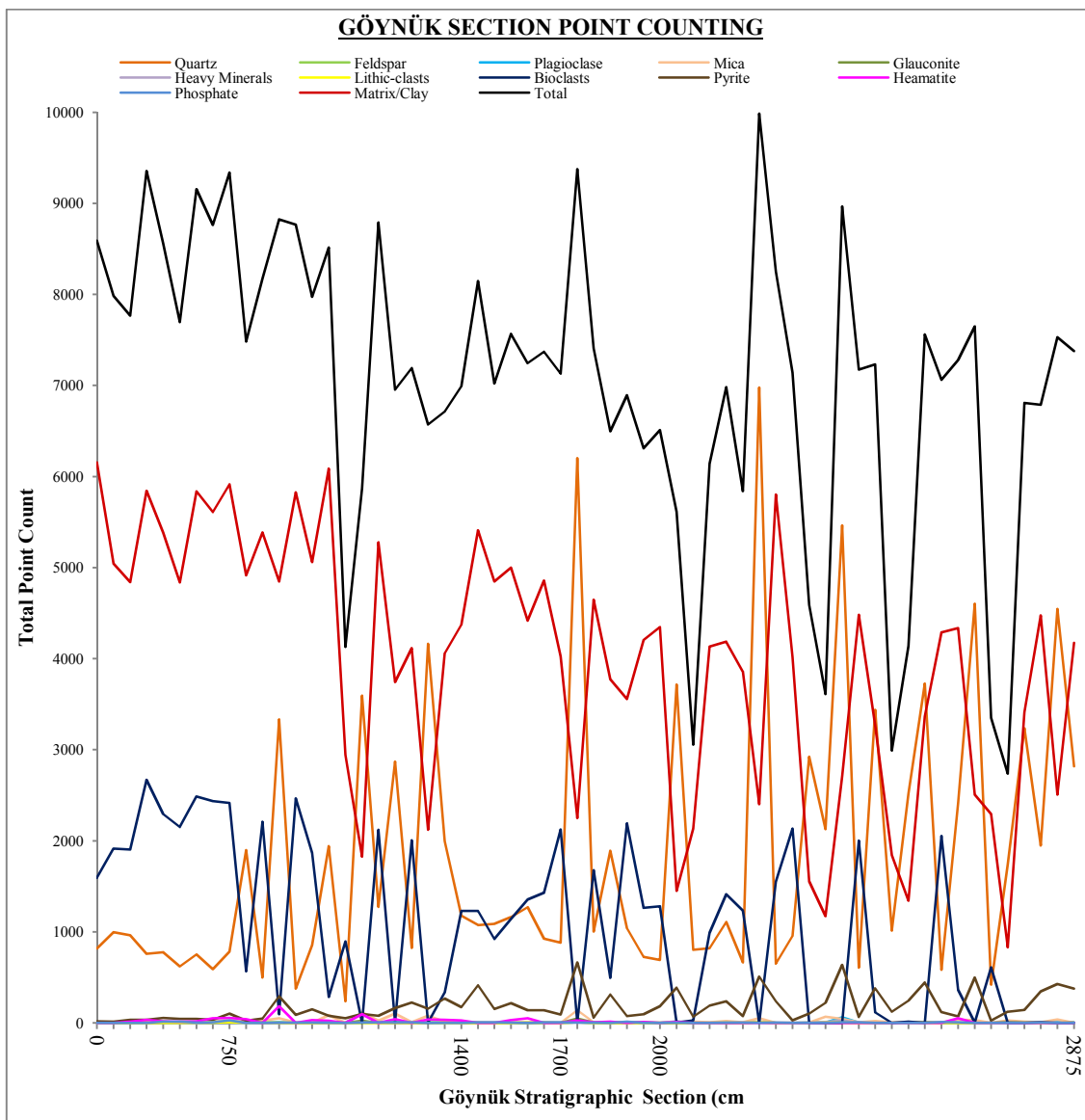


Figure 3.31: Graphic representation of quantitative studied of the Göynük samples under microscope by using point counting method (James Swift brand mechanical stage).

At 1030 cm, intensive increasing deflection in the peaks of quartz grains, feldspar, plagioclase, glauconite and heavy minerals graphic lines. At 1280 cm, another high deflective peaks was realized which is characterized by silt-size quartz grains.

Glauconitic mineral shows some strong crest pulses at different measured stratigraphic level. These crests are observed at 800 cm, 1030 cm and 1340 cm (Figure 3.32). The plagioclase curve illustrates variable crest in between 750 to 1230 cm and then followed by gradual negative linear behavior trend toward the top. The lithic graph represents minor increasing and decreasing peaks except the shrinkage at 950cm. Heavy minerals show low peaks but prominent increasing peak at 1030 cm. Pyrite curve is generally characterized as steadily increasing linear trend, where as a single sharp increased apex at 880 cm. Mica displays prominent increasing curvature near 750 cm, 1030 cm and 1280 cm. Phosphatic line indicates progressive rising and later retained to zero level (Figures 3.32-3.33). The total grains and matrix lines represent relative parallel trend (Figure 3.33).

Between 1400 to 1700 cm interval: From 1400 to 1700 cm interval, the quartz grains and bioclasts show almost uniform pattern with inconsequently increase and decrease in the quantities. At 1600 cm, the bioclastic content remained same other than a decrease in the quartz grains (Figure 3.32). The plagioclase graph represents reducing curve which shrinks at 1500 cm and is followed by a rise and then again a contract at 1700 cm. Minor increasing deflection in glauconitic line realizes near top. Pyrite line illustrates high increasing trend and then gradual decreasing deflection in the evaluation. Mica and phosphate lines exaggerated in the beginning and depleted in the middle and rise near 1600 cm (Figures 3.32-3.33).

The matrix is characterized by slowly increasing pattern while decreasing manner in the total grains graph but opposite situation near 1700 cm where sudden fall in the matrix was observed and rise in the total grains (Figure 3.33).

Between 1700 to 2000 cm interval: In the beginning, terrigenous grains represent prominent high curvature curves. The quartz grains increased from 12 % to 66 % and

also a significant increased in the other minor minerals such as feldspar, plagioclase, mica, glauconite, lithics, mica and pyrite that cause a small angle curvature in the total grains graph (Figures 3.32-3.33). Later, twisting pattern was shown by bioclastic and quartz grains (Figure 3.32). Minor amount of feldspar, plagioclase and mica were received to the basin and give few recorded magnitudes toward the top. Pulses of phosphate and glauconite mineral appeared at different measured stratigraphic levels. Pyrite indicates variable frequency crest and trough. High deflected crest was observed in the lower portion and represent gradual increasing in the top portion (Figures 3.32-3.33). The matrix line appeared as a gradual rise where as a decrease in the total grains content.

Between 2000 to 2866 cm interval: This interval represents highly fluctuated graphic presentation (Figures 3.32-3.33). Approximately, after every 200 cm, there is invasion of high terrigenous input to ocean that has been observed at 6 different measured stratigraphic levels. These are characterized by high peaks of quartz grains, plagioclase, glauconite, heavy minerals, mica, pyrite and occasional appearance of feldspar. In between these 6 intervals, these minerals demonstrate slightly increasing and decreasing manners. In these intervals, pyrite represents high value peaks at number of points while some points show decreasing peaks. Bioclastic graph mostly illustrate decreasing trend with few increasing peaks and die out near the top portion after 2680 cm. The total grains and matrix graphic lines represent sinusoidal pattern with some sharp deviations.

3.7 COMPARISON GRAPHIC REPRESENTATION BETWEEN ALAGÖZ AND GÖYNÜK SECTIONS

The graphic representation of Alagöz and Göynük sections are correlated with each other in order to get the comparison image and determined similarity trend and differences as well.

The Alagöz Section is measured up to 1900 cm where as Göynük Section is measured up to 2875 cm (Figures 2.7, 2.11). After 1900 cm, there will be an imagery linear trend drawn in the Alagöz Section to be compared with above section of Göynük section.

Table 3.7: Percent quantitative data of the Göynük samples under microscope by using point counting method (unit as number of grains percent) (James Swift brand mechanical stage). (data display in graphic curve as Figures 3.32-3.33).

Göynük Section Point Counting in Percent													
Sample No	Quartz	Feldspar	Plagioclase	Mica	Glauconite	Heavy Minerals	Lithics	Bioclasts	Pyrite	Heema-tite	Phosphate	Matrix /Clay	Total
GOZ-0	9.5	0	0	0.06	0	0	0.02	18.54	0.2	0	0.02	71.66	100
GOZ-1	12.5	0	0	0.07	0.01	0.01	0.02	23.98	0.2	0	0.01	63.19	100
GOZ-2	12.4	0.02	0	0.07	0.01	0.02	0.03	24.51	0.43	0.17	0.02	62.3	100
GOZ-3	8.1	0	0.02	0.09	0	0.01	0.02	28.56	0.35	0.38	0.02	62.43	100
GOZ-4	9.09	0	0	0.2	0	0	0	26.82	0.65	0.2	0.15	62.79	100
GOZ-5	8.08	0	0	0.05	0.06	0	0.03	27.96	0.6	0.2	0.18	62.71	100
GOZ-6	8.2	0	0	0.03	0.05	0	0.04	27.16	0.5	0.2	0.06	63.58	100
GOZ-7	6.72	0	0.02	0.3	0	0	0.03	27.81	0.4	0.6	0.08	63.98	100
GOZ-8	8.4	0	0.03	0.3	0	0	0.06	25.86	1.1	0.6	0.3	63.25	100
GOZ-9	25.36	0	0.05	0.3	0.08	0	0.06	7.54	0.32	0.55	0.03	65.18	100
GOZ-10	6.1	0	0	0.3	0	0	0.07	27.01	0.6	0	0.05	65.78	100
GOZ-11	37.76	0	0.08	0.6	0	0.01	0.06	1.1	3.3	2.1	0.05	54.16	100
GOZ-12	4.3	0	0	0.06	0	0.02	0	28.12	1	0	0.06	66.32	100
GOZ-13	10.72	0	0.03	0	0	0	0.03	23.4	1.9	0.4	0.04	62.37	100
GOZ-14	22.8	0.02	0.06	1	0	0	0.04	3.34	0.9	0.3	0.05	71.03	100
GOZ-15A	5.8	0	0	0.04	0	0	0	21.7	1.2	0	0	71.2	100
GOZ-15B	61.23	0	1.8	2	0.4	0.07	0.03	0	1.7	1.6	0.06	30.92	100
GOZ-16	14.5	0	0.03	0.3	0	0	0.02	24.13	0.9	0	0.07	60.02	100
GOZ-17	41.25	0	0.2	1.5	0	0.02	0.05	0.1	2.35	0.6	0.1	57.01	100
GOZ-18	11.45	0	0.05	0.1	0	0	0.03	27.92	3.1	0	0.1	56.94	100
GOZ-19	63.35	0	0.1	1.2	0	0.01	0.05	0	2.4	0.6	0	32.17	100
GOZ-20	29.72	0	0.08	0.2	0.08	0	0.02	4.93	4	0.5	0	60.44	100
GOZ-21	16.82	0	0.04	0	0	0.01	0.03	17.61	2.5	0.4	0.02	62.54	100
GOZ-22	13.17	0.01	0.03	0.1	0	0	0	15.11	5.1	0	0.08	66.16	100
GOZ-23	15.5	0	0	0.05	0	0	0	13.12	2.2	0	0.1	68.93	100
GOZ-24	15.35	0	0	0.1	0	0	0.02	15.11	2.9	0.4	0.05	65.83	100
GOZ-25	17.54	0	0	0.1	0	0	0.07	18.73	1.9	0.7	0.02	60.76	100
GOZ-26	12.56	0	0	0.1	0.01	0	0.04	19.4	1.9	0	0.1	65.72	100
GOZ-27	12.34	0	0	0	0	0	0	29.81	1.3	0	0.1	56.45	100
GOZ-28	66.18	0.06	0.1	1.5	0.5	0.05	0.1	0.1	7.1	0.3	0.03	24.61	100
GOZ-29	13.53	0	0	0.1	0.04	0.02	0.03	22.63	0.8	0.1	0.04	62.09	100
GOZ-30	29.1	0	0.04	0.1	0	0	0	7.63	4.8	0.21	0	57.89	100
GOZ-31	15.1	0.01	0.05	0.1	0	0	0.03	31.8	1.1	0	0.22	51.39	100

Table 3.7: Continued.

GOZ-32	11.5	0.01	0.05	0.04	0.05	0	0	20.05	1.5	0.18	0	66.52	100
GOZ-33	10.64	0	0	0.08	0	0	0	19.7	2.8	0	0	66.5	100
GOZ-34a	66.2	0.06	0.25	0	0.02	0.3	0.07	0.06	6.9	0.2	0.06	24.58	100
GOZ-34b	26.3	0	0.07	0.5	0	0	0.02	0.9	2.3	0	0.08	69.79	100
GOZ-35	13.34	0	0	0.1	0	0	0	16.12	3.1	0	0.04	67.24	100
GOZ-36	15.87	0.02	0.05	0.3	0	0.07	0.04	20.22	3.4	0	0.05	59.86	100
GOZ-37	11.35	0	0	0.1	0	0	0	21.13	1.3	0	0.06	65.92	100
GOZ-38	69.9	0.04	0.15	0.5	0.06	0.1	0.08	0.02	5.1	0	0	23.81	100
GOZ-39	7.9	0	0	0	0	0	0.01	18.8	2.9	0	0.06	70.17	100
GOZ-40	13.4	0	0.03	0	0	0	0	29.9	0.4	0	0.02	56.22	100
GOZ-41a	63.65	0	0.06	0.1	0.02	0	0.05	0	2.2	0	0	32.14	100
GOZ-41b	58.98	0	0.08	1.9	0.07	0.3	0.09	0	6.1	0	0.04	32.55	100
GOZ-42	60.95	0	0.7	0.5	0.06	0.3	0.07	0.02	7.1	0	0.1	30.28	100
GOZ-43	8.48	0	0.04	0.1	0	0	0.02	27.92	0.9	0	0.09	62.01	100
GOZ-44	47.55	0	0.05	0.3	0	0	0.03	1.6	5.25	0	0	44.75	100
GOZ-45(Lower)a	33.95	0	0.02	0.2	0.06	0.01	0	0	4.1	0	0	61.23	100
GOZ-45(Middle)b	60.82	0	0.12	0.2	0.08	0.04	0	0.38	5.9	0	0	32.35	100
GOZ-45(Upper)c	49.3	0	0.08	0.1	0.08	0.02	0	0	5.9	0	0	44.02	100
GOZ-46	8.27	0	0.03	0.1	0	0	0.01	29.05	1.7	0	0.14	60.46	100
GOZ-47	33.15	0	0	0.5	0	0	0.02	4.99	1	0.7	0.08	58.88	100
GOZ-48	60.21	0	0.04	0.4	0	0	0.02	0.07	6.5	0	0	32.75	100
GOZ-49(Lower)a	12.6	0	0.02	0	0	0	0.01	18.18	0.7	0	0	68.39	100
GOZ-49(Middle)b	63.65	0	0.05	1	0.4	0.1	0	0	4.5	0	0.04	29.53	100
GOZ-49(Upper)c	47.5	0	0	0.2	0.07	0	0	0.03	2.1	0	0	49.47	100
GOZ-50	28.7	0	0	0.1	0	0	0	0.12	5.1	0	0.08	65.12	100
GOZ-51	60.37	0	0.08	0.5	0.02	0.02	0	0	5.7	0	0	32.65	100
GOZ-52	38.2	0	0.06	0	0.07	0	0	0	5.1	0	0	56.57	100

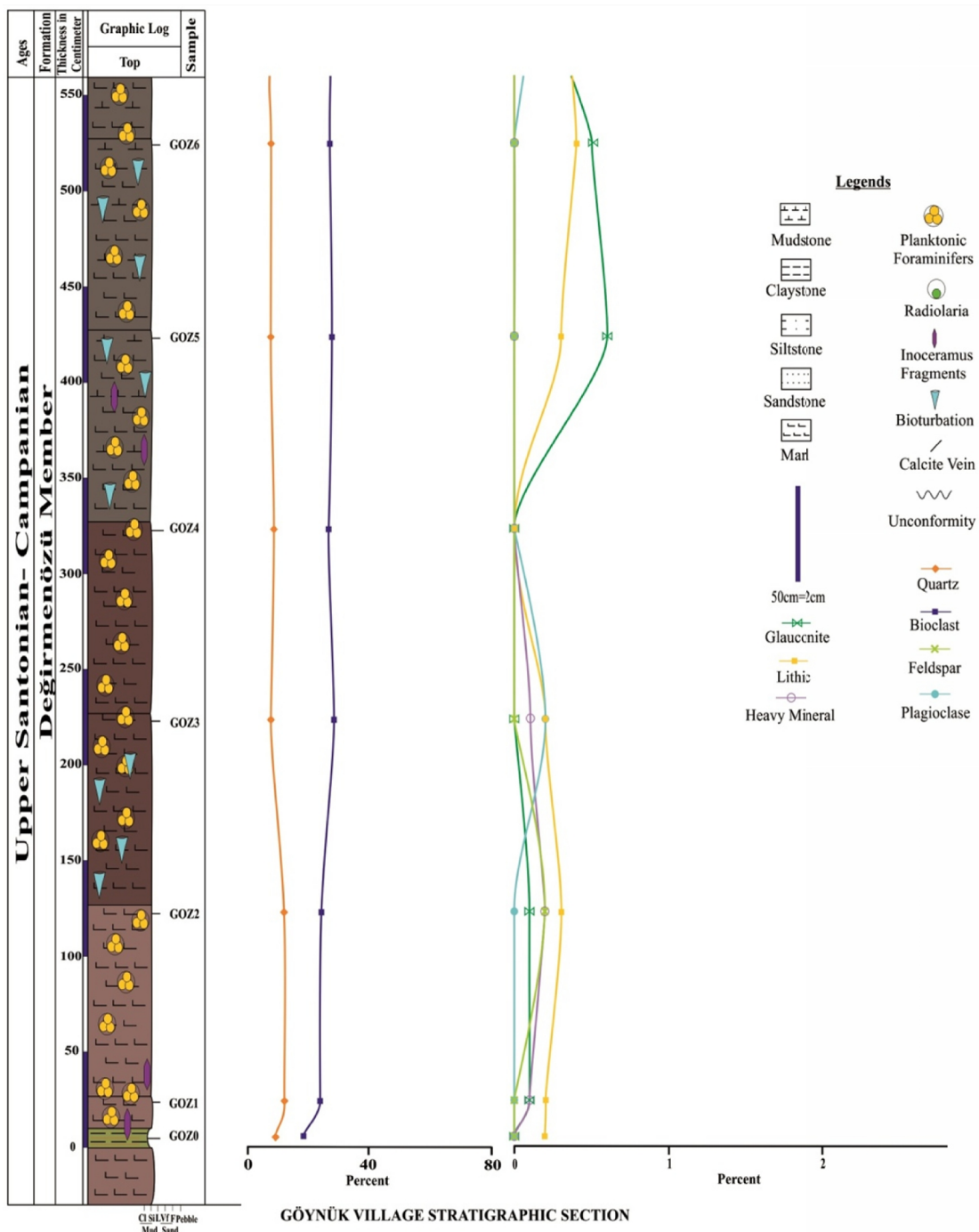


Figure 3.32: Representing Quartz-Bioclastic-Feldspar (10*)-Plagioclase (10*)-Glaucnate (10*)-Lithic(10*)-Heavy minerals(10*) graphics curve of the Göynük stratigraphic section petrographic data. (Note: 10* represents 10 time increase).

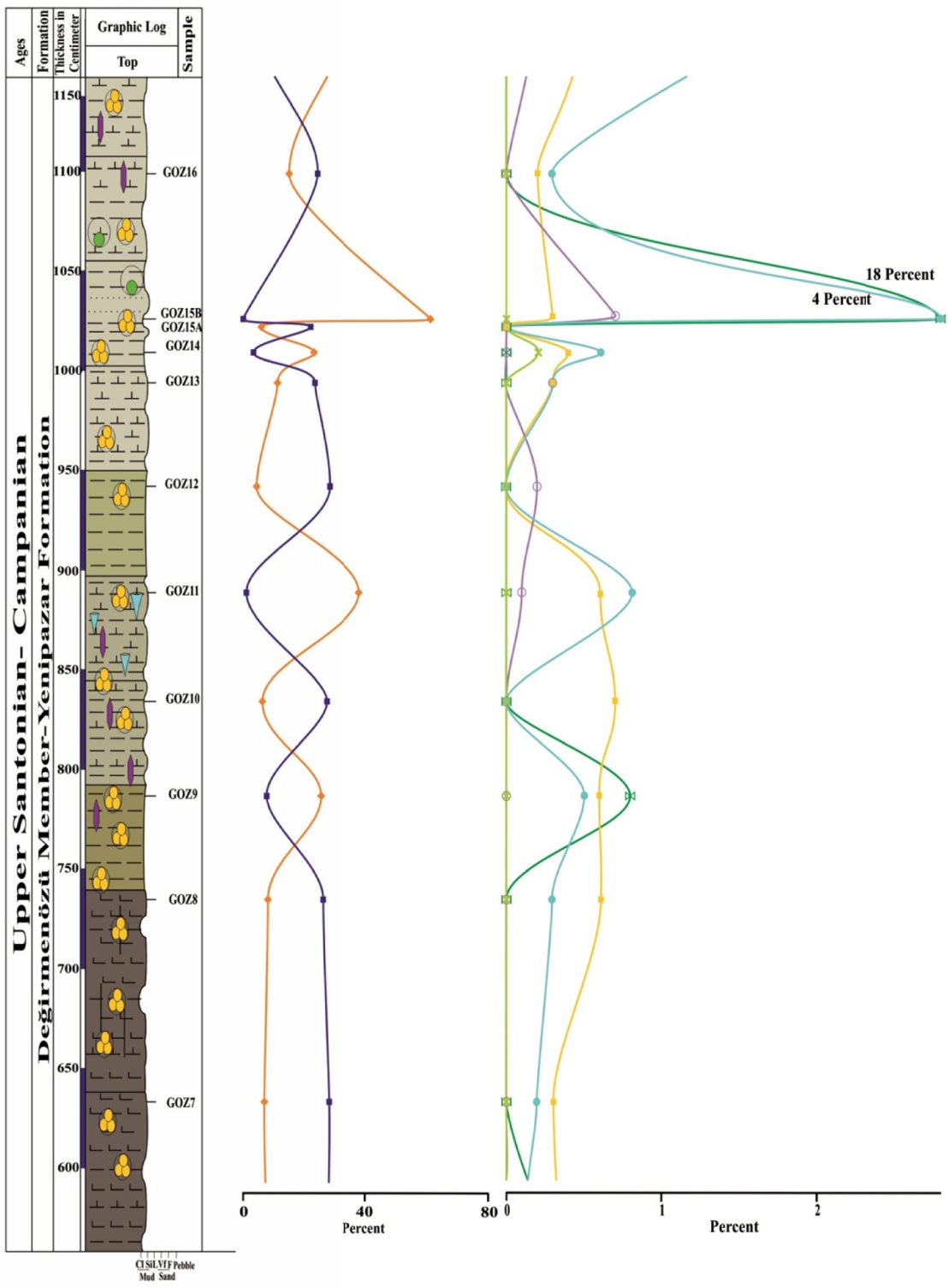


Figure 3.32: Continued.

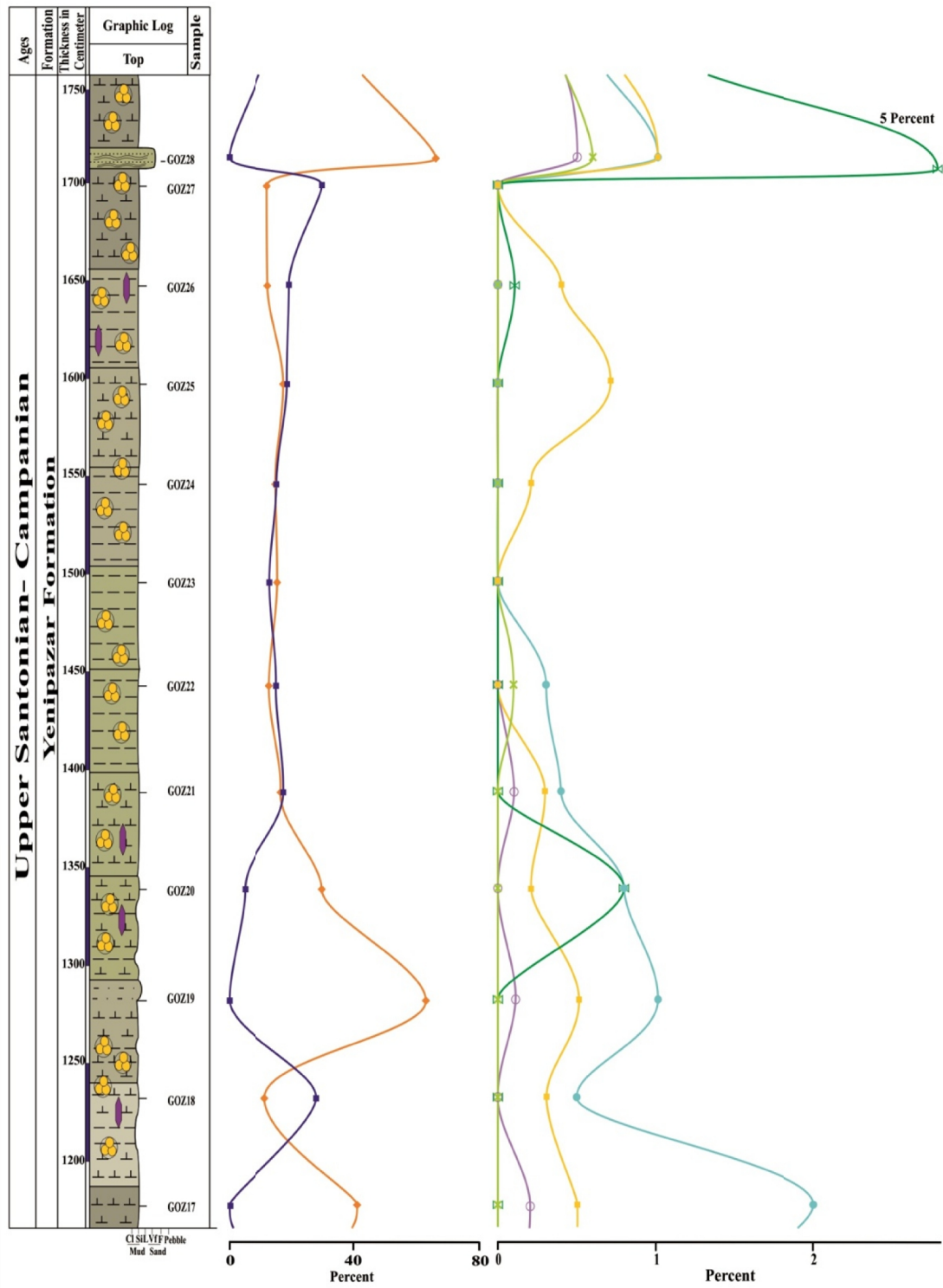


Figure 3.32: Continued.

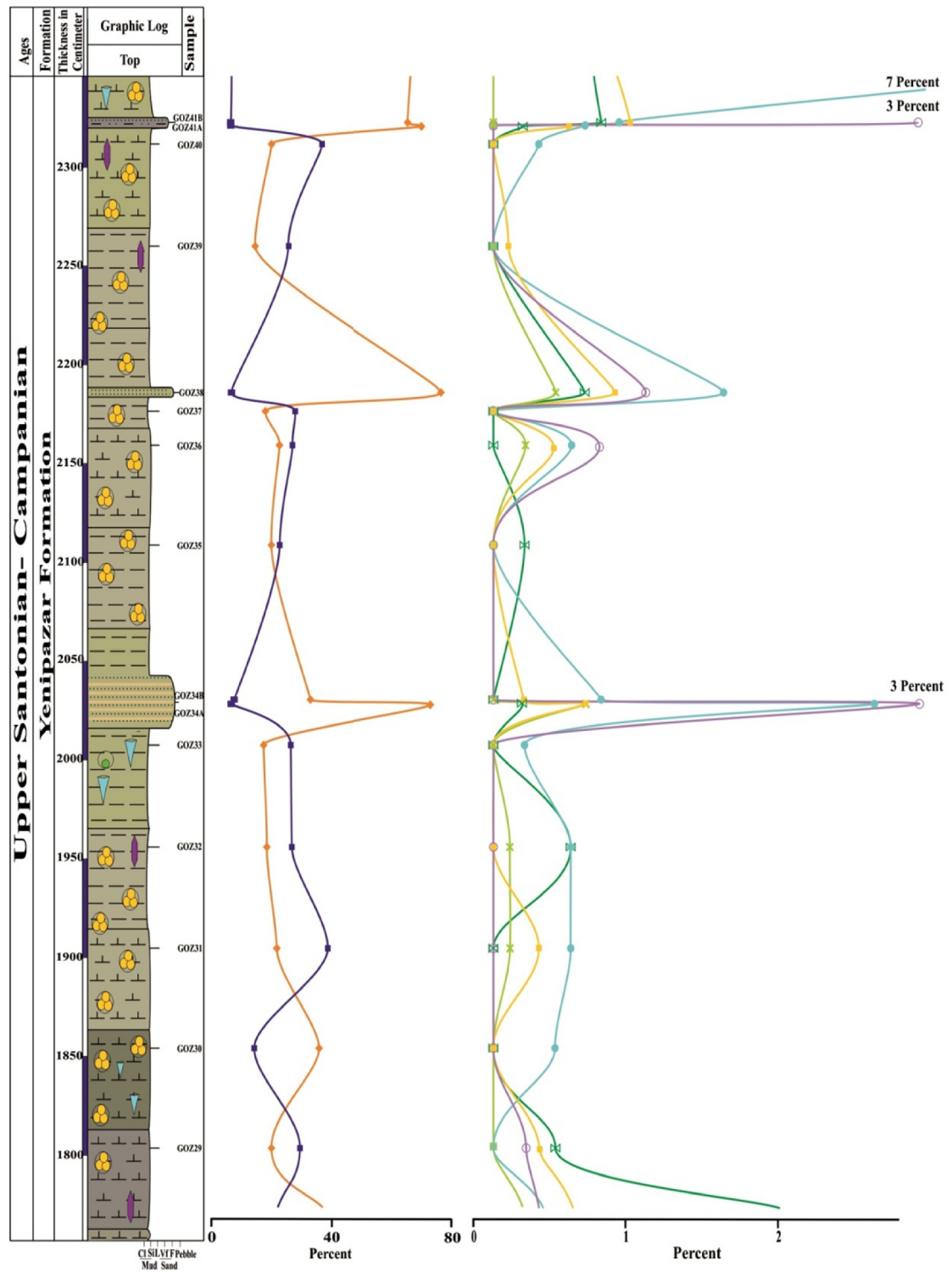


Figure 3.32: Continued.

GÖYNÜK VILLAGE STRATIGRAPHIC SECTION

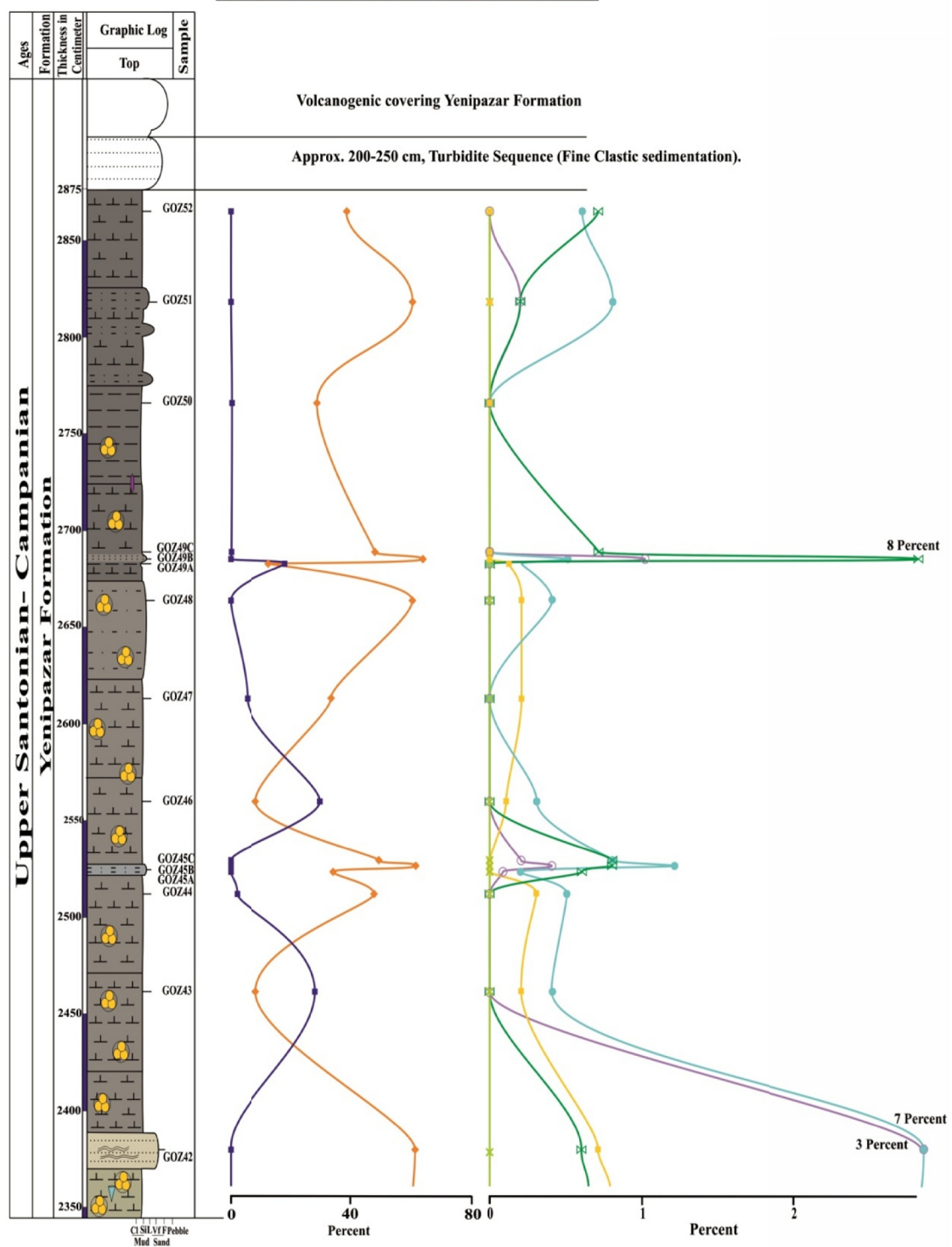


Figure 3.32: Continued.

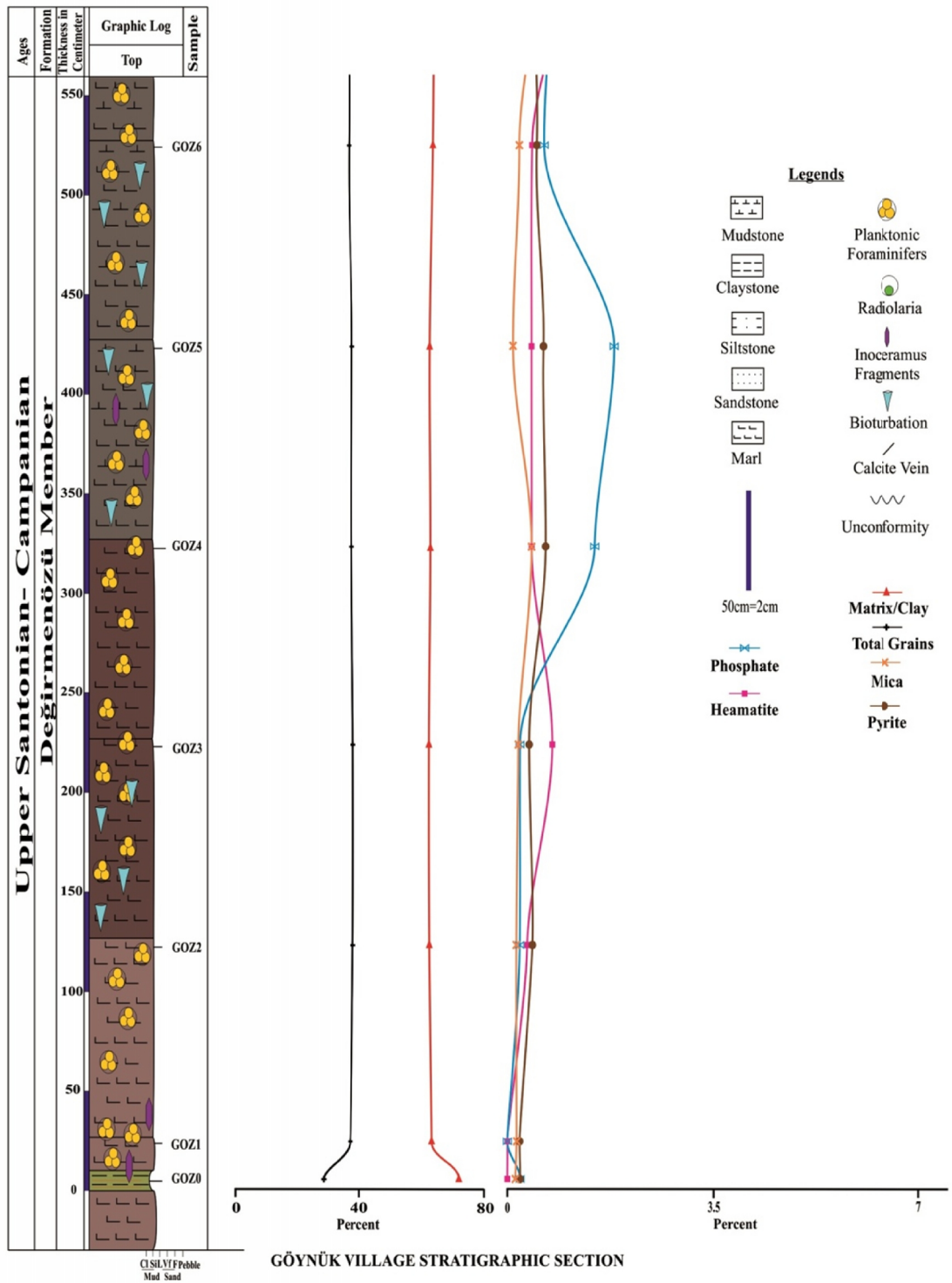


Figure 3.33: Representing Matrix-Total grains-Mica (2*)-Pyrite-Phosphate (10*) – Hematite (2*) graphic curves of the Göynük stratigraphic section petrographic data. (Note: 10* and 2* represents 10 and 2 time increase, respectively).

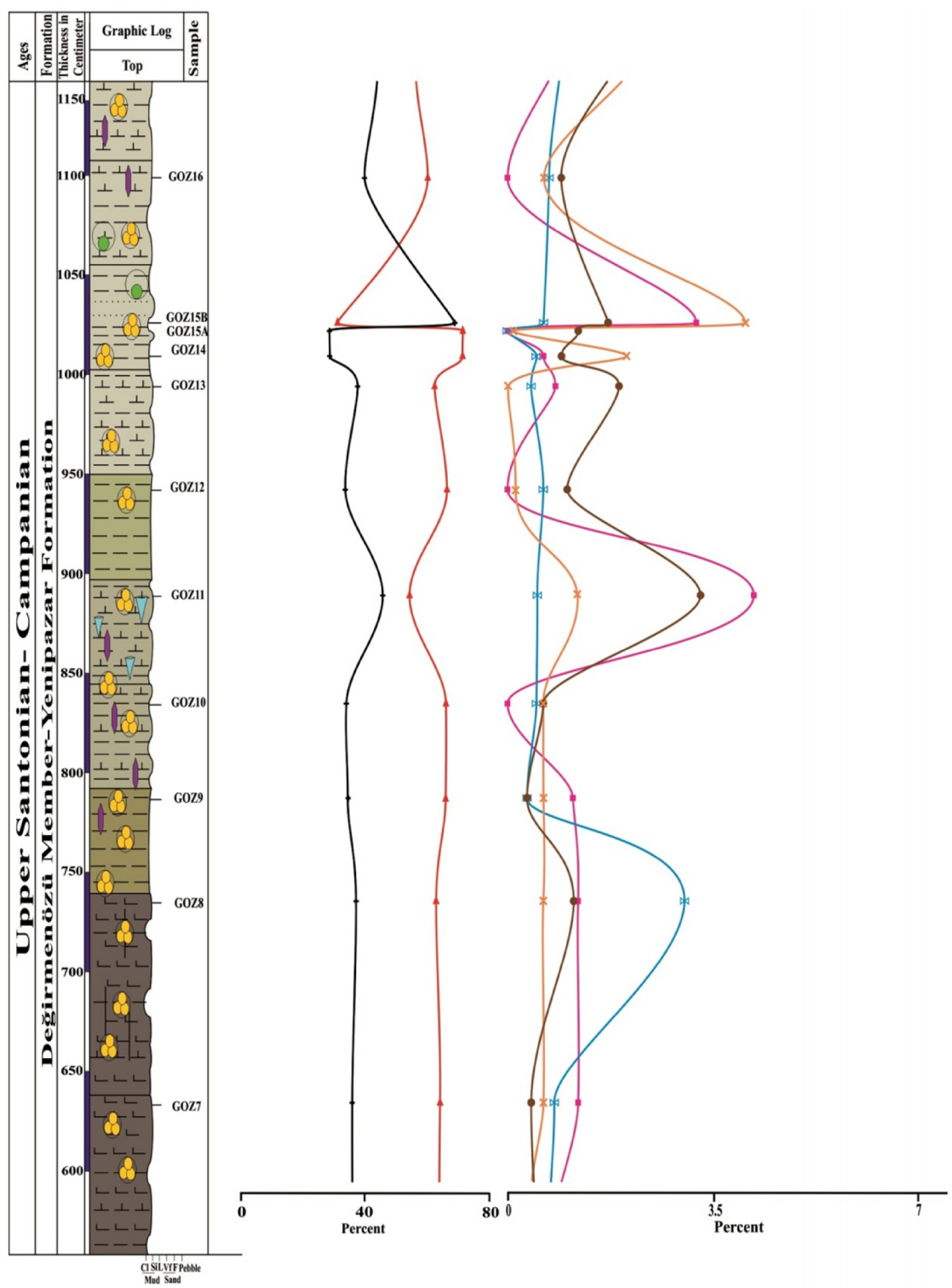


Figure 3.33: Continued.

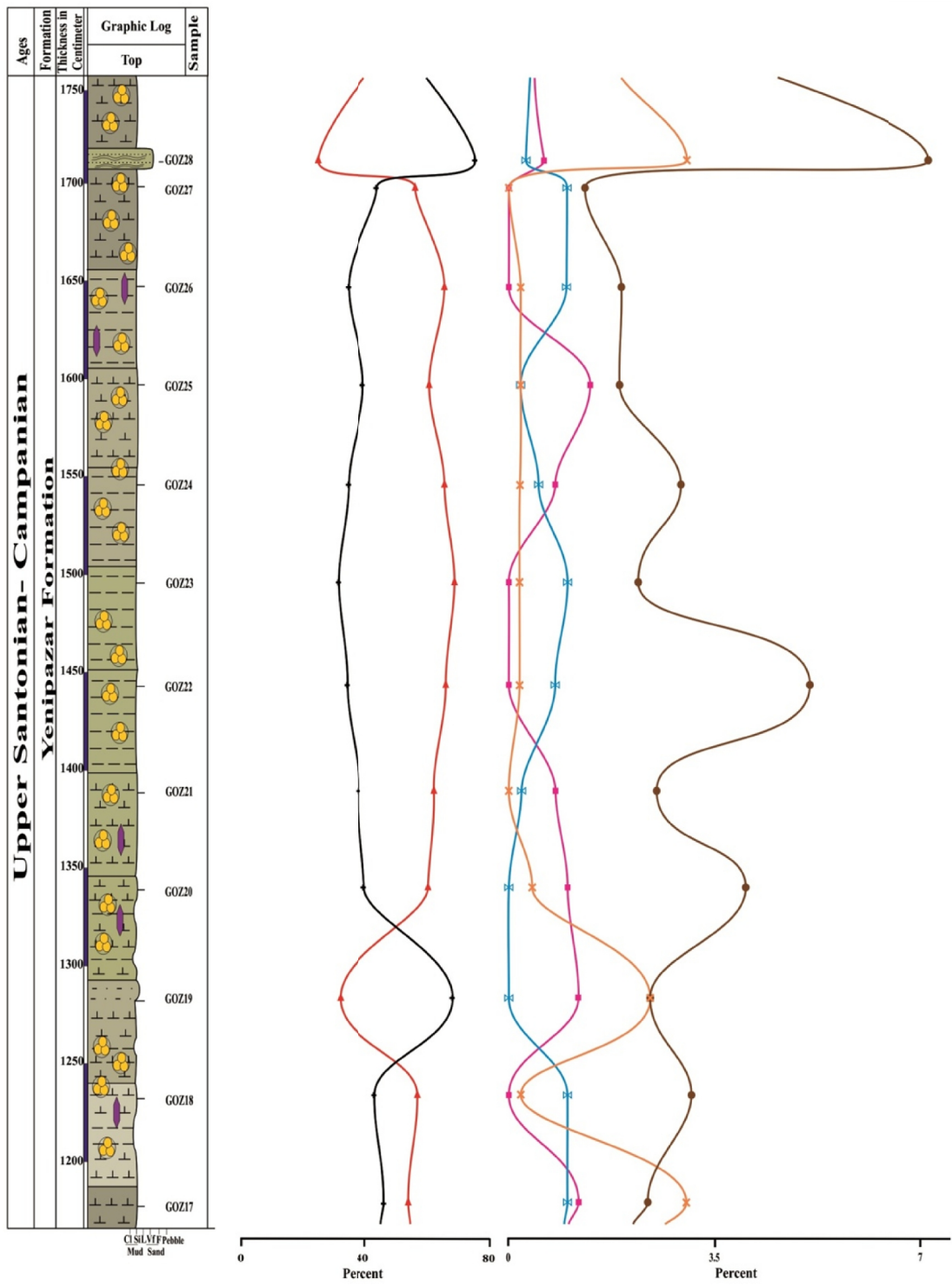


Figure 3.33: Continued.

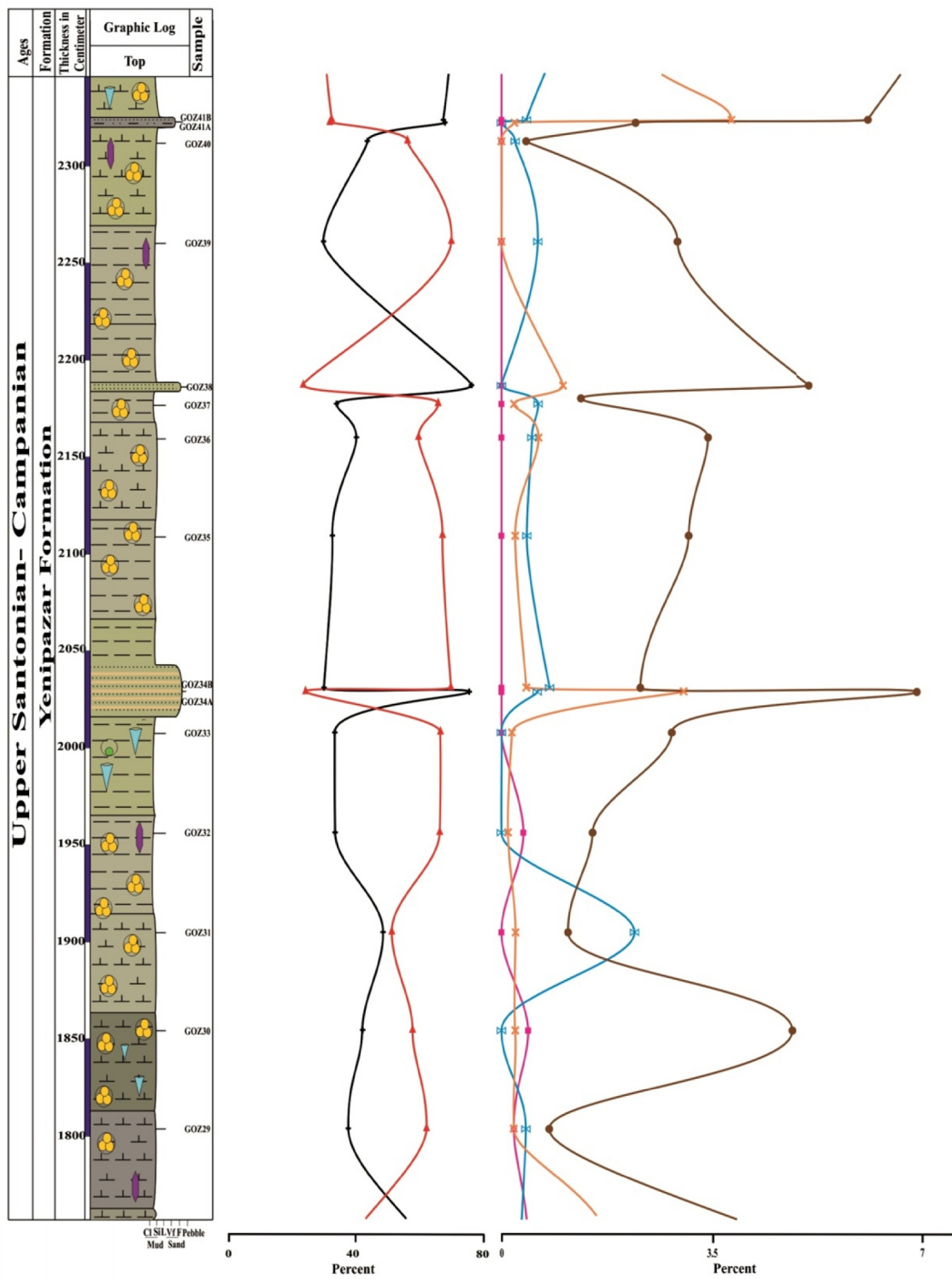


Figure 3.33: Continued.

GÖYNÜK VILLAGE STRATIGRAPHIC SECTION

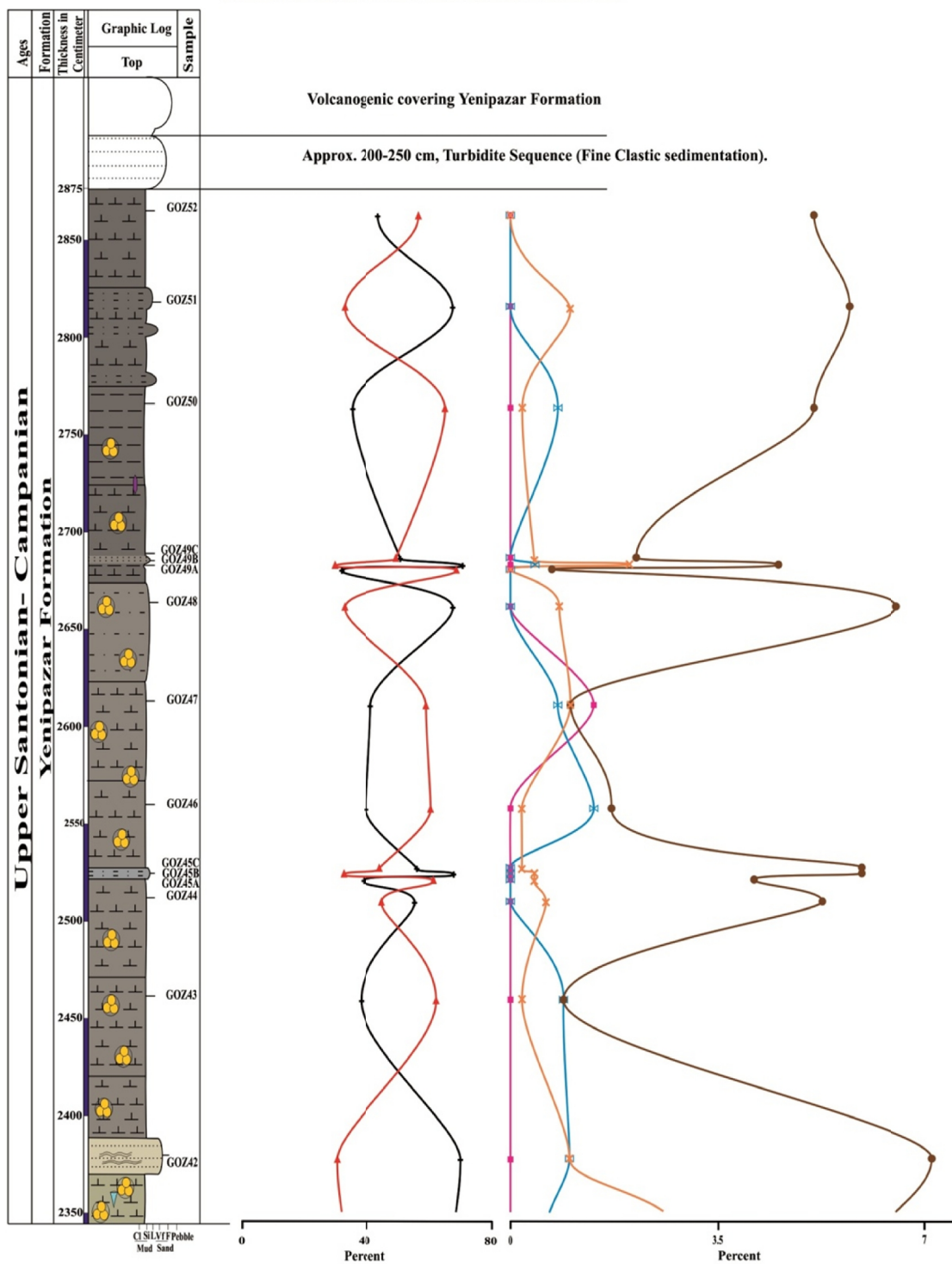


Figure 3.33: Continued.

The Alagöz Section is measured up to 1900 cm where as Göynük Section is measured up to 2875 cm (Figures 2.7, 2.11). After 1900 cm, there will be an imagery linear trend drawn in the Alagöz Section to be compared with above section of Göynük section.

The bulk composition of Alagöz and Göynük sections are composed of quartz, feldspar, plagioclase, mica, glauconite, heavy minerals, lithics, bioclasts, pyrite, hematite, phosphate and matrix (Tables 3.6-3.7). Few samples of the Alagöz Section show opaline patches within the matrix. The sections are compared on the basis of their compositional icons which are represented in the form of graphic curve to visualize the changes and similarities within the studied sections which are narrated as under:

3.7.1 QUARTZ

Quartz is one of the main fundamental units of most of the sedimentary rocks. Quartz grains have been observed in every sample in both measured stratigraphic sections, from 0.3 % minimum to 72.81% maximum. The red beds of Alagöz Section begin with low percent of quartz content and then sudden rise and subsequently followed by a slight fall in the quartz grains (Figure 3.34). The minimum and maximum values of quartz content in the red beds of the Alagöz Section is 0.3% and 72.81%, respectively (Table 3.8), with a mean value of 37.44%. The red beds of Göynük Section are represented by low quartz content as compared to the Alagöz Section with a mean of 9.19%. It shows a minimum of 6.72% and a maximum of 12.50% of quartz (Table 3.10).

In the greenish grayish bedding, the Alagöz Section quartz is characterized as falling graphic line while Göynük Section represents highly fluctuated graph curve with relative high positive peaks (Figure 3.34). The minimum to maximum values of the Alagöz and Göynük sections are 13.30% to 37.68% and 4.30% to 69.90%, respectively. The mean values are 24.87% of Alagöz and 29.88% of Göynük section (Tables 3.9-3.11). The higher mean value in the Göynük Section is because of intercalation of turbiditic fine sandstone and siltstone. The overall linear trend in these beds of Alagöz and Göynük section is relative similar (Figure 3.34).

Table 3.8: Percent date Statistical description of red beds of the Alagöz Section from Table 3.6.

	Quartz	Feldspar	Plagioclase	Mica	Glauconite	Heavy Mineral	Lithics	Bio-clasts	Pyrite	Heamatite	Phosphate	Lime Mud	Matrix /Clay	Opal	Total Grains	Total Matrix / Clay
Mean	37.4	0	0.03	1.22	0.02	0.01	5	17.2	1.78	0.46	0.02	6.04	29.26	1.5	63.2	36.8
Median	41.4	0	0.02	1.55	0.02	0.01	0.05	0.02	1.85	0.00	0.00	0.00	31.55	0	64.2	35.8
Standard Deviation	25.5	0.01	0.04	0.84	0.01	0.00	14.00	31.7	1.19	0.65	0.04	11.19	21.86	2.9	12.9	12.9
Skewness	-0.5	0.64	1.04	-0.68	0.82	-1.44	2.83	1.4	0.61	0.88	1.50	1.44	-0.29	1.7	-0.3	0.3
Minimum	0.3	0	0	0.02	0.01	0	0.02	0	0.40	0	0	0	0	0	43.1	20.7
Maximum	72.8	0.01	0.10	2.00	0.03	0.01	39.64	70.2	3.88	1.55	0.10	24.18	56.90	7.4	79.2	56.9
Count	8	8	8	8	8	8	8	8	8	8	8	8	8	8	8	8

Table 3.9: Percent date statistical description of green to gray beds of the Alagöz Section from Table 3.6.

	Quartz	Feldspar	Plagioclase	Mica	Glauconite	Heavy Mineral	Lithics	Bio-clasts	Pyrite	Heamatite	Phosphate	Lime Mud	Matrix /Clay	Opal	Total Grains	Total Matrix / Clay
Mean	24.87	0	0	0.16	0.01	0	0.01	7.93	2.37	0.39	0	0	64.26	0	35.74	64.26
Median	24.60	0	0	0.02	0	0	0.00	6.50	2.30	0.00	0	0	65.85	0	34.15	65.85
Standard Deviation	7.66	0	0	0.31	0.01	0.01	0.02	4.99	0.97	0.71	0	0	4.99	0	4.99	4.99
Skewness	0.34	4.12	2.61	2.01	0.88	2.47	1.52	0.39	-0.01	2.11	NA	NA	-0.85	NA	0.85	-0.85
Minimum	13.30	0	0	0	0	0	0	0.22	0.60	0	0	0	53.20	0	29.90	53.20
Maximum	37.68	0.01	0.01	1.00	0.03	0.02	0.05	17.00	3.90	2.50	0	0	70.10	0	46.80	70.10
Count	17	17	17	17	17	17	17	17	17	17	17	17	17	17	17	17

Table 3.10: Percent date statistical description of red beds of Göynük Section from Table 3.7.

	Quartz	Feldspar	Plagioclase	Mica	Glauconite	Heavy Mineral	Lithics	Bio-clasts	Pyrite	Heamatite	Phosphate	Matrix /Clay	Total Grains
Mean	9.19	0	0.01	0.14	0.02	0.01	0.03	26.58	0.53	0.29	0.10	63.11	36.89
Median	8.30	0	0	0.08	0.01	0	0.03	26.99	0.47	0.20	0.07	63.05	36.96
Standard Deviation	2.12	0.01	0.01	0.11	0.02	0.01	0.02	1.66	0.27	0.21	0.10	0.60	0.60
Skewness	1.01	2.83	0.89	0.80	1.36	1.32	0.25	-0.60	1.38	0.55	1.15	0.27	-0.27
Minimum	6.72	0	0	0.03	0	0	0	23.98	0.20	0	0.01	62.32	35.96
Maximum	12.50	0.02	0.03	0.30	0.06	0.02	0.06	28.56	1.10	0.60	0.30	64.04	37.68
Count	8	8	8	8	8	8	8	8	8	8	8	8	8

Table 3.11: Percent date statistical description of green to gray beds of the Göynük Section from Table 3.7.

	Quartz	Feldspar	Plagioclase	Mica	Glauconite	Heavy Mineral	Lithics	Bio-class	Pyrite	Hematite	Phosphate	Matrix /Clay	Total Grains
Mean	29.88	0	0.09	0.34	0.04	0.03	0.03	11.70	2.98	0.19	0.04	54.68	45.32
Median	20.17	0	0.04	0.10	0	0	0.02	10.38	2.38	0	0.04	60.26	39.74
Standard Deviation	21.41	0.01	0.26	0.49	0.10	0.07	0.03	11.29	2.03	0.40	0.05	14.87	14.87
Skewness	0.62	3.48	5.83	2.14	3.52	3.29	0.94	0.27	0.57	3.21	1.32	-0.87	0.87
Minimum	4.30	0	0	0	0	0	0	0	0.20	0	0	23.98	28.34
Maximum	69.90	0.06	1.80	2.00	0.50	0.30	0.10	31.80	7.10	2.10	0.22	71.66	76.02
Count	52	52	52	52	52	52	52	52	52	52	52	52	52

3.7.2 FELDSPAR AND PLAGIOCLASE

Feldspar and plagioclase are other important minerals of the sedimentary rocks. These occurred in less percent due to their instability. These are mostly associated with immature sedimentary rocks (Folk, 1974; Pettijohn, 1954).

The feldspar and plagioclase have been observed in both sections but in very small amount (Figures 3.34). In the Alagöz Section, the red beds display few peaks of feldspar and plagioclase while green-gray bedding represents feldspar at ZR07 and plagioclase at ZR05 (Figure 3.34). Where, the Göynük Section shows single feldspar and two plagioclase peaks in the red beds. Above the red beds of the Göynük Section, there are number of peaks in feldspar and plagioclase.

3.7.3 MICA

In the studied sections, mica represents ascending graphic trend with increasing terrigenous influx to the system. In the Alagöz Section, red beds have high peaks as compared to the Göynük red beds and opposite in the green-gray bedding (Figure 3.35). In the red beds, ZR03 and GOZ4 represents similar increasing pattern. Such a case has

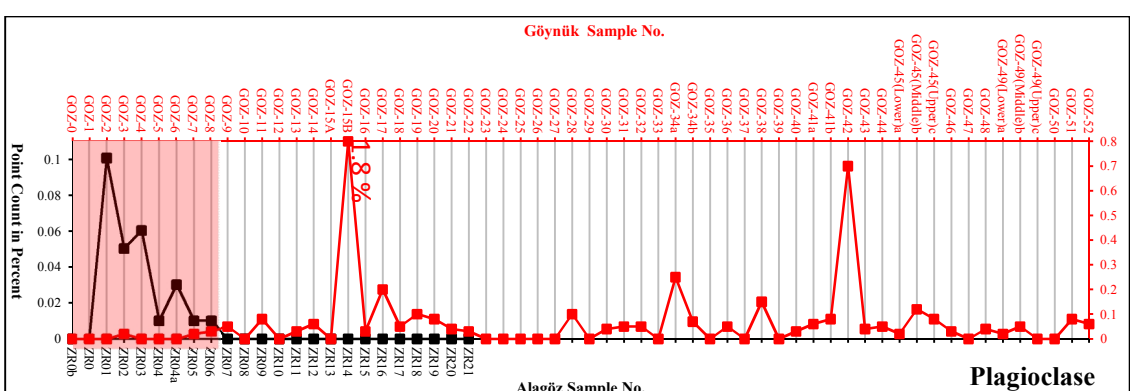
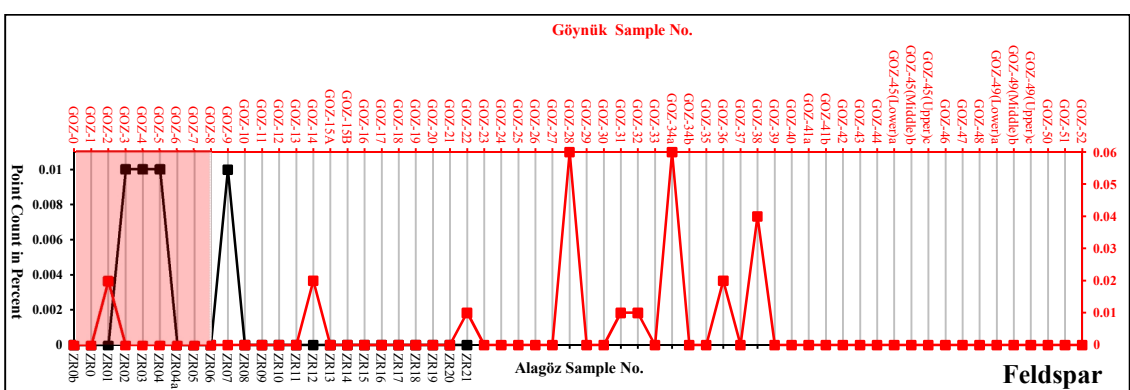
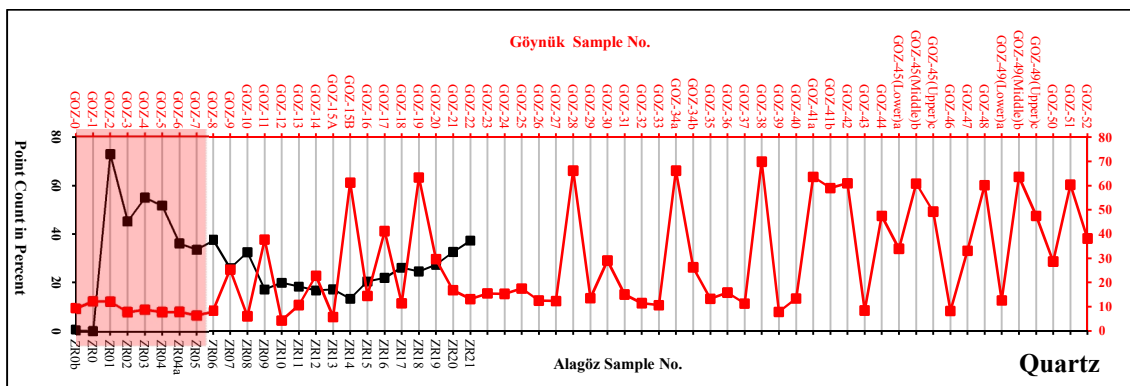


Figure 3.34: The graphic curves comparison of quartz, feldspar and plagioclase of Alagöz Section (black line) and Göynük Section (red line). (Red beds represented by red shaded area)

also been observed in the greenish grayish bedding near ZR17 and GOZ18. Overall, the Göynük Section contains more mica as compared to the Alagöz Section (Tables 3.8-3.11).

3.7.4 GLAUCONITE AND HEAVY MINERAL

The glauconite indicates zigzag pattern in the Alagöz and the Göynük sections. The ZR04 and GOZ5 represent similar direction curve with relatively high peak in the GOZ5. In the overlying greenish grayish bedding in both sections, suggests seasonal influx to the depositional environment. In the Göynük Section, after GOZ28, there is relatively uniform increasing and decreasing the curve (Figure 3.35).

The inputs of heavy minerals depend on the terrestrial source and volcanic activity. At ZR01 and GOZ2, there are similar graphic peaks in heavy minerals, which have been identified in the red beds. In the greenish grayish facies, there is also number of peaks in both sections. Relative high percent of heavy minerals curves occurred in the greenish grayish facies of the Göynük Section which have been associated with intercalated fine sandstone and siltstone (Figure 3.35).

3.7.5 LITHIC CLASTS

Lithic clasts are comprised of sedimentary and volcanic-clasts. In both studied sections, they represent moderately similar rising and falling peaks trend in the red beds (Figure 3.36). The content of lithics in the red beds of the Alagöz Section was found to be higher than the Göynük red beds. Relatively close peaks have been observed at ZR04-GOZ5, ZR05-GOZ7, ZR10-GOZ12, ZR13-GOZ15A and ZR20-GOZ22 (Figure 3.36). In the Göynük Section, the top portion indicates cyclic increase and decrease in the graphic curve of lithics.

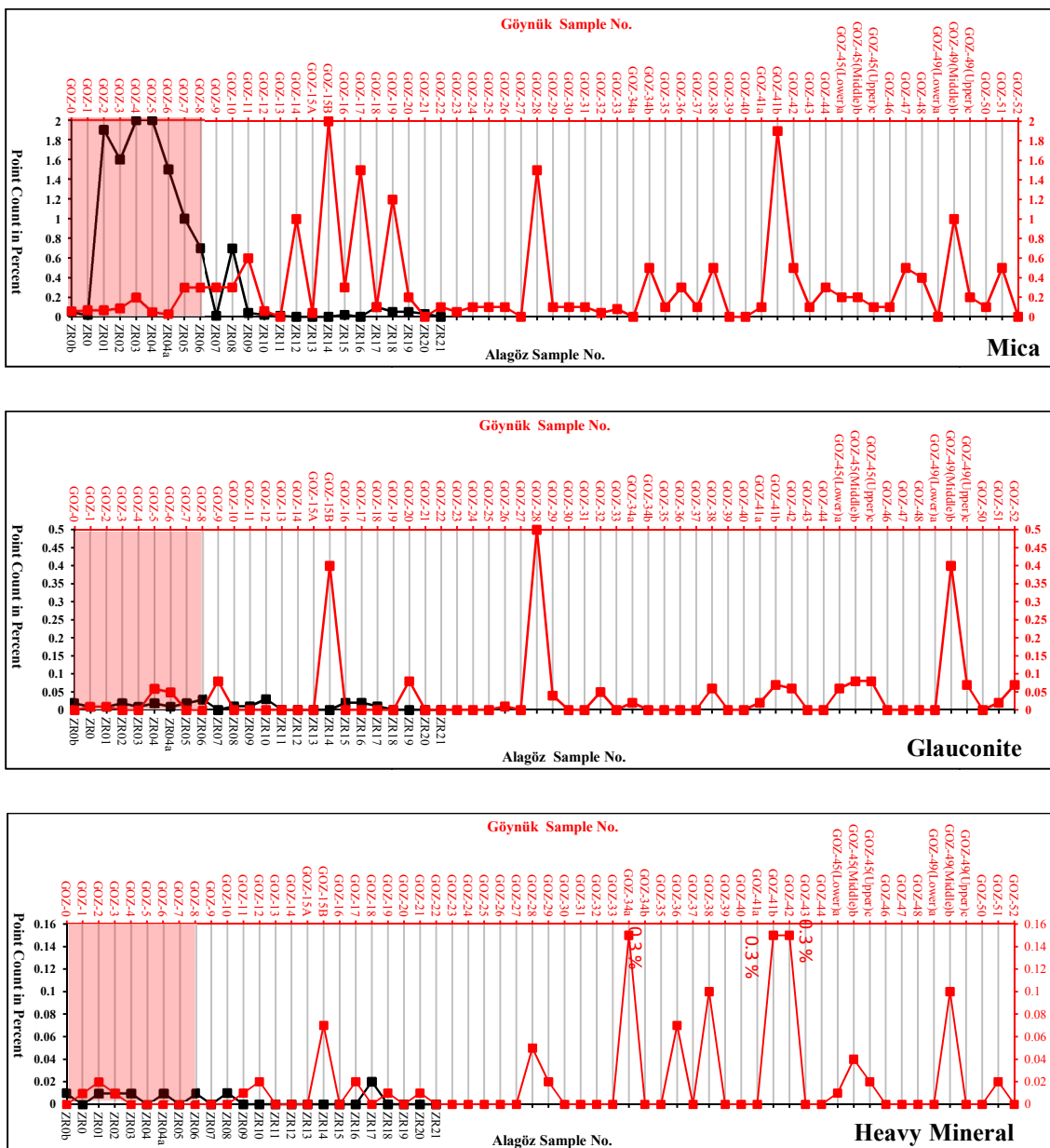


Figure 3.35: The graphic curves comparison of mica, glauconite and heavy minerals of the Alagöz Section (black line) and Göynük Section (red line) (red shade represents red beds). (Red beds represented by red shaded area)

3.7.6 BIOCLASTS

The bioclastic pattern has been mostly characterized by high planktonic foraminifers with low percent of other fossils (Tables 3.2, 3.4). In the Alagöz red beds, bioclasts are observed to be 70.24% at maximum and 0% at minimum (Table 3.8). In the contrast, the Göynük Section red beds have been noticed with 28.56 % maximum and 23.98 % minimum (Table 3.10). It is suggested that the deposition of red beds in the Göynük Section have been less interrupted by terrigenous input as compared to the Alagöz red beds. The green to gray beds of the Alagöz and Göynük sections display similar curve behavior.

From middle to top portion, the Alagöz Section shows increase trend in bioclasts curve. Similar situation occurred in the Göynük Section but represented rhythmic increase and decrease toward the upper portion that has been interrupted by turbiditic sequences (Figure 3.36).

The mean of bioclast values in the Alagöz and Göynük sections in the green to gray beds are 7.93% and 11.70%, respectively (Tables 3.9, 3.11). It indicates that the proportion of planktonic foraminifers along with other low bioclasts in the Göynük Section has been relatively high as compared to the Alagöz Section.

3.7.7 HEMATITE AND PHOSPHATE

The hematite grains have been found in the lower and middle part of the Göynük Section and random observed peaks in the Alagöz studied area (Figure 3.36). At the boundary between red beds and green-gray lithologies, there is similar increasing projection in the curve followed by declining curve line. The maximum percentage in the red beds and green-gray beds of the Alagöz succession is 1.55% and 2.50 %, respectively. On the other hand, the red beds and green-gray beds of the Göynük succession represent maximum 0.6% and 2.10%, respectively. The Alagöz red beds succession has relatively high mean values (0.46%) of hematite as compared to the Alagöz green-gray beds (0.39%), Göynük red beds (0.29 %) and green-gray beds (0.19%) (Tables 3.8-3.11).

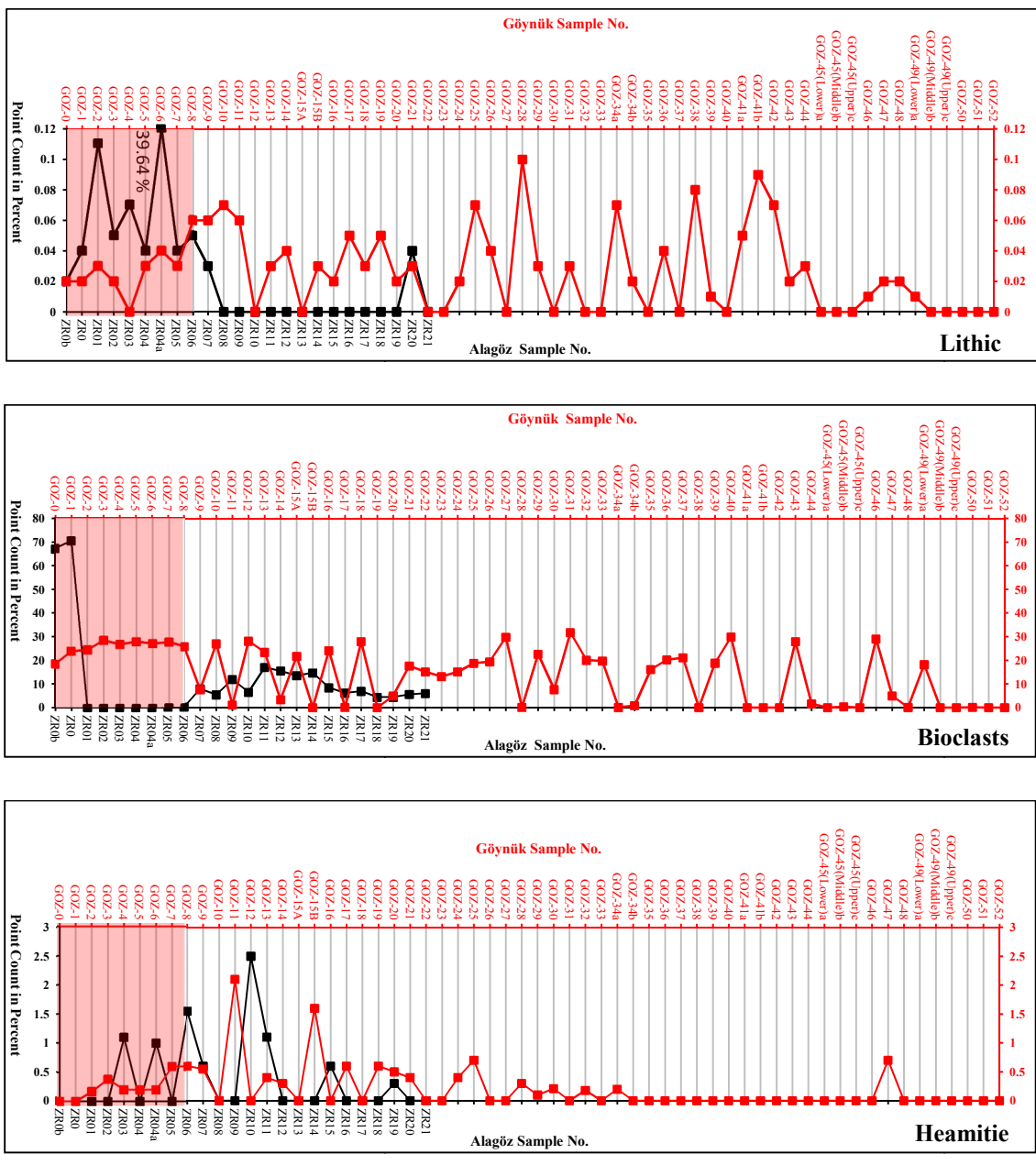


Figure 3.36: The graphic curves comparison of lithic, bioclasts and heamatite of Alagöz Section (black line) and Göynük Section (red line). (Red beds represented by red shaded area)

The presences of phosphatic grains are only restricted with few red beds in the Alagöz Section. In the Göynük Section, the red beds indicate maximum 0.3% value. Later, in the green-gray beds of Göynük strata show some crests which are below 0.15% except one sample GOZ31 (Figure 3.37).

3.7.8 PYRITE

The presences of pyrite and their occurrence in the early diagenesis depend on the environmental condition and availability of Fe source, sulfate and organic matter (Berner, 1970, 1984; Schoonen and Barnes, 1991).

Pyrite has been frequently observed in both sections with low percent. The comparison graphs of pyrite of the Alagöz and the Göynük sections show similar increasing linear trends (Figure 3.37). The maximum 7.10% value has been observed in the Göynük Section at GOZ 28 which represents fine sandstone quartz-wacke lithofacies.

3.7.9 MATRIX/CLAY

In the red beds, the Alagöz Section displays relatively low matrix content as compared to the Göynük Section. The mean of the Alagöz red beds matrix/clay is 29.26% where the Göynük red beds gives 63.11% mean value (Tables 3.8, 3.10).

In the green-gray bedding, both sections are characterized by almost similar pattern up to ZR13 and GOZ15A. After these samples, there is rapid fall in the matrix line of Göynük Section while relatively constant rate in the Alagöz Section. The upper portion of the Göynük Section is described as linear straight line but more toward the increasing percent (Figure 3.37). The matrix/clay mean of green-gray beds is 64.26% for the Alagöz section and 54.68% for the Göynük Section (Tables 11 and 13).

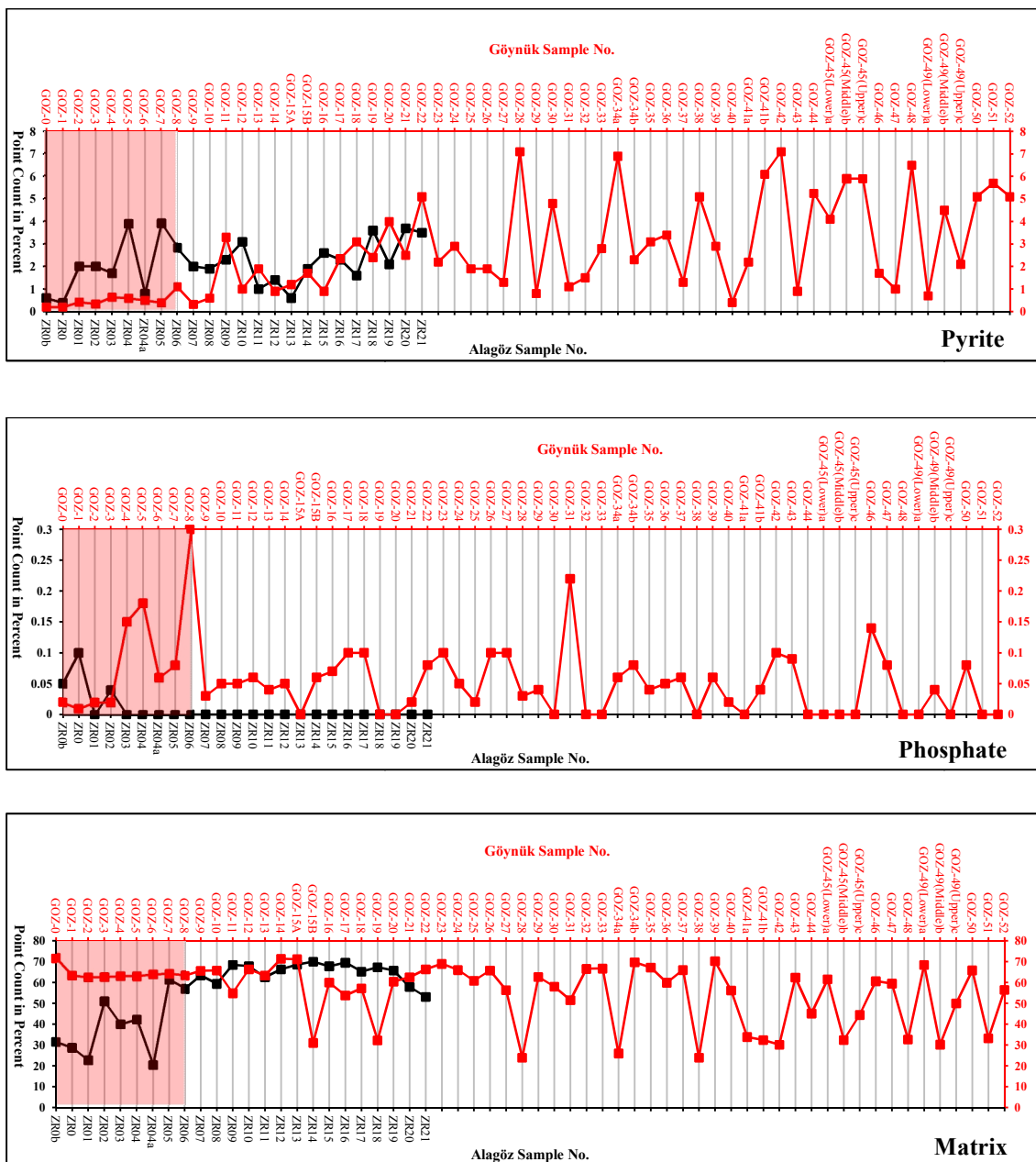


Figure 3.37: The graphic curves comparison of pyrite, phosphate and matrix comparison graphic curves of Alagöz section (black line) and Göynük Section (red line). (red beds represented by red shaded area)

3.7.10 TOTAL GRAINS

The total grains are the sum of terrigenous grains, bioclasts and all other minerals. Gradual declining in the total grains graphic curve of the Alagöz red beds sequence have been observed while relatively straight line in the red beds of Göynük Section (Figure 3.38). The average percent values of red beds of both sections are close which are 36.82% in the Alagöz red beds and 36.89% in the Göynük red beds (Tables 3.8, 3.10).

The green-gray lithologies of the studied sections are described by increasing virtual linear trend line in the total grains. Occasional high peaks are recognized in the Göynük Section green-gray lithologies which are characterized by fine sandstone and siltstone intervals within the succession (Figure 3.38). The total grains are in high proportion in the Alagöz area with a mean of 64.26% as compared to the Göynük area having 45.32 % mean value (Tables 3.9, 3.11).

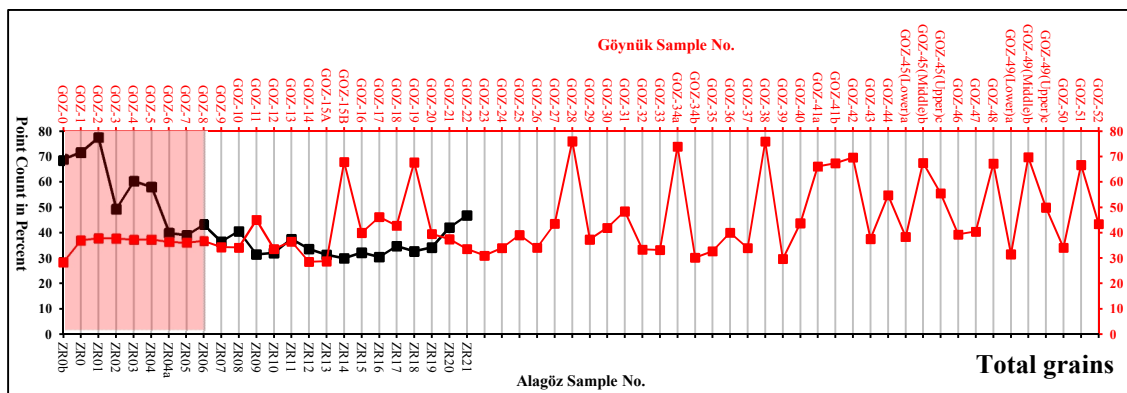


Figure 3.38: The graphic curves comparison of total grains of Alagöz Section (black line) and Göynük Section (red line). (Red beds represented by red shaded area)

3.8 INTERPRETATION AND DEPOSITIONAL ENVIRONMENT

Relative changes in the microfacies composition can be used to interpret changes in the climate as arid and humid climatic, changes in sea-level as regression and transgression and their depositional environments. According to Chamley (1989), Weaver (1989) and Li et al. (2000), change in the sediment sources are due to different climatic changes and/or sea level fluctuation (regression and transgression). In the studied sections, the green-gray fine grained siliciclastic succession is overlying the red beds which reflect transgressive condition. The depositions of the red beds were mostly occurred during low terrigenous input to system and were related with transgressive conditional environment and warmer climate, such conditions were indicated in the eastern Austrian Alps (Jansa and Hu, 2009; Wagreich et al., 2009).

The Late Cretaceous red beds and green-gray shale/mudstone are described as slope to deep marine pelagic-hemipelagic deposits which are controlled by influx of terrigenous, biogenic deposits, eustatic sea level, climate change and tectonic setting (Wang et al., 2009; Egger et al., 2002). The studied sections are characterized by silty marls, marls, mudstone, claystone and occasional limestone, siltstone and fine sandstone which interprets deep marine environment with occasional fine grained turbiditic interruption.

The colours of the pelagic lithologies give clue to the paleoceanographic condition (Colley et al., 1984; Wilson et al, 1985; Thomson et al., 1987). The low rates of sediment deposits are also responsible for the development of the red beds (Thomson et al., 1987; Eren and Kadir, 1999). Therefore, it is interpreted that the red beds in the Alagöz and the Göynük sections represent low sedimentation rate and deposited in oxic condition. These red beds of the studied sections can be comparable with Chuangde Formation of Southern Tibet (Wang et al., 2005) and Santonian strata of eastern Alps of Austria (Scott, 2009).

The overlying green-gray succession of the Alagöz and the Göynük areas indicate changes in redox condition from oxic to dysoxic condition/ oxygen depletion in the bottom water. It also suggests that relative high rate of accumulation in the deep marine environment, causes rapid burial and as a result less time for sediment to interface with

oxygen rich bottom water. Such causes are responsible in the deposition of green-gray succession in the oxygen rich bottom water and less probability of red beds (Wang et al., 2009; Wagreich et al., 2009). These green-gray successions of the Alagöz and the Göynük section can be related with Early Campanian Ultrahelvetic units of Austrain Eastern Alps where similar condition occurred. The ending of red beds in Upper Cretaceous was due to increase in the clastic influx to the depositional environment (Wagreich et al., 2009).

The boundary between the red beds and green-gray sequence in the Alagöz and Göynük measured stratigraphic sections has transitional condition. The marly red beds overlain by the fine grained green-gray turbiditic lithofacies imply transgressive condition in the studied sections (Schlager, 1991; Yilmaz et al., 2010). These may correspond to increase in the sea level and/or tectonic subsidence.

The high proportion of planktonic foraminifers and low ratio/rare benthic foraminifers in the studied sections indicates deposition of sediments in the open marine bathyal environment (Kostka, 1993).

In the red beds of studied sections, bioturbation are documented during microscopic studies which represent oxygen-rich environment (Skupien et al., 2009). While, rarely present micro-burrows in the green-gray lithologies indicate development of oxygen rich horizons during the deposition. The terrigenous influx is introduced to the deep ocean by eolian and/or turbiditic current. Overall, the red beds of both sections are interpreted as oxygen rich deep bottom water with relative slow accumulation rate. In contrast, the greenish-grayish beds of the studied section are described as relatively low oxygen/depletion in the oxygen in the deep marine environment with relatively high sedimentation rate and accompanied by increasing eustatic sea level and/or tectonic subsidence.

CHAPTER 4

GEOCHEMICAL ANALYSIS

4.1 INTRODUCTION

Geochemical studies have been carried out by analyzing the major oxides, trace element contents of the samples collected throughout the measured section in order to determine the geochemical classification of sedimentary rocks (especially fine grained mudrocks), redox-sensitive in the paleo-environmental condition, provenance character and to approach the tectonic setting of depositional sediments of the Alagöz and Göynük measured stratigraphic sections.

4.2 MAJOR OXIDES OF THE ALAGÖZ AND GÖYNÜK SECTIONS

The geochemical data of the major oxides in the studied sections are varying from facies to facies, and are correlated with one another's trend. Normally, shale and mudstone of the marine environments are characterized by high proportion of three major oxides i.e. SiO_2 (siliceous biogenic and/or quartz grains), Al_2O_3 (clayey enrichment) and CaO (related with calcareous content) (Daniel and Bustin, 2009). Similarly, in the studied sections, the dominant major oxides are SiO_2 (ranging from 15.65-70.80 wt.% Alagöz Section; 22.13-48.86 wt.% Göynük Section), Al_2O_3 (ranging from 2.53-13.18 wt.% Alagöz Section; 6.36-14.34 wt.% Göynük Section) and CaO (ranging from 7.01-39.03 wt.% Alagöz Section; 12.60-33.37 wt.% Göynük Section) with minor amount of other oxides, trace elements and rare earth elements (Tables 4.1-4.12).

Table 4.1: Major element (wt.%), REE (ppm) and normalized values of the red beds of Alagöz Section.

Sample	Type	SiO ₂	Al ₂ O ₃	Fe ₂ O ₃	MgO	CaO	Na ₂ O	K ₂ O	TiO ₂	P ₂ O ₅	MnO	Cr ₂ O ₃	TOT/C	$\sum \text{LREE}/\sum \text{HREE}$	Ce*	Eu*
ZR0b	Packstone	70.80	2.53	1.26	0.63	12.23	0.22	0.67	0.10	0.03	0.10	0.03	2.66	7.93	0.60	1.24
ZR0	Packstone	58.04	2.60	0.84	0.71	19.50	0.25	0.61	0.10	0.04	0.16	0.01	4.32	7.63	0.58	1.23
ZR2	Silty Marl	48.40	12.55	8.28	4.53	8.90	1.52	2.32	1.13	0.15	0.11	0.06	1.87	9.36	0.86	1.24
ZR3	Silty Marl	49.43	13.18	9.35	5.16	7.01	1.67	2.23	1.19	0.17	0.10	0.07	1.38	9.74	0.90	1.23
ZR4	Silty Marl	43.82	11.93	8.60	5.49	11.18	1.44	1.70	1.20	0.16	0.13	0.06	2.31	10.63	0.80	1.22
ZR6	Silty Marl	43.26	12.25	9.22	6.29	10.67	1.56	1.54	1.34	0.18	0.13	0.06	2.22	10.69	0.89	1.28
ZR1	Siltstone	49.72	12.44	8.92	3.92	8.54	1.55	2.40	1.11	0.16	0.11	0.08	1.72	9.54	0.86	1.27
ZR4a	Siltstone	15.65	3.77	3.05	2.42	39.03	0.50	0.53	0.34	0.07	0.66	0.12	8.94	12.48	0.78	1.25
Mean		47.39	8.91	6.19	3.64	14.63	1.09	1.50	0.81	0.12	0.19	0.06	3.18	9.75	0.78	1.25
Standard Deviation		15.63	4.94	3.77	2.16	10.56	0.64	0.80	0.53	0.06	0.19	0.03	2.49	1.56	0.13	0.02
Minimum		15.65	2.53	0.84	0.63	7.01	0.22	0.53	0.10	0.03	0.10	0.01	1.38	7.63	0.58	1.22
Maximum		70.80	13.18	9.35	6.29	39.03	1.67	2.40	1.34	0.18	0.66	0.12	8.94	12.48	0.90	1.28
1.	REE-Rare Earth Element, LREE-Light Rare Earth Element, HREE-Heavy Rare Earth Element															
2.	PAAS-Post-Archaean Australian Shale (Taylor and McLennan, 1985),															
3.	* PAAS normalization values															
4.	Ce/Ce* = $(\text{Ce}_{\text{sample}}/\text{Ce}^*)/[(\text{La}_{\text{sample}}/\text{La}^*)(\text{Pr}_{\text{sample}}/\text{Pr}^*)]^{0.5}$															
5.	Eu/Eu* = $(\text{Eu}_{\text{sample}}/\text{Eu}^*)/[(\text{Sm}_{\text{sample}}/\text{Sm}^*)(\text{Gd}_{\text{sample}}/\text{Gd}^*)]^{0.5}$															

Table 4.2: Major element (wt.%), REE (ppm) and normalized values of the green-gray beds of Alagöz Section.

Sample	Type	SiO ₂	Al ₂ O ₃	Fe ₂ O ₃	MgO	CaO	Na ₂ O	K ₂ O	TiO ₂	P ₂ O ₅	MnO	Cr ₂ O ₃	TOT/C	$\sum \text{LREE}/\sum \text{HREE}$	Ce*	Eu*
ZR5	Mudstone	41.27	12.47	8.15	6.97	11.98	1.63	1.47	1.35	0.17	0.15	0.07	2.47	11.51	0.89	1.35
ZR7	Mudstone	39.02	10.96	7.25	5.61	15.20	1.35	1.37	1.05	0.16	0.13	0.05	3.23	9.23	0.82	1.29
ZR8	Mudstone	30.50	8.53	5.86	4.31	24.26	1.03	1.24	0.72	0.10	0.20	0.04	5.48	9.71	0.86	1.30
ZR11	Mudstone	31.28	8.26	5.13	3.46	24.91	0.96	1.40	0.60	0.09	0.19	0.03	5.61	10.28	0.82	1.27
ZR17	Mudstone	30.68	8.97	4.95	3.33	24.84	1.07	1.49	0.68	0.11	0.17	0.03	5.64	9.95	0.85	1.25
ZR20	Mudstone	32.44	9.31	5.61	3.58	23.28	1.02	1.62	0.65	0.10	0.19	0.03	5.24	9.68	0.88	1.23
ZR21	Mudstone	34.95	10.42	6.26	4.29	19.92	1.20	1.75	0.77	0.11	0.16	0.03	4.55	10.33	0.88	1.15
ZR9	Claystone	32.69	9.07	5.72	4.18	22.51	1.09	1.53	0.68	0.11	0.16	0.03	5.08	9.99	0.84	1.16
ZR10	Claystone	35.31	10.02	6.25	4.40	19.74	1.21	1.69	0.73	0.13	0.15	0.03	4.47	10.12	0.82	1.18
ZR12	Claystone	29.01	8.30	4.94	3.62	26.37	1.08	1.34	0.59	0.10	0.18	0.02	6.02	10.26	0.86	1.22
ZR13	Claystone	29.92	8.27	5.11	3.35	25.60	0.96	1.30	0.62	0.09	0.17	0.03	5.78	9.88	0.83	1.20
ZR14	Claystone	30.12	7.62	4.61	2.77	26.53	0.87	1.31	0.52	0.08	0.19	0.02	5.99	9.85	0.78	1.19
ZR15	Claystone	32.79	9.57	5.38	3.78	22.58	1.15	1.57	0.70	0.10	0.16	0.03	5.13	9.45	0.82	1.12
ZR16	Claystone	33.85	10.00	5.34	3.65	21.63	1.12	1.83	0.64	0.09	0.16	0.02	4.97	10.14	0.82	1.14
ZR18	Claystone	34.85	10.05	5.40	3.32	21.48	1.09	1.84	0.65	0.11	0.17	0.03	4.88	9.65	0.90	1.16
ZR19	Claystone	34.71	10.39	5.78	3.84	20.76	1.16	1.86	0.72	0.12	0.18	0.03	4.66	10.08	0.92	1.15
Mean		33.34	9.51	5.73	4.03	21.97	1.12	1.54	0.73	0.11	0.17	0.03	4.95	10.01	0.85	1.21
Standard Deviation		3.34	1.24	0.91	1.01	3.95	0.18	0.21	0.20	0.02	0.02	0.01	0.96	0.50	0.04	0.07
Minimum		29.01	7.62	4.61	2.77	11.98	0.87	1.24	0.52	0.08	0.13	0.02	2.47	9.23	0.78	1.12
Maximum		41.27	12.47	8.15	6.97	26.53	1.63	1.86	1.35	0.17	0.20	0.07	6.02	11.51	0.92	1.35

Table 4.3: Trace element (ppm) concentration in the red beds of Alagöz Section.

Sample	Rock	LOI	Sc	Ba	Co	Nb	Rb	Sr	Ta	Th	U	V	Zr	Mo	Cu	Pb	Zn	Ni	Cd
ZR0b	Packstone	11.3	3	142	5.4	2.7	20.9	169.5	0.1	0.8	0.4	23	19.7	<0.1	13.4	6.4	18	20.8	<0.1
ZR0	Packstone	17.1	2	177	6.8	2.4	19.4	233.1	0.1	0.9	0.5	17	18.4	<0.1	11.2	7.7	19	19.4	<0.1
ZR2	Silty Marl	11.8	17	279	36.0	17.0	83.1	194.0	1.2	6.7	1.3	163	149.4	0.1	36.9	9.6	83	259.7	<0.1
ZR3	Silty Marl	10.2	19	293	38.3	18.1	82.0	192.7	1.2	6.7	1.3	155	156.8	0.1	31.2	10.4	90	283.6	<0.1
ZR4	Silty Marl	14.0	18	273	37.1	18.6	62.4	253.0	1.2	6.7	1.4	158	151.7	<0.1	70.5	8.7	79	270.6	<0.1
ZR6	Silty Marl	13.2	19	218	39.0	21.4	54.0	251.6	1.5	5.8	1.4	175	157.0	<0.1	41.5	7.5	86	302.1	<0.1
ZR1	Siltstone	10.9	18	314	34.3	16.6	85.5	204.4	1.0	6.6	1.3	134	143.6	0.1	20.1	12.0	83	234.8	<0.1
ZR4a	Siltstone	33.7	8	79	16.1	5.2	19.6	402.9	0.3	2.0	0.6	53	45.0	<0.1	24.7	6.6	29	268.2	0.1
Mean		15.2	13	222	26.6	12.7	53.4	237.7	0.8	4.5	1.0	110	105.2	0.04	31.2	8.61	61	207.4	0.01
Standard Deviation		7.76	7	83	14.6	7.89	29.7	73.13	0.6	2.8	0.4	67	64.81	0.05	19.1	1.95	33	117.2	0.04
Minimum		10.2	2	79	5.4	2.4	19.4	169.5	0.1	0.8	0.4	17	18.4	<0.1	11.2	6.4	18	19.4	<0.1
Maximum		33.7	19	314	39	21.4	85.5	402.9	1.5	6.7	1.4	175	157	0.1	70.5	12	90	302.1	0.1

Table 4.4: Trace element (ppm) concentration in the green-gray beds of Alagöz Section.

Sample	Type	LOI	Sc	Ba	Co	Nb	Rb	Sr	Ta	Th	U	V	Zr	Mo	Cu	Pb	Zn	Ni	Cd
ZR5	Mudstone	14.0	19	209	54.1	20.1	49.0	268.9	1.2	6.8	1.6	160	152.0	<0.1	115.7	6.5	87	404.3	0.1
ZR7	Mudstone	17.6	16	204	34.9	17.6	51.8	331.5	1.2	5.5	1.2	145	129.9	<0.1	53.9	3.8	77	271.1	<0.1
ZR8	Mudstone	23.0	13	155	25.3	10.2	43.4	404.4	0.7	4.1	1.2	108	90.5	<0.1	41.2	5.3	59	181.9	<0.1
ZR11	Mudstone	23.5	11	183	23.9	8.9	51.5	451.2	0.5	4.4	1.1	93	81.8	<0.1	23.2	5.3	57	148.4	<0.1
ZR17	Mudstone	23.5	12	184	21.3	9.9	56.5	473.0	0.7	4.6	1.0	104	88.2	<0.1	42.4	4.2	54	98.7	<0.1
ZR20	Mudstone	22.0	12	205	21.7	9.3	62.9	407.4	0.6	5.0	1.2	101	87.8	<0.1	32.9	6.0	62	137.4	0.1
ZR21	Mudstone	19.9	14	216	25.9	11.7	66.3	439.6	0.8	5.6	1.3	117	115.3	<0.1	40.9	4.6	68	151.3	<0.1
ZR9	Claystone	22.0	13	178	23.4	10.8	57.3	423.0	0.7	4.7	1.1	117	95.3	<0.1	34.0	5.3	61	158.3	0.1
ZR10	Claystone	20.1	14	198	25.2	11.8	61.8	384.8	0.8	5.7	1.1	111	107.3	<0.1	46.7	7.0	64	163.4	0.1
ZR12	Claystone	24.2	11	230	19.7	9.0	47.1	489.0	0.5	4.6	1.1	95	82.4	<0.1	34.6	4.7	55	124.1	<0.1
ZR13	Claystone	24.4	11	191	24.3	9.0	50.0	506.0	0.6	3.8	1.0	95	83.9	<0.1	31.3	5.1	59	130.0	0.2
ZR14	Claystone	25.2	10	205	19.3	7.9	49.7	415.9	0.5	4.1	1.0	93	74.5	<0.1	28.9	4.8	50	122.1	0.1
ZR15	Claystone	22.0	13	196	24.2	10.3	56.8	451.8	0.7	5.1	1.2	112	94.5	<0.1	43.5	5.5	66	152.0	<0.1
ZR16	Claystone	21.5	13	232	21.0	9.6	66.3	387.0	0.6	5.8	1.2	121	94.0	<0.1	44.2	4.8	60	123.5	0.1
ZR18	Claystone	20.8	13	257	23.7	10.9	75.2	456.5	0.6	6.2	1.4	116	100.3	<0.1	44.8	5.6	61	122.7	0.1
ZR19	Claystone	20.2	13	240	23.9	11.3	70.9	381.8	0.8	6.2	1.2	111	111.7	<0.1	39.1	5.5	65	133.8	<0.1
Mean		21.5	13	205	25.7	11.1	57.3	416.9	0.7	5.1	1.2	112	99.34	0.00	43.58	5.2	63	163.9	0.06
Standard Deviation		2.8	2.2	25.8	8.35	3.23	9.17	59.67	0.2	0.9	0.2	18.3	20.05	0.00	20.69	0.8	9	74.77	0.06
Minimum		14	10	155	19.3	7.9	43.4	268.9	0.5	3.8	1	93	74.5	0.00	23.2	3.8	50	98.7	<0.1
Maximum		25	19	257	54.1	20.1	75.2	506	1.2	6.8	1.6	160	152	0.00	115.7	7	87	404.3	0.2

Table 4.5: REE (ppm) concentration in the red beds of Alagöz Section.

Sample	Type	La	Ce	Pr	Nd	Sm	Eu	Gd	Tb	Dy	Ho	Er	Tm	Yb	Lu	\sum LREE	\sum HREE	\sum REE
ZR0b	Packstone	6.9	8.2	1.45	5.6	1.15	0.32	1.28	0.20	1.09	0.25	0.70	0.10	0.69	0.11	24.90	3.14	28.04
ZR0	Packstone	7.8	9.2	1.69	7.4	1.44	0.38	1.47	0.23	1.35	0.31	0.86	0.12	0.85	0.13	29.38	3.85	33.23
ZR2	Silty Marl	20.7	37.3	4.88	19.2	3.94	0.99	3.60	0.63	3.88	0.70	1.93	0.30	1.95	0.29	90.61	9.68	100.29
ZR3	Silty Marl	20.9	41.0	5.29	19.3	4.00	1.05	4.07	0.67	3.84	0.69	1.97	0.30	2.01	0.34	95.61	9.82	105.43
ZR4	Silty Marl	24.3	41.0	5.72	23.5	4.74	1.17	4.27	0.67	3.75	0.74	2.09	0.31	1.98	0.31	104.7	9.85	114.55
ZR6	Silty Marl	20.8	40.6	5.27	20.5	3.88	1.03	3.69	0.64	3.47	0.65	1.88	0.27	1.76	0.29	95.77	8.96	104.73
ZR1	Siltstone	19.8	39.8	5.77	22.8	4.48	1.15	4.07	0.68	4.14	0.73	2.11	0.33	1.96	0.31	97.87	10.26	108.13
ZR4a	Siltstone	16.2	25.2	3.43	14.0	2.60	0.67	2.44	0.35	2.13	0.38	1.05	0.15	0.97	0.14	64.54	5.17	69.71
Mean		17.2	30.3	4.19	16.5	3.28	0.85	3.11	0.51	2.96	0.56	1.57	0.24	1.52	0.24	75.42	7.59	83.01
Standard Deviation		6.45	14.3	1.77	6.84	1.38	0.34	1.21	0.21	1.23	0.21	0.6	0.09	0.58	0.1	32.08	3.00	35
Minimum		6.90	8.2	1.45	5.6	1.15	0.32	1.28	0.2	1.09	0.25	0.7	0.1	0.69	0.11	24.9	3.14	28.04
Maximum		24.3	41	5.77	23.5	4.74	1.17	4.27	0.68	4.14	0.74	2.11	0.33	2.01	0.34	104.7	10.26	114.55

Table 4.6: REE (ppm) concentration in the green-gray beds of Alagöz Section.

Sample	Type	La	Ce	Pr	Nd	Sm	Eu	Gd	Tb	Dy	Ho	Er	Tm	Yb	Lu	\sum LREE	\sum HREE	\sum REE
ZR5	Mudstone	23.0	45.3	5.97	23.3	4.32	1.16	3.78	0.64	3.70	0.72	1.89	0.28	1.77	0.28	106.8	9.28	116.1
ZR7	Mudstone	17.4	32.4	4.75	18.7	3.52	0.97	3.56	0.58	3.43	0.60	1.79	0.26	1.86	0.29	81.3	8.81	90.11
ZR8	Mudstone	17.0	30.1	3.88	15.2	2.92	0.76	2.60	0.46	3.02	0.53	1.51	0.23	1.48	0.23	72.5	7.46	79.92
ZR11	Mudstone	17.6	29.9	4.00	15.5	2.98	0.77	2.74	0.44	2.79	0.52	1.52	0.22	1.45	0.21	73.5	7.15	80.64
ZR17	Mudstone	15.4	27.6	3.61	14.6	2.81	0.72	2.62	0.43	2.45	0.49	1.44	0.22	1.51	0.23	67.4	6.77	74.13
ZR20	Mudstone	15.5	28.9	3.69	14.5	2.83	0.71	2.62	0.44	2.66	0.52	1.54	0.24	1.47	0.23	68.8	7.10	75.85
ZR21	Mudstone	18.5	34.2	4.30	16.3	3.11	0.77	3.21	0.53	2.89	0.53	1.51	0.25	1.78	0.29	80.4	7.78	88.17
ZR9	Claystone	16.1	28.5	3.77	14.2	2.71	0.68	2.79	0.44	2.61	0.47	1.45	0.20	1.47	0.24	68.8	6.88	75.63
ZR10	Claystone	19.2	32.0	4.24	16.4	3.45	0.82	3.10	0.48	2.92	0.56	1.66	0.26	1.68	0.27	79.2	7.83	87.04
ZR12	Claystone	16.4	28.2	3.51	14.0	2.43	0.63	2.45	0.43	2.41	0.48	1.43	0.20	1.40	0.24	67.6	6.59	74.21
ZR13	Claystone	14.5	24.5	3.21	12.3	2.41	0.62	2.44	0.39	2.22	0.44	1.25	0.20	1.35	0.22	60.0	6.07	66.05
ZR14	Claystone	14.5	23.2	3.26	13.5	2.63	0.64	2.45	0.38	2.26	0.43	1.32	0.20	1.32	0.20	60.2	6.11	66.29
ZR15	Claystone	15.9	27.3	3.72	15.0	3.12	0.67	2.54	0.45	2.76	0.53	1.55	0.23	1.47	0.23	68.3	7.22	75.47
ZR16	Claystone	18.6	29.9	3.78	14.2	2.73	0.64	2.55	0.47	2.69	0.54	1.47	0.23	1.49	0.25	72.4	7.14	79.54
ZR18	Claystone	17.6	31.5	3.68	14.0	2.63	0.66	2.75	0.51	2.70	0.61	1.71	0.25	1.52	0.25	72.8	7.55	80.37
ZR19	Claystone	17.2	33.7	4.14	16.1	3.34	0.78	3.07	0.48	2.79	0.54	1.62	0.25	1.82	0.27	78.3	7.77	86.10
Mean		17.1	30.5	3.97	15.5	3.00	0.75	2.83	0.47	2.77	0.53	1.54	0.23	1.55	0.25	73.63	7.34	80.98
Standard Deviation		2.1	4.97	0.66	2.55	0.49	0.14	0.41	0.07	0.39	0.07	0.16	0.02	0.17	0.03	10.9	0.86	11.7
Minimum		14.5	23.2	3.21	12.3	2.41	0.62	2.44	0.38	2.22	0.43	1.25	0.2	1.32	0.2	59.98	6.07	66.05
Maximum		23	45.3	5.97	23.3	4.32	1.16	3.78	0.64	3.7	0.72	1.89	0.28	1.86	0.29	106.8	9.28	116.1

Table 4.7: Major element (wt. %), REE (ppm) and normalized values of the red beds of Göynük Section.

Sample	Type	SiO ₂	Al ₂ O ₃	Fe ₂ O ₃	MgO	CaO	Na ₂ O	K ₂ O	TiO ₂	P ₂ O ₅	MnO	Cr ₂ O ₃	TOT/C	$\sum \text{LREE}/\sum \text{HREE}$	Ce*	Eu*
GOZ1	Marl	22.13	6.36	3.07	1.46	33.37	0.55	1.46	0.30	0.08	0.15	0.007	7.55	30.16	0.35	0.47
GOZ2	Marl	24.16	7.17	3.38	1.44	31.84	0.57	1.68	0.32	0.07	0.13	0.007	7.10	32.00	0.40	0.53
GOZ3	Marl	25.74	7.93	3.52	1.56	30.83	0.63	1.87	0.36	0.07	0.11	0.008	6.72	32.43	0.40	0.56
GOZ4	Marl	25.16	7.71	3.37	1.56	32.80	0.63	1.82	0.36	0.09	0.14	0.009	7.07	32.63	0.40	0.56
GOZ5	Marl	25.09	7.84	3.59	1.65	32.69	0.63	1.89	0.37	0.07	0.15	0.008	7.05	30.83	0.38	0.52
GOZ6	Marl	25.60	8.10	3.80	1.61	31.25	0.69	1.97	0.38	0.08	0.14	0.010	6.81	30.97	0.40	0.51
GOZ7	Marl	28.72	8.82	4.06	1.74	28.76	0.67	2.20	0.40	0.08	0.12	0.009	6.22	31.45	0.44	0.58
GOZ8	Marl	25.41	7.71	3.76	1.68	31.28	0.63	1.91	0.36	0.10	0.15	0.008	6.87	33.78	0.45	0.60
Mean		25.25	7.71	3.57	1.59	31.60	0.63	1.85	0.36	0.08	0.14	0.01	6.92	31.78	0.4	0.54
Standard Deviation		1.83	0.71	0.31	0.1	1.45	0.05	0.22	0.03	0.01	0.02	0	0.38	1.16	0.03	0.04
Minimum		22.1	6.36	3.07	1.4	28.76	0.55	1.46	0.3	0.07	0.11	0.01	6.22	30.16	0.35	0.47
Maximum		28.7	8.82	4.06	1.7	33.37	0.69	2.2	0.4	0.1	0.15	0.01	7.55	33.78	0.45	0.6

Table 4.8: Major element (wt. %), REE (ppm) and normalized values of the green-gray beds of Göynük Section.

Sample	Type	SiO ₂	Al ₂ O ₃	Fe ₂ O ₃	MgO	CaO	Na ₂ O	K ₂ O	TiO ₂	P ₂ O ₅	MnO	Cr ₂ O ₃	TOT/C	$\sum \text{LREE}/\sum \text{HREE}$	Ce*	Eu*
GOZ11	Mudstone	31.01	9.64	4.13	1.87	25.42	0.83	2.43	0.40	0.08	0.12	0.01	5.51	33.47	0.47	0.73
GOZ13	Mudstone	30.96	9.32	4.16	1.95	26.14	0.90	2.25	0.40	0.07	0.14	0.01	5.66	35.13	0.47	0.66
GOZ16	Mudstone	30.64	8.98	3.84	1.97	27.63	0.80	2.10	0.39	0.06	0.17	0.01	5.95	34.47	0.48	0.62
GOZ17	Mudstone	37.88	11.67	5.01	2.16	20.09	1.07	2.80	0.50	0.08	0.11	0.01	4.09	34.35	0.53	0.77
GOZ18	Mudstone	30.32	8.72	3.80	1.94	27.53	0.84	2.00	0.39	0.11	0.19	0.01	5.92	33.34	0.43	0.56
GOZ20	Mudstone	35.01	10.23	4.85	2.23	22.37	0.95	2.45	0.46	0.09	0.13	0.01	4.78	33.66	0.48	0.67
GOZ21	Mudstone	32.67	9.61	4.70	2.09	23.85	0.87	2.28	0.42	0.10	0.16	0.01	5.19	34.30	0.48	0.63
GOZ25	Mudstone	44.79	13.34	5.46	2.61	13.69	1.01	3.10	0.66	0.08	0.06	0.01	2.92	32.44	0.38	0.60
GOZ27	Mudstone	36.09	8.78	4.32	2.02	23.99	0.74	1.82	0.41	0.18	0.18	0.01	5.28	37.30	0.64	0.71
GOZ29	Mudstone	36.07	8.67	3.85	1.93	24.17	0.79	1.75	0.40	0.10	0.16	0.01	5.30	38.03	0.54	0.70
GOZ30	Mudstone	40.01	9.22	4.30	2.13	21.28	0.90	1.91	0.43	0.14	0.13	0.01	4.54	39.19	0.72	0.78
GOZ31	Mudstone	31.75	8.52	3.74	1.76	27.01	0.89	1.68	0.34	0.17	0.21	0.01	5.90	42.90	1.04	0.88
GOZ36	Mudstone	30.61	8.39	4.21	1.81	26.67	0.74	1.93	0.36	0.15	0.21	0.01	5.76	32.75	0.60	0.68
GOZ40	Mudstone	27.18	7.74	3.86	1.77	29.64	0.67	1.75	0.36	0.11	0.23	0.01	6.50	33.42	0.47	0.62
GOZ43	Mudstone	31.75	9.30	4.24	1.89	25.72	0.66	2.16	0.38	0.12	0.18	0.01	5.46	35.44	0.72	0.86
GOZ44	Mudstone	31.97	9.20	4.61	1.93	25.17	0.71	2.24	0.41	0.22	0.20	0.01	5.43	36.64	0.64	0.77
GOZ46	Mudstone	31.35	8.61	4.56	1.88	26.22	0.70	2.15	0.38	0.18	0.22	0.01	5.64	32.58	0.51	0.60
GOZ47	Mudstone	44.34	12.98	6.46	2.86	13.63	1.13	3.07	0.61	0.10	0.11	0.02	2.88	29.04	0.52	0.74
GOZ52	Mudstone	32.81	9.08	4.22	1.86	25.23	0.76	2.18	0.39	0.07	0.17	0.03	5.51	35.71	0.57	0.69
GOZ0	Claystone	31.69	9.43	3.64	1.77	26.08	0.68	2.00	0.40	0.07	0.09	0.01	5.54	27.95	0.44	0.56
GOZ9	Claystone	37.63	11.56	5.20	2.26	19.58	0.90	3.11	0.55	0.10	0.09	0.02	4.11	33.81	0.48	0.71
GOZ10	Claystone	25.68	7.59	3.55	1.67	30.32	0.62	1.83	0.33	0.08	0.17	0.01	6.78	34.88	0.46	0.55
GOZ12	Claystone	24.47	7.14	3.05	1.59	31.91	0.68	1.74	0.31	0.07	0.18	0.01	7.16	34.04	0.41	0.57
GOZ14	Claystone	32.02	9.48	4.40	1.96	25.70	0.86	2.27	0.39	0.11	0.14	0.01	5.43	33.70	0.56	0.69
GOZ22	Claystone	28.27	7.74	3.92	1.79	28.74	0.69	1.69	0.36	0.11	0.20	0.01	6.45	39.55	0.47	0.56
GOZ23	Claystone	30.93	8.69	4.22	2.01	26.38	0.73	1.93	0.38	0.25	0.17	0.01	5.73	37.99	0.55	0.65
GOZ24	Claystone	32.37	9.11	4.09	1.92	25.56	0.81	1.92	0.41	0.06	0.14	0.01	5.64	35.68	0.58	0.72
GOZ26	Claystone	33.37	8.76	4.06	1.94	25.68	0.74	1.87	0.42	0.10	0.18	0.01	5.62	34.12	0.46	0.62
GOZ32	Claystone	31.47	8.67	3.80	1.86	26.81	0.85	1.82	0.39	0.15	0.23	0.01	5.83	38.94	0.49	0.62
GOZ33	Claystone	34.17	8.31	4.25	1.93	24.91	0.81	1.79	0.39	0.12	0.21	0.01	5.52	36.54	0.50	0.62
GOZ35	Claystone	36.92	9.48	4.83	2.10	22.15	0.84	2.06	0.43	0.09	0.14	0.01	4.77	34.10	0.53	0.71
GOZ37	Claystone	37.20	10.49	4.96	2.36	20.79	0.96	2.28	0.53	0.08	0.13	0.01	4.47	28.20	0.47	0.67
GOZ39	Claystone	28.99	8.22	4.20	1.84	27.72	0.68	1.86	0.37	0.12	0.21	0.01	6.06	33.04	0.45	0.62
GOZ50	Claystone	47.14	13.92	5.25	2.67	12.36	1.08	2.92	0.57	0.09	0.07	0.01	2.34	38.28	0.52	0.69
GOZ19	Siltstone	42.95	13.10	5.22	2.69	15.01	1.08	2.85	0.56	0.11	0.09	0.01	2.98	33.94	0.59	0.84
GOZ48	Siltstone	43.98	12.16	5.74	2.76	15.25	1.12	2.74	0.60	0.08	0.09	0.02	3.25	29.21	0.42	0.66
GOZ51	Siltstone	48.86	12.70	5.18	2.39	13.62	1.72	2.25	0.69	0.11	0.11	0.01	2.54	37.93	0.59	0.88
GOZ28	Sandstone	42.54	8.68	2.68	1.35	22.74	1.37	1.25	0.43	0.10	0.12	0.01	4.76	35.80	0.59	0.80
GOZ28	Sandstone	42.54	8.68	2.68	1.35	22.74	1.37	1.25	0.43	0.10	0.12	0.01	3.79	35.80	0.59	0.80
GOZ38	Sandstone	44.01	10.84	4.37	1.83	18.74	1.70	1.90	0.72	0.17	0.11	0.02	2.82	34.03	0.58	1.00
GOZ42	Sandstone	45.45	14.26	3.97	1.58	15.24	2.13	2.80	0.60	0.10	0.09	0.01	2.39	33.79	0.57	1.00
GOZ15	Mixed	46.10	14.34	5.90	2.43	12.63	1.32	3.85	0.59	0.11	0.08	0.01	2.82	36.96	0.47	0.83
GOZ34	Mixed	47.46	12.41	5.08	2.28	14.48	1.56	2.14	0.67	0.10	0.09	0.01	2.76	33.70	0.50	0.81
GOZ41	Mixed	46.87	13.01	5.64	2.64	13.05	1.37	2.89	0.65	0.10	0.10	0.02	2.80	31.52	0.49	0.77
GOZ45	Mixed	47.31	12.47	5.65	2.55	14.27	1.66	2.63	0.77	0.11	0.10	0.02	3.19	30.47	0.52	0.86
GOZ49	Mixed	44.25	11.70	6.00	2.80	15.42	1.12	2.54	0.63	0.07	0.10	0.02	5.54	32.73	0.54	0.67
Mean		36.43	10.14	4.51	2.08	22.24	0.98	2.24	0.47	0.11	0.14	0.01	4.75	34.56	0.53	0.71
Standard Deviation		6.87	2.01	0.80	0.36	5.65	0.34	0.51	0.12	0.04	0.05	0.00	1.35	3.04	0.11	0.11
Minimum		24.47	7.14	2.68	1.35	12.36	0.62	1.25	0.31	0.06	0.06	0.01	2.34	27.95	0.38	0.55
Maximum		48.86	14.34	6.46	2.86	31.91	2.13	3.85	0.77	0.25	0.23	0.03	7.16	42.90	1.04	1.00

Table 4.9: Trace element (ppm) concentration in the red beds of Göynük Section.

Sample	Rock	LOI	Sc	Ba	Co	Nb	Rb	Sr	Ta	Th	U	V	Zr	Mo	Cu	Pb	Zn	Ni	Cd
GOZ1	Marl	30.9	7	628	9.2	4.9	58.4	573.2	0.4	5.7	1.1	68	58.1	0.3	22.0	8.9	32	19.6	<0.1
GOZ2	Marl	29.1	8	279	9.5	5.1	65.0	556.4	0.3	6.3	0.9	78	63.1	0.2	23.1	12.3	34	24.0	0.1
GOZ3	Marl	27.2	9	282	11.2	5.7	69.3	526.2	0.3	6.4	0.8	84	70.2	0.2	24.3	10.3	37	23.8	<0.1
GOZ4	Marl	26.2	8	214	12.5	5.8	65.9	539.9	0.3	5.9	1.0	73	65.0	0.2	20.1	8.7	36	24.8	0.1
GOZ5	Marl	25.9	9	414	12.1	5.7	67.4	534.5	0.3	5.8	1.1	77	65.6	0.2	22.9	9.7	35	26.9	<0.1
GOZ6	Marl	26.2	9	231	13.0	5.1	74.1	497.1	0.3	5.4	1.1	86	68.1	0.2	20.1	8.9	37	32.2	<0.1
GOZ7	Marl	24.3	10	223	13.1	5.4	79.4	481.5	0.3	6.4	0.9	97	71.9	0.2	30.1	9.0	37	30.8	<0.1
GOZ8	Marl	26.8	9	311	12.6	4.9	71.2	532.5	0.4	6.1	1.3	83	68.9	<0.1	31.2	8.2	37	23.4	<0.1
Mean		27.1	9	323	11.6	5.3	68.8	530.2	0.3	6.0	1	81	66.4	0.19	24.2	9.5	36	25.7	0.03
Standard Deviation		2.05	1	139	1.54	0.4	6.32	29.61	0.1	0.4	0.2	8.9	4.4	0.08	4.23	1.3	1.9	4.13	0.05
Minimum		24.3	7	214	9.2	4.9	58.4	481.5	0.3	5.4	0.8	68	58.1	0	20.1	8.2	32	19.6	<0.1
Maximum		30.9	10	628	13.1	5.8	79.4	573.2	0.4	6.4	1.3	97	71.9	0.3	31.2	12.3	37	32.2	0.1

Table 4.10: Trace element (ppm) concentration in the green-gray beds of Göynük Section.

Sample	Type	LOI	Sc	Ba	Co	Nb	Rb	Sr	Ta	Th	U	V	Zr	Mo	Cu	Pb	Zn	Ni	Cd
GOZ11	Mudstone	23.9	10	392	11.0	5.7	77.9	485.1	0.4	7.2	1.3	101	78.9	<0.1	36.4	11.7	44	25.2	<0.1
GOZ13	Mudstone	23.5	10	512	13.9	6.4	77.7	497.7	0.4	8.1	1.6	105	85.7	0.1	34.8	14.1	39	26.6	<0.1
GOZ16	Mudstone	23.2	10	225	10.9	5.7	77.6	532.4	0.3	7.0	1.8	124	77.9	<0.1	42.2	11.5	38	32.0	0.2
GOZ17	Mudstone	18.4	12	805	13.6	7.8	95.8	526.0	0.5	12.2	2.1	122	113.0	0.2	50.1	15.4	44	32.3	<0.1
GOZ18	Mudstone	24.0	10	241	13.9	5.8	82.9	545.9	0.4	6.8	1.9	91	76.7	<0.1	45.3	11.7	39	35.6	0.2
GOZ20	Mudstone	21.1	12	264	17.0	6.5	93.8	464.1	0.5	8.0	1.8	99	85.4	0.3	43.2	13.5	44	41.7	<0.1
GOZ21	Mudstone	23.1	10	277	10.5	6.3	89.3	520.8	0.4	8.1	1.5	94	84.7	0.1	35.1	11.7	42	32.6	<0.1
GOZ25	Mudstone	15.0	15	463	16.6	9.6	124.2	443.5	0.6	11.1	2.3	139	113.9	0.1	42.8	19.9	52	51.0	0.1
GOZ27	Mudstone	21.3	10	209	10.3	6.5	85.0	508.5	0.4	6.7	2.4	92	80.3	0.2	32.0	11.5	45	41.4	<0.1
GOZ29	Mudstone	21.9	9	232	10.3	5.7	78.4	553.9	0.4	6.3	1.6	87	75.8	<0.1	39.2	12.1	45	41.7	<0.1
GOZ30	Mudstone	19.3	9	265	12.7	6.3	82.7	559.3	0.4	7.7	1.9	88	83.2	0.1	33.7	12.7	48	43.2	<0.1
GOZ31	Mudstone	23.7	8	274	6.6	5.2	68.7	695.3	0.4	8.2	2.3	72	75.6	0.2	36.0	11.9	35	21.5	<0.1
GOZ36	Mudstone	24.8	8	212	8.8	5.7	85.8	544.7	0.5	6.8	1.9	81	73.2	<0.1	41.6	10.6	38	29.2	<0.1
GOZ40	Mudstone	26.5	8	187	7.8	5.6	82.0	512.5	0.4	5.8	1.5	79	69.4	<0.1	32.5	10.1	35	28.4	0.1
GOZ43	Mudstone	23.4	9	292	7.3	7.6	94.5	638.4	0.5	8.2	2.1	93	96.1	<0.1	34.5	11.0	41	31.2	0.1
GOZ44	Mudstone	23.2	9	228	8.7	6.7	105.8	501.8	0.5	8.8	2.7	89	90.0	<0.1	33.6	14.1	39	33.2	<0.1
GOZ46	Mudstone	23.6	9	221	9.7	6.2	100.8	494.2	0.4	6.9	2.3	88	78.5	0.1	29.8	10.8	37	34.2	<0.1
GOZ47	Mudstone	14.5	13	416	18.0	10.2	134.6	330.7	0.7	9.5	1.8	130	120.2	0.2	47.0	14.2	64	67.1	<0.1
GOZ52	Mudstone	23.0	9	252	7.0	7.0	90.1	648.5	0.4	7.8	1.9	69	79.7	<0.1	30.3	12.8	38	33.2	0.1
GOZ0	Claystone	23.9	10	281	10.1	8.0	79.5	482.7	0.5	9.1	1.8	129	81.8	11.9	34.4	10.9	38	24.9	0.2
GOZ9	Claystone	18.8	13	415	16.0	8.4	97.8	397.0	0.5	9.2	2.1	115	103.9	0.1	56.2	16.7	54	50.6	<0.1
GOZ10	Claystone	28.0	8	220	10.5	5.3	68.5	547.7	0.3	5.7	1.3	75	68.4	<0.1	24.4	10.4	37	29.5	0.1
GOZ12	Claystone	28.7	8	214	9.8	4.6	60.8	577.6	0.3	5.7	2.2	98	64.7	<0.1	40.6	10.2	33	20.6	0.2
GOZ14	Claystone	22.5	10	524	13.2	5.9	75.5	491.9	0.4	7.8	1.8	95	80.9	<0.1	44.9	13.2	42	32.7	<0.1
GOZ22	Claystone	26.3	9	209	11.6	5.0	73.0	579.4	0.3	6.0	1.5	76	66.7	0.3	24.2	10.2	34	32.3	<0.1
GOZ23	Claystone	24.1	9	234	9.6	5.6	83.4	505.3	0.4	6.7	2.9	86	74.3	0.1	31.1	11.2	41	34.7	<0.1
GOZ24	Claystone	23.4	10	233	10.4	6.3	82.1	494.9	0.4	7.2	1.6	100	78.3	<0.1	42.6	11.5	44	37.0	<0.1
GOZ26	Claystone	22.7	10	214	12.7	5.8	87.4	485.2	0.4	6.0	1.3	90	72.5	<0.1	32.7	10.9	43	42.4	<0.1
GOZ32	Claystone	23.8	9	242	10.3	5.2	81.5	592.2	0.4	6.8	2.0	92	72.2	<0.1	31.4	10.9	38	31.1	0.1
GOZ33	Claystone	22.9	9	261	8.5	6.1	79.2	534.4	0.4	6.7	1.9	88	73.1	<0.1	31.1	10.8	38	36.2	<0.1
GOZ35	Claystone	20.8	10	254	11.6	7.4	92.0	505.9	0.5	7.1	1.5	84	81.7	0.1	33.0	12.6	44	45.2	<0.1
GOZ37	Claystone	20.0	12	237	11.6	8.3	102.4	357.5	0.6	7.5	1.3	98	92.9	0.1	39.8	12.9	50	55.4	<0.1
GOZ39	Claystone	25.6	8	204	8.8	6.2	90.5	494.5	0.3	6.2	1.7	76	70.6	0.1	25.1	11.2	39	41.6	<0.1
GOZ50	Claystone	13.7	13	493	14.0	10.2	122.2	745.4	0.7	14.2	2.8	120	145.1	0.1	46.8	18.6	60	37.3	0.2
GOZ19	Siltstone	16.1	13	570	11.8	9.5	100.8	544.7	0.6	12.5	2.4	142	128.7	<0.1	67.0	16.4	58	38.1	0.1
GOZ48	Siltstone	15.3	13	304	16.4	9.2	123.9	324.1	0.7	7.4	1.6	118	107.5	0.2	45.5	14.1	62	67.5	0.1
GOZ51	Siltstone	12.2	13	386	24.6	9.9	76.5	537.0	0.7	7.6	3.6	115	136.4	0.3	34.3	15.0	52	48.4	<0.1
GOZ28	Sandstone	18.4	8	1763	6.2	6.4	45.2	959.9	0.5	7.0	2.0	67	118.3	0.7	10.5	9.8	29	23.3	<0.1
GOZ38	Sandstone	15.4	14	334	18.7	9.1	59.4	371.9	0.7	7.1	1.8	114	127.9	0.7	28.7	9.9	45	45.5	<0.1
GOZ42	Sandstone	13.5	13	559	16.7	10.6	68.6	530.7	0.6	12.2	3.5	116	142.5	0.3	31.5	19.2	49	26.8	0.1
GOZ15	Mixed	12.4	15	802	19.5	9.5	113.2	498.3	0.5	14.3	2.5	143	133.0	0.3	62.9	19.5	55	40.9	<0.1
GOZ34	Mixed	13.5	14	444	20.0	8.9	73.2	543.5	0.6	8.9	2.1	123	128.4	0.2	37.5	12.0	49	39.9	0.1
GOZ41	Mixed	13.5	14	328	15.4	9.6	115.3	324.4	0.7	9.2	1.8	119	130.3	<0.1	45.4	14.1	61	56.1	<0.1
GOZ45	Mixed	12.3	14	359	25.2	10.0	84.9	325.5	0.8	8.0	2.2	124	131.6	0.2	39.4	12.7	55	58.7	<0.1
GOZ49	Mixed	15.2	14	309	16.1	9.4	124.3	363.7	0.7	7.9	1.5	122	115.6	0.2	34.5	13.0	56	60.1	0.1
Mean		20.5	11	364	12.7	7.3	88.6	513.8	0.5	8.12	1.9	102	94.79	0.4	37.7	12.9	45	38.6	0.05
Standard Deviation		4.68	2.2	259	4.44	1.8	18.9	114.6	0.1	2.11	0.5	20.5	24.35	1.8	9.94	2.64	8.5	11.5	0.07
Minimum		12.2	8	187	6.2	4.6	45.2	324.1	0.3	5.7	1.3	67	64.7	0	10.5	9.8	29	20.6	<0.1
Maximum		28.7																	

Table 4.11: REE (ppm) concentration in the red beds of Göynük Section.

Sample	Type	La	Ce	Pr	Nd	Sm	Eu	Gd	Tb	Dy	Ho	Er	Tm	Yb	Lu	\sum LREE	\sum HREE	\sum ΣREE
GOZ1	Marl	17.20	28.0	3.45	12.40	2.47	0.51	2.63	0.34	0.00	0.44	1.25	0.00	0.00	0.18	66.66	2.21	68.87
GOZ2	Marl	16.90	31.5	3.45	12.80	2.43	0.57	2.43	0.34	0.00	0.40	1.27	0.00	0.00	0.18	70.08	2.19	72.27
GOZ3	Marl	17.40	31.7	3.62	13.80	2.55	0.61	2.63	0.36	0.00	0.43	1.24	0.00	0.00	0.20	72.31	2.23	74.54
GOZ4	Marl	17.40	31.5	3.50	12.80	2.45	0.60	2.24	0.34	0.00	0.39	1.23	0.00	0.00	0.20	70.49	2.16	72.65
GOZ5	Marl	16.40	30.3	3.43	11.90	2.36	0.56	2.25	0.31	0.00	0.43	1.25	0.00	0.00	0.19	67.20	2.18	69.38
GOZ6	Marl	16.40	31.5	3.39	12.70	2.27	0.55	2.26	0.34	0.00	0.44	1.26	0.00	0.00	0.19	69.07	2.23	71.30
GOZ7	Marl	18.00	35.0	3.90	15.10	2.78	0.63	2.59	0.38	0.00	0.46	1.43	0.00	0.00	0.21	78	2.48	80.48
GOZ8	Marl	18.40	35.6	3.77	13.90	2.73	0.65	2.64	0.38	0.00	0.45	1.24	0.00	0.00	0.23	77.69	2.30	79.99
Mean		17.26	31.9	3.56	13.2	2.51	0.59	2.46	0.35	0.00	0.43	1.27	0.00	0.00	0.20	71.4	2.25	73.69
Standard Deviation		0.71	2.44	0.18	1.03	0.18	0.05	0.19	0.02	0.00	0.02	0.07	0.00	0.00	0.02	4.34	0.1	4.43
Minimum		16.4	28	3.39	11.9	2.27	0.51	2.24	0.31	0.00	0.39	1.23	0.00	0.00	0.18	66.66	2.16	68.87
Maximum		18.4	35.6	3.9	15.1	2.78	0.65	2.64	0.38	0.00	0.46	1.43	0.00	0.00	0.23	78	2.48	80.48

Table 4.12: REE (ppm) concentration in the green-gray beds of Göynük Section.

Sample	Type	La	Ce	Pr	Nd	Sm	Eu	Gd	Tb	Dy	Ho	Er	Tm	Yb	Lu	\sum LREE	\sum HREE	\sum ΣREE
GOZ11	Mudstone	20.4	37.1	4.29	16.9	3.27	0.79	2.94	0.41	0.00	0.45	1.46	0.00	0.00	0.24	85.69	2.56	88.25
GOZ13	Mudstone	20.4	37.1	4.15	15.4	3.23	0.71	2.96	0.38	0.00	0.44	1.36	0.00	0.00	0.21	83.95	2.39	86.34
GOZ16	Mudstone	19.3	37.9	4.03	15.1	2.94	0.67	2.78	0.38	0.00	0.46	1.34	0.00	0.00	0.22	82.72	2.40	85.12
GOZ17	Mudstone	22.9	42.3	4.82	18.3	3.5	0.83	3.19	0.46	0.00	0.57	1.51	0.00	0.00	0.25	95.84	2.79	98.63
GOZ18	Mudstone	17.9	34.3	3.83	14.1	2.87	0.61	2.41	0.35	0.00	0.44	1.3	0.00	0.00	0.19	76.02	2.28	78.30
GOZ20	Mudstone	20.3	38.1	4.23	16.8	3.15	0.72	2.87	0.41	0.00	0.5	1.44	0.00	0.00	0.21	86.17	2.56	88.73
GOZ21	Mudstone	20.2	37.9	4.11	15.5	3.28	0.68	2.7	0.39	0.00	0.46	1.37	0.00	0.00	0.24	84.37	2.46	86.83
GOZ25	Mudstone	16.4	30.6	3.52	14.3	2.78	0.65	2.46	0.36	0.00	0.44	1.18	0.00	0.00	0.2	70.71	2.18	72.89
GOZ27	Mudstone	29.5	50.6	5.72	20.6	3.85	0.77	3.46	0.47	0.00	0.54	1.79	0.00	0.00	0.27	114.50	3.07	117.57
GOZ29	Mudstone	26.3	42.7	4.63	19.3	3.27	0.76	3.05	0.42	0.00	0.52	1.46	0.00	0.00	0.23	100.01	2.63	102.64
GOZ30	Mudstone	29.7	57.6	6.09	23.3	4.09	0.84	3.78	0.52	0.00	0.6	1.81	0.00	0.00	0.27	125.40	3.20	128.60
GOZ31	Mudstone	43.2	82.5	8.68	31.4	5.35	0.95	5.08	0.66	0.00	0.82	2.29	0.00	0.00	0.36	177.16	4.13	181.29
GOZ36	Mudstone	26.1	47.4	5.46	19.6	3.65	0.73	3.16	0.47	0.00	0.54	1.96	0.00	0.00	0.27	106.10	3.24	109.34
GOZ40	Mudstone	19.9	37.4	4.22	15.4	2.77	0.67	2.86	0.4	0.00	0.46	1.43	0.00	0.00	0.2	83.22	2.49	85.71
GOZ43	Mudstone	32	57.5	6.54	24.5	4.65	0.93	4.31	0.6	0.00	0.75	2.03	0.00	0.00	0.3	130.43	3.68	134.11
GOZ44	Mudstone	27.8	50.9	5.87	20.8	4.1	0.83	3.66	0.53	0.00	0.53	1.77	0.00	0.00	0.28	113.96	3.11	117.07
GOZ46	Mudstone	21.8	40.3	4.76	17.4	3.13	0.65	2.86	0.43	0.00	0.5	1.63	0.00	0.00	0.23	90.90	2.79	93.69
GOZ47	Mudstone	21.9	41.4	5.04	18.6	3.67	0.8	3.27	0.49	0.00	0.6	1.88	0.00	0.00	0.29	94.68	3.26	97.94
GOZ52	Mudstone	22.2	45.4	4.82	16.9	3.64	0.75	3.07	0.5	0.00	0.51	1.47	0.00	0.00	0.23	96.78	2.71	99.49
GOZO	Claystone	19	35.4	3.92	14.5	2.91	0.6	3.06	0.45	0.00	0.53	1.63	0.00	0.00	0.23	79.39	2.84	82.23
GOZ9	Claystone	20.2	38.1	4.38	15.2	3.32	0.77	2.89	0.42	0.00	0.48	1.38	0.00	0.00	0.23	84.86	2.51	87.37
GOZ10	Claystone	19.1	36.4	3.99	14.7	2.98	0.59	2.47	0.37	0.00	0.4	1.35	0.00	0.00	0.18	80.23	2.30	82.53
GOZ12	Claystone	17.4	32.3	3.58	14.2	2.73	0.62	2.36	0.31	0.00	0.4	1.25	0.00	0.00	0.19	73.19	2.15	75.34
GOZ14	Claystone	23.4	44.6	4.92	17.5	3.52	0.74	3.4	0.47	0.00	0.56	1.63	0.00	0.00	0.25	98.08	2.91	100.99
GOZ22	Claystone	20	37.6	4.05	15.8	2.7	0.61	2.68	0.36	0.00	0.41	1.11	0.00	0.00	0.23	83.44	2.11	85.55
GOZ23	Claystone	24.8	43.4	4.83	17.8	3.44	0.7	3.05	0.43	0.00	0.5	1.42	0.00	0.00	0.23	98.02	2.58	100.60
GOZ24	Claystone	23.8	46.3	5.03	20.2	3.41	0.78	3.25	0.46	0.00	0.53	1.62	0.00	0.00	0.27	102.77	2.88	105.65
GOZ26	Claystone	20.3	36.5	4.12	15.6	3.03	0.67	2.68	0.38	0.00	0.48	1.37	0.00	0.00	0.2	82.90	2.43	85.33
GOZ32	Claystone	23	38.9	4.29	16.6	2.95	0.67	2.76	0.38	0.00	0.46	1.24	0.00	0.00	0.21	89.17	2.29	91.46
GOZ33	Claystone	23.8	40.1	4.47	17.2	2.95	0.67	2.88	0.4	0.00	0.5	1.41	0.00	0.00	0.21	92.07	2.52	94.59
GOZ35	Claystone	23.4	42.3	5.04	19.5	3.66	0.77	3.19	0.48	0.00	0.51	1.61	0.00	0.00	0.27	97.86	2.87	100.73
GOZ37	Claystone	19.4	37.3	4.49	16.1	3.29	0.72	3.01	0.47	0.00	0.55	1.72	0.00	0.00	0.25	84.31	2.99	87.30
GOZ39	Claystone	19.6	35.5	4.27	15.3	3.12	0.67	2.83	0.42	0.00	0.5	1.33	0.00	0.00	0.21	81.29	2.46	83.75
GOZ50	Claystone	22.9	41.4	4.81	18.2	3.03	0.74	2.71	0.41	0.00	0.45	1.35	0.00	0.00	0.24	93.79	2.45	96.24
GOZ19	Siltstone	23.6	47.2	5.28	20.6	3.73	0.91	3.55	0.5	0.00	0.62	1.69	0.00	0.00	0.28	104.87	3.09	107.96
GOZ48	Siltstone	18.4	33.1	4.02	15.6	2.96	0.71	2.62	0.42	0.00	0.5	1.51	0.00	0.00	0.22	77.41	2.65	80.06
GOZ51	Siltstone	25.5	46.9	5.49	21.4	3.82	0.95	3.27	0.49	0.00	0.55	1.55	0.00	0.00	0.24	107.33	2.83	110.16
GOZ28	Sandstone	28.4	47	5.14	19.5	3.64	0.86	3.23	0.48	0.00	0.55	1.77	0.00	0.00	0.21	107.77	3.01	110.78
GOZ38	Sandstone	24.5	46	5.47	21	4.12	1.08	3.67	0.55	0.00	0.61	1.72	0.00	0.00	0.23	107.77	3.01	108.95
GOZ42	Sandstone	24.5	45.3	5.41	19.3	3.66	1.08	3.48	0.53	0.00	0.61	1.7	0.00	0.00	0.2	105.84	3.11	105.77
GOZ15	Mixed	20.1	37.3	4.22	16.7	3.02	0.9	2.77	0.4	0.00	0.4	1.31	0.00	0.00	0.19	102.73	3.04	87.31
GOZ34	Mixed	21.7	39.8	4.85	17.9	3.48	0.87	3.06	0.45	0.00	0.49	1.56	0.00	0.00	0.22	85.01	2.30	94.38
GOZ41	Mixed	20.2	39.1	4.74	17.5	3.2	0.83	3.01	0.46	0.00	0.53	1.58	0.00	0.00	0.24	91.66	2.72	91.39
GOZ45	Mixed	21.5	41.1	4.9	18.2	3.64	0.93	3.27	0.5	0.00	0.52	1.82	0.00	0.00	0.23	88.58	2.81	96.61
GOZ49	Mixed	22.3	42.7	4.63	16.4	3.27	0.72	2.94	0.44	0.00	0.53	1.64	0.00	0.00	0.23	93.54	3.07	95.80
Mean		22.9	42.2	4.78	17.9	3.39	0.77	3.09	0.45	0.00	0.52	1.55	0.00	0.00	0.24	95.06	2.75	97.81
Standard Deviation		4.63	8.51	0.89	3.19	0.52	0.12	0.49	0.07	0.00	0.08	0.24						

4.2.1 MAJOR OXIDES OF THE RED BEDS OF THE ALAGÖZ AND GÖYNÜK SECTIONS

The red beds of the Alagöz Section are composed of three different facies such as packstone (limestone), silty marl and siltstone, while the red beds of the Göynük Section are composed dominantly of marly facies. The average major oxides values are given in Table B28. The red beds of the Alagöz Section are composed of SiO_2 (15.65-70.80 wt.%, mean of 47.39 wt.%), Al_2O_3 (2.53-13.18 wt.%, mean of 8.91 wt.%), Fe_2O_3 (0.84-9.35 wt.%, mean of 6.19 wt.%), MgO (0.63-6.29 wt.%, mean of 3.64 wt.%), CaO (7.01-39.03 wt.%, mean of 14.63 wt.%) and less than 2 wt.% mean of Na_2O , K_2O , TiO_2 , P_2O_5 , MnO and Cr_2O_3 (Table 4.2). It has been noticed that the maximum value, 70.80 wt.% of SiO_2 in the red beds of Alagöz Section is due to high ratio of siliceous radiolaria and occurrence of patchy opaline within matrix (Samples ZR0 and ZR0b). The minimum value 15.65 wt.% of SiO_2 is represented by siltstone as occurrence of calcareous intra-clasts (ZR04a) (Table 4.1).

The major oxides of red beds of the Göynük Section is represented by SiO_2 (22.13-28.72 wt.%, mean of 25.25 wt.%), Al_2O_3 (6.36-8.82 wt.%, mean of 7.71 wt.%), Fe_2O_3 (3.07-4.06 wt.%, mean of 3.57 wt.%), CaO (28.86-33.37 wt.%, mean of 31.60 wt.%) and less than 2 wt.% mean of MgO , Na_2O , K_2O , TiO_2 , P_2O_5 , MnO and Cr_2O_3 (Table C1).

The total average values of SiO_2 , Fe_2O_3 , MgO , TiO_2 , Na_2O , P_2O_5 , MnO and Cr_2O_3 in the red beds of the Alagöz Section are relatively higher than those in the Göynük red beds (Table C1). The Al_2O_3 values are comparatively similar in the both sections and lower than PAAS (Taylor and McLennan, 1985). Higher Fe_2O_3 values have been shown by the red beds of Alagöz samples as compared to the Göynük samples and smaller than PAAS (Taylor and McLennan, 1985). The samples from the Göynük Section are represented by higher total average value of CaO (Table C1).

$\text{SiO}_2/\text{Al}_2\text{O}_3$ indicates high proportion of quartz input. The average $\text{SiO}_2/\text{Al}_2\text{O}_3$ of the red beds of Alagöz section is 3.78 excluding red packstone facies reading (Table 4.1). Overall $\text{SiO}_2/\text{Al}_2\text{O}_3$ of Alagöz red facies are relatively higher than Göynük red facies, and PAAS (Taylor and McLennan, 1985) (Table B28).

4.2.2 MAJOR OXIDES OF THE GREEN-GRAY BEDS OF ALAGÖZ AND GÖYNÜK SECTIONS

The green-gray beds of Alagöz Section are characterized by high weight percent of SiO_2 (29.01-41.27 wt.%, mean as 33.34 wt.%), Al_2O_3 (7.62-12.47 wt.%, mean as 9.51 wt.%), Fe_2O_3 (4.61-8.15 wt.%, mean as 5.73 wt.%), MgO (2.77-6.97 wt.%, mean as 4.03 wt.%), CaO (11.98-26.53 wt.%, mean as 21.97 wt.%) and other remaining oxides have less than 2 wt.% mean value (Table 4.1).

The green-gray beds of Göynük Section have dominantly SiO_2 (24.47-48.86 wt.%, mean value as 36.43 wt.%), Al_2O_3 (7.14-14.34 wt.%, mean value as 10.14 wt.%), Fe_2O_3 (2.68-6.46 wt.%, mean value as 4.51 wt.%), MgO (1.35-2.86 wt.%, mean value as 2.08 wt.%), CaO (12.36-31.91 wt.%, mean value as 31.91 wt.%), K_2O (1.25-3.85 wt.%, mean value as 2.24 wt.%) and the other are less than 2 wt.% (Na_2O , TiO_2 , P_2O_5 , MnO and Cr_2O_3) (Table 4.8). In the green-gray succession of the Göynük Section; the siltstone, sandstone and mixed facies represent high average proportions of SiO_2 , Al_2O_3 , Fe_2O_3 and less percentage of CaO (Table B25).

The average values of SiO_2 , Al_2O_3 , CaO in the mudstone and claystone of the both sections are relatively comparable and lesser than PAAS (Taylor and McLennan, 1985) except CaO (Table B25). The high weight percentage of CaO in these siliciclastic facies may be as a result of micritic matrix and calcareous fossils. The Fe_2O_3 values have been observed in relatively high proportion near to 6 wt.% in the green-gray beds of Alagöz intervals, while around 5 wt.% in the Göynük green-gray lithologies (Table B25). Increasing value of K_2O in the green-gray beds of the Göynük lithologies indicate relative more feldspar and plagioclase occurrences that suggest the presence of clay minerals in the studied sections (Fu et al., 2010) (Table B25). The averages P_2O_5 in the green-gray facies of the studied sections are relatively matching with one another and lower than PAAS (Taylor and McLennan, 1985) (Table B25). The averages $\text{SiO}_2/\text{Al}_2\text{O}_3$ of the green-gray beds are around 3.5 weight percent in the both sections which are slightly higher than PAAS (Taylor and McLennan, 1985) (Table B25).

4.2.3 VERTICAL DISTRIBUTION OF THE MAJOR OXIDES AND THEIR COMPARISON

Generally, the major oxides and Al-normalized patterns of the Alagöz Section graphical representation is more consistent as compared to the Göynük Section.

In the bedding comparison, the patterns of major elements Si, Al, Fe, Ti, Mg, Ca, P in the red beds of Alagöz Section are highly inconsistent than the Göynük Section red beds. The green-grayey beds of Alagöz Section have comparatively rational graphic curves, compared to green-grayey beds of Göynük section having an irregular pattern (Figures 4.1-4.2). TiO_2 , Fe_2O_3 , Al_2O_3 and MnO graphic line are comparably similar to each other in both studied sections.

The vertical distributions of major oxides of the studied sections have been represented along the measured stratigraphic sections and their graphic curves have been compared with one another (Figure 4.1-4.2). In the graphic representation of SiO_2 - Al_2O_3 , there is relatively rapid fall in the SiO_2 curve in the red beds of the Alagöz Section and a very low value of Al_2O_3 curve. Al_2O_3 curve of the red beds of Alagöz section shows rapid increase followed by slightly uniform pattern and again a sharp fall in the SiO_2 and Al_2O_3 line but for a short period of time. In the green-grey beds of the studied section, there is gradually falling trend in SiO_2 curves and then uniform trend in SiO_2 , while Al_2O_3 remain constant (Figure 4.1). On the other hand, SiO_2 - Al_2O_3 curves in the Göynük red beds display moderately uniform trend after falling at GOZ1 sample (Figure 4.1). In the green-grayey beds of Göynük Section that demonstrates high fluctuation in the SiO_2 graphic curve but represent increasing linear trend in the SiO_2 . The Al_2O_3 in the Göynük green-gray beds samples have faintly uniform linear trend and masking the Al_2O_3 graphic curve line of the Alagöz Section. The Al_2O_3 wt.% are similar in both section. Whereas, the SiO_2 values are higher in the red beds of Alagöz Section but relatively similar in green-gray beds in studied sections.

The Fe_2O_3 - CaO graphic curves are highly variable in the red beds of Alagöz section. In the Göynük section, Fe_2O_3 represents slightly uniform graphic curve while irregular curve of CaO (Figure 4.1; Table B26). The Fe_2O_3 curves have almost similar linear trend

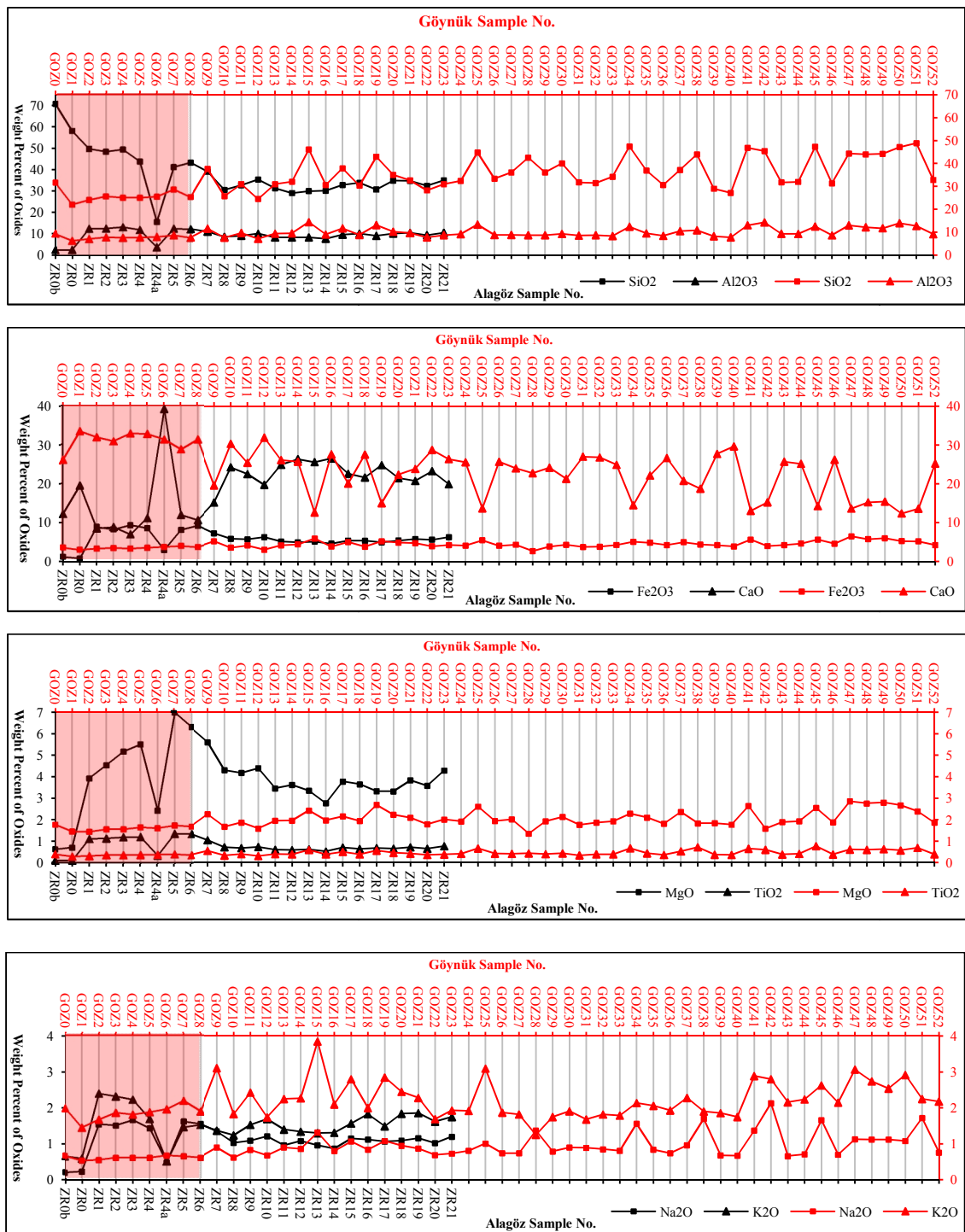


Figure 4.1: SiO_2 , Al_2O_3 , MgO , Fe_2O_3 , CaO , TiO_2 , Na_2O and K_2O wt.% geochemical data graphs of the Alagöz Section (black line) and Göynük Section (red line) and their relationship. (red shade represents red beds)

and somewhat similar low and high peaks in the CaO curve of the studied sections but increasing linear trend in the CaO of Alagöz section and declining CaO linear trend in the Göynük section. The MgO-TiO₂ and Na₂O-K₂O graphic curves exhibit fairly same crest and trough morphology in the Alagöz red beds and Göynük red beds (Figure 4.1). Similar situations have been observed in the green-gray beds of the studied sections. The TiO₂ curve lines of both sections are overlapping and show similar behaviour in the green-gray beds (Figure 4.1).

P₂O₅ and Cr₂O₃ graphic curves are highly inconsistent in the studied sections (Figure 4.2). The P₂O₅ curves of both sections characterize frequent rising and falling lobs. However, most of the points represent similar pattern of rising and falling character between the Alagöz and Göynük sections. The Cr₂O₃ curve of Alagöz section indicates a fluctuation in the red beds and then followed by gradual decline. In the Cr₂O₃ curve of Göynük section relatively uniform trend with few increasing peaks have been observed.

MnO graphic representation of the Alagöz and Göynük sections have superimposed at the number of points. The MnO curves in the green-gray beds of the Göynük Section demonstrate inconsistent pattern in the upper portion (Figure 4.2).

4.3 TRACE ELEMENT OF THE ALAGÖZ AND GÖYNÜK SECTIONS

The concentration of trace elements in the modern and ancient depositional basin are used to determine the different redox-condition, source rock character (provenance studies) and tectonic setting of the sediments (Calvert and Pedersen, 1993; Jones and Manning, 1994; Crusius et al., 1996; Wignall, 1994; Dean et al., 1997, 1999; Yarincik et al., 2000; Morford et al., 2001; Pailler et al., 2002). Different trace elements are used for geochemical characteristic, which are listed in the tables (Tables 4.3-4.4 for Alagöz Section; Tables 4.9-4.10 for Göynük Section).

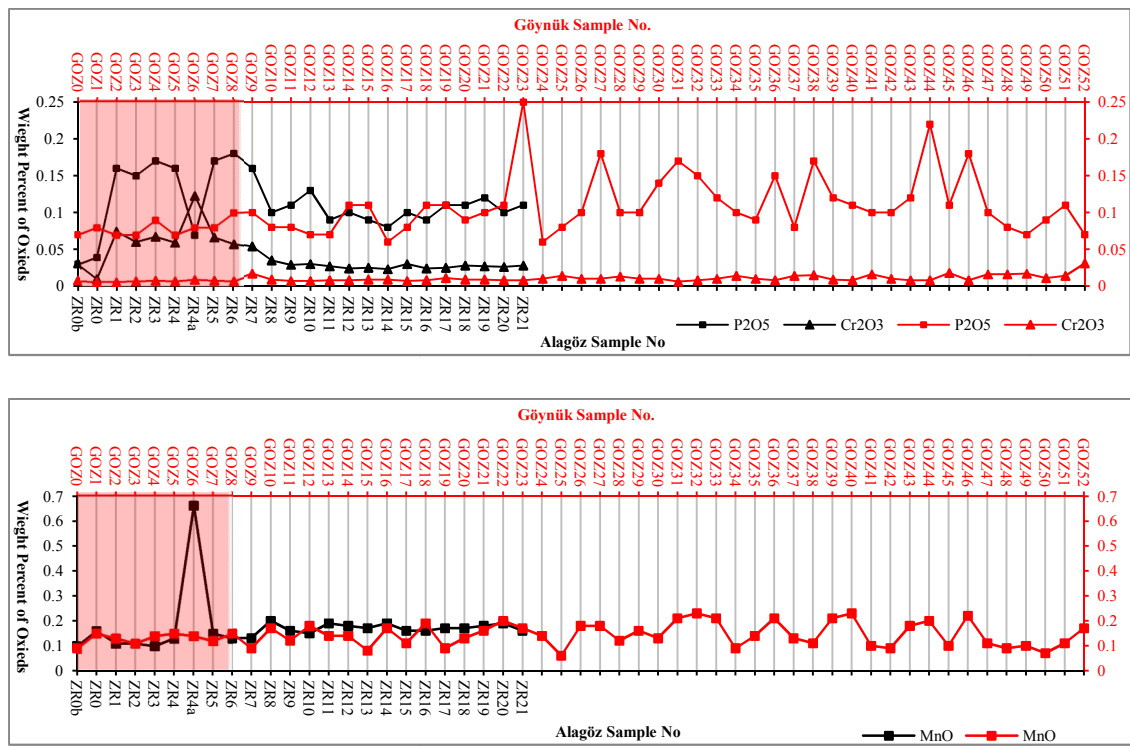


Figure 4.2: P_2O_3 , Cr_2O_3 and MnO wt.% geochemical data graphs of the Alagöz Section (black line) and Göynük Section (red line) and their relationship. (red Shade represents red beds)

4.3.1 TRACE ELEMENTS OF THE RED BEDS OF ALAGÖZ AND GÖYNÜK SECTIONS

The trace elements of red beds of the Alagöz Section are higher than the Göynük red beds samples and PAAS (Taylor and McLennan, 1985), except few trace element and limestone and limestone bearing clasts samples (ZR0b, ZR0 and ZR4a) as shown in Figures 4.3 A, 4.4 A. The higher values of PAAS-normalized trace elements in the red beds of the Alagöz Section are due to relative high terrigenous influx than in the Göynük red beds.

4.3.2 TRACE ELEMENT OF THE GREEN-GRAY BEDS OF ALAGÖZ AND GÖYNÜK SECTIONS

The trace elements of green-gray beds of the Alagöz Section and the Göynük Section indicate relatively similar normalized graphic representation except Ni. Generally, most of the trace elements from the green-gray beds of the both section are below 1, which represents lower values than PAAS (Taylor and McLennan, 1985) (Figures 4.3 B, 4.4 B). The green-gray beds of Alagöz Section represent high average values of Sc, Co, Nb, Ta, V, Cu, Ni, Cd compared to Göynük Section and higher values of Nb, Sr, Ni. Higher average values in the Göynük green-gray beds are possessed by Ba, Rb, Th, U, Zr, Mo, Pb as compared to Alagöz section green-gray beds.

4.4 AL-NORMALIZED MAJOR AND TRACE ELEMENTS OF THE ALAGÖZ AND GÖYNÜK SECTIONS

Different elements are used to normalize the major and trace elements i.e. Al (Murray et al., 1991b), Li (Loring, 1990) and Fe (Schiff and Weisberg, 1999). However, Al is commonly used and is more convenient than other. As, it is found as immobile, resistive, abundantly occurs in the sediments and conservatively in marine environment (Bertin and Goldberg, 1977; Covelli and Fontolan, 1997; Yilmaz et al., 2010). Therefore, it is used as normalization element to examine the major and trace elements as naturally occurring deposit elements without any dilution. The Al-normalization of the trace elements is used to determine the affiliation of the trace elements with terrestrial input and to distinguish from the anthropogenic sources of trace elements. The major oxides are converted to elements form by using stoichiometric method of conversion. All the major and trace elements are normalized by Aluminum as shown in the lists (Tables B1-B2, B21-B22 for Alagöz Section and Tables B3-B4, B23-B24 for Göynük Section).

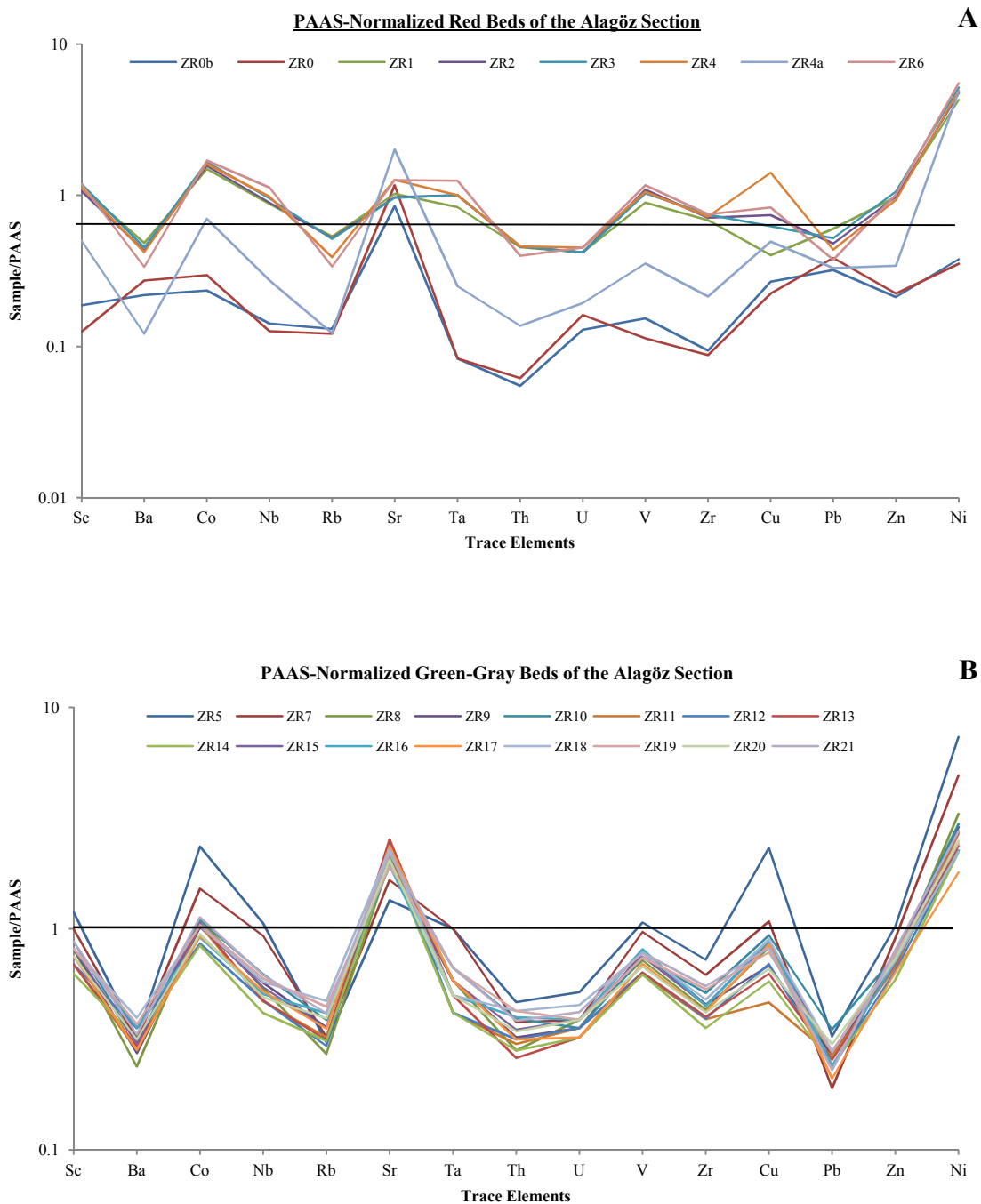


Figure 4.3: PAAS-normalized trace elements of the Alagöz Section samples plot. PAAS (Taylor and McLennan, 1985) values are used for normalization. (A: Red Beds and B: Green-gray Beds)

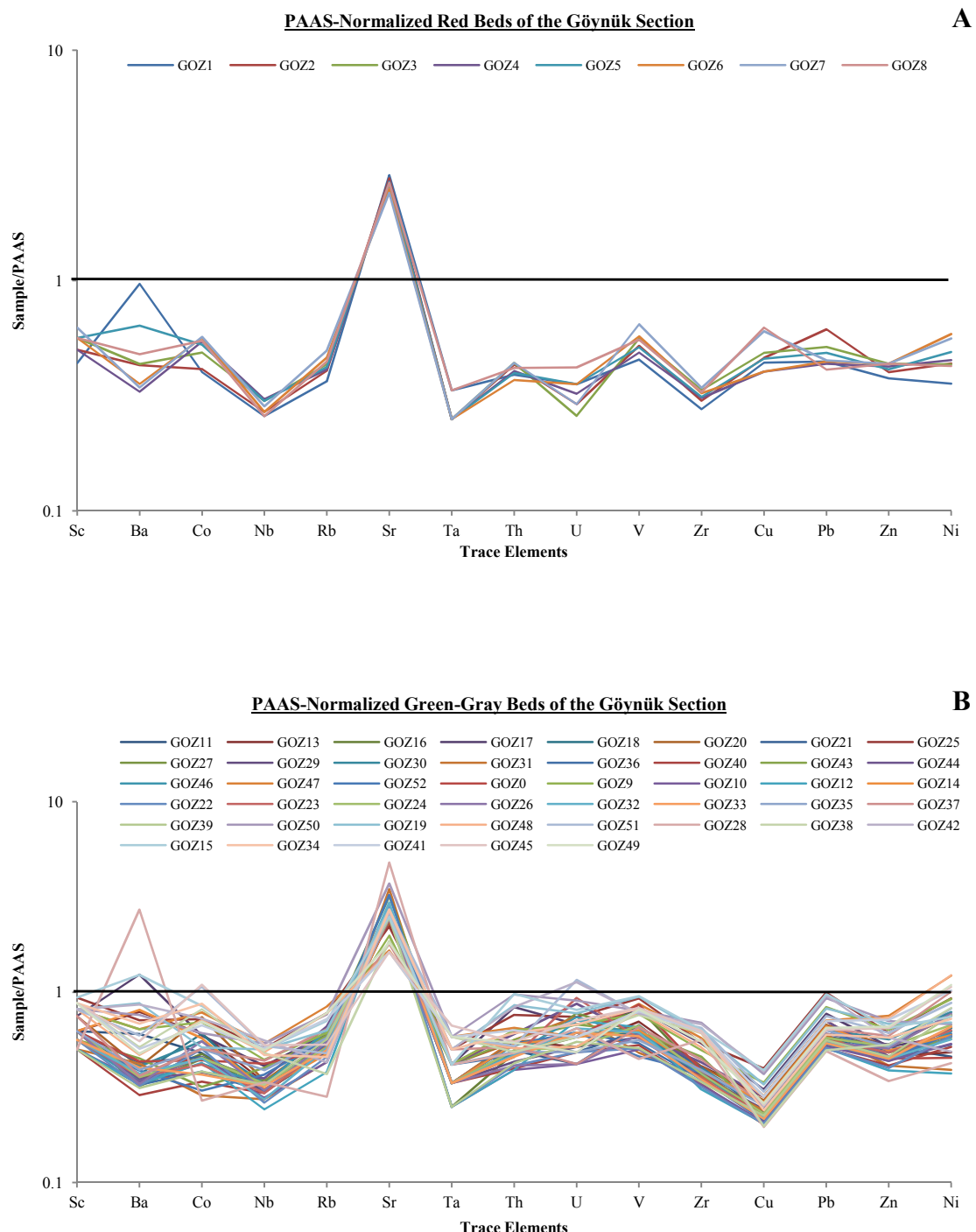


Figure 4.4: PAAS-normalized trace elements of the Göynük Section samples plot. PAAS (Taylor and McLennan, 1985) values are used for normalization. (A: Red Beds and B: Green-gray Beds)

4.4.1 VERTICAL DISTRIBUTION OF AL-NORMALIZED MAJOR AND TRACE ELEMENTS OF THE ALAGÖZ AND GÖYNÜK SECTIONS

Al-normalized elements of the Alagöz and Göynük sections have been plotted along the measured stratigraphic section with associated sample distribution. These graphic representations are described and compared with each other (Figures 4.5-4.6).

I. VERTICAL DISTRIBUTION OF AL-NORMALIZED MAJOR ELEMENTS OF THE ALAGÖZ AND GÖYNÜK SECTIONS

The Si to Al graphic lines of the studied sections is overlapping on each other after first two samples at the base (Figure 4.5). Si to Al graphic curves demonstrate uniform trend in both measured lithologies except ZR0b-ZR0 (siliceous limestone) of Alagöz Section and GOZ28 (sandstone) of Göynük Section.

In the Alagöz Section, the Fe to Al curve line indicates low value and then increasing to certain samples and starts decline toward the upper portion. While in the Göynük Section, it shows relatively uniform projection from red beds toward the top. But in the middle of the portion, it demonstrates inconsistent lobs in the graphic line. Generally, the Alagöz Section Fe/Al curve represents higher values than the Fe/Al values from the Göynük Section (Figure 4.5).

Normalized Mg curve displays gradual rising in the red beds and steadily falling in the green-grayey beds of Alagöz Section. The Mg to Al curve of Göynük Section remains relatively consistent with few low lobs (Figure 4.5).

The red bed of Alagöz Ca to Al ratio curve has sharp fluctuation (Figure 4.5). In the Göynük Ca to Al ratio curve, there is progressively decreasing in the graphic line from red beds to green-grayey beds with few high and low peaks (Figure 4.5). K to Al and Na to Al graphs represent opposite increment and decline trend in the curves line of each section along the studied stratigraphic section (Figures 4.5-4.6). In the Alagöz Section, there is falling trend in the K to Al and rising trend in the Na to Al in the red beds which

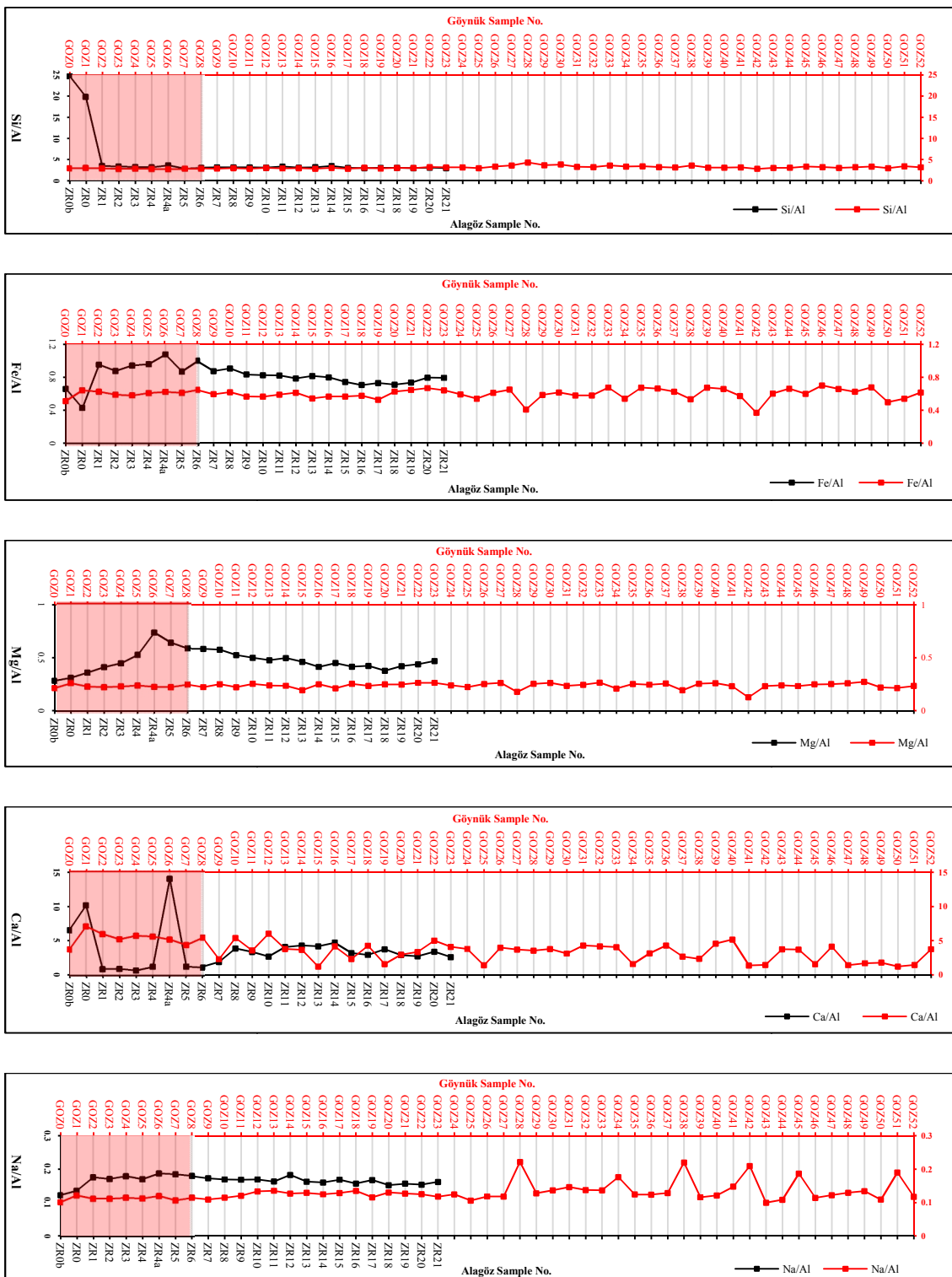


Figure 4.5: Graphic representation of Si/Al, Fe/Al, Mg/Al, Ca/Al and Na/Al of the Alagöz (black line) and Göynük (red line) sections. (red shade represents red beds)

is followed by positive deviation in K to Al and small negative deviation in the Na to Al curves in the green-grayey beds. In the Göynük Section, K to Al and Na to Al curves in the red beds have relative similar pattern. Whereas, in the green-grayey beds of the Göynük section, there is slightly declining curve pattern in K to Al and normal progressive pattern in Na to Al with some fluctuation frequency in the upper portion of Na to Al line (Figure 4.5-4.6).

In the Alagöz area, ZR0b and ZR0 limestone samples represent low Ti to Al graphic curve. After these samples, the Ti to Al ratio curve shows increasing behavior and pursued by decreasing pattern in the green-grayey beds of Alagöz Section and then relatively uniform with some fluctuation in the curve line (Figure 4.6). The Göynük section Ti to Al ratio curve demonstrates normal pattern with a few relatively high frequency peaks in the top portion (Figure 4.6). The P to Al ratio curve in the Alagöz and Göynük Sections represent frequently high peaks. The Alagöz Section P to Al ratio curve shows declining trend and small negative deviation in the P to Al Göynük ratio curve trend (Figure 4.6). Generally, P/Al curves are identical to each other after the red beds and represent relatively inconsistent pattern.

Mn to Al ratios have uniform trend with two sharp fluctuations in the Alagöz Section (Figures 4.5-4.6). In the Göynük Section, Mn to Al ratio represents inconsistent low graphic line but uniform linear trend. The Cr to Al ratio curve is slowly declining linear trend in the Alagöz Section while relatively uniform linear trend in the Göynük Section Cr to Al ratio line (Figure 4.6).

II. VERTICAL DISTRIBUTION OF AL-NORMALIZED TRACE ELEMENTS OF THE ALAGÖZ AND GÖYNÜK SECTIONS

Trace elements such as Sc, Ba, Co, Nb, Rb, Sr, Ta, Th, U, V, Zr, Mo, Cu, Pb, Zn, Ni, Cd are normalized by Al element of the samples and obtained data are represented in the lists (Tables B21-B22 for Alagöz Section; Tables B23-B24 for Göynük Section).

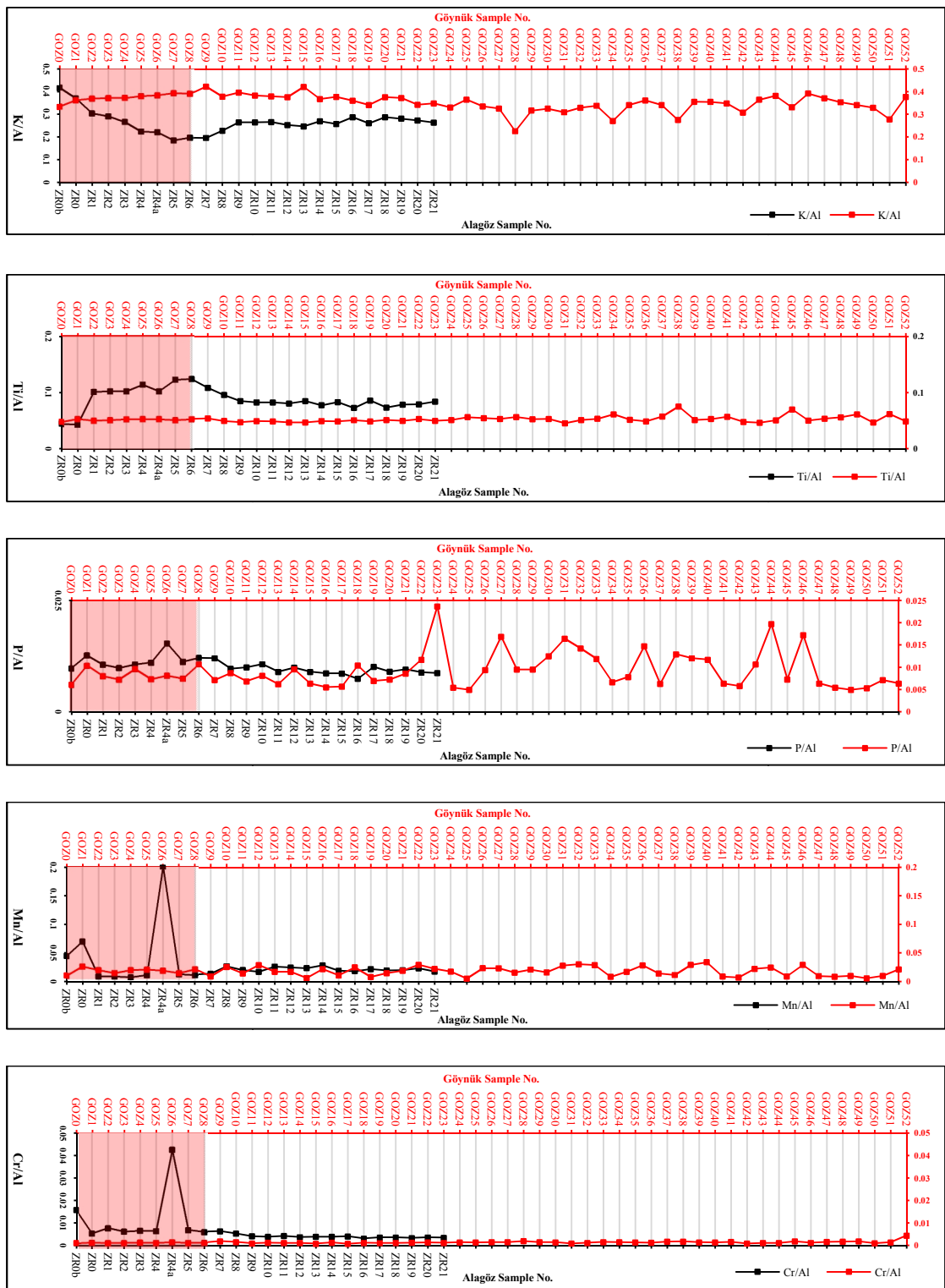


Figure 4.6: Graphic representation of K/Al, Ti/Al, P/Al, Mn/Al and Cr/Al of the Alagöz (black line) and Göynük (red line) sections. (red shade represents red beds).

The concentration of Al-normalized trace elements in the studied sections are either relatively similar or highly inconsistent ratio with one another sections and also show similar behavior by comparing with PAAS (Taylor and McLennan, 1985) (Table B27).

The total average ratios of Sc/Al, Co/Al, Nb/Al, Ta/Al, V/Al, Zr/Al, Zn/Al, Ni/Al of the Alagöz Section are comparable higher than Göynük section, PAAS (Taylor and McLennan, 1985). Whereas, Ba/Al, Rb/Al, Sr/Al, U/Al total average ratios of the Göynük Section are greater from Alagöz Section. The average ratios of Th/Al, Cu/Al, Pb/Al and Cd/Al of both studied sections are comparatively similar to each other. High Mo to Al ratio is represented by green-gray beds of Göynük Section but lower than PAAS (Taylor and McLennan, 1985) (Table B27).

In the Alagöz Section Al-normalized graphic representation, most of the trace elements show an increasing graphic trend compared to the Göynük Section (Figures 4.7-4.10). The Sc/Al, Co/Al, Nb/Al, Sr/Al, Ta/Al, V/Al, Zr/Al, Zn/Al, Cu/Al, Ni/Al graphic representation curves of the Alagöz Section illustrate relatively similar projection of curve line with each other. In the red beds of Alagöz Section, these curves show similar decreasing pattern, followed by gradual to rapid increasing pattern and then gradual declining (Figures 4.7-4.10). In the green-grayey beds of Alagöz Section, these curves are consistent with gradual declining and then uniform linear trend except Ta to Al ratio which shows crest and trough topography in upper section (Figure 4.8). Ba/Al, U/Al, Pb/Al ratio curves demonstrate sudden decreasing, then gradual falling and followed by slightly increasing pattern (Figures 4.7-4.9). Th/Al curve represents rapid increase and continue with relatively uniform cresting and trough morphology (Figure 4.8). Rb to Al ratio graphic line represents stepwise declining and followed by stepwise ascending pattern (Figure 4.7). Mo to Al ratio curve show only pulses in the red beds (Figure 4.9).

In the Göynük Section, the Al-normalized trace elements show highly inconsistent pattern but uniform linear trend with few in declining curves drift (Figures 4.7-4.10). Certain Al-normalized trace elements display zig-zag pattern from bottom to top. Some Al-normalized trace elements are characterized by consistent curves in the red beds and then followed by zig-zag pattern in the green-grayey beds (Figures 4.7-4.10).

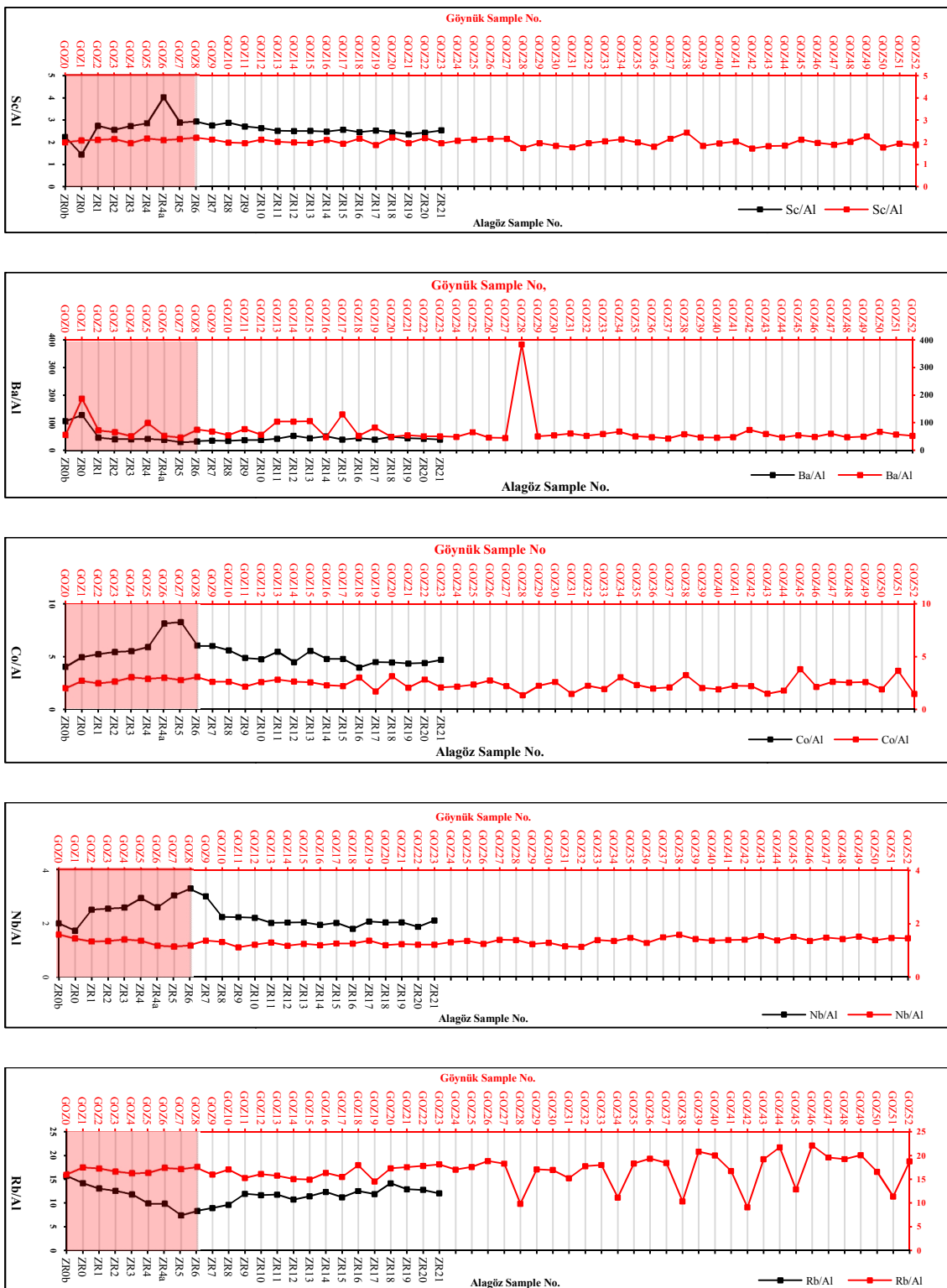


Figure 4.7: Graphic representation of Sc/Al, Ba/Al, Co/Al, Nb/Al and Rb/Al of the Alagöz (black line) and Göynük (red line) sections. (red shade represents red beds)

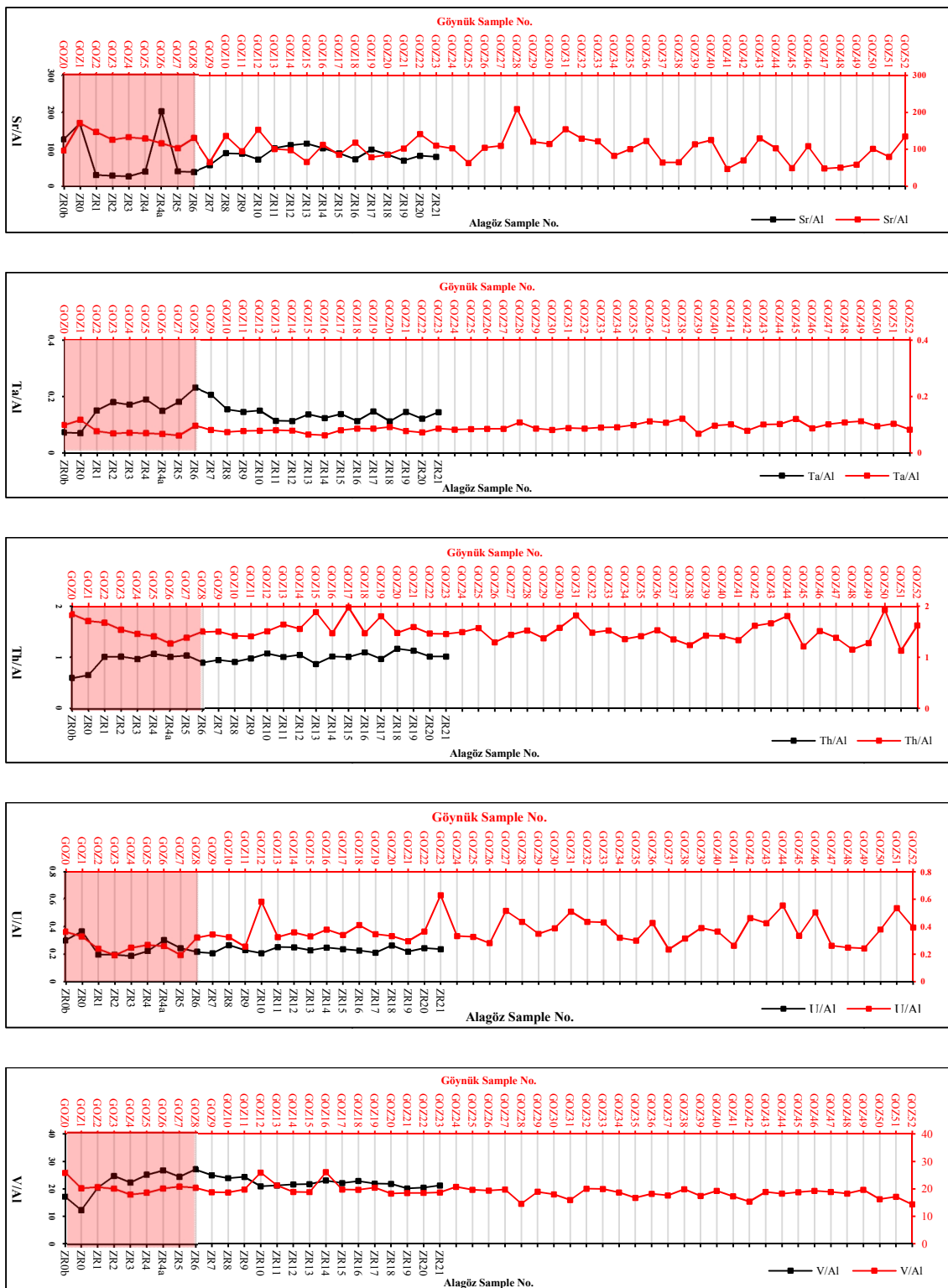


Figure 4.8: Graphic representation of Sr/Al, Ta/Al, Th/Al, U/Al and V/Al of the Alagöz (black line) and Göynük (red line) sections. (red shade represents red beds)

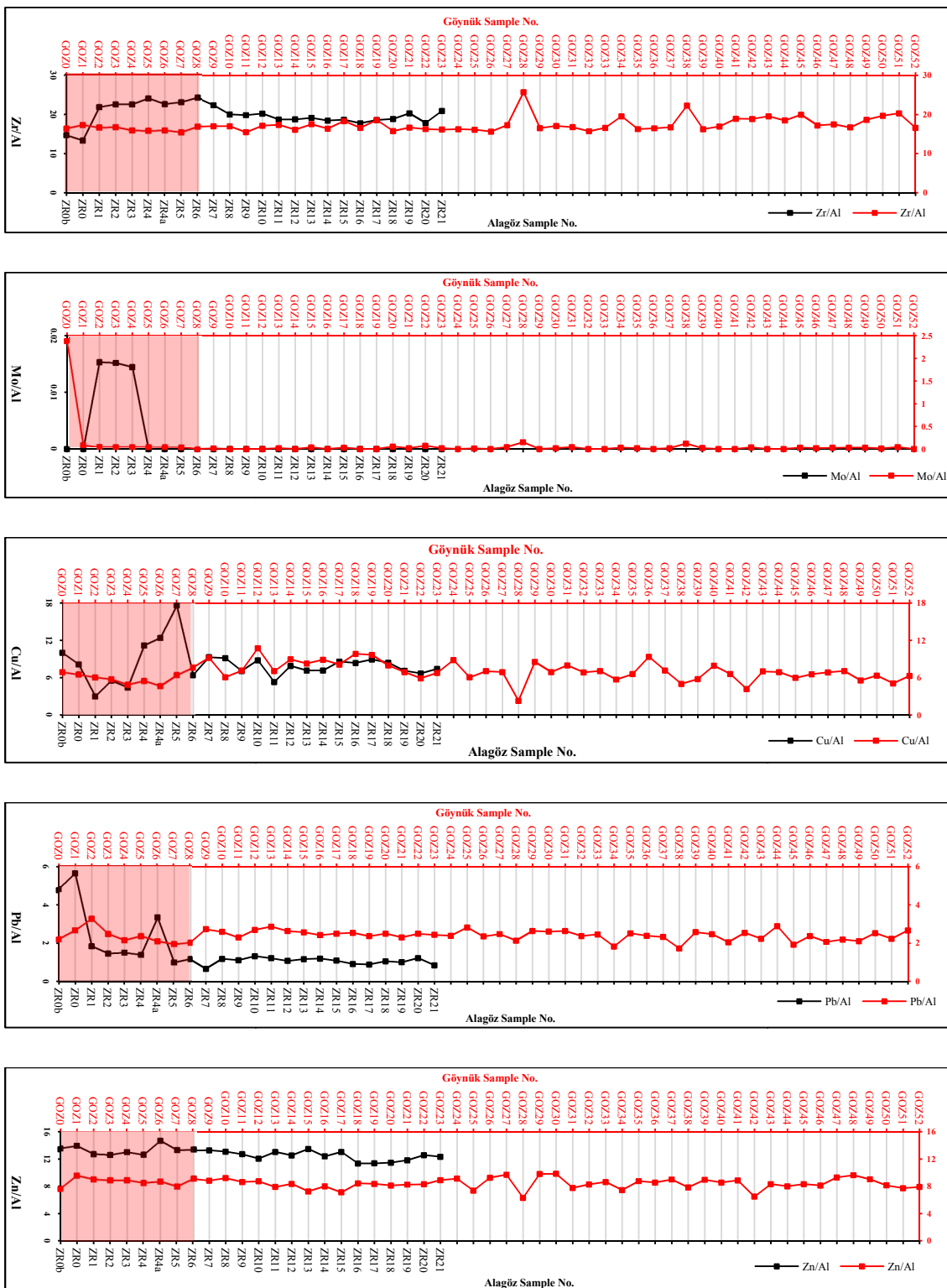


Figure 4.9: Graphic representation of Zr/Al, Mo/Al Cu/Al, Pb/Al and Zn/Al of the Alagöz (black line) and Göynük (red line) sections. (red shade represents red beds)

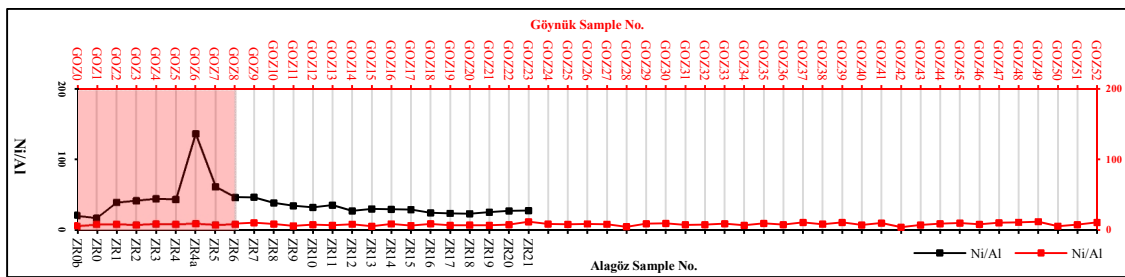


Figure 4.10: Graphic representation of Ni/Al of the Alagöz (black line) and Göynük (red line) sections. (red shade represents red beds)

4.5 RARE EARTH ELEMENTS OF THE ALAGÖZ AND GÖYNÜK SECTIONS

The concentration of rare earth elements (REE) in the studied samples are listed in the tables (Tables 4.4-4.6 for Alagöz Section and tables 4.11-4.12 represent Göynük Section).

The average concentrations of $\sum\text{REE}$ are ranging from 30.64-106.25 ppm in the red bed lithologies and from 76.74-86.42 ppm in the green-gray bed lithologies of Alagöz Section (Table B25). The low concentration of $\sum\text{REE}$ is given by limestone microfacies in the red bed of the Alagöz Section. In the Göynük Section, the average values of $\sum\text{REE}$ are 73.69 ppm in the red strata and from 90.64-102.77 ppm in the green-gray strata (Table B25). The overall average values of $\sum\text{REE}$ in the Alagöz and Göynük sections are lower than PAAS (184.77 ppm; Taylor and McLennan, 1985) (Table B25). Higher concentration of light rare earth elements ($\sum\text{LREE}$) have been noticed in the studied sections. Generally, high occurrences of $\sum\text{LREE}$ as compared to heavy rare earth elements ($\sum\text{HREE}$) in the sediments represent shale or limestone facies (Gromet et al., 1984; Condie, 1991; Armstrong-Altrin et al., 2003, 2004; Ketris and Yudovich, 2009).

4.5.1. VERTICAL DISTRIBUTION OF THE RARE EARTH ELEMENTS OF ALAGÖZ AND GÖYNÜK SECTIONS

The rare earth elements graphic curves in the Alagöz Section are slightly declining form from base to top. In the Göynük Section, the REE shows a more proper trend with increasing from base to top (Figures 4.11-4.14).

From the geochemical data, graphic display and comparison with major oxide elements, it is interpreted that REE fluctuations in the studied sections are controlled by terrestrial influx to the basin. According to Wang et al. (2004) and Fu et al. (2009), terrestrial input to depositional basin is responsible to increase the concentration of the REE. Increase in the REE content along with terrestrial influx is mostly characterized by changes in depositional environment, tectonic setting and fluctuation in sea level.

4.5.2 REE-NORMALIZATION OF THE ALAGÖZ AND GÖYNÜK SECTIONS

The REE of Alagöz and Göynük sections are normalized by using PAAS values of Taylor and McLennan (1985). The normalized calculated values are listed in the tables (PAAS-normalized Alagöz and Göynük sections tables B5-B6, B7-B8, respectively).

The PAAS-normalized diagrams of the red beds and green-grayey beds of Alagöz Section exhibit relatively similar pattern with Göynük beds normalized diagrams (Figures 4.15-4.16). Very low value curves of normalized REE in the Alagöz Section are indicated by limestone facies and high value curve of normalized REE is shown by GOZ31 of the Göynük Section. Both studied sections illustrate weak negative Cerium (Ce) anomalies and weak positive Europium (Eu) anomalies. The normalization diagrams of the studied sections display gentle slope-pattern in the LREE and flat pattern in the HREE (Figures 4.15-4.16).

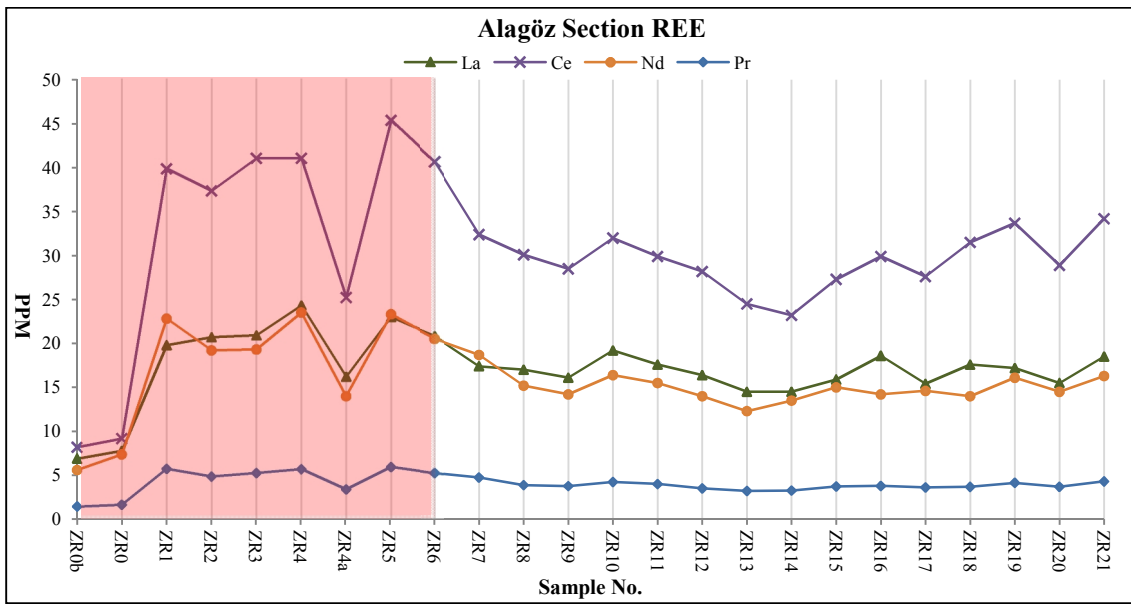


Figure 4.11: La, Ce, Nd and Pr geochemical data graph of the Alagöz Section. (red shade represents red beds)

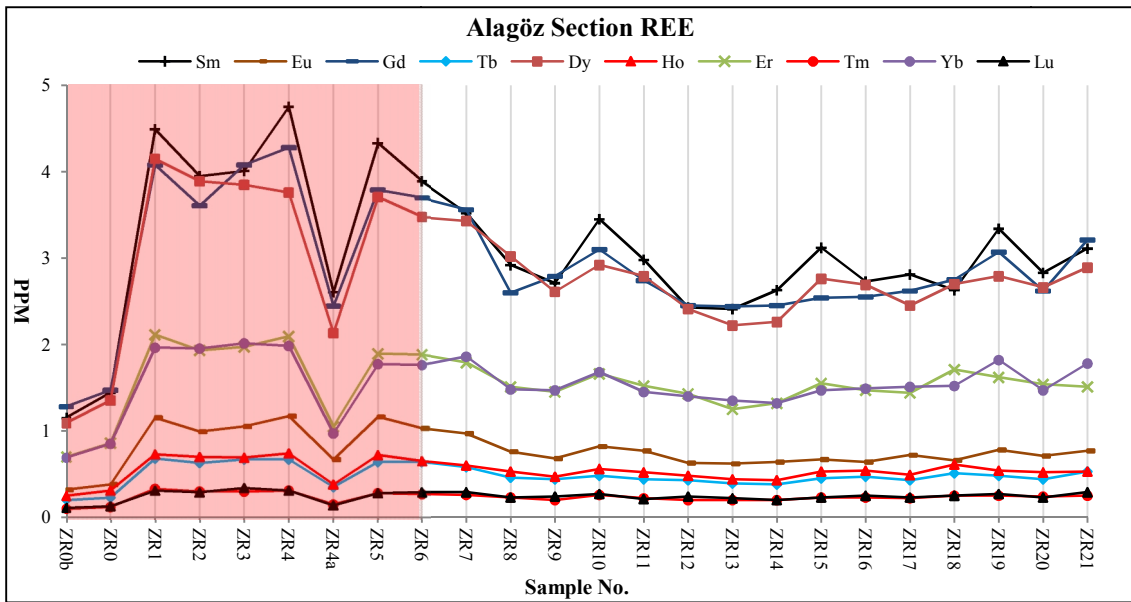


Figure 4.12: Sm, Eu, Gd, Tb, Dy, Ho, Er, Tm, Yb and Lu geochemical data graphs of the Alagöz Section. (red shade represents red beds)

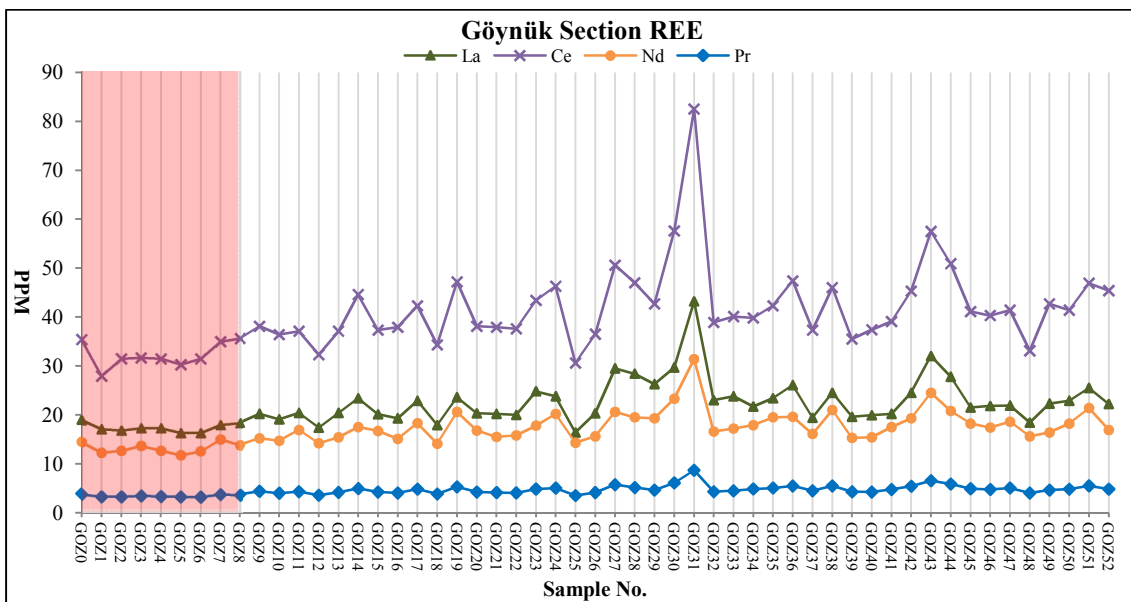


Figure 4.13: La, Ce, Nd and Pr geochemical data graph of the Göynük Section. (red shade represents red beds)

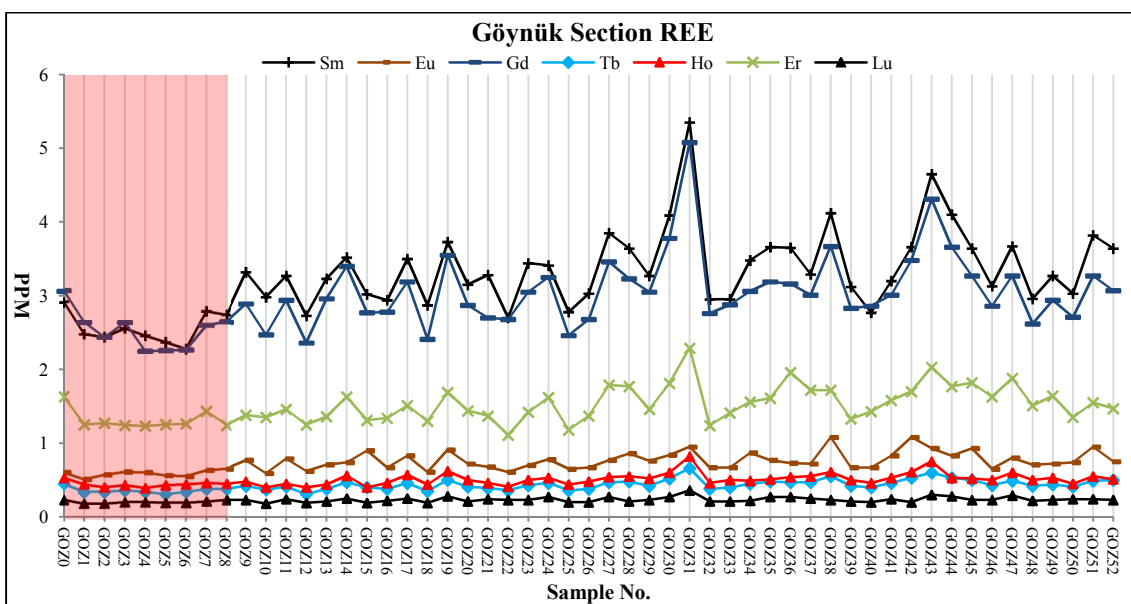


Figure 4.14: Sm, Eu, Gd, Tb, Dy, Ho, Er, Tm, Yb and Lu geochemical data graph of the Göynük Section. (red shade represents red beds)

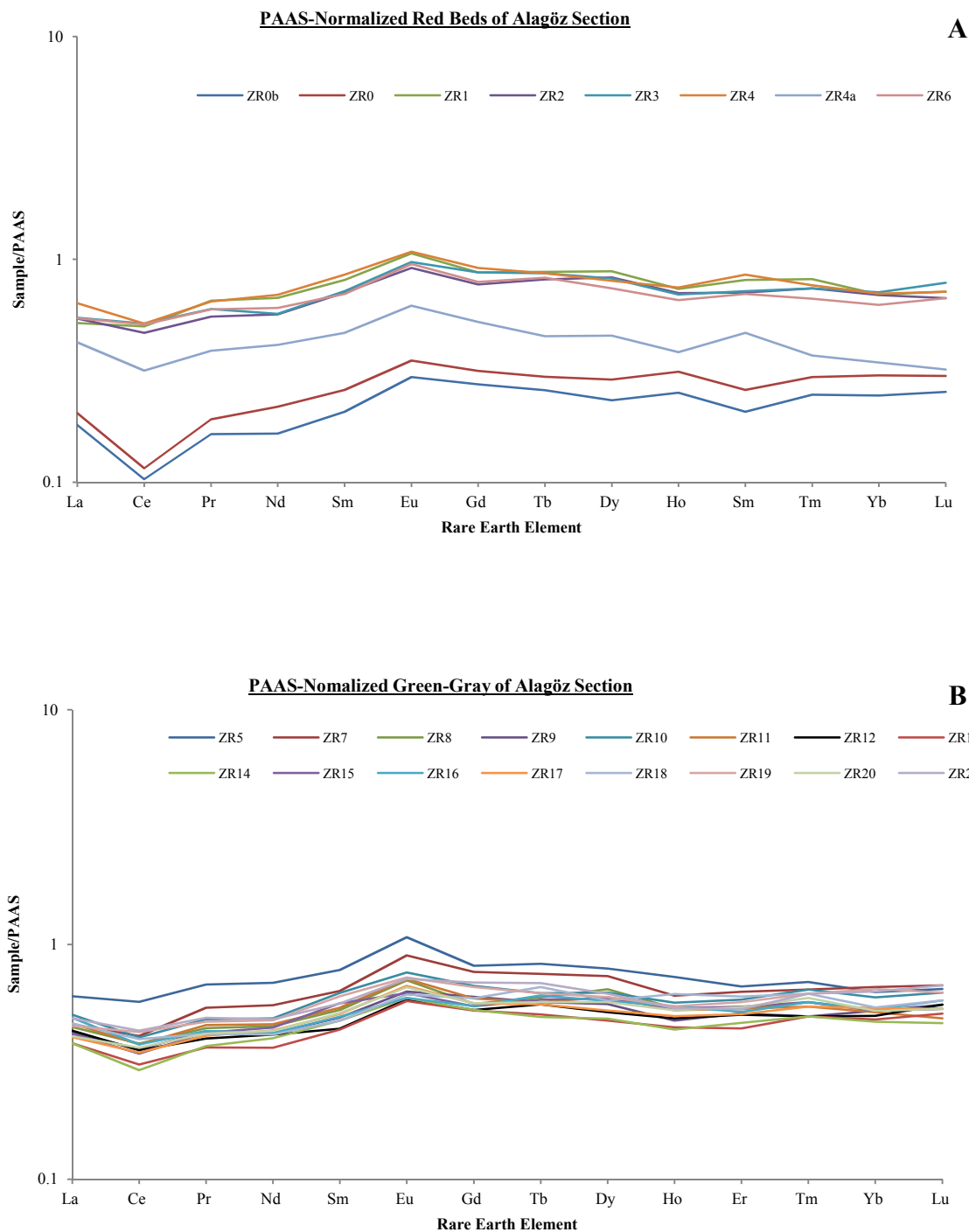


Figure 4.15: PAAS-normalized REE of the Alagöz Section samples plot. PAAS (Taylor and McLennan, 1985) values are used for normalization. (A: Red beds and B; Green-gray beds)

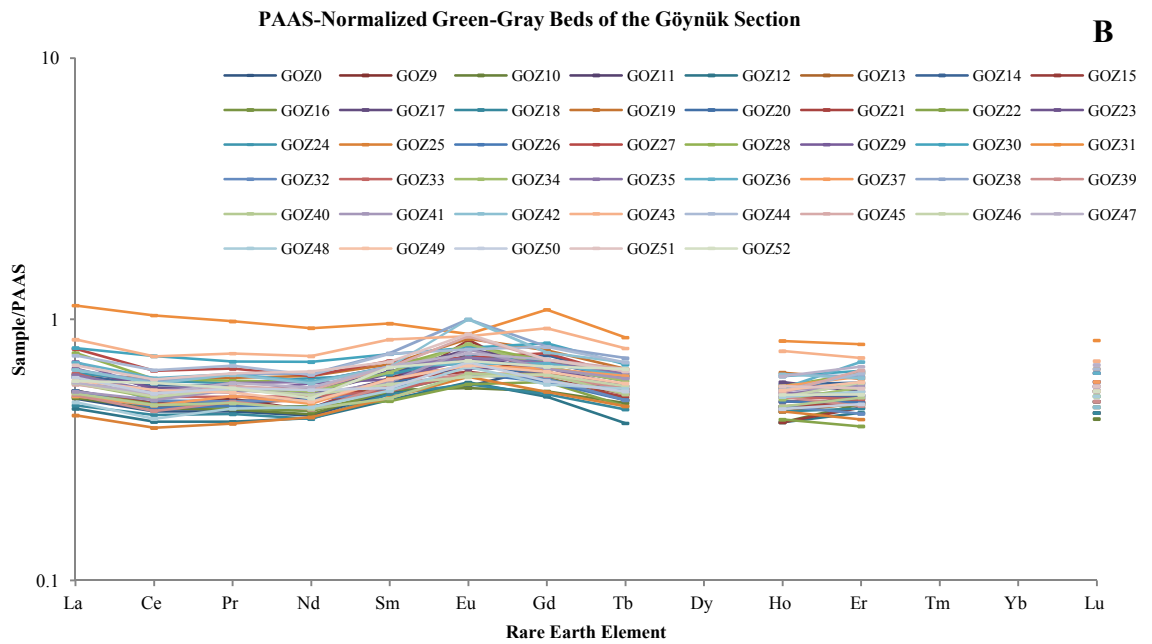
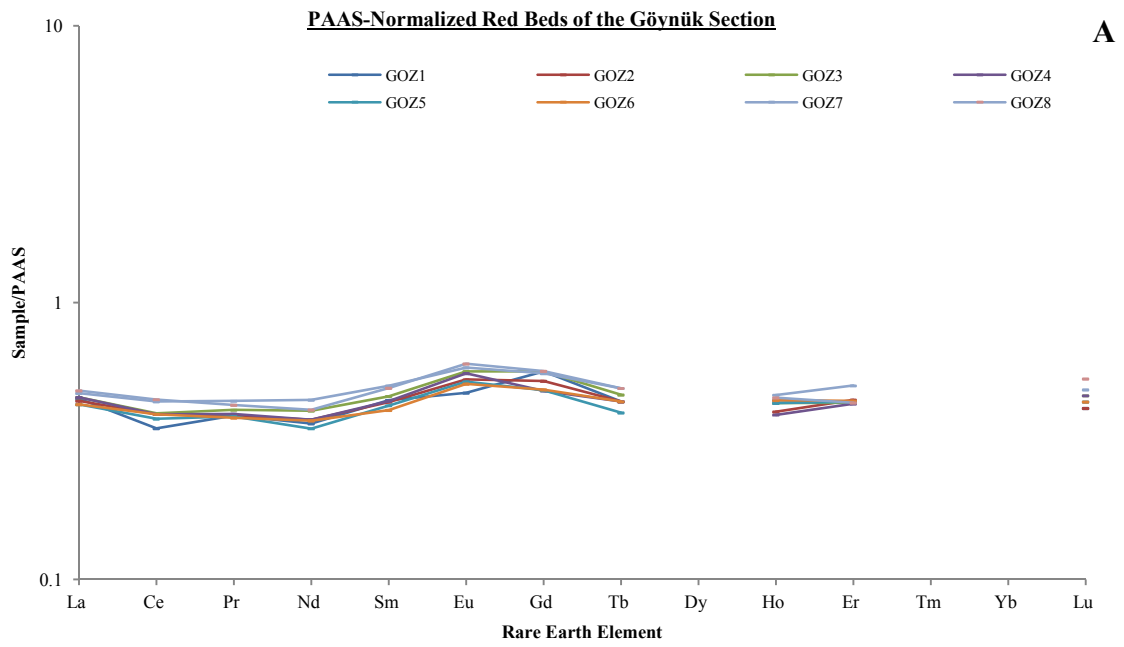


Figure 4.16: PAAS-normalized REE of the Göynük Section samples plot. PAAS (Taylor and McLennan, 1985) values are used for normalization. (A: Red beds and B; Green-gray beds)

4.6 INTERPRETATION OF GEOCHEMICAL DATA

4.6.1 PEARSON'S CORRELATION COEFFICIENT OF THE ALAGÖZ AND GÖYNÜK SECTIONS

The Pearson's correlation coefficient is the matrix technique to evaluate the linear relation strength between the variables (Rollinson, 1993). The Pearson's correlation coefficient values are ranging from -1 to 1. If the obtained values are 1 or near to 1, then it interprets strong relation between the variables. In case of zero, there is no linear relation in between the two or more variants. While, strong inverse linear relation in the variables are indicated by -1 value of the Pearson's correlation coefficient. In this study, it is used to determine the geochemical relation for the interpretation of the geological and physiochemical parameters of the studied sections.

The positive statistical correlation between Al_2O_3 and TiO_2 is generally associated with terrestrial invasion. Similarly, the positive correlation of SiO_2 , MgO , K_2O , P_2O_5 with Al_2O_3 suggests the terrestrial invasion to the system (Ogala, 2012). The geochemical data of the Alagöz red and green-gray beds represent positive correlation of SiO_2 , MgO , K_2O , P_2O_5 with Al_2O_3 which indicates terrigenous input except red beds correlation coefficient between SiO_2 and Al_2O_3 (Tables 4.13-4.14). The negative correlation is because of high siliceous biogenic content. The terrigenous interruption in the Alagöz succession is also supported by the positive correlation between Al_2O_3 and TiO_2 (Tables 4.13-4.14). Similar positive correlation coefficients have been observed in the Göynük succession which also indicates the terrigenous incursion (Tables 4.15-4.16). The negative correlation of CaO with SiO_2 , Al_2O_3 , Fe_2O_3 , TiO_2 and K_2O also supports the clastic invasion in both the sections (Tables 4.13-4.16).

The strong positive correlation between Fe_2O_3 and Al_2O_3 has been documented in the studied sections (Tables 4.13-4.16). Such a strong relation of Fe_2O_3 and Al_2O_3 provides the indication of Fe association with detrital input. According to the Berner (1984), during decomposition of the organic matter in the reducing environment, the sulfate reducing bacteria produces H_2S in the sediments that react with detrital Fe/reactive Fe in

Table 4.13: Pearson's correlation coefficient of major element, REE and normalized values of the red beds of Alagöz Section.

	SiO ₂	Al ₂ O ₃	Fe ₂ O ₃	MgO	CaO	Na ₂ O	K ₂ O	TiO ₂	P ₂ O ₅	MnO	Cr ₂ O ₃	TOT/C	Σ LREE	Σ HREE	Σ REE	LREE/HREE	Ce*	Eu*
SiO ₂	1	-0.11	-0.19	-0.32	-0.68	-0.16	0.06	-0.19	-0.23	-0.83	-0.88	-0.68	-0.40	-0.21	-0.39	-0.93	-0.46	-0.24
Al ₂ O ₃		1	0.99	0.92	-0.65	1.00	0.94	0.99	0.98	-0.45	0.22	-0.66	0.94	0.99	0.95	0.27	0.90	0.15
Fe ₂ O ₃			1	0.95	-0.59	1.00	0.90	0.99	0.99	-0.37	0.31	-0.59	0.97	0.98	0.97	0.37	0.93	0.22
MgO				1	-0.45	0.93	0.73	0.97	0.97	-0.25	0.33	-0.46	0.94	0.90	0.94	0.51	0.91	0.24
CaO					1	-0.61	-0.72	-0.59	-0.56	0.96	0.50	1.00	-0.39	-0.56	-0.41	0.50	-0.31	0.06
Na ₂ O						1	0.92	0.99	0.99	-0.40	0.27	-0.62	0.95	0.99	0.96	0.32	0.92	0.18
K ₂ O							1	0.86	0.86	-0.53	0.15	-0.72	0.82	0.93	0.83	0.05	0.79	0.06
TiO ₂								1	1	-0.38	0.27	-0.59	0.96	0.97	0.96	0.37	0.91	0.23
P ₂ O ₅									1	-0.35	0.30	-0.56	0.97	0.97	0.97	0.39	0.93	0.25
MnO										1	0.72	0.96	-0.16	-0.35	-0.18	0.69	-0.05	0.14
Cr ₂ O ₃											1	0.50	0.48	0.32	0.46	0.90	0.58	0.30
TOT/C												1	-0.40	-0.57	-0.41	0.49	-0.31	0.06
ΣLREE													1	0.97	1.00	0.55	0.94	0.20
ΣHREE														1	0.97	0.34	0.90	0.14
ΣREE															1	0.53	0.94	0.19
LREE/HREE																1	0.60	0.32
Ce*																1	0.34	
Eu*																	1	

Table 4.14: Pearson's correlation coefficient of major element, REE and normalized values of the green-gray beds of Alagöz Section.

	SiO ₂	Al ₂ O ₃	Fe ₂ O ₃	MgO	CaO	Na ₂ O	K ₂ O	TiO ₂	P ₂ O ₅	MnO	Cr ₂ O ₃	TOT/C	Σ LREE	Σ HREE	Σ REE	LREE/HREE	Ce*	Eu*
SiO ₂	1	0.96	0.91	0.84	-0.99	0.90	0.36	0.87	0.89	-0.73	0.82	-0.99	0.88	0.93	0.89	0.35	0.33	0.26
Al ₂ O ₃		1	0.87	0.81	-0.96	0.93	0.48	0.85	0.85	-0.69	0.74	-0.95	0.88	0.91	0.89	0.40	0.50	0.18
Fe ₂ O ₃			1	0.97	-0.95	0.92	0.07	0.96	0.92	-0.63	0.92	-0.96	0.91	0.93	0.92	0.42	0.32	0.50
MgO				1	-0.91	0.93	-0.07	0.97	0.91	-0.61	0.95	-0.92	0.90	0.88	0.90	0.49	0.25	0.59
CaO					1	-0.95	-0.28	-0.92	-0.92	0.74	-0.87	1.00	-0.91	-0.95	-0.91	-0.38	-0.33	-0.33
Na ₂ O						1	0.20	0.94	0.92	-0.71	0.87	-0.94	0.92	0.90	0.93	0.52	0.37	0.38
K ₂ O							1	-0.04	0.08	-0.24	-0.20	-0.24	0.21	0.25	0.22	0.06	0.50	-0.62
TiO ₂								1	0.92	-0.61	0.97	-0.94	0.90	0.89	0.91	0.48	0.30	0.59
P ₂ O ₅									1	-0.70	0.88	-0.93	0.85	0.90	0.86	0.34	0.34	0.49
MnO										1	-0.55	0.72	-0.48	-0.58	-0.49	-0.07	0.08	0.02
Cr ₂ O ₃											1	-0.89	0.84	0.85	0.84	0.39	0.17	0.69
TOT/C												1	-0.90	-0.94	-0.91	-0.38	-0.32	-0.37
ΣLREE													1	0.93	1.00	0.66	0.45	0.47
ΣHREE														1	0.94	0.33	0.41	0.42
ΣREE															1	0.64	0.45	0.47
LREE/HREE																1	0.31	0.34
Ce*																1	0.03	
Eu*																	1	

Table 4.15: Pearson's correlation coefficient of major element, REE and normalized values of the red beds of Göynük Section.

	SiO ₂	Al ₂ O ₃	Fe ₂ O ₃	MgO	CaO	Na ₂ O	K ₂ O	TiO ₂	P ₂ O ₅	MnO	Cr ₂ O ₃	TOT/C	ΣLREE	ΣHREE	ΣREE	LREE/HREE	Ce*	Eu*
SiO ₂	1	0.97	0.91	0.82	-0.89	0.80	0.97	0.91	0.07	-0.54	0.63	-0.98	0.73	0.76	0.73	0.28	0.77	0.71
Al ₂ O ₃		1	0.92	0.83	-0.81	0.90	0.99	0.97	0.04	-0.48	0.73	-0.94	0.61	0.62	0.61	0.24	0.70	0.64
Fe ₂ O ₃			1	0.88	-0.85	0.85	0.96	0.90	0.17	-0.29	0.65	-0.91	0.70	0.75	0.71	0.23	0.81	0.63
MgO				1	-0.64	0.79	0.89	0.89	0.35	-0.04	0.59	-0.76	0.66	0.69	0.66	0.22	0.72	0.63
CaO					1	-0.62	-0.82	-0.69	0.00	0.67	-0.41	0.95	-0.79	-0.88	-0.80	-0.23	-0.77	-0.65
Na ₂ O						1	0.90	0.95	0.17	-0.24	0.92	-0.78	0.42	0.44	0.42	0.15	0.55	0.44
K ₂ O							1	0.97	0.12	-0.39	0.72	-0.94	0.67	0.69	0.67	0.26	0.76	0.67
TiO ₂								1	0.13	-0.30	0.81	-0.86	0.53	0.55	0.53	0.19	0.64	0.58
P ₂ O ₅									1	0.44	0.26	-0.02	0.50	0.21	0.50	0.57	0.50	0.46
MnO										1	-0.11	0.63	-0.37	-0.38	-0.38	-0.17	-0.27	-0.38
Cr ₂ O ₃											1	-0.58	0.22	0.27	0.23	0.04	0.35	0.24
TOT/C												1	-0.76	-0.79	-0.76	-0.29	-0.78	-0.71
ΣLREE													1	0.80	1.00	0.66	0.95	0.91
ΣHREE														1	0.81	0.08	0.70	0.55
ΣREE															1	0.65	0.95	0.91
LREE/HREE																1	0.70	0.84
Ce*																	1	0.92
Eu*																		1

Table 4.16: Pearson's correlation coefficient of major element, REE and normalized values of the green-gray beds of Göynük Section.

	SiO ₂	Al ₂ O ₃	Fe ₂ O ₃	MgO	CaO	Na ₂ O	K ₂ O	TiO ₂	P ₂ O ₅	MnO	Cr ₂ O ₃	TOT/C	ΣLREE	ΣHREE	ΣREE	LREE/HREE	Ce*	Eu*
SiO ₂	1	0.89	0.69	0.68	-0.97	0.83	0.59	0.92	-0.11	-0.79	0.49	-0.97	0.08	0.21	0.08	-0.16	0.04	0.61
Al ₂ O ₃		1	0.78	0.74	-0.96	0.74	0.86	0.88	-0.21	-0.84	0.38	-0.96	-0.07	0.09	-0.07	-0.27	-0.10	0.53
Fe ₂ O ₃			1	0.93	-0.81	0.38	0.81	0.74	-0.09	-0.58	0.43	-0.79	-0.12	0.08	-0.12	-0.36	-0.14	0.24
MgO				1	-0.79	0.30	0.73	0.71	-0.18	-0.61	0.41	-0.76	-0.16	0.01	-0.16	-0.33	-0.17	0.11
CaO					1	-0.76	-0.75	-0.92	0.15	0.82	-0.48	1.00	0.01	-0.15	0.01	0.24	0.04	-0.54
Na ₂ O						1	0.40	0.83	-0.08	-0.63	0.35	-0.78	0.09	0.20	0.09	-0.13	0.05	0.75
K ₂ O							1	0.63	-0.24	-0.69	0.28	-0.75	-0.24	-0.08	-0.23	-0.32	-0.24	0.26
TiO ₂								1	-0.14	-0.77	0.53	-0.92	-0.09	0.11	-0.09	-0.34	-0.13	0.55
P ₂ O ₅									1	0.43	-0.26	0.14	0.47	0.34	0.47	0.40	0.45	0.20
MnO										1	-0.39	0.83	0.17	-0.01	0.17	0.36	0.19	-0.39
Cr ₂ O ₃											1	-0.46	-0.10	0.06	-0.10	-0.27	-0.09	0.20
TOT/C												1.00	-0.01	-0.17	-0.01	0.23	0.03	-0.57
ΣLREE													1	0.86	1.00	0.56	0.99	0.60
ΣHREE														1	0.87	0.06	0.85	0.64
ΣREE															1	0.55	0.99	0.61
LREE/HREE																1	0.56	0.17
Ce*																	1	0.56
Eu*																		1

the sediments and lead to the formation of pyrite. The phenomena of pyrite formation in the studied sediments elaborate the reducing environment and their formation depends on the availability of Fe in the sediments.

4.6.2 GEOCHEMICAL CLASSIFICATION OF THE SAMPLES FROM ALAGÖZ AND GÖYNÜK SECTIONS

The interpretation of major oxides and their cross plot diagrams are useful tools to classify and determine the maturity of sedimentary rocks (Pettijohn et al., 1972; Potter, 1978; Herron, 1988). Pettijohn et al. (1972) purposed cross plots diagram of $(\text{Na}_2\text{O}/\text{K}_2\text{O})$ vs $\log(\text{SiO}_2/\text{Al}_2\text{O}_3)$ to classify the terrigenous sandstone. Later, Herron (1988) modified the Pettijohn's sandstone classification and introduce the shale along with sandstone and used Fe_2O_3 instead of Na_2O in the cross plot diagram [$\log(\text{Fe}_2\text{O}/\text{K}_2\text{O})$ vs $\log(\text{SiO}_2/\text{Al}_2\text{O}_3)$]. Due to the inclusion of Fe_2O_3 in the diagram, there is also addition of Fe-rich sediment quadrants (Figures 4.17-4.18).

The values of $\log(\text{Fe}_2\text{O}/\text{K}_2\text{O})$ vs $\log(\text{SiO}_2/\text{Al}_2\text{O}_3)$ are calculated from present studies to evaluate the geochemistry classification of the sediments (Tables B9-B12). The calculated values of the present sections are plotted on the Herron's (1988) shale-sandstone classification diagram (Figures 4.17-4.18). The red beds and green-grayey beds of Alagöz Section are classified as more Fe-shale rocks and few lies in the shale quadrant (Figure 4.17). In the Göynük measured stratigraphic section, the red beds samples represent shale rock geochemistry. The green-grayey samples of Göynük Section lies in the shale regime but close to the wacke dividing line (Figure 4.18). Single sample in the green-grayey lithology encounter the wacke portion in the $\log(\text{Fe}_2\text{O}/\text{K}_2\text{O})$ vs $\log(\text{SiO}_2/\text{Al}_2\text{O}_3)$ cross plot. Overall, Herron's (1988) classification indicates that the Alagöz Section is composed of Fe-rich shale and shale. Göynük Section is comprised of shale and single sample represents wacke composition (Figure 4.18).

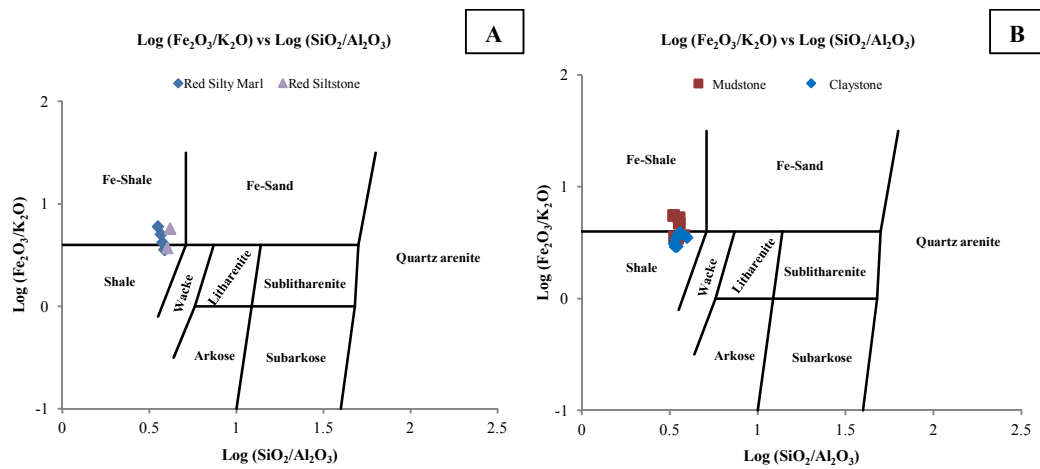


Figure 4.17: Log ($\text{Fe}_2\text{O}_3/\text{K}_2\text{O}$) vs Log ($\text{SiO}_2/\text{Al}_2\text{O}_3$) graph of **A)** red beds and **B)** green-gray beds of the Alagöz Section by Herron (1988) for sandstone and shale classification.

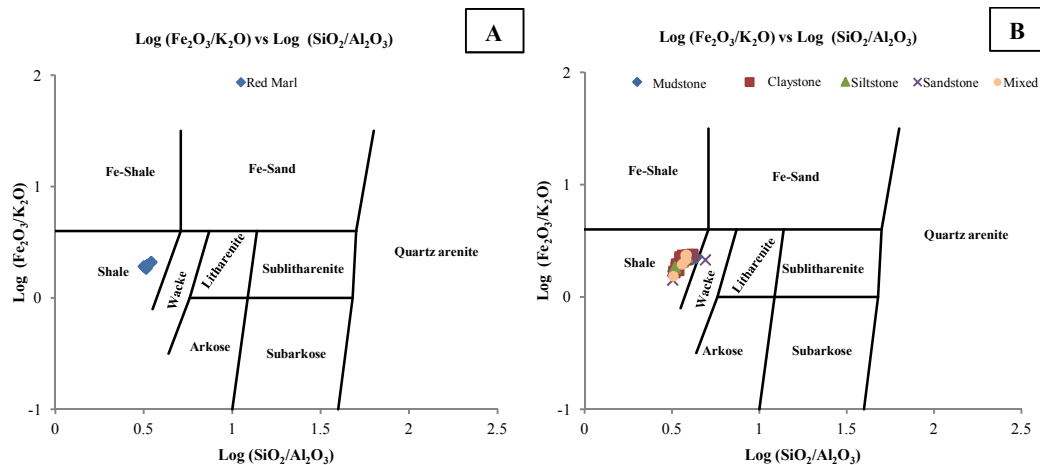


Figure 4.18: Log ($\text{Fe}_2\text{O}_3/\text{K}_2\text{O}$) vs Log ($\text{SiO}_2/\text{Al}_2\text{O}_3$) graph of **A)** red beds and **B)** green-gray beds of the Göynük Section by Herron (1988) for sandstone and shale classification.

4.6.3 PROVENANCE STUDIES OF THE ALAGÖZ AND GÖYNÜK SECTIONS

Geochemical data of the sedimentary rocks have been carried out to identify the provenance of the studied areas. Different geochemical parameters and their cross plots are used to determine the source rock of the sedimentary rocks (Taylor and McLennan, 1985; Condie et al., 1992; Cullers, 1995; Madhavaraju and Ramasamy, 2002; Armstrong-Altrin et al., 2004).

The ratio of $\text{Al}_2\text{O}_3/\text{TiO}_2$ constitutes are helpful to provide the clues regarded to the parent rock composition of the deposited sediments. The Al_2O_3 to TiO_2 ratios are characterized as felsic rock between 21 to 70 Al_2O_3 to TiO_2 ratios, intermediate rock between 8 to 21 Al_2O_3 to TiO_2 ratios and mafic rock between 3 to 8 Al_2O_3 to TiO_2 ratios (Hayashi et al., 1997). The Al_2O_3 ratio of red beds and green-grayey bed sample in the Alagöz Section are ranging from 9.14 to 11.21 and 9.24 to 15.63, respectively (Tables B9-B10). The Alagöz Section samples indicate intermediate rocks (mafic+felsic) character apart from two samples in red beds of packstone which represent felsic composition (25.15 Al_2O_3 to TiO_2 average ratios; Table B28). In the Göynük samples, the ratios of Al_2O_3 to TiO_2 are ranging from 21.19 to 22.41 in the red lithologies and 15.06 to 25.06 in the green grayey lithologies (Tables B11-B12). The Göynük Section represent felsic rock content in the red beds and intermixing of felsic-intermediate rock composition (magmatic) in the green-grayey beds but majority are in felsic ratio (Table B28). The low occurrences of Cr_2O_3 and Ni in the clastic sediments also support the composition of felsic origin for the Göynük Section (Wrafter and Graham, 1989) (Tables B25-B26). Thus, it is interpreted that the sediments in the Alagöz Section and Göynük Section are originated from intermediate rock and more felsic to few intermediate rock, respectively.

In addition, La/Sc - Th/Co and Th/Sc ratios also provide the clues to evaluate the provenance of the studied regions (Wronkiewicz and Condie, 1990; Cox et al., 1995; Cullers, 1995; 2002). In the graph of Th/Co vs La/Sc , red beds and green gray beds of the Alagöz Section lies between felsic and mafic rock which also support the

intermediate origin of the rock samples (Figure 4.19). In the Th/Co vs La/Sc diagram of Göynük Section, the ratio of Th/Co and La/Sc of samples lie in the felsic regime and in between felsic and mafic but more close to felsic region (Figure 4.20). Similarly, the specific range of Th/Sc ratios are categorized to determine the provenance of the detrital grain i.e. felsic derived rock has high ratio of Th/Sc and low for mafic source rock (Alvarez and Roser, 2007). The low concentration of Th/Sc ratios in the Alagöz Section characterized as near to mafic origin sediments. In the Göynük Section, the Th/Sc ratios are falling around felsic origin ratio of Th/Sc (Table 4.17).

The strong positive statistical correlation between TiO_2 and P_2O_5 are related with basic rocks (Ogala et al., 2009). The Alagöz Section indicates strong positive correlation between TiO_2 and P_2O_5 in the red (0.94) and green-grayey samples (1) (Tables 4.13-4.14) which also support the mafic origin of the sediments. While, weak positive correlation (0.13) between $\text{TiO}_2\text{-P}_2\text{O}_5$ in the red beds and negative correlation (-0.14) between $\text{TiO}_2\text{-P}_2\text{O}_5$ in the green-gray beds of Göynük Section represent felsic source rock (Tables 4.15-4.16).

The differences in the values of REE and Eu-anomaly in the sedimentary rocks are also important tools to suggest the parent rock of the area (Taylor and McLennan, 1985). The Eu anomalies will be considered negative, if the values are less than one (which provided by taking log of Eu anomalies) and positive, if the values are greater than one. The higher ratio of LREE/HREE and negative Eu anomaly will propose felsic source rock, where the mafic source rock is characterized by low LREE/HREE ratio and positive Eu anomaly (Cullers, 1995). Eolian input, diagenesis and/or clastic from active ridge system can caused the positive Eu anomaly in the oceanic environment (Michard et al., 1983; Elderfield, 1988; Murray et al., 1991b). From the geochemical data and normalization values, the Alagöz Section represents low $\sum\text{LREE}/\sum\text{HREE}$ ratios and weak positive Eu anomalies (Table B25; Figure 4.15). It indicates more mafic character in the Alagöz sediments. On the other hand, the Göynük Section represents high $\sum\text{LREE}/\sum\text{HREE}$ ratios and very weak positive Eu anomaly as compared to the Alagöz Section (Table B25, Figure 4.16). This suggests felsic origin for the Göynük sediments.

In addition, the positive Eu anomalies in the studied sections may be as a result of eolian input.

4.6.4 CLASTIC INFLUX AND PRIMARY PRODUCTIVITY IN THE ALAGÖZ AND GÖYNÜK SECTIONS

The values of Si to Al ratio should be greater than 1 that represent high proportion of detrital grain and should be less than 1 to indicate clayey rich sediments (Potter, 1978). Very high ratio of Si to Al has been documented from the red beds of Alagöz Section that is due to the presence of high proportion of siliceous radiolarian in the limestone (packstone). Generally, Si to Al ratio in the red beds and green-gray beds are around 3 - 3.50 in the Alagöz Section (Table B27). The average ratio of Si to Al in the Alagöz section are decreasing from packstone (22.21) > siltstone (3.60) > silty marl (3.27) > claystone (3.12) > mudstone (3.09). In the Göynük section, average ratios of Si to Al are reported as 2.9 for red marl and 3.19 for mudstone, 3.16 for siltstone, 3.15 for claystone, 3.58 for sandstone, 3.22 for mixed. Si to Al ratios of Alagöz and Göynük section are close to the PAAS (Taylor and McLennan, 1985) (Table B27).

The low K to Al ratio and high SiO₂ concentration convey dry, semi-arid warm climate (Niebuhr, 2005). Generally, the studied sections are regarded by low K to Al ratio with moderate SiO₂ concentration. K to Al ratios of the red beds of Alagöz Section are relatively parallel to PAAS (Taylor and McLennan, 1985). However, red beds of the Göynük Section K to Al ratios are greater than the red beds of Alagöz Section and PAAS (Taylor and McLennan, 1985) (Table C4). The average K/Al ratio of green-gray lithologies of the Alagöz section are comparatively similar to the red beds of Alagöz section while Göynük green-gray represent 0.35 average K to Al ratio (Table C4).

The primary productivity of marine is essentially controlled by phosphorous. The low value of P to Al concludes insufficient supply of nutrient to marine condition and causes low bioproductivity (Broecker and Peng, 1982; Böning et al., 2004; Schenau et al., 2005). Average P to Al ratio in the Alagöz Section and Göynük Section are similar

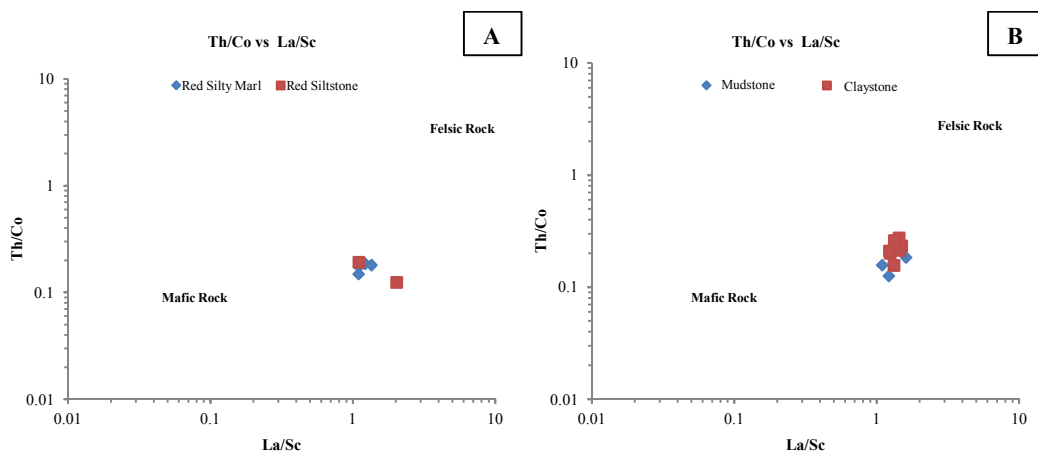


Figure 4.19: Th/Co vs La/Sc graph of **A)** red beds and **B)** green-gray beds of the Alagöz Section. (terrigenous source from Cullers, 2002).

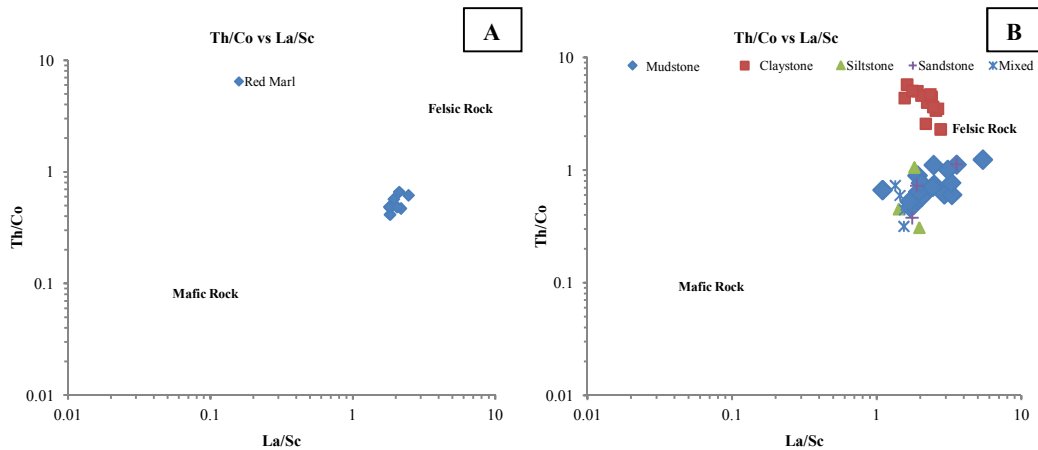


Figure 4.20: Th/Co vs La/Sc graph of **A)** red beds and **B)** green-gray beds of the Göynük Section. (terrigenous source from Cullers, 2002).

Table 4.17: Range of La/Sc, Th/Co, Th/Sc ratios of the Alagöz and Göynük sections compared with felsic and mafic sediments origin ratio
(¹Cullers, 1994; 2002; ²Taylor and McLennan, 1985)

	Red Beds of Alagöz Section			Green-gray Beds of Alagöz Section			Red Beds of Göynük Section			Green-gray Beds of Göynük Section			Range of Sediments ¹			PAAAS ²
Element Ratio	Packstone	Silty Marl	Siltstone	Mudstone	Claystone	Marl	Mudstone	Claystone	Siltstone	Sandstone	Mixed	Felsic rocks	Mafic rocks			
La/Sc	2.3-3.9	1.09-1.35	1.1-2.03	1.09-1.6	1.22-1.49	1.80-2.46	1.09-5.4	1.62-2.76	1.42-1.96	1.75-1.88	1.34-1.59	2.53-16.3	0.43-0.86	2.39		
Th/Co	0.13-0.15	0.15-0.19	0.12-0.19	0.13-0.23	0.16-0.28	0.42-0.66	0.47-1.24	0.47-1.01	0.31-1.06	0.38-1.13	0.32-0.73	0.67-19.4	0.04-1.4	0.63		
Th/Sc	0.27-0.45	0.31-0.39	0.25-0.35	0.32-0.42	0.35-0.48	0.6-0.81	0.67-1.03	0.6-1.09	0.57-0.96	0.51-0.94	0.56-0.95	0.84-20.5	0.05-0.22	0.91		

values (Table C4). These studied sections indicate low productivity as lacking of nutrient in the marine environment. Barium is also important trace element for enrichment of the primary productivity. It is transported to the depositional basin in the form of barite (McManus et al., 1998; Tribouillard et al., 2006). The average values of the Ba/Al in the Alagöz Section samples are lower than from the average values of the Ba/Al Göynük Section samples (Table C4). It represents that Göynük Section samples have relatively organic rich sediments than from the Alagöz Section samples except ZR0b, ZR0 (limestone). The Cu/Al and Ni/Al trace elements and their correlation with Ba/Al also suggest the enrichment of primary productivity in the ancient marine environment (Brumsack, 1989; Calvert and Pedersen, 1993). Overall, both studied section samples illustrate low values of Ba/Al, Cu/Al and Ni/Al which reflect low primary productivity during deposition of these sediments.

4.6.5 GEOCHEMICAL APPROACH TO THE TECTONIC SETTING OF ALAGÖZ AND GÖYNÜK SECTIONS

Several geochemical parameters are utilized to approach the tectonic setting of the depositional sediments (Bhatia, 1983; Taylor and McLennan, 1985; Bhatia and Crook, 1986; Roser and Korsch, 1986; Condie et al., 1992; Cullers, 1995; Armstrong-Altrin et al., 2004). Roser and Korsch (1986) purposed three types of tectonic setting for sandstone and mudstone by using cross plot between $\log(K_2O/Na_2O)$ and SiO_2 . These three types of tectonic setting of Roser and Korsch (1986) are island arc (oceanic arc and continental arc), active continental margin and passive margin. The $\log(K_2O/Na_2O)$ values of the Alagöz (Tables B9-B10) and Göynük (Tables B11-B12) sections are determined. These values are plotted against SiO_2 values of the studied sections in the scatter diagram of sandstone-mudstone tectonic setting of Roser and Korsch (1986). In the $\log(K_2O/Na_2O)$ vs SiO_2 diagram, all the red beds and green-gray beds samples of Alagöz section encountered the island arc tectonic setting regime (Figure 4.21). Similarly, all the red beds and green-gray beds samples of Göynük section are placed in island arc tectonic setting region of the $\log(K_2O/Na_2O)$ vs SiO_2 diagram (Figure

4.22). Therefore, it is interpreted that the Alagöz and Göynük sections are deposited in the island arc tectonic setting.

4.6.6 REDOX SENSITIVE ELEMENTS IN THE DEPOSITIONAL ENVIRONMENTS OF THE ALAGÖZ AND GÖYNÜK SECTIONS

Different elements and element ratios in the sedimentary rocks are used to detect the redox condition of marine environment during the deposition (Hallberg, 1976; Dill, 1986; Hatch and Leventhal, 1992; Jones and Manning, 1994; Nath et al., 1997; Rimmer, 2004). Mo, Ni, Cr, V, U, Co and Th have been considered as characteristic trace elements to evaluate the reducing and oxidizing condition during sedimentation (Dean et al., 1997).

The low ratio of Mo/Al, Cd/Al, V/Al and U/Al trace element in the sediments suggest sufficient oxygen availability in the marine environment (Francois, 1988; Crusius et al., 1996; Helz et al., 1996; Dean et al., 1997; Brumsack, 2006). The presence of low concentration of Mo/Al, Cd/Al, V/Al and U/Al ratios in the present studied sections indicate deposition in oxygenated condition environment (Tables B21-B22 for Alagöz Section; Tables B23-B24 for Göynük Section). However, relatively high values of Mo and Cd are observed in few samples of the green-gray beds of Göynük Section which indicates comparatively oxygen deficient environment as compared to Alagöz Section (Tables 4.4, 4.10).

The values of Cu/Zn, U/Th and (Cu+Mo)/Zn ratios are useful redox parameter (Hallberg, 1976; Nath et al., 1997). The concentration of U/Th ratio below 1.25 represent oxic environment and above than 1.25 indicates suboxic/anoxic marine condition (Neth et al., 1997). Overall, the U/Th ratios of all samples from Alagöz and Göynük stratigraphic sections are less than 1.25 which shows sufficient oxygen during the deposition of sediments. Similarly, the low ratios of Cu/Zn and (Cu+Mo)/Zn in the Alagöz and Göynük sections indicate oxidizing marine environments (Tables B13-B14 for Alagöz Section; Tables B15-B16 for Göynük Section).

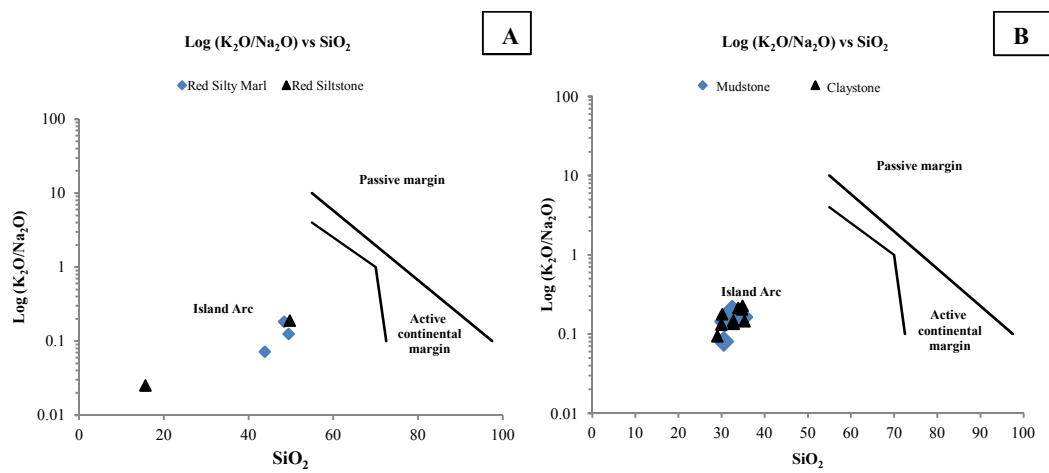


Figure 4.21: $\text{Log}(\text{K}_2\text{O}/\text{Na}_2\text{O})$ vs SiO_2 graph of **A)** red beds and **B)** green-gray beds of the Alagöz Section. (sandstone-mudstone tectonic setting by Roser and Korsch, 1986)

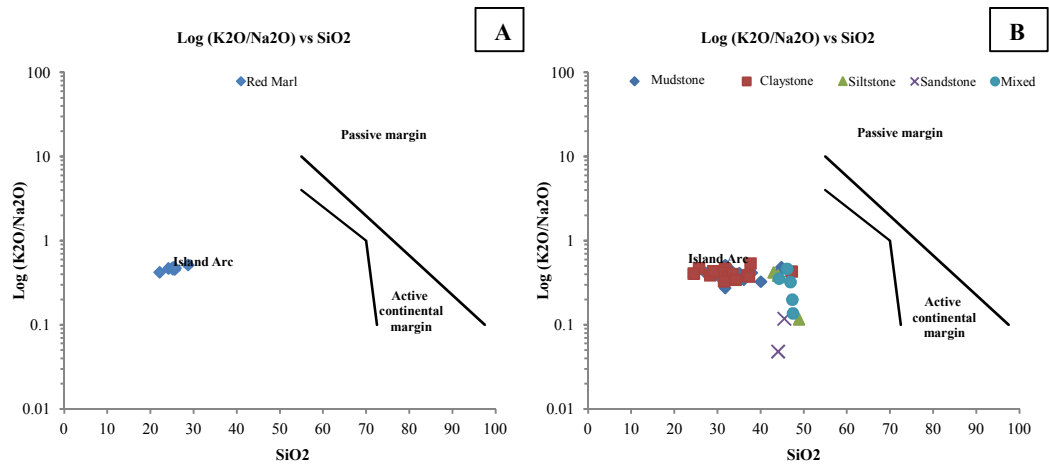


Figure 4.22: $\text{Log}(\text{K}_2\text{O}/\text{Na}_2\text{O})$ Vs SiO_2 graph of **A)** red beds and **B)** green-gray beds of the Göynük Section. (sandstone-mudstone tectonic setting by Roser and Korsch, 1986)

In addition, trace elements ratio such as Ni/Co, V/Cr, V/(V+Ni) ratios and graphic representation also provide useful guideline to diagnose oxic/dysoxic/anoxic marine environment of the sediments during deposition. It has been noticed that the ratios of these elements are inversely proportional to availability of oxygen (Hatch and Leventhal, 1992; Jones and Manning, 1994; Rimmer, 2004). The ratio of Ni/Co are defined as oxic condition below 5, dysoxic between 5 to 7, and anoxic condition above 7. Similarly, the ratios of V/Cr are categorized as oxic condition below 2, dysoxic between 2 to 4.25 and anoxic environment > 4.25 . V/(V+Ni) ratio interprets euxinic (>0.84), dysoxic (0.46 to 0.60) and anoxic (0.54 to 0.82) environments (Hatch and Leventhal, 1992).

In the Alagöz Section, the red beds represent 2.85 to 16.66 Ni/Co ratio, 0.17 to 0.53 V/(V+Ni) ratio and exceptional very high ratio of V/Cr (629.75 to 4409.70) (Table B13; Figure 4.23). The green-grayey beds of Alagöz Section show 4.63 to 7.77 Ni/Co ratio, 0.28 to 0.51 V/(V+Ni) ratio and 3490.15 to 7368.40 V/Cr ratio (Table B14; Figure 4.24). The Ni/Co vs V/(V+Ni) and Ni/Co vs V/Cr graphic representation of Alagöz Section suggests oxic to dysoxic marine environmental condition. As, The V/(V+Ni) and V/Cr ratios are plotted in the dysoxic/suboxic condition for red and green-grayey beds of the Alagöz Section (Figures 4.23-4.24). While, Ni/Co values of the studied section represent oxic to suboxic condition for red beds and almost all of the green-grayey beds lie in the dysoxic environmental condition (Figures 4.23-4.24). Thus, it is interpreted that red stratigraphic portion of the Alagöz section are deposited under oxic to dysoxic condition and then progressively dysoxic marine condition during the deposition of remaining green-grayey stratigraphic portion of the Alagöz Section (Table B28).

In the Göynük Section, the red beds represent 1.86 to 2.53 Ni/Co ratio, 0.73 to 0.78 V/(V+Ni) ratio and unusual V/Cr ratio (11854.39 to 16285.29) (Table B15; Figure 4.25). Where, the green-grayey beds has 1.30 to 4.78 Ni/Co ratio, 0.64 to 0.84 V/(V+Ni) ratio and odd V/Cr ratio (3253.02 to 25471.86) (Table B16; Figure 4.26). The graphic representation of Ni/Co vs V/(V+Ni) and Ni/Co vs V/Cr of the Göynük Section suggests oxic to anoxic oceanic condition. As, the values of V/(V+Ni) and V/Cr of the Göynük Section samples encounter the anoxic marine environment (Figure 4.25-4.26). While,

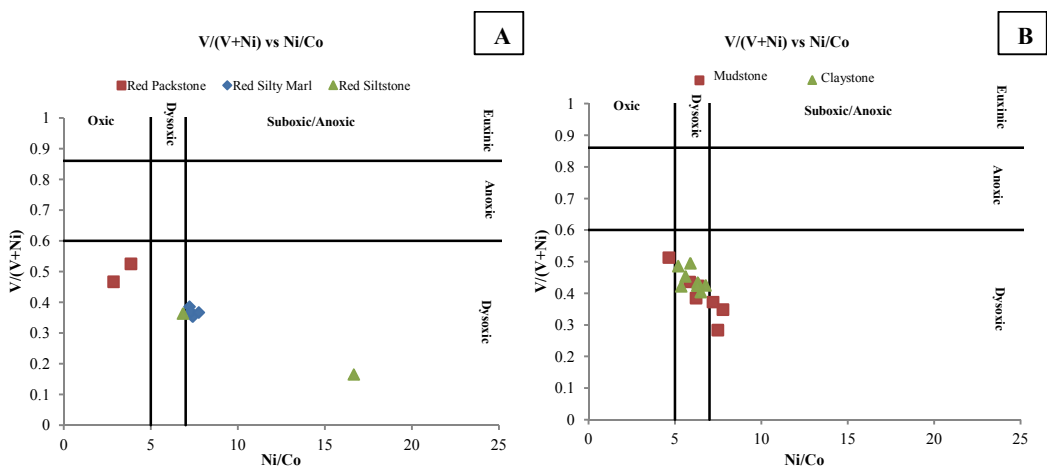


Figure 4.23: Ni/Co vs V/(V+Ni) graph of A) red beds and B) green-gray beds of the Alagöz Section for redox-sensitive cross plots (Hatch and Levenchal, 1992).

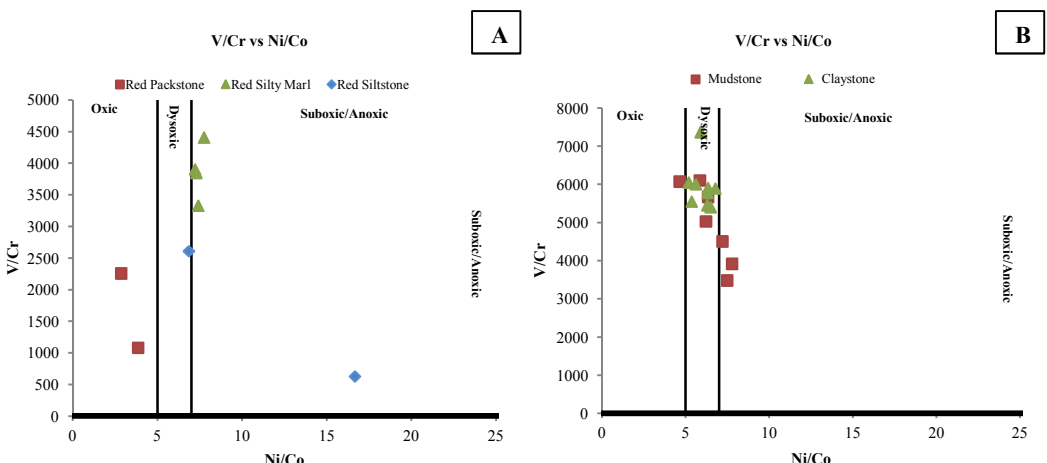


Figure 4.24: Ni/Co vs V/Cr graph of A) red beds and B) green-gray beds of the Alagöz Section for redox-sensitive cross plots (Jones and Manning, 1994).

Ni/Co values of the red and green-grayey beds of Göynük Section represent oxic environment (Figures 4.25-4.26). Thus, it is interpreted that Göynük Section is progressively deposited under oxic to anoxic marine condition (Table B28).

Cerium (Ce) anomalies in the sedimentary strata are also used to approach the redox-condition during the deposition of the sediments (Taylor and McLennan, 1995). The Ce anomalies will be considered negative, if the values are less than one (which provided by taking log of the Ce anomalies) and positive, if the values are greater than one. According to Wilde (1987), Wright et al. (1987) and Murray et al. (1990, 1991a), the Ce-anomalies in oxic sediments represent less negative to positive (>-0.1) and predicts oxic depositional environment with persistent dry cooler climates and regressive condition. The negative Ce-anomalies suggest anoxic sediment with warmer climate and transgressive depositional environment. In the studied sections, the values of Ce-anomalies are considered as negative because obtained values of Ce-anomalies are less than 1 in the Alagöz and Göynük Section (Tables B17-B18 for Alagöz; Tables B19-B20 for Göynük). The Log (Ce/Ce*) anomalies are plotted along the measured stratigraphic sections (Figures 4.27-4.28). The graphic representation of Log (Ce/Ce*)_{PAAS} anomalies, both studied sections are laying toward the negative portion. Thus, based on the Murry et al. (1990, 1991a) and Wilde (1987) Ce anomaly scatter graphic diagram, both studied sections interpret warmer climate, transgressive condition with very weakly reducing environment. Further interpretation, the Ce anomaly and Nd (ppm) values from the studied section samples are plotted on the Ce anomaly-Nd (ppm) graph of Wright et al. (1987) (Figures 4.29-4.32) . This diagram indicates that almost all the samples from both studied sections are lying near the oxic-anoxic boundary but dominantly in the anoxic quadrant (Figures 4.29-4.32). It shows that the studied sections were deposited under suboxic condition.

Overall, the Alagöz and Göynük sections are interpreted as oxic to suboxic marine redox condition. The cross plot of the SiO₂ vs Al₂O₃ and log (Ce/Ce*) anomaly graphs of the Alagöz and Göynük Sections suggested identical depositional environment in the studied section (Figures 4.33-4.34).

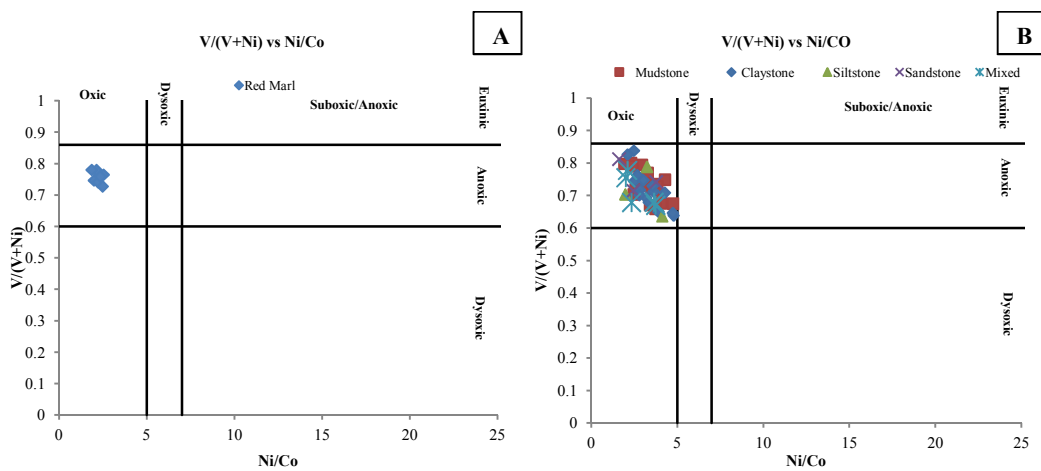


Figure 4.25: Ni/Co vs $V/(V+Ni)$ graph of A) red beds and B) green-gray beds of the Göynük Section for redox-sensitive cross plots (Hatch and Levenchal, 1992).

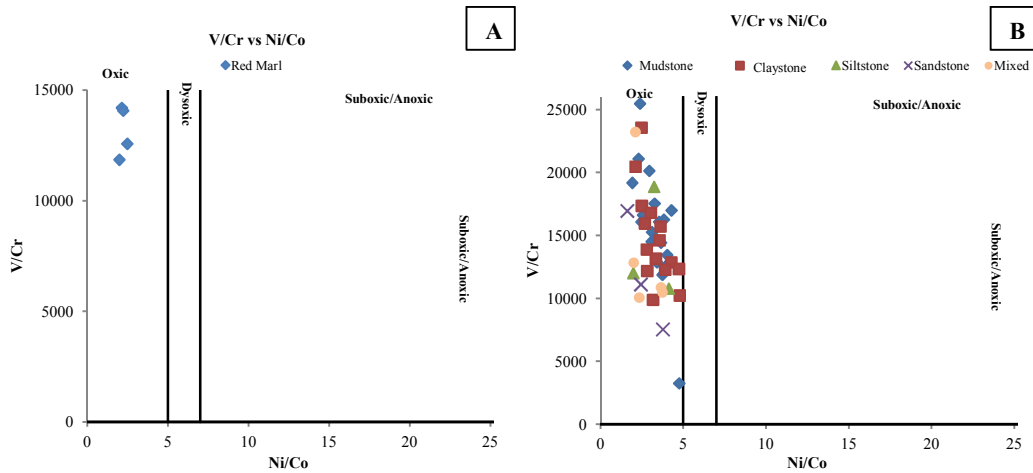


Figure 4.26: Ni/Co vs V/Cr graph of A) red beds and B) green-gray beds of Göynük Section for redox-sensitive cross plots (Jones and Manning, 1994).

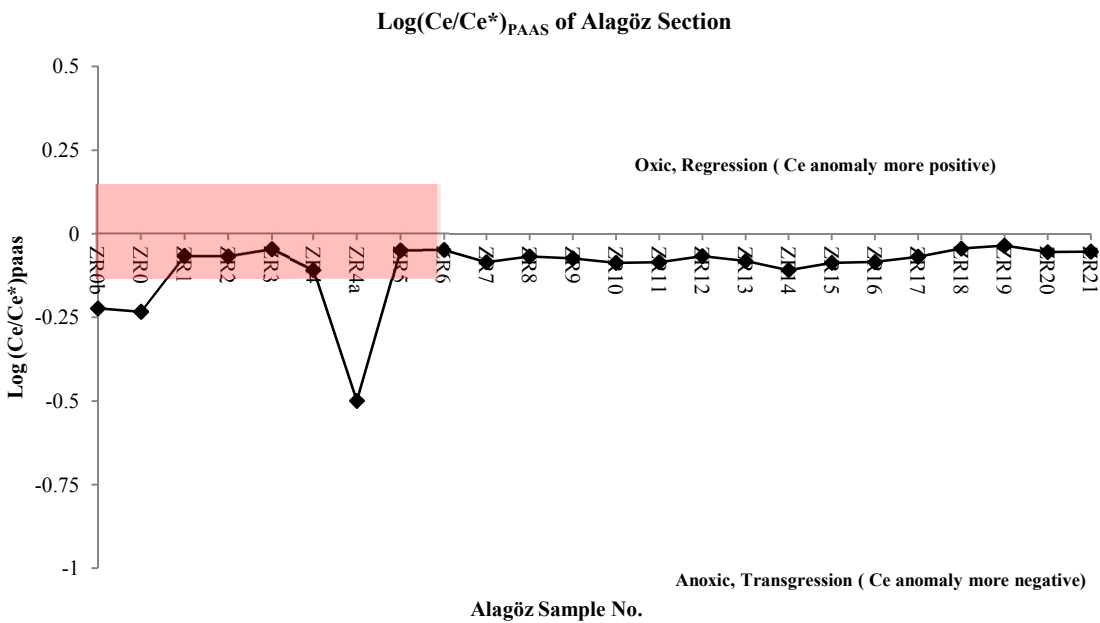


Figure 4.27: Representing Ce anomalies along measured stratigraphic samples of the Alagöz Section to observe the redox sensitive marine condition. (red shade represents red beds: * PAAS- Taylor and McLennan, 1985)

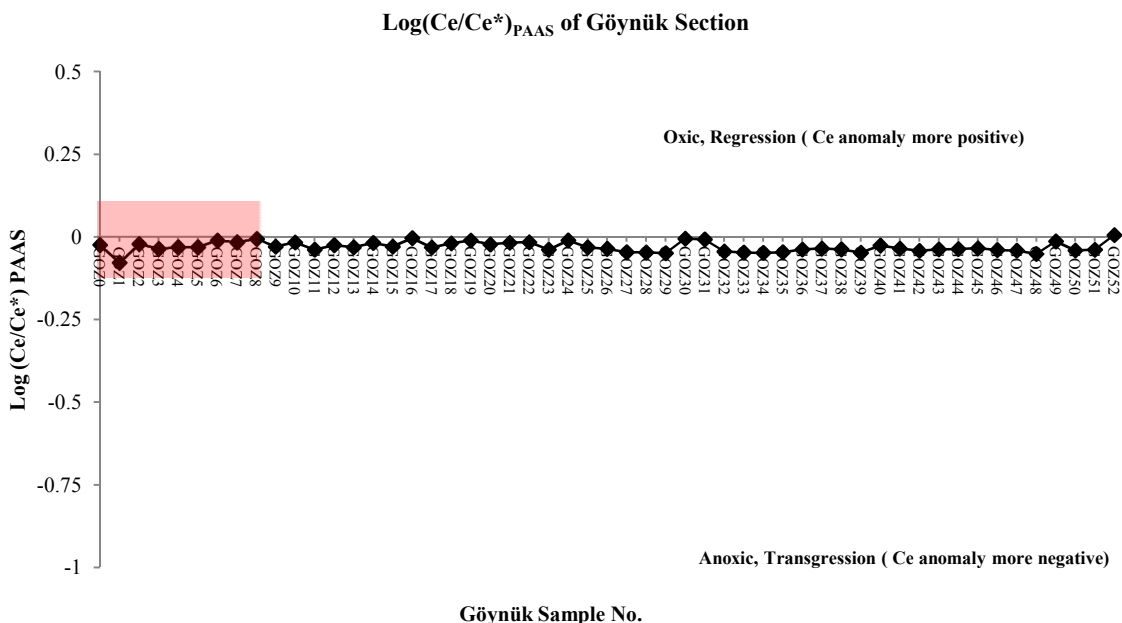


Figure 4.28: Representing Ce anomalies along measured stratigraphic samples of the Göynük Section to observe the redox sensitive marine condition. (red shade represents red beds: * PAAS- Taylor and McLennan, 1985)

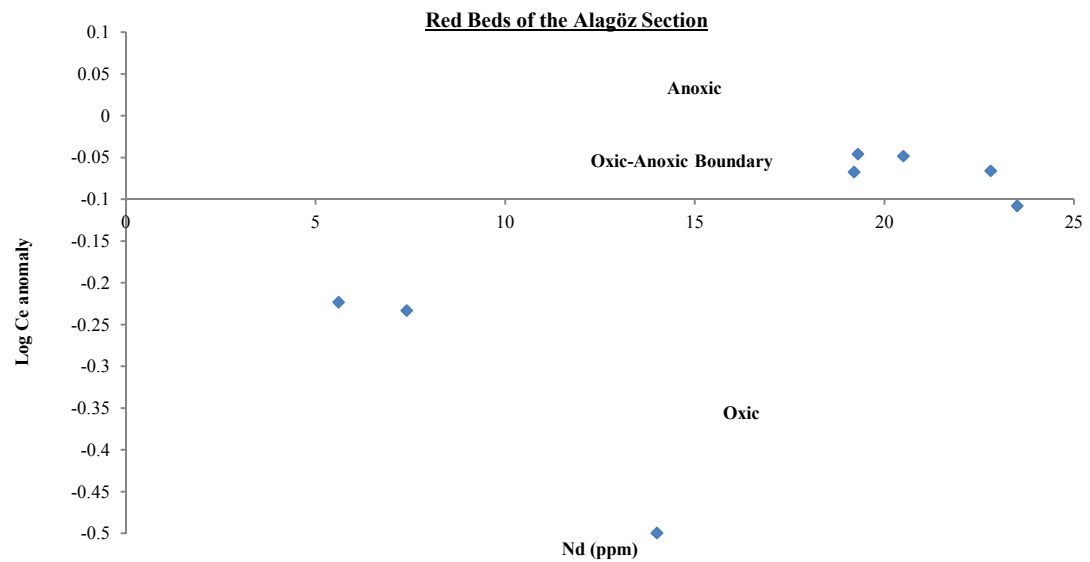


Figure 4.29: Ce-Anomaly vs Nd (ppm) graph of red beds of the Alagöz Section (Ce-anomaly vs Nd (ppm) graph of Wright et al., 1987).

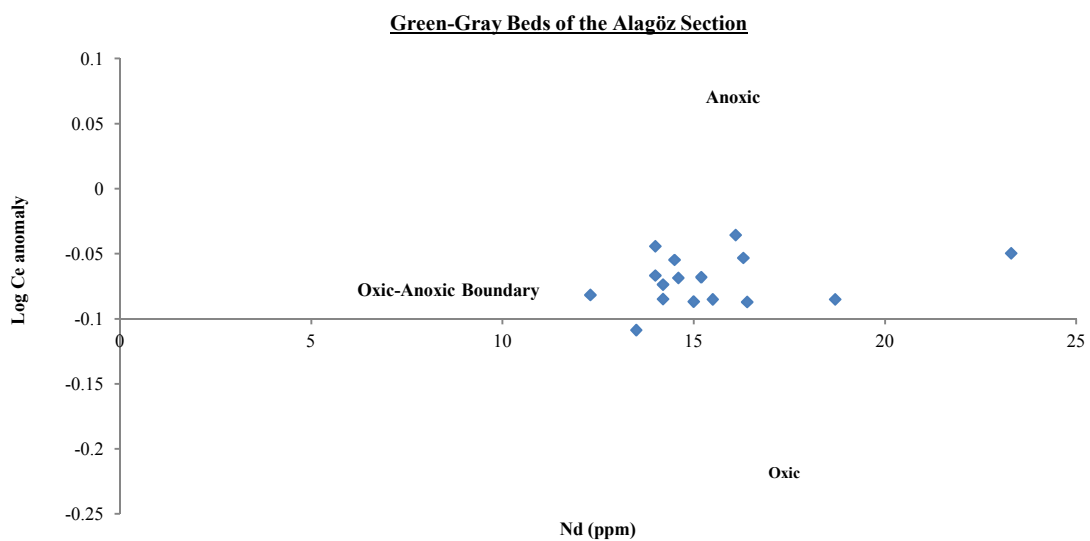


Figure 4.30: Ce-Anomaly vs Nd (ppm) graph of green-gray beds of the Alagöz Section (Ce-anomaly vs Nd (ppm) graph of Wright et al., 1987).

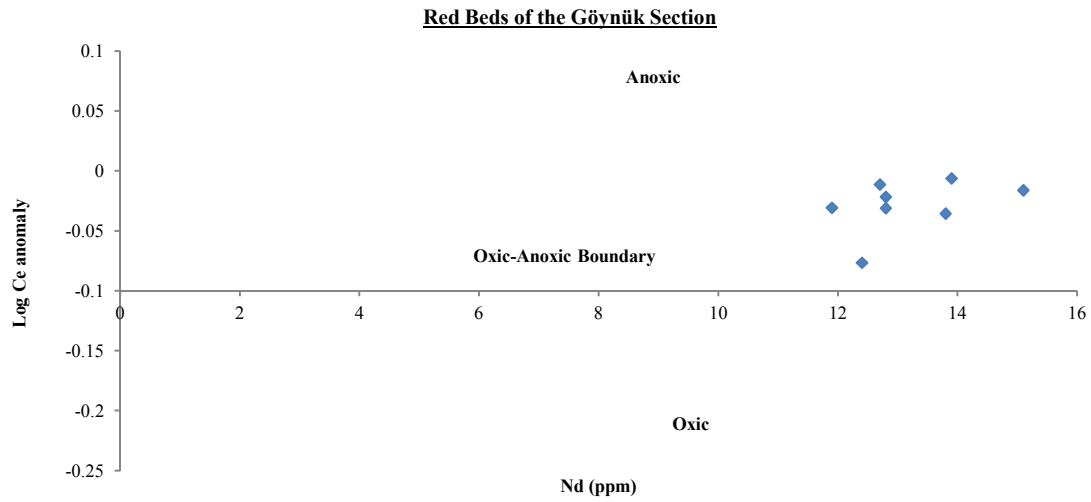


Figure 4.31: Ce-Anomaly vs Nd (ppm) graph of red beds of the Göynük Section (Ce-anomaly vs Nd (ppm) graph of Wright et al., 1987).

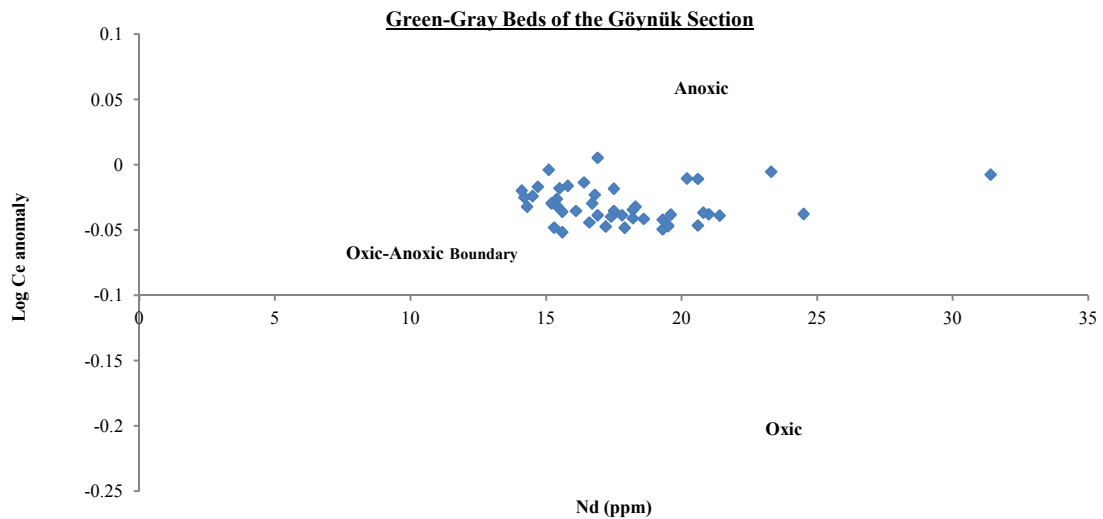


Figure 4.32: Ce-Anomaly vs Nd (ppm) graph of green-gray beds of the Göynük Section (Ce-anomaly vs Nd (ppm) graph of Wright et al., 1987).

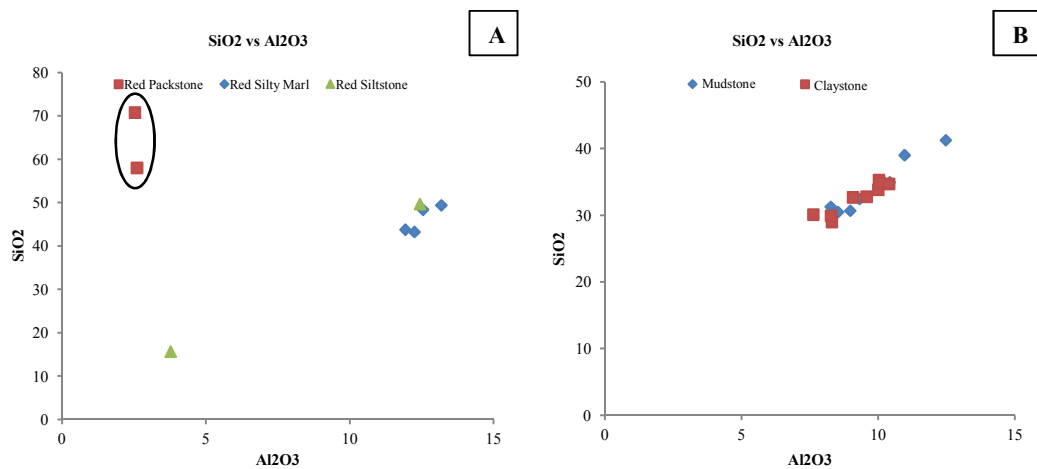


Figure 4.33: SiO_2 vs Al_2O_3 graph of **A)** red beds and **B)** green-gray beds of the Alagöz Section.

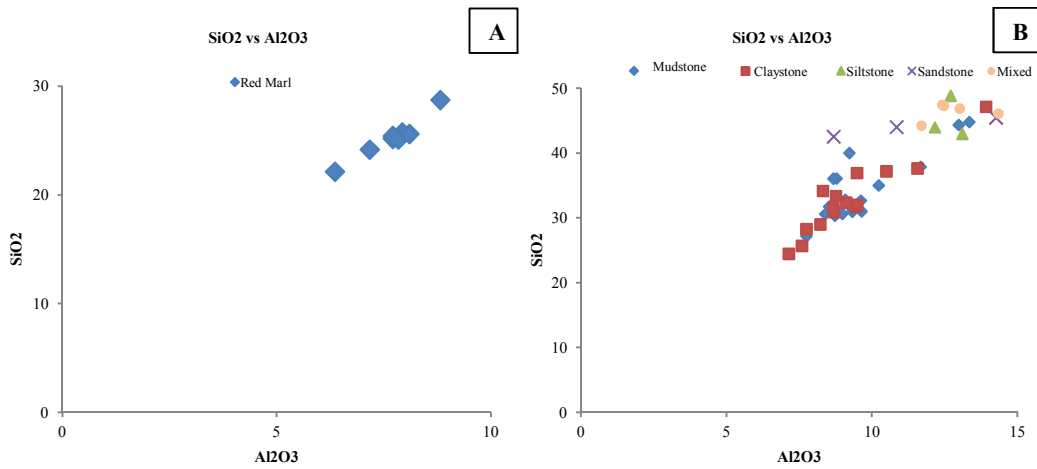


Figure 4.34: SiO_2 vs Al_2O_3 graph of **A)** red beds and **B)** green-gray beds of the Göynük Section.

CHAPTER 5

CYCLOSTRATIGRAPHY

5.1 CYCLOSTRATIGRAPHY

Cyclostratigraphy is defined as the stratigraphic studies to analyze the depositional cyclic/rhythmic patterns which are caused by orbital or internal parameters of the earth (Einsele et al., 1991; Schwarzacher, 1993). The climatic changes that occur due to the earth's orbital variations, could be responsible for these short period sedimentary cycles (mainly Milankovitch cycles) (Einsele et al., 1991). The time period variation in the earth's orbital parameters are categorized as eccentricity (100 ka to 400ka), obliquity (41ka) and precession (21ka) in the Milankovitch cycles (Einsele et al., 1991). In the cyclostratigraphy, the sedimentary cycles are characterized by two different time cycles. One is the cyclic bedding or periodic cycles that are generally used for the orderly repetition of two or more lithological strata, other one is the discyclic bedding or episodic bedding, which is related with abrupt changes in the sediment depositions that is caused by the catastrophic event for short period of time. These are also characterized as rhythmic bedding which reflects the repetitions of the two lithologies, associated with repeated episodic phenomena i.e. tempestities and turbidities (Einsele, 2001).

In the Cretaceous epoch, the cyclic/rhythmic beddings are observed in the alternation of pelagic and hemi-pelagic succession in many places in Europe and USA such as Umbria-Marche Basin of Italy, Vocontian Basin of NE France, Niobrara of Western interior of USA and Mooreville Chalk of Mexico (Barron et al., 1985; Mount and Ward, 1986; Bottjer et al., 1986; Hattin, 1986; Ditchfield and Marshall, 1989; Gale, 1995; Bellanca et al., 1996; Mutterlose and Ruffell, 1999; Stage, 1999; Wendler et al., 2002; Lu, 2007; Locklair and Sagmen, 2008).

In the studied sections, the cyclostratigraphic patterns are determined by using field observations and microfacies analysis of the measured stratigraphic section. The cm to

meter-scale cycles are documented in the studied sections. A total of three cyclic bedding in the Alagöz Section and four cyclic bedding in the Göynük sections are recognized (Figures 5.1, 5.2).

5.2 CYCLOSTRATIGRAPHY OF THE ALAGÖZ SECTION

Total thickness of the Alagöz Stratigraphic Section is 19 m (1900 cm) and a total of 24 samples were collected (Figure 5.1). The succession is composed of very thin to medium bedded, limestone, silty marls, siltstone and alternating mudstone-claystone. In the Alagöz Section, three cyclic bedding patterns with subtypes are identified. The cycles in the studied section begin with red radiolarian limestone and overlain by the green-gray fine grained siliciclastic succession. The microbioturbation have been observed as sedimentary structures in the Alagöz Section.

In the Alagöz Section, three types of cycles, A, B and C, have been recognized along the measured stratigraphic section (Figure 5.1). The details for the documented cycles are as follows:

5.2.1 CYCLE TYPE A

The cycle type A, starts with the red radiolarian packstone and finishes with silty marl with occasional interbedded siltstone and mudstone (Figure 5.1). This type represents deepening upward succession. The cycle-A type is divided into two subtypes. Cycle-A1 subtype contains red to green radiolarian limestone and overlain by siltstone. The cycle-A2 is composed of dominantly silty marl and is capped by mudstone and intra-clastic bearing siltstone. The silty marl also includes microbioturbation features. The centimeter-scale intra-clastic bearing siltstone bedding may belong to the result of an episodic event for short period of interval.

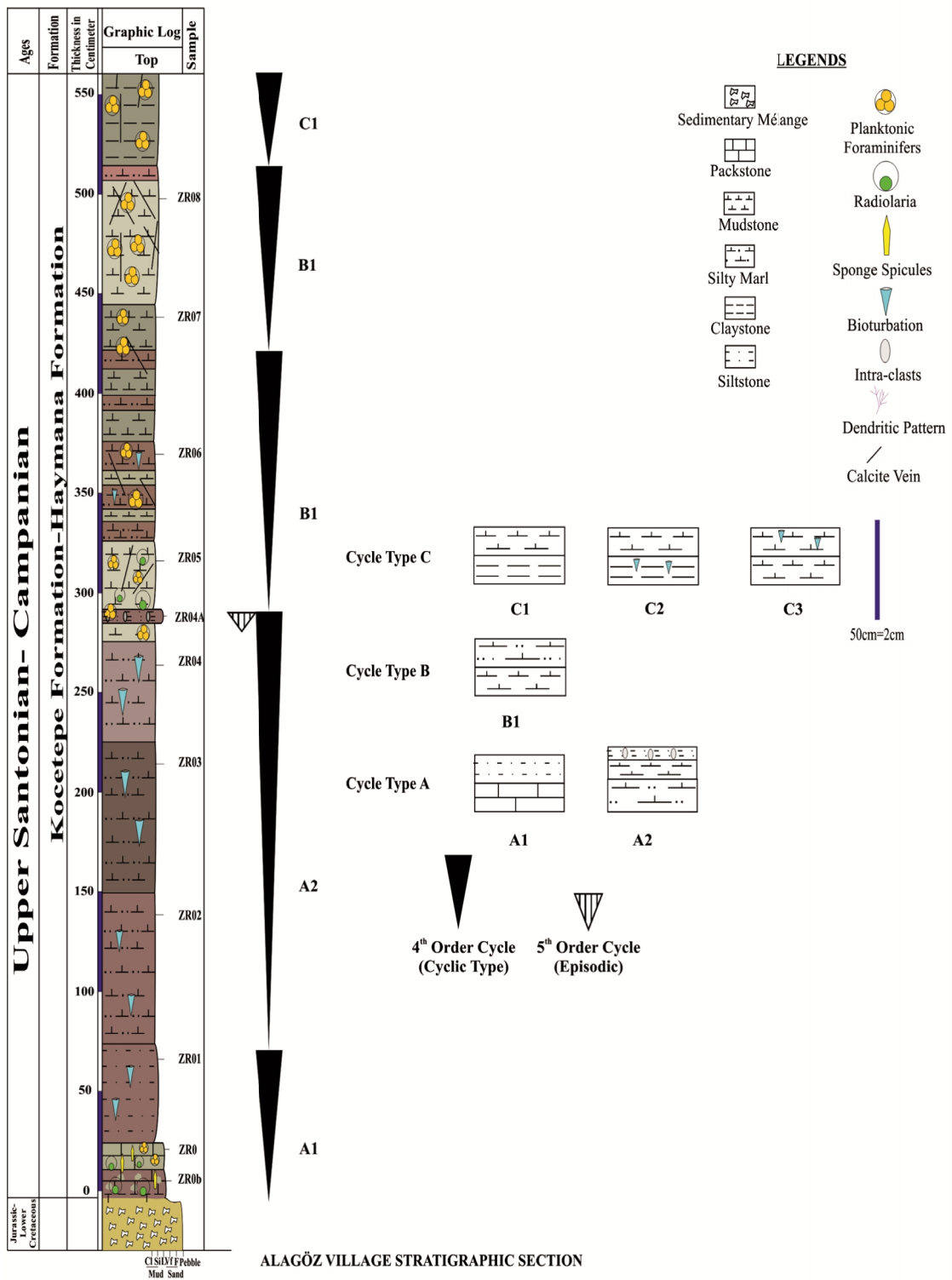


Figure 5.1: Cyclostratigraphic framework in the Alagöz Stratigraphic Section (0-550 cm).

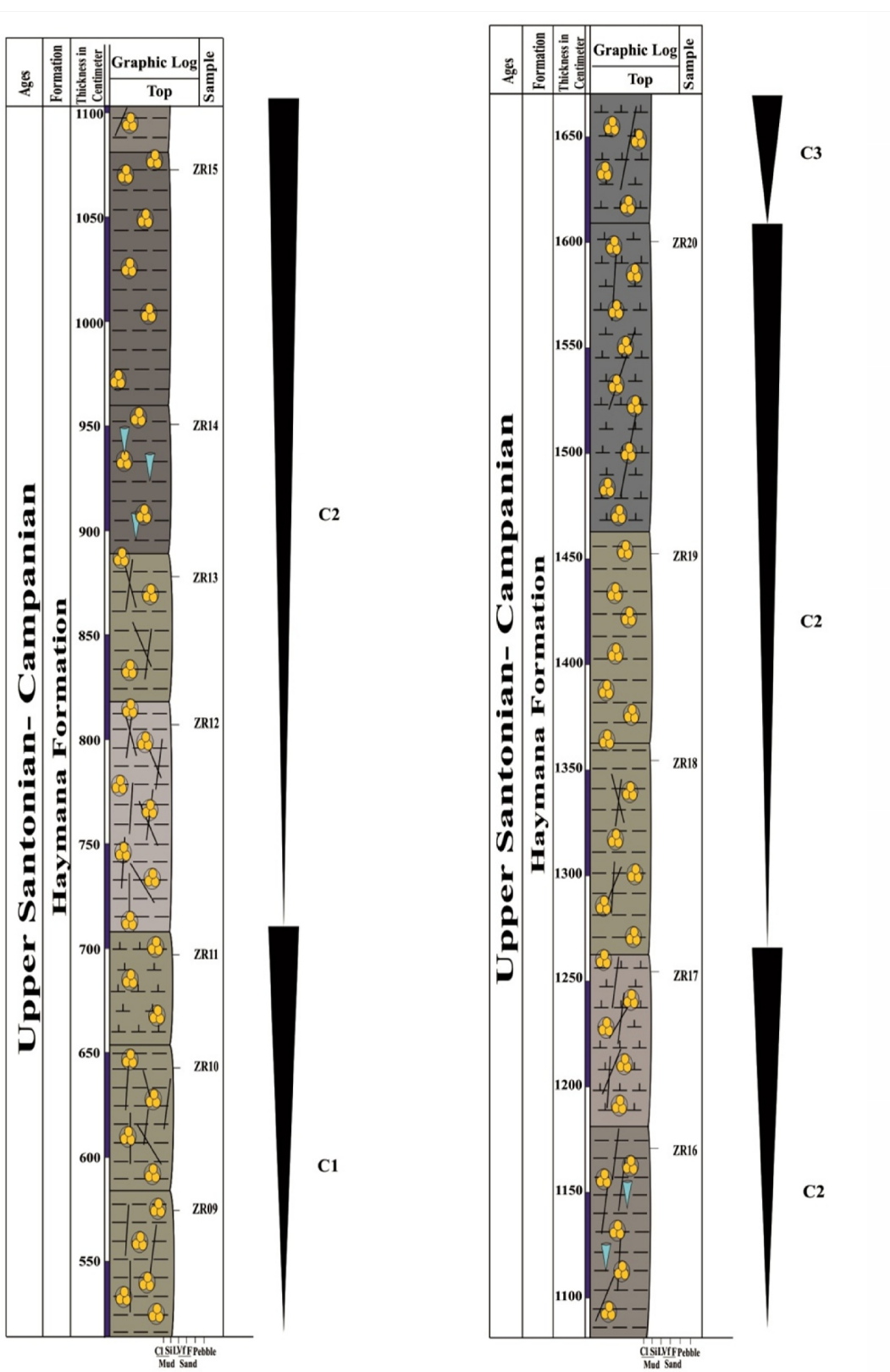


Figure 5.1: Continued. (550-1650 cm)

ALAGÖZ VILLAGE STRATIGRAPHIC SECTION

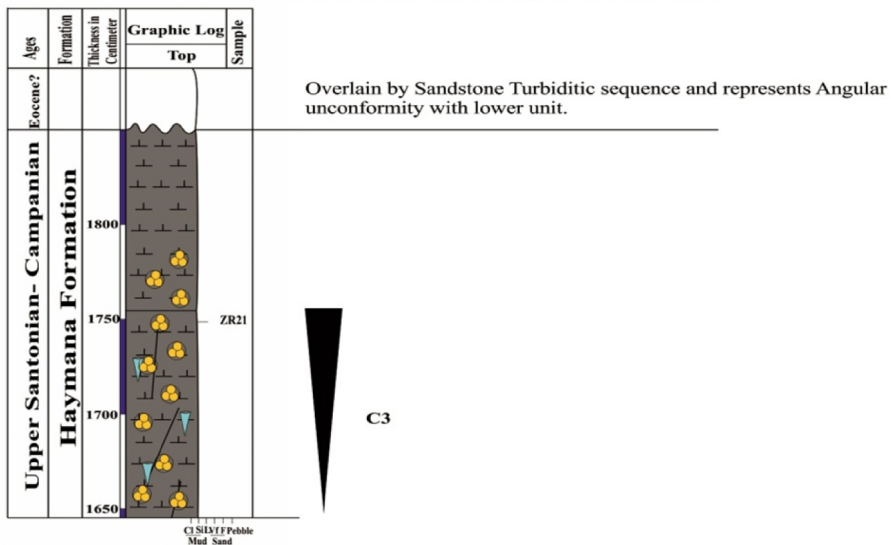


Figure 5.1: Continued. (1650-1900 cm)

5.2.2 CYCLE TYPE B

Cycle-B type represents repeated cyclic bedding alternation of green-gray mudstone and red silty marl (Figure 5.1) which may demonstrate transitional conditions in red beds and green gray beds. The total interval thickness of this repeated cyclic bedding interval is between 280 cm to 520 cm (Figure 5.1). Variations in the colour of facies are due to changes in redox condition in the deep marine environment. These changes may be as a result of increase in the temperature which limited the dissolution of oxygen in bottom water and/or increasing the organic matter (Schieber, 1994; Hu et al., 2009).

5.2.3 CYCLE TYPE C

Cycle type-C is comprised of mudstone and claystone alternation with dominant planktonic foraminifers and occasional bioturbation (Figure 5.1). This cycle suggests changes in the terrigenous influx and primary productivity. In the cycle C, there is low terrigenous content in the bottom and relative high proportion of terrigenous and bioclastic content in the cycle top. This cycle indicates repeated alternation of mudstone-

claystone. It is further subdivided into three types. Cycle-C1 commences with claystone which is characterized by low terrigenous influx, planktonic foraminifers and dominantly matrix/clay proportion. These are topped by mudstone with relatively high proportion of siliciclastic and bioclastic content. C2 cycles are similar to those of C1 cycles but claystone is characterized by microbioturbation. Cycle-C3 is composed of meter-scale mudstone overlain by micro-bioturbated mudstone (Figure 5.1).

5.3 CYCLOSTRATIGRAPHY OF GÖYNÜK SECTION

The Göynük Section consists of dominantly fine grained siliciclastic sediments. The sedimentary structures such as parallel lamination, asymmetrical ripples and microbioturbation have been observed at different stratigraphic level. The detailed study of the microfacies and their vertical arrangement along the studied succession, which is 28.75m (2875 cm) and collection of 53 samples, are illustrated by four types of cycles, A, B, C and D along with their subtypes. The recognized cyclic beddings with the superimposed occasional rhythmic beddings are described in the details as below;

5.3.1 CYCLE TYPE A

The cycle type-A is composed of red marl with occasional interbedded beds of claystone and mudstone (Figure 5.2). They are represented in centimeter to meter scale cyclic pattern and are lying under green-gray siliciclastic lithofacies. The cycle is further categorized into three subtypes A1, A2 and A3. A1 cycle is characterized as claystone at the base and marl at the top. Cycle-A2 has marl with microbioturbation at the bottom and mudstone at the top and is represented in cm to dm-scale repeated cyclic bedding. Cycle-A3 subtype represents cyclicity of alternating claystone-marl-mudstone.

5.3.2 CYCLE TYPE B

The Cycle type B consists of alternating mudstone-claystone with bioturbation. These are resting over red beds of the studied section. They represent cyclic bedding throughout the measured stratigraphic section (Figure 5.2). These siliciclastic lithofacies contained relative proportions of terrigenous materials and planktonic foraminifers. The cycle-B is separated into two subtypes. Cycle-B1 subtype shows cyclic intercalation of claystone and mudstone. Cycle-B2 subtype represents mudstone at the base and microbioturbation mudstone at the top with microbioturbation.

5.3.3 CYCLE TYPE C

The cycle-C is documented as in low siliciclastic content at the lower part and high siliciclastic at the upper part (Figure 5.2). The high siliciclastic interbeds may be due to episodic interruption of event deposits such as turbiditic current. Due to the high influx of terrestrial clasts, it may have affected bioproductivity in the studied section (Einsele et al., 1991). This cycle is classified into three subtype cycles as C1, C2 and C3. Cycle-C1 is characterized by the couplets of mudstone and sandstone. Cycle-C2 consists of mudstone having siltstone in between. The cycle-C3 starts with claystone, followed by mudstone and finishes with sandstone.

5.3.4 CYCLE TYPE D

Cycle-D is composed of mudstone, claystone, siltstone and sandstone (Figure 5.2). This cycle has been observed as an alternating couplet of mudstone-sandstone, mudstone-siltstone and mudstone-claystone-siltstone. The cycle may indicate repeated invasion of turbiditic current deposits and represents coarsening upward. Cycle-D type is subdivided into four subtypes of cycles as D1, D2, D3 and D4. In the cycle-D1 subtype, the bottom is composed of bioturbated mudstone and top includes sandstone with ripple marks. Cycle-D2 subtype consists of mudstone and siltstone couplets. Cycle-D3 is characterized by mudstone-claystone-sandstone cyclic pattern. Cycle subtype D4 starts with mudstone, then pass into claystone and ends with siltstone.

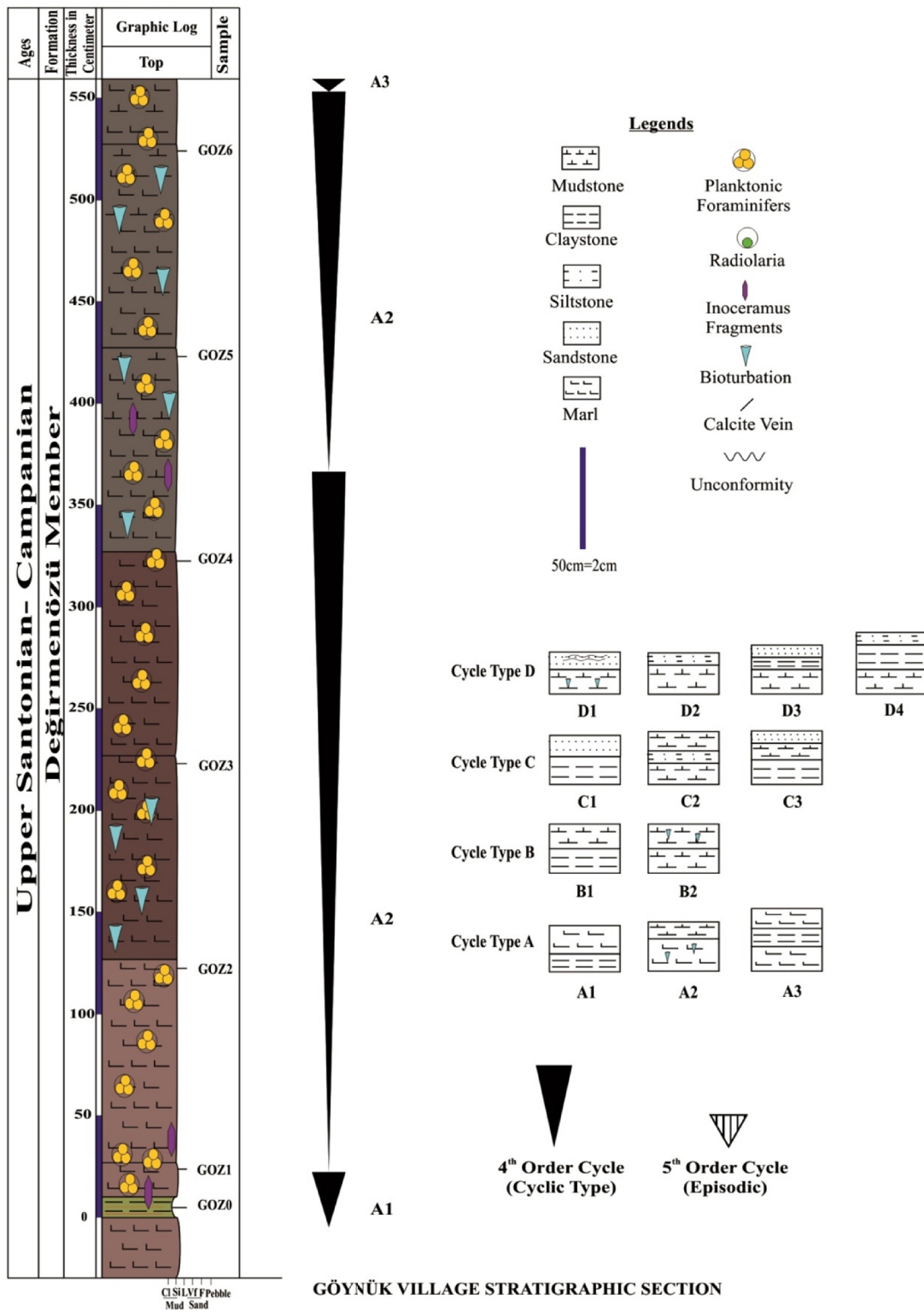


Figure 5.2: Cyclostratigraphic framework in the Göynük Stratigraphic Section (0-550 cm).

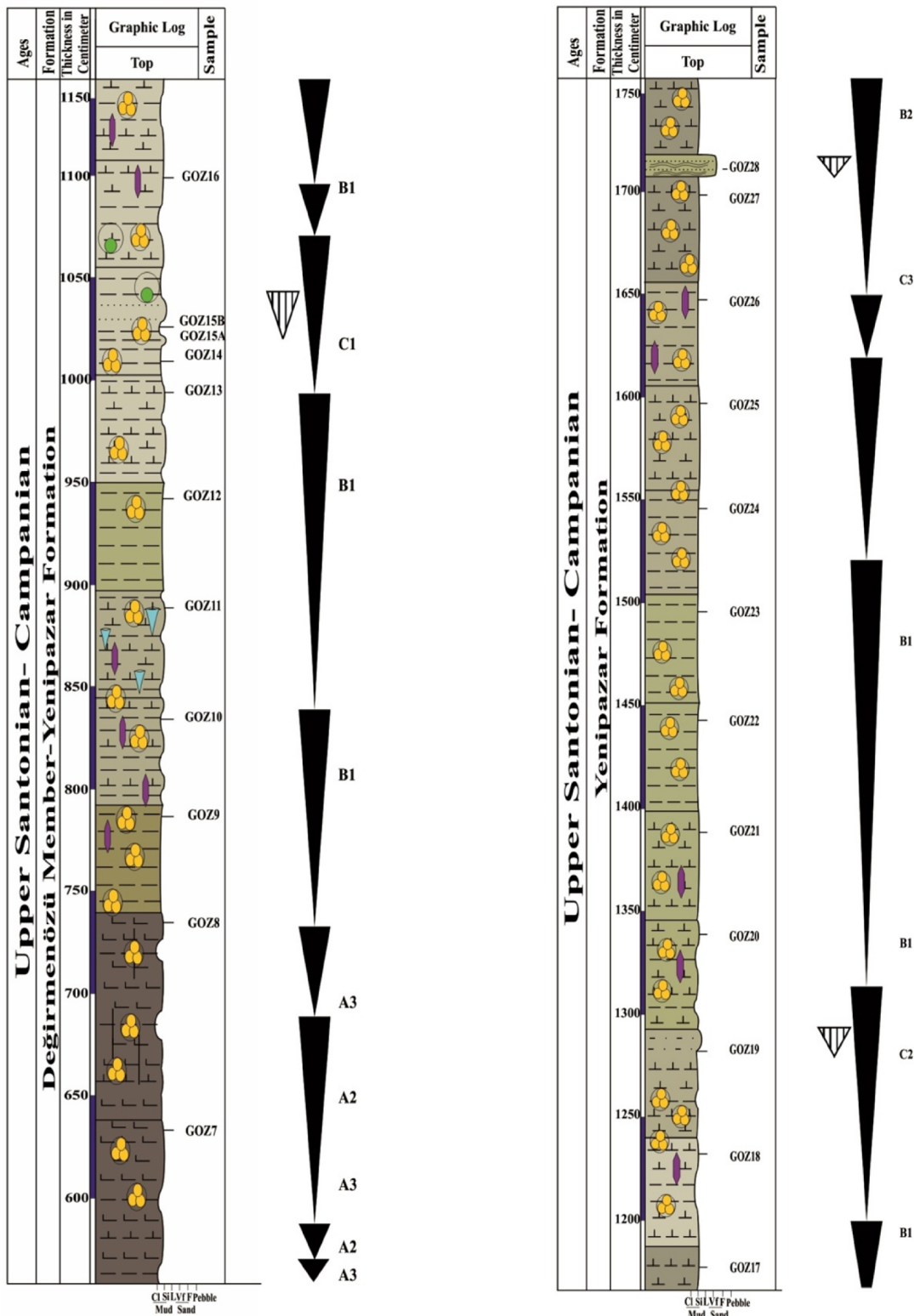


Figure 5.2: Continued. (550-1750 cm)

GÖYNÜK VILLAGE STRATIGRAPHIC SECTION

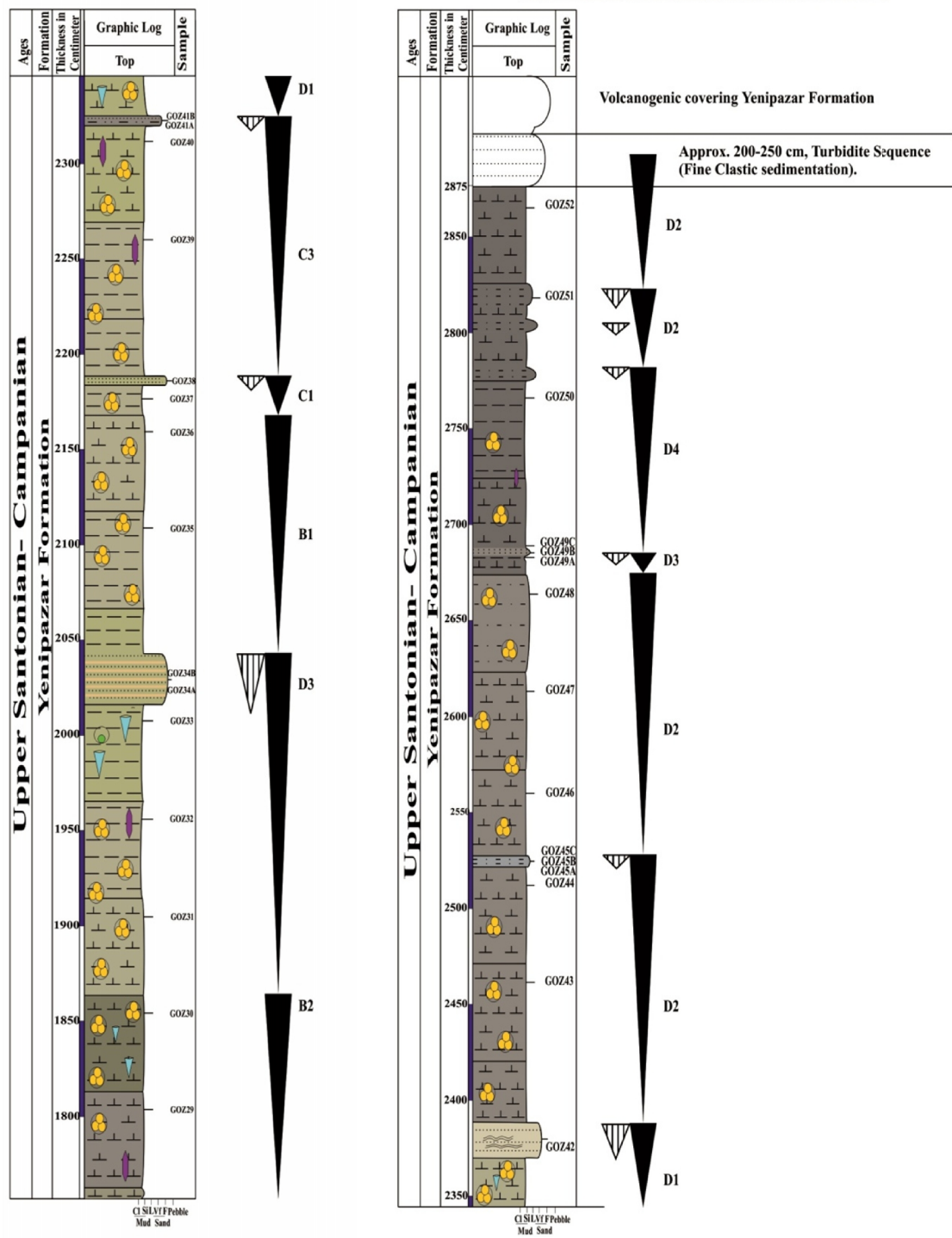


Figure 5.2: Continued. (1750-2875 cm)

5.4 INTERPRETATION

The documented cycles in the studied sections are interpreted as centimeter to meter-scale cyclic bedding with occasional superimposed episodic bedding, under the definition of cyclostratigraphy (Einsele et al., 1991). The red radiolarian limestone, silty marl and siltstone in the Alagöz Section and red marly facies in the Göynük Section are overlain by the green-gray fine grained siliciclastic successions which imply deepening event (Einsele et al., 1991; Schlager, 1999; Yılmaz et al, 2010). It also indicates transgressive condition during the deposition of Upper Santonian-Campanian studied sections. According to the Milankovitch cycles (Einsele et al., 1991), the documented centimeter to meter cycles in the studied section may be characterized as 4th order cycle and may be related with climatic changes. The episodic or rhythmic bedding superimposed 4th order cycles in the studied section are due to turbiditic invasion and are characterized as 5th order cycles. The upper portions of the Göynük Section represent repeated fine grained turbiditic current deposits and imply the onset of the regression as the succession capped by turbiditic and volcanogenic beds. According to Açıkalın (2011), at the Campanian-Maastrichtian boundary, the Central Sakarya Region was characterized by beginning of cooling climate and falling of the sea level. The cycle types of the Alagöz section represents fluctuation in the clastic supply and bioproductivity and has generally similar cyclic pattern as in the Göynük cycle types. Overall, the cyclic pattern of the alternating lithofacies in the studied sections may be produced by small scale sea level fluctuation and/or combination of tectonic setting and productivity changes. Such conditions are interpreted in the Neo-Tethyan Ocean during Cretaceous period from northern Turkey and northern Syria (Al-Riyami and Robertson, 2002; Tüysüz and Tekin, 2007).

CHAPTER 6

DISCUSSIONS AND RESULTS

The Upper Cretaceous (Upper Santonian-Campanian) successions from two different basins, Haymana basin and Mudurnu-Göynük basin in Turkey, were measured for detailed studies. These detailed studies include the identification of vertical changes in the facies, interpretation of depositional environment, geochemical characteristic, changes in the redox condition and recognition of cyclic vertical stacking pattern. The total thicknesses of the measured stratigraphic sections are 1900 cm (19 m) in the Alagöz region and 2785 cm (27.85m) in the Göynük region. A total of 24 samples were collected from Alagöz Section and 53 samples from Göynük Section. These Upper Santonian-Campanian strata are formalized in the stratigraphy as Kocatepe Formation-Haymana Formation in the Haymana Basin and Değirmenözü Member-Yenipazar Formation in Mudurnu-Göynük basin. The lower portions of the two measured stratigraphic sections are composed of red beds which are characterized by radiolarian limestone, silty marl, siltstone in the Alagöz Section and marl in the Göynük Section. These red beds are overlain by green-gray mudstone-claystone. Occasional intercalation of parallel to cross laminated fine grained sandstone and siltstone are observed in green-gray beds of the Göynük Section. Turbiditic sequences and volcanogenic beds are unconformably overlying the two measured stratigraphic sections. The lower contact of Alagöz section is sharp with sedimentary mélange and is unexposed in the Göynük Section. Microscopic and point counting studies have been carried out in order to identify the lithofacies and establish graphic comparisons. A total of 5 microfacies are identified in each studied sections. The Alagöz Section is characterized by red radiolarian packstone, silty marl, siltstone and green-gray mudstone, claystone from bottom to top. The Göynük Section comprises of red marl and green-gray beds of mudstone, claystone with occasional intercalation of the siltstone and fine grained quartzwacke sandstone from base to top. The presences of microfossils within the thin

sections such as planktonic foraminifers, inceramus fragments, sponge spicule, siliceous and calcited radiolaria and less percentage of benthic foraminifers, bivalve and echinoidea. The grains are mostly quartz with less percent of other minerals such as feldspar, plagioclase, gluaconite, mica, rock fragments, heavy mineral (muscovite, chlorite, biotite, zircon, rutile, blue and green tourmaline and monazite) and association of random distribution of pyrite, pyritized fossils, phosphate and heamatite but rarely observed phosphate in the Alagöz Section. Generally, the grains ratio is higher in the red beds of the Alagöz Section and green-gray beds of the Göynük Section. The observed sedimentary structures are parallel to cross laminations, asymmetrical ripples, iron nodules and few microscopic bioturbation in the Göynük Section, while only micro-bioturbation as sedimentary structure has been observed in the Alagöz Section.

The field observation and microfacies studies of the measured sections indicate the deposition in the pelagic to hemipelagic environment with occasional interruption of the turbiditic current. The vertical changes and repetition in the microfacies illustrate small scale fluctuation in the transgressive phase of sea level. The variation from red beds to green-gray beds in the studied successions reflects the changes in the redox conditions from oxic to dysoxic environment and/or minor increase in the organic matter. The green-gray succession of Alagöz and Göynük sections indicate relatively high sedimentation rate, gradual subsidence in the areas/ increasing eustatic sea level and relative rapid burial condition, as overlain by fine to coarse volcanogenic turbiditic succession. The high concentrations of planktonic foraminifers and low ratio/rare benthic foraminifers in the studied sections also suggest deposition of sediments in the open marine bathyal environment. The terrigenous sediments were transported to deep marine environment either by eolian and/or turbiditic current. The Al/ (Al+Fe+Mn) ratio (express as D*) and correlation with Ti/Al is used to approaches the terrigenous input source to the depositional basin (Machhour et al., 1994). Generally, the D* geochemical relationship is related with the fluvial clastic influx. The Ti/Al values correspond to the eolian supply of the clastic materials (Rachold and Brumsack, 2001). At the Alagöz Section, the average D* values are 0.53 in red beds and 0.55 in green-gray beds (Tables B1-B2). While, the average D* values for red beds and green-gray beds of the Göynük

Section are 0.61 and 0.62, respectively (Tables B3-B4). Both studied sections indicates relatively high D* values and low Ti/Al ratio, which suggests that the clastic input to the deep marine environment may be controlled by fluvial run off. The low Ti/Al values in the studied sections show reduction in the grain size, which reflects transgressive condition in the studied sections. The bioturbation in the sections may be local occurrence of oxic horizons and/or fluctuation of dysoxic to oxic deep marine environment during the deposition.

Based on the colour, deposition environmental condition and clastic influx, the red beds of the studied sections can be comparable with Chuangde Formation of Southern Tibet (Wang et al., 2005) and Santonian strata of eastern Alps of Austria (Scott, 2009), and the green-gray successions of the studied section can be related with Early Campanian Ultrahelvetic units of Austrain Eastern Alps (Wagreich et al., 2009).

Geochemical parameters described the geochemical classification of sediments, redox condition, provenance studies and tectonic setting of the studied sections. The abundant major oxides in the studied sections are SiO₂, Al₂O₃, CaO and around 4-5 % Fe₂O₃. The total average values of major oxides are relatively higher in the Alagöz red beds than Göynük red beds, while relatively closer values in the green-gray beds of both sections. The positive correlation of the Al₂O₃ with SiO₂, Fe₂O₃, MgO, K₂O, P₂O₅ and negative correlation with CaO indicate terrestrial invasion during the deposition of studied sections. Terrigenous influx to the studied regimes is also supported by strong positive correlation between Al₂O₃ and TiO₂. The low concentrations of P to Al ratio in the studied sediments suggest low nutrient supply and low bioproductivity during the deposition. The Cu/Al and Ni/Al trace elements and their correlation with Ba/Al also indicate the low primary productivity during deposition of these sediments.

The chemical classification indicates that the Alagöz Section is comprised of Fe-rich and Fe-poor microfacies, while the Göynük Section lithologies are characterized by Fe-poor composition. The Al₂O to TiO₂ ratio and strong positive correlation between TiO₂-P₂O₅ indicates intermediate type source rock (basaltic and granitic) and of the Alagöz sediment and more felsic to intermediate origin source rock for Göynük sediments.

Similarly, the trace element ratio such as Th/Co, La/Sc, Th/Sc ratio and normalized Eu anomalies also suggest more mafic source rock character in the Alagöz section and more felsic rock type origin in the Göynük Section. The (K_2O/Na_2O) ratio against the SiO_2 in the scatter graph plot represent island arc tectonic setting during the deposition of the studied sections. Geochemical parameters such as U/Th, Cu/Zn, Mo/Al, U/Al, Cd/Al, ($Cu+Mo/Zn$, Ni/Co, V/Cr, V/(V+Ni) and Ce anomaly interpret the oxic to dysoxic depositional marine environment in the Upper Santonian-Campanian studied sections. The SiO_2 vs Al_2O_3 and Ce anomalies suggest relatively similar depositional environment in the studied sections.

The high resolution cyclostratigraphy of the Alagöz and Göynük sections indicate cm to meter-scale 4th order cycles (Cyclic bedding) with occasional 5th order cycles (Episodic bedding). The 4th order cycles may be characterized as short eccentricity cycles of the Milankovitch band and may be related with change in climatic condition. The vertical stacking patterns in the studied sections have mainly cyclic bedding and are rarely intercalated by episodic bedding. Generally, the cyclic patterns of the alternating lithofacies in the studied sections may be due to the small scale sea level fluctuation along with changes in the tectonic setting and primary productivity.

Table 6.1: Correlation of the CORBs characteristic from different regions of the world (modified from Chen et al., 2007 and Hu et al., 2005)

Area	North Atlantic Ocean	South Atlantic Ocean	Pacific Ocean	Indian Ocean	Tethyan realm	New Zealand	Austrian Eastern Alps	Turkey (Kapanboğazi Formation)	Tibet	Present studies
Age range	Turonian-Maastrichtian	Campanian-Maastrichtian	Campanian-Maastrichtian	Campanian-Maastrichtian	Late Santonian-Maastrichtian	Upper Cenomanian-Coniacian	Santonian-Campanian	Cenomanian-Campanian	Santonian-Campanian	Upper Santonian-Campanian
Colour	Yellowish brown, reddish brown, light brown, reddish pink, yellow, variegated	Light brown, pink, pinkish gray, reddish yellow, variegated	Brown, light brown, brownish white, reddish brown, red pink, pinkish white, variegated	Yellow brown, yellowish brown, brown, light brown, red, orange pink, variegated	Red, pink, variegated	Red, green, olive gray	Red, gray	Red	Red	Red to brown, green to gray, yellowish
Lithology	Mainly clays and Claystones, few chalks; minor mudstones, oozes, dolomite	Mainly chalks, few oozes, clays, minor shales	Mainly clays, claystones and zeolitic clays, few chalks and limestone; minor oozes, mudstones and marly limestone	Mainly chalks and clays; few oozes, clayey sands	Marlstone, shales, limestone, mudstone	Mudstone, limestone	Marl, limestone, fine siliciclastic turbidites (sandstone, siltstone)	Limestone, marlstone	Shale, marlstone, chert	Marl, silty marl, mudstone, claystone and occasional interbedded fine siliciclastic turbidites (siltstone and sandstone) and radiolarian limestone
Thickness (m)	30-60	30-80	0.7-150	13-115	10-600	0.5-10	-	40	30	19-27.85
Accumulation rate (mm/ka)	2-5	5-15	10	10-20	<10	-	1.5-12	-	2-10	-
Depositional Environment	Slope to pelagic basin: bathyal to abyssal, below or above CCD	Mainly pelagic basins; few slopes and plateaus, above or below CCD	Mainly pelagic basins and submarine plateaus; below or above CCD	Mainly pelagic basins; few submarine plateau, ridges, and shelves, above or below CCD	Mainly pelagic basins to slopes, few shelf environment, below or above CCD	Mid-shelf depth	Pelagic-hemipelagic: below CCD	Pelagic: above CCD	Pelagic slope to basin	Hemipelagic slope to basin above and below CCD

CHAPTER 7

CONCLUSION

1. 1900 cm (19 m) and 2875 cm (28.75 m) thick Upper Cretaceous (Upper Santonian-Campanian) successions were measured from two different basins in the Central Anatolian region of the Turkey, Alagöz Section (Haymana basin) and Göynük Section (Mudurnu-Göynük basin), respectively. A total of 24 samples and 53 samples were collected from Alagöz Section and Göynük Section, respectively. The Upper Santonian-Campanian measured sections are comprised of Kocatepe Formation-Haymana Formation in the Haymana Basin and Değirmenözü Member-Yenipazar Formation in the Mudurnu-Göynük Basin.
2. A total of five facies are identified from each section i.e radiolarian packstone, silty marl, marl, alternating mudstone-claystone and occasional siltstone and sandstone. Based on the board colour contrast, the measured stratigraphic sections are divided into red beds and green-gray beds from bottom to top. The red beds are characterized by radiolarian limestone, silty marl, siltstone in the Alagöz Section and marl in the Göynük Section. The green-gray beds are resting over red beds and are comprised of alternating mudstone-claystone and occasional intercalation of parallel to cross laminated fine grained quartzwacke sandstone and siltstone. Turbiditic sequences and volcanogenic beds are unconformably overlying the two measured stratigraphic sections.
3. During microscopic studies, the observed microfossils are planktonic foraminifers, inceramus fragments, sponge spicule, siliceous-calcited radiolaria and less percentage of benthic foraminifers, bivalve and echinoidea. The grains are mostly quartz with less percent of other minerals such as feldspar, plagioclase, gluaconite, mica, rock fragments, heavy mineral (muscovite, chlorite, biotite, zircon, rutile, blue

and green tourmaline and monazite) and association of random distribution of pyrite, pyritized fossils, phosphate and hematite.

4. The studied sections were deposited in the pelagic to hemipelagic marine environment with occasional interruption of the turbiditic current. The transition from red beds to green-gray beds in the studied successions reflects the changes from oxic to dysoxic condition and/or minor increase in the organic matter. It also reflects transgressive environmental condition.
5. The green-gray succession of Alagöz and Göynük sections indicate relatively high sedimentation rate, gradual subsidence in the areas/ increasing eustatic sea level and relative rapid burial condition as overlain by fine to coarse turbiditic succession.
6. P/Al, Ba/Al, Cu/Al and Ni/Al ratios illustrate low nutrient supply and low primary productivity. The geochemical classification of samples indicates Fe-rich to Fe-poor lithologies in the Alagöz Section and Fe-Poor lithologies in the Göynük Section.
7. The major elements, trace elements and their ratio in the studied sections indicate terrigenous influx to the depositional basin. The relatively high D* values and low Ti/Al in the studied sections imply fluvial supply clastic to the deep marine environment. The low Ti/Al values in the studied sections also reflect transgressive condition during the deposition of the studied sections.
8. The provenance of the Alagöz Section is characterized by intermediate type source rock (basaltic and granitic) and intermediate to more felsic origin source rock for Göynük Sections. The tectonic environment approaches to provenance studies suggest island arc type provenance.
9. Geochemical parameters such as U/Th, Cu/Zn, Mo/Al, U/Al, Cd/Al, (Cu+Mo)/Zn, Ni/Co, V/Cr, V/(V+Ni) and Ce anomaly interpret oxic to dysoxic depositional marine environment in the Upper Santonian-Campanian Alagöz and Göynük sections.

10. All the field observations and microscopic studies, geochemical calculations, properties and their interpretations indicate that the studied sections were deposited in oxic to suboxic marine environmental conditions.
11. Cm to meter-scale 4th order cycles (Cyclic bedding) of the studied sections may be belongs to the short eccentricity cycles of the Milankovitch band and may be linked with changes in climatic condition. The cyclic patterns in the studied sections may also be controlled by the small scale sea level fluctuation and/or association of tectonic setting and changes in the productivity.

REFERENCES

- Abdüsselemoğlu, S., 1959. Almacıkdağı ile Mudurnu ve Göynük civarının jeolojisi, İstanbul Üniversitesi, Fen Fakültesi Monografileri, pp. 14.
- Acer, A., Sarı, A., Sonel, N. and Aliyev, S., 2007. Source Rock Characterization and Depositional Environment of the Late Cretaceous Haymana Formation in the Salt Lake Basin of Turkey. Mineral Research and Exploration Institute Ankara, Turkey. Energy Sources, Part A, Vol. 29, pp. 277-291.
- Açıklan, S., 2011. Orta Sakarya bölgesi kretase - tersiyer istifinin kaynak bölge ve iklimsel açılardan incelenmesi / Provenance and climatic investigation of cretaceous ? tertiary succession in the central Sakarya region, Ph.D Thesis, (in Turkish with English Abstract).
- Aghayev, R., 2008. Sedimentological and cyclostratigraphic analysis of Upper part of the Kartal Formation, SW Ankara. MS Thesis, Middle East Technical University, Turkey.
- Aliyev, S., Sarı, A., Koralay, D. B. and Koç, S., 2009. Investigation of organic carbon and trace metal enrichments of rocks at the Paleocene-Eocene boundary, NW Turkey. Petroleum Science and Technology, Vol. 27: 56-71.
- Al-Riyami, K. and Robertson, A., 2002. Mesozoic sedimentary and magmatic evolution of the Arabian continental margin, northern Syria: evidence from the Baer-Bassit Melange. Geological Magazine, Vol. 139, (4), pp. 395-420.
- Allix, P., Burnham, A., Herron, M. and Kleinberg, R., 2010. Gas Shale, Oil Shale, and Oil-Bearing Shale: Similarities and Differences: American Association of Petroleum Geologists Search and Discovery, Abstract.
- Akarsu, I., 1971. II Geological report of the AR/TPO/747 area. Türkiye Petrolleri Anonim Ortaklıği (unpublished).

Altiner, D., 1991. Microfossil biostratigraphy (mainly foraminifers) of the Jurassic-Lower Cretaceous carbonate successions in Northwestern Anatolia (Turkey). *Geologica Romana*, Vol. 27, pp. 167-215.

Altiner, D. and Özkan S., 1991. Calpionellid zonation in North-Western Anatolia (Turkey) and calibration of the stratigraphic ranger of some benthic Foraminifera at the Jurassic-Cretaceous boundary. *Geologica Romana*, Vol. 27 (1), pp. 215-236.

Altiner, D., Koçyiğit, A., Farinacci, A., Nicosia, U. and Conti, M.A., 1989. Geology and paleontology of western Pontides, Turkey, Tübitak, TBAG-1, pp.270

Altiner, D., Koçyiğit, A., Farinacci, A., Nicosia, U. and Conti, M.A., 1991. Jurassic-Lower Cretaceous stratigraphy and paleogeographic evolution of the southern part of North-Western Anatolia (Turkey). *Geologica Romana*, Vol. 27, pp. 13-81.

Altiner, D., Özgül, N., Yılmaz, İ. Ö., Akçar, N., Bayazıtoglu, M. and Gaziulusoy, Z., 1998. Batı Toroslar'ın Üst Jura-Alt Kretase devirsel karbonat istiflerinde yörüngeisel, östatik veya tektonik olayların etkileri. YDABCAG-163 nolu TÜBİTAK Projesi, Proje Final Raporu, pp. 199.

Altiner, D., Yılmaz, İ. Ö., Özgül, N., Akçar, N., Bayazıtoglu, M. and Gaziulusoy, Z., 1999. High Resolution sequence stratigraphic correlation in the Upper Jurassic (Kimmeridgian)-Upper Cretaceous (Cenomanian) peritidal carbonates deposits (Western Taurides, Turkey). In: Bozkurt, E., Rowbotham, G. (eds), "Advances in Turkish Geology, Part I: Tethyan Evolution and Fluvial-Marine Sedimentation", Geological Journal Special Issue, Vol. 34, (1-2), pp. 139-158.

Altinli, E., 1977. Geology at the eastern territory of Nallihan (Ankara, province). *Istanbul Üniveritesi Fen Fakültesi, Mecmuası*, B, Vol. 42, (1-2), pp. 29-44.

Alvarez, N. O. C. and Roser, B. P., 2007. Geochemistry of black shales from the Lower Cretaceous Paja Formation, Eastern Cordillera, Colombia: Source weathering, provenance and tectonic setting. *Journal of South American Earth Sciences*, Vol. 23, pp. 271-289.

Arabu, N., 1934-1935. Contribution a l'etude qeologique des environs de la mer de Marmara. C.R. geological institute of Romanie, pp. 23.

Arikan, Y., 1975. Tuzgölü havzasının jeolojisi ve petrol imkanları. Mineral Research and Exploration of Turkey, No. 85, pp. 17-38.

Armstrong-Altrin, J.S., Lee, Y.I., Verma, S.P., Madhavaraju, J. and Ramasamy, S., 2003. Geochemistry of Upper Miocene Kudankulam limestones, southern India. International Geological Review, Vol. 45, pp. 16-26.

Armstrong-Altrin, J.S., Lee, Y.I., Verma, S.P. and Ramasamy, S., 2004. Geochemistry of sandstones from the upper Miocene Kudankulam Formation Southern India: implications for provenance, weathering and tectonic setting. Journal of Sedimentary Research, Vol. 74, pp. 285-297.

Aydemir, A. and Ateş, A., 2006. Structural interpretation of the Tuzgölü and Haymana Basins, Central Anatolia, Turkey, using seismic, gravity and aeromagnetic data. Earth Planets and Space, Vol. 58, pp. 951-961.

Aydemir, A., 2011. An integrated geophysical investigation of Haymana Basin and hydrocarbon prospective Kırkkavak Formation in Central Anatolia, Turkey. Petroleum Geoscience, Vol. 17, pp. 91-100.

Aygen, T., 1956. Balya bölgesi jeolojisinin incelenmesi. Mineral Research and Exploration Institute (MTA) of Turkey publication Bulletin, No. 11, pp. 1-95.

Barron, E. J., Arthur, M. A. and Kauffman, E. G., 1985. Cretaceous rhythmic bedding sequences: a plausible link between orbital variations and climate. Earth and Planetary Science Letters, Vol. 72, pp. 327-340.

Bellanca, A., Claps, M., Erba, E., Masetti, D., Neri, R., Premoli Silva, I. and Venezia, F., 1996. Orbitally induced limestone/marlstone rhythms in the AlbioneCenomanian Cismon section (Venetian region, northern Italy) sedimentology, calcareous and siliceous plankton distribution, elemental and isotope geochemistry. Palaeogeography, Palaeoclimatology, Palaeoecology, Vol.126, pp. 227-260.

Berner, R.A., 1970. Sedimentary pyrite formation. American Journal of Sciences, Vol. 268, pp. 1-23.

Berner, R.A., 1984. Sedimentary pyrite formation: an update. *Geochimica et Cosmochimica Acta*, Vol. 48, (4), pp. 605-615.

Bertine K.K. and Goldberg E.D., 1977, History of heavy metal contamination in shallow coastal sediments around Mitelene, Greece. *International Journal of Environmental Analytical Chemistry*, Vol. 68, pp. 281-293.

Bhatia, M. R., 1983. Plate tectonics and geochemical composition of sandstones. *Journal of Geology*, Vol. 91, pp. 611-627.

Bhatia, M. R. and Crook, K. A. W., 1986. Trace element characteristics of graywackes and tectonic setting discrimination of sedimentary basins. *Contributions to Mineralogy and Petrology*, Vol. 92, pp. 191-193.

Bottjer, D. J., Arthur, M. A., Dean, W. E., Hattin, D. E. and Savrda, C.E., 1986. Rhythmic bedding produced in Cretaceous pelagic carbonate environments: sensitive recorders of climatic cycles. *Paleoceanography*, Vol. 1, pp. 467-481.

Böning, P., Brumsack, H.-J., Böttcher, M.E., Schnetger, B., Kriete, C., Kallmeyer, J. and Borchers, S.L., 2004. Geochemistry of Peruvian near-surface sediments. *Geochimica et Cosmochimica Acta*, Vol. 68, (21), pp. 4429-4451.

Bralower, T. J., Arthur, M. A., Leckie, R. M., Sliter, W. V., Allard, D. J. and Schlanger, S. O., 1994. Timing and paleoceanography of oceanic dysoxia/anoxia in the Late Barremian to Early Aptian (Early Cretaceous). *Palaios*, Vol. 9, pp. 335-369.

Broecker, W.S. and Peng, T.-H., 1982. Tracers in the Sea. Eldigio Press, Palisades, New York.

Brumsack, H.J., 1989. Geochemistry of recent TOC-rich sediments from the Gulf of California and the Black Sea. *Geol. Rundsch.* Vol. 78, pp. 851-882.

- Brumsack, H.-J., 2006. The trace metal content of recent organic carbon-rich sediments: implications for Cretaceous black shale formation. *Palaeogeography, Palaeoclimatology, Palaeoecology*, Vol. 232, pp. 344-361.
- Calvert, S.E. and Pedersen, T.F., 1993. Geochemistry of Recent oxic and anoxic marine Sediments: implications for the geological record. *Marine Geology*, Vol. 113, pp. 67-88.
- Chamley, H., 1989. *Clay sedimentology*: New York, Springer-Verlag, pp. 623.
- Chaput, E., 1932. Observations géologiques en Asie Mineure: Le Crétacé supérieur dans l'Anatolie Centrale. *C. R. A. S.*, Vol. 194, pp. 1960-1961.
- Chaput, E., 1935a. L'Eocene du plateau de Galatia (Anatolie Centrale). *C. R. A. S.*, Vol. 200, pp. 767-768.
- Chaput, E., 1935b. Les plissements Tertiare de l'Anatolie Centrale. *C. R. A. S.*, Vol. 201, pp. 1404-1405.
- Chaput, E., 1936. Voyages d'études géologiques et géomorphologiques en Turquie. Mém. Institute of Françaiş D'Archaéo. İstanbul, II, pp. 312.
- Chen, X., Wang, C. S., Li, X. and Hu, X., 2005. Characteristics and correlation of Upper Cretaceous oceanic red beds in Alps-Carpathian area. *Earth Science Frontiers*, Vol. 12, (2), pp. 61-68 (in Chinese with English abstract).
- Chen, X., Wang, C., Hu, X., Huang, Y., Wand, P., Jansa, L. and Zeng, X., 2007. Cretaceous Oceanic Red Beds: Distribution, Lithostratigraphy and Paleoenvirons. *Acta Geologica Sinica*, Vol. 81, (6), pp. 1070-1086.
- Claps, M. and Masetti, D., 1994. Milankovitch periodicities recorded in Cretaceous deep sea sequences from the southern Alps (Northern Italy). In: DE BOER, P.L. and SMITH, D.G. (eds), *Orbital Forcing and Cyclic Sequences*. Special Publication of Internal Association of Sedimentologists, Vol. 19, pp. 99-109.

Claps, M., Erba, E., Masetti, D. and Melchiorri, F., 1995. Milankovitch-type cycles recorded in Toarcian black shales from the Belluno trough (Southern Alps, Italy). Memorie di Scienze Geologiche, Vol. 47: 179-188.

Coccioni, R., Luciani, V. and Marsili, A., 2006. Cretaceous oceanic anoxic events and radially elongated chambered planktonic foraminifera: Paleoecological and paleoceanographic implications. Palaeogeography, Palaeoclimatology, Palaeoecology, Vol. 235, pp. 66-92.

Colley, S., Wilson, T.R.S. and Higgs, N.C., 1984. Post-depositional migration of elements during diagenesis in brown clay and turbidity sequences in the North East Atlantic. *Geochimica et Cosmochimica Acta*, Vol. 48, pp. 1223-1235.

Condie, K.C., 1991. Another look at rare earth elements in shales. *Geochimica et Cosmochimica Acta*, *Geochimica et Cosmochimica Acta*, Vol. 55, pp. 2527-2531.

Condie, K. C., Boryta, M. D., Liu, J. and Quian, X., 1992. The origin of khondalites: geochemical evidence from the Archean to Early Proterozoic granulitic belt in the North China Craton: *Precambrian Research*, Vol. 59, (3-4), pp. 207-223.

Covelli, S. and Fontolan, G., 1997. Application of a normalization procedure in determining regional geochemical baselines. *Environmental Geology*, Vol. 30, pp. 34-45.

Coşkun, B., Özdemir, A. ve İşık, V., 1990. Haymana-Mandıra-Dereköy arasındaki sahanın petrol imkanları. *Türkiye Petrol Jeologları Derneği Bülteni*, Vol. 2, pp. 135-143.

Cox, R., Lowe, D.R. and Cullers, R.L., 1995. The influence of sediment recycling and basement composition on evolution of mud rock chemistry in the southwestern United States: *Geochimica et Cosmochimica Acta*, Vol. 59, (14), pp. 2919-2940.

Crusius, J., Calvert, S., Pedersen, T. and Sage, D., 1996. Rhenium and molybdenum enrichments in sediments as indicators of oxic, suboxic and sulfidic conditions of deposition. *Earth Planetary Science Letters*, Vol. 145, pp. 65-78.

Cullers, R. L., 1994. The controls on the major and trace element variation of shales, siltstones, and sandstones of Pennsylvanian-Permian age from uplifted continental blocks in Colorado to platform sediment in Kansas, USA. *Geochim. Cosmochim. Acta*, Vol. 58, pp. 4955-4972.

Cullers, R. L., 1995. The controls on the major and trace element evolution of shales, siltstones and sandstones of Ordovician to Tertiary age in the Wet Mountain region, Colorado, U.S.A: *Chemical Geology*, Vol. 123, (1-4), pp. 107-131.

Cullers, R. L., 2002. Implications of elemental concentrations for provenance, redox conditions, and metamorphic studies of shales and limestones near Pueblo, CO, USA: *Chemical Geology*, Vol. 191, (4), pp. 305-327.

Çemen, İ., Göncüoğlu, M. C. and Dirik, K., 1999. Structural evolution of the Tuzgölü basin in Central Anatolia, Turkey. *The Journal of Geology*, Vol. 107, pp. 693-706.

Çetin, H., Demirel, İ. H. ve Gökçen, S. L., 1986. Haymana'nın (SW Ankara) doğusu ve batisındaki Üst Kretase-Alt Tersiyer istifinin sedimentolojik ve sedimanter petrolojik incelemesi. *Türkiye Jeoloji Kurultayı Bülteni*, Vol. 29, (2), pp. 21-33.

Çimen, O., Koç, Ş. and Sarı, A., 2013. Rare Earth Element (REE) geochemistry and Genesis of oil shales around Dağhacilar Village, Göynük-Bolu, Turkey. *Oil Shale*, Vol. 30, (3), pp. 419-440.

Çiner, A., 1992. *Sédimentologie et stratigraphie séquentielle du bassin d' Haymana à l'Eocene moyen Turquie*. PhD Thesis, l'University of Louis Pasteur, France, pp. 190.

Çiner, A., Deynoux, M., Koşun, E. ve Gündoğdu, N., 1993a. Yamak turbidit karmaşığının (YTK) sekansiyel stratigrafik analizi: Haymana Baseni (Orta Eosen). *Sekans Stratigrafisi, Sedimentoloji Çalışma Grubu Özel Yayıını*, Vol. 1, pp. 53-70.

Çiner, A., Deynoux, M., Koşun, E. ve Gündoğdu, N., 1993b. Beldede örgülü-delta karmaşığının (BÖDK) sekans stratigrafik analizi: Polatlı-Haymana baseni (Orta Eosen) Orta Anadolu. *Yerbilimleri*, Vol. 16, pp. 67-92.

Çiner, A., Deynoux, M., Ricou, S. and Koşun, E., 1996a. Cyclicity in the middle Eocene Çayraz Carbonate Formation, Haymana Basin, Central Anatolia. *Palaeogeography, Palaeoclimatology, Palaeoecology*, Vol. 121, pp. 313-329.

Çiner, A., Deynoux, M. and Koşun, E., 1996b. Cyclicity in the Middle Eocene Yamak turbidite complex of the Haymana basin, Central Anatolia, Turkey. *Geologische Rundschau*, Vol. 85, pp. 669-682.

Daniel, J. K. R. and Bustin, R. M., 2009. Investigating the use of sedimentary geochemical proxies for paleo-environment interpretation of thermally mature organic-rich strata: Examples from the Devonian-Mississippian shales, Western Canadian Sedimentary Basin. *Chemical Geology*, Vol. 206, pp. 1-19.

Dean, W.E., Gardner, J.V. and Piper, D.Z., 1997. Inorganic geochemical indicators of glacial-interglacial changes in productivity and anoxia of the California continental margin. *Geochimica et Cosmochimica Acta*, Vol. 61, pp. 4507- 4518.

Dean, W.E., Piper, D.Z. and Peterson, L.C., 1999. Molybdenum accumulation in Cariaco basin sediment over the past 24 k.y.: a record of water-column anoxia and climate. *Geology*, Vol. 27, pp. 507-510.

Delaloye, M. and Bingöl, E., 2000. Granitoids from western and northwestern Anatolia: Geochemistry and modeling of geodynamic evolution. *International Geology Review*, Vol. 42, pp. 241-268.

Demirel, H. İ. ve Şahbaz, A., 1994. Haymana, Paşadağ-Aladağ havzalarının petrofasiyes ve provenans karakteristikleri ile petrol potansiyeli. *Türkiye 10. Petrol Kongresi ve Sergisi (Geology)*, pp. 5-19.

Diaz, H. G-, Miller, C. and Lewis, R., 2012. sCore: A Classification Scheme for Organic Mudstones Based on Bulk Mineralogy. American Association of Petroleum Geologists, Southwest section convention, Fort worth, Texas.

Dickinson, W. R., and Seely, D. R., 1979. Structure and stratigraphy of fore-arc regions: American Association of Petroleum Geologists Bulletin, Vol. 63, pp. 2-31.

- Dill, H., 1986. Metallogenesis of Early Paleozoic graptolite shales from the Graefenthal Horst (Northern Bavaria-Federal Republic of Germany). *Economic Geology*, Vol. 81, pp. 889-903.
- Ditchfield, P. and Marshall, J.D., 1989. Isotopic variation in rhythmically bedded chalks: paleotemperature variation in the Upper Cretaceous. *Geology*, Vol. 17, pp. 842-845.
- Druitt, C. E. and Reckamp J. U., 1959. Çaldağ columnar section. *Türkiye Petrolleri Anonim Ortaklığı Arşivi*, Ankara.
- Dunham, R. J., 1962. Classification of carbonate rocks according to depositional texture. In: Ham, W.E.(ed.). *Classification of carbonate rocks*. Bulletin, American Association of Petroleum Geologists. Memoir, Vol. 1, pp. 108-121.
- Egeran, N. ve Lahn, E., 1951. Kuzey ve Orta Anadolu'nun tektonik durumu hakkında not. Mineral Research and Exploration Institute (MTA) of Turkey Bülteni, No. 41, pp. 23-28.
- Egger, H., Homayoun, M., and Schnabel, W., 2002. Tectonic and climatic control of Paleogene sedimentation in the Rhenodanubian Flysch basin (Eastern Alps, Austria): *Sedimentary Geology*, Vol. 152, pp. 247-262.
- Einsele, G., Ricken, W. and Seilacher, A., 1991. *Cycles and Events in Stratigraphy*. Springer-Verlag, Berlin.
- Einsele, G., 2001. *Sedimentary Basins: Evolution, Facies and Sediment Budget*. Springer-Verlag, Berlin.
- Elderfield, H., 1988. The oceanic chemistry of the rare-earth elements. *Philos. Transactions Royal Society of London*, Vol. 325, pp. 105-126.
- Erba, E., 2004. Calcareous nannofossils and Mesozoic oceanic anoxic events. *Marine Micropaleontology*, Vol. 52, pp. 85-106.

Eren, M. and Kadir, S., 1999. Colour origin of upper Cretaceous pelagic red sediments within the Eastern Pontides, northeast Turkey. International Journal of Earth Sciences, Vol. 88, pp. 593-595.

Eren, M. and Taslı, K., 2002. Kliop Cretaceous hardground (Kale, Gümüşhane, NE Turkey): description and origin. Journal of Asian Earth Sciences, Vol. 20, pp. 433-448.

Erk, S., 1942. Etude géologique de la région entre Gemlik et Bursa. Mineral Research and Exploration Institute (MTA) of Turkey publication Bulletin, No. 9.

Erol, O., 1961. Ankara Bölgesinin tektonik gelişmesi. Türkiye Jeoloji Kurultayý Bülteni, Vol. 7, (1), pp. 57-85.

Esmeray, S., 2008. Cretaceous/Paleogene boundary in the Haymana basin, Central Anatolia, Turkey: Micropaleontological, Mineralogical and Sequence Stratigraphic Approach. MS Thesis; Middle East Technical University, Ankara.

Folk, R.L., 1962, Spectral subdivision of limestone types, in Ham, W.E., ed., Classification of carbonate Rocks-A Symposium: American Association of Petroleum Geologists Memoir 1, pp. 62-84,

Folk, R. L., 1965. Petrology of Sedimentary Rocks. 2nd Edition Hemphill, Bookstore, Austin.

Folk, R. L., 1974. Petrology of Sedimentary Rocks. 3rd Edition Hemphill, Austin, Texas.

Fourquin, C., 1975. L'anatolie du Nord-Ouest, marge méridionale du continent européen, histoire paléogéographique, tectonique et magmatique durant le Secondaire et Tertiaire. Bulletin Society of Géology of France, Vol. 7, pp. 1058-1070.

Francois, R., 1988. A study on the regulation of the concentrations of some trace metals (Rb, Sr, Zn, Pb, Cu, V, Cr, Ni, Mn and Mo) in Saanich Inlet sediments, British Columbia, Canada. Marine Geology, Vol. 83, pp. 285-308.

Fu, X. G., Wang, J., Zeng, Y. H., Li, Z. X. and Wang, Z. J., 2009. Geochemical and palynological investigation of the Shengli River marine oil shale (China): implications

for paleoenvironment and paleoclimate. International Journal of Coal Geology, Vol. 78, pp. 217-224.

Fu, X.G., Wang, J., Zeng, Y.H., Tan, F.W. and Feng, X.L., 2010. REE Geochemistry of marine oil shale from the Changshe Mountain area, Northern Tibet, China. International Journal of Coal Geology, Vol. 81, pp. 191-199.

Gale, A. S., 1995. Cyclostratigraphy and correlation of the Cenomanian Stage in Western Europe. House, M. R. and GALE, A. S. (eds), 1995; Orbital Forcing Timescales and Cyclostratigraphy, Geological Society Special Publication, No. 85, pp. 177-197.

Gökçen, S. L., 1976. Haymana güneyinin sedimentolojik incelemesi. I. Stratigrafik birimler ve tektonik. Yerbilimleri, Vol. 2, pp. 161-201.

Gökçen, S., L., 1977. Sedimentology and provenance of resedimented deposits in part of the Haymana basin-Central Anatolia. Yerbilimleri, Vol. 3, pp. 13-23.

Gökçen, S. L. ve Kelling, G., 1983. The Paleogene Yamak sand-rich submarinefan complex, Haymana basin, Turkey. Sedimentary Geology, Vol. 34, pp. 219-243.

Göncüoğlu, M. C., 2010. Introduction to Geology of Turkey: Alpine and pre-Alpine geodynamic evolution of tectonic units. Mineral Research and Exploration of Ankara, Turkey, Monograph Series, No. 5, pp. 1-69.

Görür, N. and Derman, A. S., 1978. Stratigraphic and tectonic analysis of the Tuzgölü-Haymana basin (In turkish). Türkiye Petrolleri Anonim Ortaklığı (TPAO) report, No. 1514 (unpublished).

Görür, N., 1981. Tuzgölü-Haymana havzasının stratigrafik analizi. Türkiye Jeoloji Kurultayı, İç Anadolu'nun Jeolojisi Simpozyumu, Ankara, pp. 60-66.

Görür, N., Oktay, F. Y., Seymen, İ. and Şengör, A. M. C., 1984. Paleotectonic evolution of the Tuzgölü Basin complex, central Turkey: Sedimentary record of the Neo-Tethyan closure. In: Dixon J. and Robertson A. H. F. (eds), The Geological Evolution of the

Eastern Mediterranean. Geological Society of London, Special Publication, Vol. 17, pp. 467-481.

Görür, N., Tüysüz, O., Akyol, A., Sakinç, M., Yititbaç, E. Ö. and Akkök, R., 1993. Cretaceous red pelagic carbonates of northern Turkey: their place in the opening history of Black Sea. *Eclogae Geologicae Helvetiae*, Vol. 36, pp. 819-838.

Görür, N., Tüysüz, O. and Şengör, A. M. C., 1998. Tectonic evolution of the Central Anatolian basins. *International Geology Review*, Vol. 40, pp. 831-850.

Görür, N. and Tüysüz, O., 2001. Cretaceous to Miocene palaeogeographic evolution of Turkey: Implications for hydrocarbon potential. *Journal of Petroleum Geology*, Vol. 24, (2), pp. 119-146.

Gromet, L. P., Dymek, R. F., Haskin, L. A. and Korotev, R. L., 1984. The "North American shale composite": its compilation, major and trace element characteristics. *Geochimica et Cosmochimica Acta*, Vol. 48, pp. 2469-2482.

Grovel, W. K., Silverman, R. M., Rasmussen, R. D., Penfield, T. G., Gurnert, R. W. and Grataler, V., 2000. American Petroleum Association of Geologista, Regional international conference, Istanbul Turkey.

Gülbay, R. K. and Korkmaz, S., 2008. Organic geochemistry, depositional environment and hydrocarbon potential of the tertiary oil shale deposits In NW Anatolia, Turkey. *Oil Shale*, Vol. 25, (4), pp. 444-464.

Gümbel, C.W., 1861. Geognostische Beschreibung des bayerischen Alpengebirges und seines Vorlandes. J. Perthes, Gotha.

Hallberg, R. O., 1976. A geochemical method for investigation of palaeoredox conditions in sediments : *Ambio, Special Report*, Vol. 4, pp. 139-147.

Hatch, J. R. and Leventhal, J. S., 1992. Relationship between inferred redox potential of the depositional environment and geochemistry of the Upper Pennsylvanian (Missourian) stark shale member of the Dennis limestone, Wabaunsee country, Kansas, USA. *Chemical Geology*, Vol. 99, pp. 65-82.

Hattin, D.E., 1986. Interregional model for deposition of Upper Cretaceous pelagic rhythmites, U.S. Western Interior. *Paleoceanography*, Vol. 1, pp. 483-494.

Hayashi, K., Fujisawa, H., Holland, H. and Ohmoto, H., 1997. Geochemistry of ~1.9 Ga sedimentary rocks from northeastern Labrador, Canada: *Geochimica et Cosmochimica Acta*, Vol. 61, (19), pp. 4115-4137.

Helz, G. R., Miller, C. V., Charnock, J. M., Mosselmans, J. F. W., Pattrick, R. A. D., Garner, C. D. and Vaughan, D. J., 1996. Mechanism of molybdenum removal from the sea and its concentration in black shales: EXAFS evidence. *Geochimica et Cosmochimica Acta*, Vol. 60, pp. 3631-3642.

Herbert, T.D. and Fischer, A.G., 1986. Milankovitch climatic origin of Mid-Cretaceous black shale rhythms in central Italy. *Nature*, Vol. 321, pp. 739-743.

Herrle, J.O., Pross, J., Friedrich, O., Kosler, P. and Hemleben, C., 2003. Forcing mechanisms for mid-Cretaceous black shale formation: evidence from the Upper Aptian and Lower Albian of the Vocontian Basin (SE France). *Palaeogeography, Palaeoclimatology, Palaeoecology*, Vol. 190, pp. 399-426.

Herron, M. M., 1988. Geochemical classification of terrigenous sands and shales from core or log data. *Journal of Sedimentary Petrology*, Vol. 58, pp. 820-829.

House, M.R. and Gale, A.S., 1995. Orbital Forcing Time Scales and Cyclostratigraphy. Geological Society, London Special Publications, No. 85.

Hu, X., Jansa, L., Wang, C., Sarti, M., Bak, K., Wagreich, M., Michalik, J. and Sotak, J., 2005. Upper Cretaceous oceanic red beds (CORBs) in the Tethys: occurrences, lithofacies, age, and environments. *Cretaceous Research*, Vol. 26, pp. 3-20.

Hu, X., Jansa, L. and Sarti, M., 2006a. Mid-Cretaceous oceanic red beds in the Umbria-Marche Basin, central Italy: constraints on paleoceanography and paleoclimate. *Palaeogeography, Palaeoclimatology, Palaeoecology*, Vol. 233, (3-4), pp. 163-186.

Hu, X., Wang, C., Scott, R. W., Wagreich, M. and Jansa, L., 2009. Cretaceous Oceanic Red Beds; Stratigraphy, Composition, Origins and Paleoceanographic and Paleoclimatic Significance. SEPM Special Publication No.91.

Hu, X., Zhao, K., Yılmaz, İ. Ö. and Li, Y., 2012. Stratigraphic transition and palaeoenvironmental changes from the Aptian oceanic anoxic event 1a (OAE1a) to the oceanic red bed 1(ORB1) in the Yenicesihlar section, Central Turkey. Cretaceous Research, Vol. 38, pp. 40-51.

Hüseyinov, A., 2007. Sedimentary cyclicity in the Upper Cretaceous successions of the Haymana Basin, Turkey: Depositional sequences as response to relative sea-level changes. MS Thesis; Middle East Technical University, Turkey.

Janse, L. and Hu, X., 2009. Cretaceous pelagic black shales and red beds in western Tethys: origin, paleoclimate, and paleoceanographic implications. SEPM Special Publication, No. 91, pp. 59-72.

Jenkyns, H. C., 1980. Cretaceous anoxic events: from continents to oceans. Journal of the Geological Society of London, Vol. 137, pp. 171-188.

Jenkyns, H. C. and Clayton, C., 1986. Black shale and carbon isotope in pelagic sediments from the Tethyan lower Jurassic. Sedimentology, Vol. 33, pp. 87-106.

Jenkyns, H. C. and Wilson, P. A., 1999. Stratigraphy, paleoceanography, and evolution of Cretaceous pacific guyots: relics from a greenhouse earth. American Journal of Science, Vol. 299, pp. 341-392.

Jones, B. and Manning, D.A.C., 1994. Comparison of geochemical indices used for the interpretation of palaeoredox conditions in ancient mudstones. Chemical Geology, Vol. 111, pp. 111-129.

Kaymakçı, N., 2000. Tectono-stratigraphical evolution of the Çankırı Basin (Central Anatolia, Turkey). Geologica Ultraictina, No. 190, pp. 247.

Ketin, İ., 1966. Tectonic units of Anatolia (Asia Minor). Mineral Research and Exploration Institute of Turkey Bulletin, No. 66, pp. 23-34.

- Ketris, M.P. and Yudovich, Y.E., 2009. Estimations of clarkes for carbonaceous biolithes: world average for trace element contents in black shales and coals. International Journal of Coal Geology, Vol. 78, pp. 135-148.
- Kostka, A., 1993. The age and microfacies of the Maruszyna Succession (Upper Cretaceous-Paleogene), Pieniny Klippen Belt, Carpathians, Poland, *Studia Geologica Polonica*, Vol. 102, pp. 7-134.
- Koçyiğit, A., 1987. Tectonostratigraphy of the Hasanoğlan region: Evolution of the Karakaya Orogen. Hacettepe University, Earth Science, Vol. 14, pp. 269-293.
- Koçyiğit, A., 1989. Suşehri basin: an active fault wedge basin on the North Anatolian Fault Zone. *Tectonophysics*, Vol. 167, pp. 13-29.
- Koçyiğit, A., Özkan, S. and Rojay, B., 1988. Examples of the fore-arc basin remnants at the active margin of northern Neo-Tethys: development and emplacement ages of the Anatolian Nappe, Turkey. Middle East Technical University Journal of Pure and Applied Sciences, Vol. 3, pp. 183-210.
- Koçyiğit, A., 1991. An example of an accretionary fore-arc basin from Central Anatolia and its implications for the history of subduction of Neo-Tethys in Turkey. Geological Society of American Bulletin, Vol.103, (1), pp. 22-36.
- Koçyiğit, A., Altiner, D., Farinacci, A., Nicosia, U. and Conti, M.A., 1991. Late Triassic-Aptian evolution of the Sakarya divergent margin: implications for the opening history of the Northern Neo-Tethys, in the North-Western Anatolia, Turkey. *Geologica Romana*, Vol. 27, pp. 81-101.
- Koçyiğit, A. and Altiner, D., 2002. Tectonostratigraphic evolution of the North Anatolian Palaeorift (NAPR): Hettangian-Aptian passive continental margin of the Northern Neo-Tethys, Turkey. *Turkish Journal of Earth Sciences*, Vol. 11, pp. 169-191.
- Lahn, E., 1949. Orta Anadolu'nun jeolojisi hakkında, *Türkiye Jeoloji Kurultayý Bülteni*, Vol. 1, pp. 1.

Lefebvre, C., Meijers, M. J. M., Kaymakci, N., Peynircioğlu, A., Langereis, C. G. and van Hinsbergen, D., J. J., 2013. Reconstructing the geometry of central Anatolia during the late Cretaceous: Large-scale Cenozoic rotations and deformation between the Pontides and Taurides. *Earth and Planetary Science Letters*, Vol. 366, pp. 83-98.

Li, L., Keller, G., Adatte, T. and Stinnesbeck, W., 2000. Late Cretaceous sea level changes in Tunisia: A multi-disciplinary approach. *Journal of the Geological Society, London*, Vol. 157, pp. 447-458.

Lu, K., 2007. Sequence stratigraphy and orbital cyclostratigraphy of the Mooreville Chalk (Santonian-Campanian), northeastern Gulf of Mexico area, USA. *Cretaceous Research*, Vol. 28, pp. 405-418.

Locklair, R. E. and Sageman, B. B., 2008. Cyclostratigraphy of the Upper Cretaceous Niobrara Formation, Western Interior, U.S.A.: A Coniacian-Santonian orbital timescale. *Earth and Planetary Science Letters*, Vol. 269, pp. 540-553.

Lokman, K. ve Lahn, D., 1946. Haymana bölgesi jeolojisi. Mineral Research and Exploration Institute (MTA) of Turkey Bülteni, No. 36, pp. 292-300.

Loring D.H., 1990. Lithium -a new approach for the granulometric normalization of trace metal data. *Marine Chemistry*, Vol. 29, pp. 155-168.

Machhour, L., Philip, J. and Oudin, J.L., 1994) Formation of laminate deposits in anaerobic-dysaerobic marine environments. MCG, Vol. 99, pp. 65-82.

Madhavaraju, J. and Ramasamy, S., 2002. Petrography and geochemistry of Late Maastrichtian-Early Paleocene sediments of Tiruchirapalli Cretaceous, Tamil Nadu-Paleo-weathering and provenance implications: *Journal of the Geological Society of India*, Vol. 59, pp. 133-142.

Mcmanus, J., Berelson, W.M., Klinkhammer, G.P., Johnson, K.S., Coale, K.H., Anderson, R.F., Kumar, N., Burdige, D.J., Hammond, D.E., Brumsack, H.-J., McCorkle, D.C. and Rushdi, A., 1998. Geochemistry of barium in marine sediments: implications for its use as a paleoproxy. *Geochim. Cosmochim. Acta*, Vol. 62, pp. 3453-3473.

Menegatti, A. P., Weissert, H., Brown, R. S., Tyson, R. V., Farrimond, P., Strasser, A. and Caron, M., 1998. High-resolution $d^{13}C$ stratigraphy through the Early Aptian “Livello Selli” of the Alpine Tethys. *Paleoceanography*, Vol. 13, pp. 530-545.

Michard, A., Albarede, F., Michard, G., Minister, J. F. and Charlou, J. L., 1983. Rare earth elements and uranium in high temperature solutions from East-Pacific Rise hydrothermal vent field (13°N). *Nature*, Vol. 303, pp. 795-797.

Moix, P., Beccaletto, L., Kozur, H. W., Hochard, C., Rosselet, F. and Stampfli, G. M., 2008. A new classification of the Turkish terranes and sutures and its implication for the paleotectonic history of the region. *Tectonophysics*, Vol. 451, pp. 7-39.

Morford, J.L., Russell, A.D. and Emerson, S., 2001. Trace metal evidence for changes in the redox environment associated with the transition from terrigenous clay to diatomaceous sediment, Saanlich Inlet, BC. *Marine Geology*. Vol. 174, pp. 355-369.

Mount, J. F. and Ward, P., 1986. Origin of limestone/marl alterations in the upper Maastrichtian of Zumaya, Spain. *Journal of Sedimentary Petrology*, Vol. 56, pp. 228-236.

Murray, R. W., Buchholtz ten Brink, M. R., Jones, D. L., Gerlach, D. C. and Price Russ, G., 1990. Rare earth elements as indicators of different marine depositional environments in chert and shale. *Geology*, Vol. 18, (3), pp. 268-271.

Murray, R. W., Buchholtz, M. R. and Brumsack, H. J., 1991a. Rare earth elements in Japan Sea sediments and diagenetic behavior of Ce/Ce*, results from ODP leg 127. *Geochimica et Cosmochimica Acta*, Vol. 55, pp. 2453-2466.

Murray, R. W., Buchholtz Brink, M. R., Brink, M. R., Gerlach, D. C., Russ III, G. P. and Jones, D. L., 1991b. Rare earth, major and trace elements in chert from the Franciscan complex and Monterey group, California: assessing REE sources to fine grained marine sediments. *Geochimica et Cosmochimica Acta*, Vol. 55, pp. 1875-1895.

Mutterlose, J. and Ruffell, A., 1999. Milankovitch-scale palaeoclimate changes in pale-dark bedding rhythms from the Early Cretaceous (Hauterivian and Barremian) of eastern

England and northern Germany. Palaeogeography, Palaeoclimatology, Palaeoecology, Vol. 154, pp. 133-160.

Nath, B. N., Bau, M., Ramalingeswara Rao, B. and Rao, Ch .M., 1997. Trace and rare earth elemental variation in Arabian Sea sediments through a transect across the oxygen minimum zone: *Geochimica et Cosmochimica Acta*, Vol. 61, (12), pp. 2375-2388.

Norman, T., 1973. Ankara Yahşihan bölgesinde Üst Kretase-Alt Tersiyer sedimentasyonu. *Türkiye Jeoloji Kurultayý Bülteni*, Vol. 16, pp. 67-81.

Norman, T., 1975. Flow features of Ankara mélange. 9th International Congress on Sedimentology, Nice (France), Vol. 4, pp. 261-269.

Norman, T., Gökçen S. L. and Şenalp M., 1980. Sedimentation pattern in Central Anatolia at the Cretaceous-Tertiary boundary. *Cretaceous Research*, Vol. 1, pp. 61-84.

Niebuhr, B., 2005. Geochemistry and time-series analyses of orbitally forced Upper Cretaceous marl-limestone rhythmites, Lehrte West Syncline, northern Germany. *Geological Magazine*, Vol. 142, (1), pp. 31-55.

Ocakoğlu, F., Yılmaz, Ö. İ., Demircan, H., Özkan-Altiner, S., Hakyemez, A., İslamoğlu, Y., Tekin, U. K., Önoğlu, N., Yıldız, A., Uchman, A., Szulc, A., 2007. Orta Sakarya bölgesi Geç Kretase-Paleojen çökellerinin sekans stratigrafisi. TUBITAK Proje No.: YDABÇAG 104Y153, 447s.

Ogala, J. E., Akaegbobi, I. M., Omo-Irabor, O. O., and Finkelman, R. B., 2009. Statistical analysis of geochemical distribution of major and trace elements of the Maastrichtian coal measures in the Anambra Basin, Nigeria. *Petroleum and Coal*, Vol. 54, (4), pp. 261-270.

Ogala, J. E., 2012. The geochemistry of lignite from the Neogene Ogwashi-Asaba Formation, Niger Delta Basin, Southern Nigeria. *Earth Sciences Research Journal*, Vol. 16, (2), pp. 151-164.

Okay, A. İ., 1986. Tectonic units and sutures in the Pontides. *Tectonic evolution of the Tethyan region*, Kluwer Academic Publishers; 109-116.

Okay, A. İ., Siyako, M. and Burkan, K. A., 1991. Geology and tectonic evolution of the Biga Peninsula, northwestern Turkey. *Bulletin of Istanbul Technical University, Turkey*, Vol. 44, pp. 91-256.

Okay, A. İ. and Monié, P., 1997. Early Mesozoic subduction in the Eastern Mediterranean: Evidence from Triassic eclogite in northwest Turkey. *Geology*, Vol. 25, pp. 595-598.

Okay, A. İ. and Tüysüz, O., 1999. Tethyan sutures of northern Turkey. In: Durand, B., Jolivet, L., Horváth, D., and Séranne, M. (eds) *The Mediterranean basins: Tertiary extension within the Alpine Orogen*: Geological Society of London, Special Publication, Vol. 156, pp. 475-515.

Okay, A. İ., 2001. Stratigraphic and metamorphic inversions in the central Menderes massif: a new structural model. *International Journal of Earth Sciences*, Vol. 89, (4), pp. 709-727.

Okay, A. İ., Tüysüz, O. and Tansel, I., 2001. Obduction, subduction and collision as reflected in the Upper Cretaceous-Lower Eocene sedimentary record of western Turkey. *Geological Magazine UK*, Vol. 138, (2), pp. 117-142.

Okay, A. İ., Monod, O. and Monié, P., 2002. Triassic blueschists and eclogites from northwest Turkey: vestiges of the Paleo-Tethyan subduction. *Lithos*, Vol. 64, pp. 155-178.

Okay, A. İ., Satir, M. and Siebel, W., 2006. Pre-Alpide Palaeozoic and Mesozoic orogenic events in the Eastern Mediterranean region In: Gee, D. G. and Stephenson, R. A. (eds). *European Lithosphere Dynamics*. Geological Society of London, Memoirs, Vol. 32, pp. 389-405.

Okay, A. İ., 2008. Geology of Turkey: A synopsis. *Anschnitt*, Vol. 21, pp. 19-42.

Özcan, E., 2002. Cuisian orthophragminid assemblages (*Discocyclina*, *Orbitoclypeus* and *Nemkovella*) from the Haymana-Polatlı Basin (Central Turkey): biometry and description of two new taxa. *Eclogae Geologicae Helvetiae*, Vol. 95, pp. 75-97.

Özcan, E. and Özkan-Altiner, S., 1997. Late Campanian-Maastrichtian evolution of orbitoid foraminifera in Haymana basin succession (Ankara, Central Turkey). *Revue de Paléobiologie*, Vol. 16, (1), pp. 271-290.

Özcan, E. and Özkan-Altiner, S., 1999. The genus *Lepidorbitoides* and *Orbitoides*: Evolution and stratigraphic significance in some Anatolian basins (Turkey). *Geological Journal*, Vol. 34, (3), 275-286.

Özcan, E. and Özkan-Altiner, S., 2001. Description of an early ontogenetic evolutionary step in *Lepidorbitoides*: *Lepidorbitoides bisambergensis asymmetrica* subsp. n., Early Maastrichtian (Central Turkey). *Rivista Italiana di Paleontologia e Stratigrafia*, Vol. 107, pp. 137-144.

Özcan, E., Sirel, E., Özkan-Altiner, S. and Çolakoğlu, S., 2001. Late Paleocene Orthophragmina (foraminifera) from the Haymana-Polatlı Basin, Central Turkey) and description of a new taxon, *Orbitoclypeus haymanaensis*. *Micropaleontology*, Vol. 47, (4), pp. 339-357.

Özkan-Altiner, S., 1996. Calcareous nannofossil biostratigraphy of Valanginian-Aptian in Northwest Anatolia, Turkey. *Revue de Paléobiologie*, Vol. 15, (2), pp. 479-498.

Özkan-Altiner, S., 1999. Rock-forming Nannofossils in Uppermost Jurassic-Lower Cretaceous Rock Units of Northwest Anatolia: *Nannoconus* and Its Revised Taxonomy. *Turkish Journal of Earth Sciences*, Vol. 8, pp. 19-43.

Özkan, S., 1993a. Calcareous nannofossil and calpionellid biostratigraphy of the Upper Jurassic-Lower Cretaceous in Northwest Anatolia, Turkey. Ph.D. Thesis, University College London, pp. 336.

Özkan, S., 1993b. Calcareous nannofossils from the Late Jurassic-Early Cretaceous of Northwest Anatolia, Turkey. *Geological Journal*, Vol. 28, pp. 295-307.

Paillet, D., Bard, E., Rostek, F., Zheng, Y., Mortlock, R. and van Geen, A., 2002. Burial of redox-sensitive metals and organic matter in the equatorial Indian Ocean linked to precession. *Geochimica et Cosmochimica Acta*, Vol. 66, pp. 849-865.

- Pettijohn, F. J., 1954. Classification of sandstones: *Journal of Geology*, Vol. 62, pp. 360-365.
- Pettijohn, F. J., Potter, P. E. and Siever, R., 1972. *Sand and Sandstones*. Springer-Verlag, New York.
- Pettijohn, F. J., 1975. *Sedimentary Rocks*, 3rd Edition, Harper and Row, New York.
- Picard, M., 1971. Classification of fine-grained sedimentary rock: *Journal of Sedimentary Petrology*, Vol. 41, pp. 179-195.
- Potter, P. E., 1978. Petrology and chemistry of modern big river sands. *Journal of Geology*, Vol. 86, (4), pp. 423-449.
- Potter, P.E., J.B. Maynard, and P.J. Depetris, 2005. Mud and mudstones introduction and overview: New York, Springer Berlin Heidelberg, pp. 297.
- Price, G.D., 2003. New constraints upon isotope variation during the Early Cretaceous (Barremian-Cenomanian) from the Pacific Ocean. *Geological Magazine*, Vol. 140, pp. 513-522.
- Rachold, V. and Brumsack, H. J., 2001. Inorganic geochemistry of Albian sediments from the Lower Saxony basin, NW German: paleoenvironmental constraints and orbital cycles, *Palaeogeography, Palaeoclimatology, Palaeoecology*, Vol. 174, pp. 123-144.
- Reckamp, J. U. and Özbeý, S., 1960. Petroleum geology of Temelli and Kugtepe structures, Polatlı area: Pet. iş. Gen. Md., Ankara (Unpublished).
- Rigo da Righi, M. and Cortesini, A., 1959. Regional studies central Anatolian basin, progress report 1. Turkish Gulf Oil Company: Pet. iş. Gen. Md., Ankara (Unpublished).
- Rimmer, S. M., 2004. Geochemical paleoredox indicators in Devonian-Mississippian black shales, central Appalachian basin (USA). *Chemical Geology*, Vol. 206, pp. 373-391.

Rojay, B. 2013: Tectonic evolution of the Cretaceous Ankara OphioliticMélange during the Late Cretaceous to pre-Miocene intervalin Central Anatolia, Turkey. *J. Geodynamics*, Vol. 65, pp. 66-81.

Rojay, B. and Altiner, D., 1998. Middle Jurassic-Lower Cretaceous biostratigraphy in central Pontides (Turkey): remarks on the paleogeography and tectonic evolution. *Rivista Italiana di Paleontologia e Stratigrafia*, Vol. 104, (2), pp. 167-180.

Rojay, B. and Süzen, L., 1997. Tectonostratigraphic evolution of the Cretaceous dynamic basins on accretionary ophiolitic mélange prism, SW of Ankara region. *Turkish Association of Petroleum Geologists Bülteni*, Vol. 9, (1), pp. 1-12.

Rojay, B., Yalınız, K. and Altiner, D., 2001. Age and origin of some pillow basalts from Ankara mélange and their tectonic implications to the evolution of northern branch of Neo-Tethys, Central Anatolia. *Turkish Journal of Earth Sciences*, Vol. 10, pp. 93-102.

Rojay, B., Altiner, D., Özkan-Altiner, S., Önen, P., James, S. and Thirwall, M., 2004. Geodynamic significance of the Cretaceous pillow basalts from North Anatolian Mélange Belt (Central Anatolia, Turkey): geochemical and paleontological constraints. *Geodinamica Acta*, Vol. 17, (5), pp. 349-361.

Rollinson, H., 1993, Using Geochemical Data: Evaluation, Presentation, Interpretation: New York, Longman Scientific and Technical.

Roser, B. P. and Korsch, R. J., 1986. Determination of tectonic setting of sandstone-mudstone suites using SiO₂content and K₂O/Na₂O ratio. *Journal of Geology*, Vol. 94, pp. 635-650.

Saner, S., 1980a. Batı Ponditler'in kom^ou havzaların oluşumlarının levha tektoniği kuramıyla açıklaması, Mineral Research and Exploration Institute (MTA) of Turkey Publications, No. 93/94, pp. 1-20.

Saner, S., 1980b. The paleogeographical interpretation of the Mudurnu-Göynük basin based on the depositional features of the Jurassic and later ages: Türkiye Jeoloji Kurultayı Bülteni, Vol. 23, pp. 39-52.

Sari, A. and Geze, Y., 2008. Organic geochemical valuations of bituminous rock and coals in Miocene Himmetoglu Basin (Bolu, Turkey). Petroleum Science and Technology, Vol. 26, (6), pp. 649-664.

Schenau, S.J., Reichart, G.-J. and de Lange, G.J., 2005. Phosphorus burial as a function of paleoproductivity and redox conditions in Arabian Sea sediments. *Geochimica et Cosmochimica Acta*, Vol. 69, (4), pp. 919-931.

Schieber, J., 1994. Evidence for episodic high energy events and shallow water deposition in the Chattanooga Shale, Devonian, central Tennessee, U.S.A. *Sedimentary Geology*, Vol. 93, pp. 193-208.

Schiff K.C. and Weisberg S.B., 1999, Iron as a reference element for determining trace metal enrichment in Southern California costal shelf sediments. *Marine Environmental Research*, Vol. 48, pp. 161-176.

Schlager, W., 1991. Depositional bias and environmental changedimportant factors in sequence stratigraphy. *Sedimentary Geology*, Vol. 70, pp. 109-130.

Schlager, W., 1999. Type-3 sequence boundaries. In: Harris, P. M., Saller, A. H. and Simo, J. A. T. (eds). *Advances in carbonate sequence stratigraphy: application to reservoirs, outcrops and models*. Society for Sedimentary Geology (SEPM), Special Publication, No.63, pp. 35-45.

Schlanger, S. O. and Cita, M. B., 1982. *Nature and Origin of Cretaceous Carbon-rich Facies*. Academic Press, London.

Schlanger, S. O. and Jenkyns, H. C., 1976. Cretaceous oceanic anoxic events – causes and consequences. *Geologie en Mijnbouw*, Vol. 55, pp. 179-184.

Schmidt, G., C., 1960. AR/MEM/365-266-367 sahalarının nihai terk raporu. Pet. İş. Gen. Md., Ankara.

Schoonen, M. A. A. and Barnes, H. L., 1991. Reactions forming pyrite and marcasite from solution, II. Via FeS precursors below 100°C: *Geochimica et Cosmochimica Acta*, Vol. 55, pp. 1505-1514.

Schwarzacher, W., 1993. Milankovitch cycles in the pre-Pleistocene stratigraphic record: a review. In: Hailwood, E.A., Kidd, R.B. (Eds.), High Resolution Stratigraphy. Geological Society, London, Special Publication, Vol. 70, pp. 187-194.

Scott, R. W., 2009. Chronostratigraphic database for Upper Cretaceous oceanic red beds (CORBs). SEPM Special Publication No. 91, pp. 35-57.

Sirel, E., 1975. Polatlı (GB Ankara) güneyinin stratigrafisi. Türkiye Jeoloji Kurultayı Bülteni, Vol. 18, (2), pp. 181-192.

Skelton, P. W., Spicer, R., Kelley, S. P. and Gilmour, I., 2003. The Cretaceous World. The Open University, Cambridge University Press, Cambridge.

Skupien, P., Bubík, M., Švábenická, L., Mikuláš, R., Vašíček, Z. and Matýsek, D., 2009. Cretaceous Oceanic Red Beds in the Outer Western Carpathians of Czech Republic. SEPM Special Publication No. 91, pp. 99-109.

Stage, M., 1999. Signal analysis of cyclicity in Maastrichtian pelagic chalks from the Danish North Sea. Earth and Planetary Science Letters, Vol. 173, pp. 75-90.

Stoll, H. M. and Schrag, D. P., 2000. High-resolution stable isotope records from the Upper Cretaceous rocks of Italy and Spain: Glacial episodes in a greenhouse planet? Geological Society of America Bulletin, Vol. 112, pp. 308-319.

Stow, D. A. V., 2005. Sedimentary rocks in the field: A colour guide: Manson Publishing.

Şenalp, M. and Gökçen, L. S., 1978. Sedimentological Studies of the Oil-Saturated Sandstones of the Haymana Region. Geological Society of Turkey, Vol. 21, pp. 87-94 (in Turkish).

Şener, M. and Şengüler, I., 1998. Geological, mineralogical and geochemical characteristics of oil shale bearing deposit in the Hatıdağ oil shale field, Göynük, Turkey. Fuel, Vol. 77, (8), pp. 871-880.

Şengör, A. M. C. and Yılmaz, Y., 1981. Tethyan evolution of Turkey: a plate tectonic approach. *Tectonophysics*, Vol. 75, pp. 181-241.

Şengör, A. M. C., Yılmaz, Y. and Sungurlu, O., 1984. Tectonics of the Mediterranean Cimmerides: nature and evolution of the western termination of Paleo-Tethys. In: Dixon, J. E., and Robertson, A. H. F., (eds). *The geological evolution of the Eastern Mediterranean*. Geological Society of London, Special Publication, Vol.17, pp. 77-112.

Šturm, D., 1860. Bericht über die geologische übersichts -Aufnahmed. Wassergebietes der Waag und Meutra. *Geologische Reichsanstalt, Jahrbuch*, Vol. 11, pp. 17-149.

Taylor, S.R. and McLennan, S.M. 1985. The continental crust: its composition and evolution. Blackwell Scientific Publication, Oxford, pp. 57-72.

Taylor, S.R., and McLennan, S.M., 1995. The geochemical evolution of the continental crust: *Reviews of Geophysics*, Vol. 33, pp. 241-265.

Tekeli, O., 1981. Subduction complex of pre-Jurassic age, northern Anatolia, Turkey. *Geology*, Vol. 9, pp. 68-72.

Thomson, J., Colley, S., Higgs, N.C., Hydes, D.J., Wilson, T.R.S., Sorensen, J., 1987. Geochemical oxidation trends in NE Atlantic distal turbidites and their effects in the sedimentary record. In: Weaver, P.P.E., Thomson, J. (Eds.), *Geology and Geochemistry of Abyssal Plains*. Geological Society, London, Special Publication, Vol. 31, pp. 167-177.

Timur, E. ve Aksay, A., 2002. 1/100 000 Ölçekli Türkiye Jeoloji Haritaları No: 39, Adapazarı-H26 Paftası [1/100 000 Scale Geological Maps of Turkey No: 39, Adapazarı-H26 Sheet. Mineral Research and Exploration Institute (MTA) of Turkey Publications.

Toker, V., 1975. Haymana yöreninin (SW Ankara) planktonik foraminifera ve nannoplanktonlarla biyostratigrafik incelenmesi. PhD. Thesis, Ankara Üniversitesi Fen Fakültesi, pp. 1-57.

Toker, V., 1977. Haymana ve Kavak formasyonlarındaki planktonic foraminifera ve nannoplanktonlar. *TBTAK VI. Bilim Kongresi*, pp. 57-70.

Toker, V., 1980. Haymana yöresi (GB Ankara) nannoplankton biyostratigrafisi. Türkiye Jeoloji Kurultayý Bülteni, Vol. 23, (2), pp. 165-178.

Topuz, G., Altherr, R., Schwartz, W. H., Dokuz, A. and Meyer, H. P., 2007. Variscan amphibolites-facies rocks from the Kurtoðlu metamorphic complex (Gümüşhane area, Eastern Pontides, Turkey). International Journal of Earth Sciences, Vol. 96, pp. 861-873.

Tribovillard N., Algeo T. J., Lyons T. and Riboulleau, A., 2006. Trace metals as paleoredox and paleoproductivity proxies: Chemical Geology Vol. 232, pp. 12-32

Turgay, M. I. and Kurtulus, C., 2000. Seismic reflection studies in Polatlı region, Turkey. Mineral Research and Exploration Institute of Turkey Publications, No. 103/104, pp. 41-49.

Turkunal, S., 1960. Field study:Nallıhan, Mudurnu ve Seben Arasında Kalan Bölgenin jeolojisi. In 1963 reported his findings in the Bulletin of the Geological Society of Turkey (Manuscript received February 1961), pp. 55-84

Tüysüz, O., 1999. Geology of the Cretaceous sedimentary basins of the Western Pontides. Geological Journal, Vol. 34, pp. 75-93.

Tüysüz, O., 2002. Upper Cretaceous red pelagic limestones in the Pontides, northern Turkey and their significance on the geological evolution of Black Sea. Inaugural Workshop of IGCP 463, Ancona, Italy, Program and Abstracts, pp. 30.

Tüysüz, O., 2003. Oceanic red beds within the Neo-Tethyan suture zone, Northern Turkey. Workshop of Upper Cretaceous Red Beds IGCP 463, Bartın Turkey, August 23-28, Abstract Book, pp. 24.

Tüysüz, O. and Tekin, U.K., 2007. Timing of imbrication of an active continental margin facing the northern branch of Neotethys, Kargı Massif, northern Turkey. Cretaceous Research, Vol. 28, pp. 754-764.

Tüysüz, O. and Yiðitbaþ, E., 1994. The Karakaya Basin: a Palaeo-Tethyan marginal basin and its age of opening. Acta Geologica Hungarica, Vol. 37, (3-4), pp. 327-350.

Ünalan, G., Yüksel, V., Tekeli, T., Göneç, O., Seyirt, Z. and Hüseyin, S., 1976. Stratigraphy and paleogeographical evolution of Upper Cretaceous- lower Tertiary sediments in the Haymana-Polatlı region (SW Ankara): Geological Society of Turkey Bulletin, Vol. 19, pp. 159-176.

Ünalan, G. ve Yüksel, V., 1985. Haymana-Polatlı havzasının jeolojisi ve petrol olanakları. Mineral Research and Exploration Institute (MTA) of Turkey, Petrol ve Jeotermal Enerji Dairesi Raporu.

Wagreich, M. and Krenmayr, H.G., 2005. Upper Cretaceous oceanic red beds (CORB) in the Northern Calcareous Alps (Nierental Formation, Austria): slope topography and clastic input as primary controlling factors. *Cretaceous Research*, Vol. 26, pp. 57-64.

Wagreich, M., Neuhuber, S., Egger, J., Wendler, I., Scott, R.W., Malata, E. and Sanders, D., 2009. Cretaceous oceanic red beds (CORBs) in the Austrian Eastern Alps: passive-margin vs. active-margin depositional settings. In: Hu, X.M., Wang, C.S., Scott, R.W., Wagreich, M., Jansa, L. (Eds.), SEPM Special Publication, Tulsa, Oklahoma, No. 91, pp. 37-91.

Wang, J., Tan, F. W., Li, Y. L., Li, Y. T., Chen, M., Wang, C. S., Guo, Z. J., Wang, X.L., Du, B.W. and Zhu, Z.F., 2004. The Potential of the Oil and Gas Resources in Major Sedimentary Basins on the Qinghai-Xizang Plateau. Geological Publishing House, Beijing, pp. 34-88 (in Chinese with English abstract).

Wang, C., Hu, X., Sarti, M., Scott, R.W. and Li, X. 2005. Upper Cretaceous oceanic red beds in southern Tibet: a major change from anoxic to oxic, deep-sea environments. *Cretaceous Research*, Vol. 26, pp. 21-32.

Wang, C., Hu, X., Huang, Y., Scott, R. and Wagreich, M., 2009. Cretaceous oceanic red beds (CORB): a window on global oceanic/climatic change. In: Hu, X., Wang, C., Scott, R.W., Wagreich, M., Jansa, L. (Eds.), *Cretaceous Oceanic Red Beds: Stratigraphy, Composition, Origins and Paleoceanographic/Paleoclimatic Significance*, SEPM Special Publication, Tulsa, Oklahoma No. 91:13-33.

Weaver, C. E., 1989. Clays, muds and shales. Development in sedimentology. Vol. 44, Elsevier.

Weissert, H. and Breheret, J. G., 1991. A carbonate carbon-isotope record from Aptian-Albian sediments of the Vacontian trough (SE France). Bulletin de la Societe Geologique de France, Vol. 162, pp. 1133-1140.

Wei, Y. and Wang, C., 2005. Correlation of Cretaceous oceanic red beds in Turkey, Caucasus and Himalaya. Earth Science Frontiers, Vol. 12. (2), pp. 51-59 (in Chinese with English abstract).

Wendler, J., Gräfe, K.-U. and Willems, H., 2002. Reconstruction of mid-Cenomanian orbitally forced paleoenvironmental changes based on calcareous dinoflagellate cysts. Palaeogeography, Palaeoclimatology, Palaeoecology, Vol. 179, pp. 19-41.

Wignall, P. B., 1994. Black Shales. Clarendon Press, Oxford;127.

Wilde, P., 1987. Model of progressive ventilation of the late Precambrian-early Paleozoic Ocean. American Journal of Science, Vol. 287, pp. 442-459.

Wilson, J. L., 1975. Carbonate Facies in geologic history. Springer-Verlag Berlin.

Wilson, T.R.S., Thomson, J., Colley, S., Hydes, D. J., Higgs, N.C. and Sorensen, J., 1985. Early organic diagenesis; the significance of progressive subsurface oxidation fronts in pelagic sediments. Geochimica et Cosmochimica Acta, Vol. 49, pp. 811-822.

Wrafter, J. P. and Graham, J. R., 1989. Ophiolitic detritus in the Ordovician sediments of South Mayo Ireland: Journal of the Geological Society, London, Vol. 146, pp. 213-215.

Wright, J., Schrader, H. and Holser, W., 1987. Paleoredox variations in ancient oceans recorded by rare earth elements in fossil apatite. Geochim Cosmochim Acta, Vol. 51, pp. 631-644

Wronkiewicz, D. J. and Condie, K. C., 1990. Geochemistry and mineralogy of sediments from the Ventersdorp and Transvaal Supergroups, South Africa: Cratonic

evolution during the early Proterozoic: *Geochimica et Cosmochimica Acta*, Vol. 54, (2), pp. 343-354.

Yalınız, M. K., Göncüoğlu, M. C., Özkan-Altiner, S. and Parlak, O., 2000. Formation and emplacement ages of the SSZ-type Neotethyan Ophiolites in Central Anatolia, Turkey: Paleotectonic implications. *Geological Journal*, Vol. 35, (2), pp. 53-68.

Yarincik, K.M., Murray, R.W., Lyons, T.W., Peterson, L.C. and Haug, G.H., 2000. Oxygenation history of bottom waters in the Cariaco Basin, Venezuela, over the past 578 k.y: results from redox-sensitive metals (Mo, V, Mn, and Fe). *Paleoceanography*, Vol. 15, pp. 593-604.

Yılmaz, İ. Ö., and Altiner, D., 2001. Use of sedimentary structures in the recognition of sequence boundaries in the Upper Jurassic (Kimmeridgian) – Upper Cretaceous (Cenomanian) peritidal carbonates of the Fele (Yassibel) area (Western Taurides, Turkey). *International Geology Review*, Vol. 43, (8), pp. 736-754.

Yılmaz, İ.Ö., 2002. Applications of cyclostratigraphy and sequence stratigraphy in determination of the hierarchy in peritidal and pelagic successions (NW, SW and WNW of Turkey) by using sedimentology and sedimentary geochemistry (Stable isotopes). Ph. D Thesis, Middle East Technical University, Ankara, Turkey.

Yılmaz, İ. Ö., 2008. Cretaceous Pelagic Red Beds and Black Shales (Aptian-Santonian), NW Turkey: Global Oceanic Anoxic and Oxic Events. *Turkish Journal of Earth Sciences*, Vol. 17, pp. 263-296.

Yılmaz, İ. Ö., Altiner, D. and Özkan- Altiner, S., 2000. Record of Milankovitch cyclicity within the Barremian-Aptian pelagic successions of NW Turkey: Preleminary results. 6 th International Cretaceous Symposium, August 27–September 4, Vienna, Austria. Abstract Book, pp. 153.

Yılmaz, İ. Ö., Vennemann, T., Altiner, D. and Satır, M. 2004a. Stable isotope evidence for meter-scale sea level changes in lower Cretaceous inner platform and pelagic carbonate successions of Turkey. *Geologica Carpathica*. Vol. 55, pp. 19-36.

Yılmaz, İ. Ö., Vennemann, T., Altiner, D., Özkan- Altiner, S. and Satır, M. 2004b. Cyclic records of pelagic carbonate successions (Barremian-Aptian) in NW Turkey: internal structure of the Sellı anoxia level and interpretation of anoxic-oxic changes. International Workshop Meeting “Upper Cretaceous Oceanic Red Beds: Response to Ocean/Climate Global Change, International Geological Correlation Program Project 463 and 494, Workshop, Romanian Carpathians, Bucharest, August 15–18, Abstract Book, pp. 34-35.

Yılmaz, İ. Ö., and Altiner, D., 2005a. Cyclostratigraphic, sequence stratigraphic and sedimentological approaches in platform to platform and platform to basin correlations (Tauride and Pontide platforms and Mudurnu-Nallıhan basins (Barremian-Aptian), SW, CW and NW Turkey). 7th International Symposium on the Cretaceous, 5-7 September, Neuchatel, Switzerland, Abstract Book, pp. 239-240.

Yılmaz, İ. Ö., and Altiner, D., 2005b. Records of Early Cretaceous (Aptian-Albian) and Late Cretaceous (Santonian-Campanian) Red Beds and possible Oceanic Anoxic Events: their meaning in Sequence Stratigraphic framework (NW Turkey). International Geosciences Program Project (IGCP) 463 and 494, Workshop on Cretaceous Oceanic Red Beds, 1-2 September, Neuchatel, Switzerland, Abstract Book, pp. 240-241.

Yılmaz, İ. Ö., and Altiner, D., 2006a. Fischer plot analysis, sedimentology and cyclostratigraphy of the turbidite succession above a drowning unconformity recorded in a pelagic sequence (Aptian-Cenomanian, NW Turkey). 4th Annual conference of Society for Sedimentary Geology. Göttingen, Germany, Abstract Book, pp. 187.

Yılmaz, İ. Ö., and Altiner, D., 2006b. Anoxic Event and Red Beds across the Cenomanian/ Turonian Boundary (NW Turkey). Hu, X., Wang, Y., Huang, Y. (eds.,). International Symposium on Cretaceous Major Geological Events and Earth System-Workshop on Cretaceous Oceanic Red Beds: Paleoclimate, Paleoceanography and Ocean-Land interaction (IGCP 463 and 494). 3-5 September, Beijing, China, Abstract Book, pp. 105.

Yılmaz, İ. Ö., Altiner, D., Tekin, U. K., Tuysuz, O., Ocakoğlu, F. and Acikalin, S., 2010. Cenomanian-Turonian Oceanic Anoxic Event (OAE2) in the Sakarya Zone,

Northwestern Turkey: Sedimentological, cyclostratigraphic, and geochemical records. Cretaceous Research, Vol. 31, pp. 207-226.

Yilmaz, İ. Ö., Ocakoglu, F. and Wagreich, M., 2012. The Santonian-Campanian oceanic anoxic deposits in the Mudurnu-Göynük and Haymana basins, NW Turkey: a possible paleoceanographic link. 34th International Geological Congress, Brisbane, Australia, pp. 3900.

Yilmaz, İ. Ö., Altiner, D., Tekin, U. K. and Ocakoğlu, F., 2012. The first record of the “Mid-Barremian” Oceanic Anoxic Event and the Late Hauterivian platform drowning of the Bilecik platform, Sakarya Zone, Western Turkey. Cretaceous Research, Vol. 38, pp. 19-39.

Yilmaz, Y., 1981. Sakarya kıtasının güney kenarının tektonik evrimi : İstanbul Üniversitesi, Yerbilimleri, Vol. 1, pp. 33-52.

Yurtsever, T. Ş., Tekin, U. K. and Demirel, İ. H., 2003. First evidence of the Cenomanian/Turonian boundary event (CTBE) in the Alakırçay Nappe of the Antalya Nappes, southwest Turkey. Cretaceous Research, Vol. 24, pp. 41-53.

Yüksel, S., 1970. Etude géologique de la region d’Haymana (Turquie Centrale). Thèse Faculty of Sciences, University of De Nancy, pp. 1-179.

Munsell rock color chart, Geological society of America, 2009

APPENDIX A

POINT COUNTING OF THE STUDIED SECTIONS

Table A1: Quantitative data of the Alagöz samples under microscope by using point counting method (Unit as number of grains) (James Swift brand mechanical stage).

Sample No	Quartz	Feldspar	Plagioclase	Mica	Glauconite	Heavy Minerals	Lithics	Bioclasts	Pyrite	Hematite	Phosphate	Matrix/Clay			Total
												Lime Mud	Matrix /Clay	Opal	
ZR0b	63	0	0	5	3	1	2	7032	62	0	5	2531	0	779	10483
ZR0	30	0	0	2	1	0	4	6967	39	0	7	2398	0	467	9915
ZR01	6549	0	9	171	1	1	10	3	180	0	0	0	2071	0	8995
ZR02	3812	1	4	135	2	1	5	0	168	0	4	0	4293	0	8425
ZR03	4858	1	5	177	1	1	6	0	150	98	0	0	3539	0	8836
ZR04	5008	1	1	194	2	0	4	0	376	0	0	0	4102	0	9688
ZR04a	3724	0	3	154	1	1	4076	0	84	101	0	0	2137	0	10281
ZR05	2737	0	1	81	2	0	4	18	316	0	0	0	4973	0	8132
ZR06	2968	0	1	55	3	1	5	19	223	122	0	0	4483	0	7879
ZR07	1826	1	0	1	0	0	3	557	140	42	0	0	4468	0	7038
ZR08	1997	0	0	43	1	1	0	332	117	0	0	0	3649	0	6140
ZR09	1117	0	0	3	1	0	0	775	149	0	0	0	4459	0	6504
ZR10	1263	0	0	1	2	0	0	413	197	159	0	0	4321	0	6356
ZR11	1647	0	0	1	0	0	0	1529	90	99	0	0	5631	0	8997
ZR12	1189	0	0	0	0	0	0	1104	99	0	0	0	4728	0	7120
ZR13	1395	0	0	0	0	0	0	1095	49	0	0	0	5573	0	8112
ZR14	1002	0	0	0	0	0	0	1107	143	0	0	0	5281	0	7533
ZR15	1609	0	0	2	2	0	0	660	204	47	0	0	5333	0	7857
ZR16	1853	0	0	0	2	0	0	519	194	0	0	0	5879	0	8447
ZR17	1822	0	0	7	1	2	0	481	112	0	0	0	4554	0	6976
ZR18	1562	0	0	3	0	0	0	279	229	0	0	0	4277	0	6350
ZR19	1788	0	0	3	0	0	0	288	137	20	0	0	4312	0	6548
ZR20	2329	0	0	2	0	0	3	399	264	0	0	0	4134	0	7131
ZR21	2978	0	0	0	0	0	0	479	280	0	0	0	4248	0	7985

Table A2: Quantitative studied of the Göynük samples under microscope by using point counting method (Unit as number of grains) (James Swift brand mechanical stage).

Sample No	Quartz	Feldspar	Plagioclase	Mica	Glaucocite	Heavy Minerals	Lithics	Bioclasts	Pyrite	Haematite	Phosphate	Matrix /Clay	Total
GOZ-0	816	0	0	5	0	0	2	1592	17	0	2	6156	8590
GOZ-1	998	0	0	6	1	1	2	1914	16	0	1	5045	7983
GOZ-2	963	2	0	5	1	2	2	1904	33	13	2	4840	7767
GOZ-3	758	0	2	8	0	1	2	2671	33	35	2	5842	9354
GOZ-4	778	0	0	17	0	0	0	2295	56	17	13	5383	8559
GOZ-5	622	0	0	4	5	0	2	2151	46	15	14	4836	7695
GOZ-6	751	0	0	3	5	0	4	2487	46	18	5	5837	9155
GOZ-7	589	0	2	26	0	0	3	2437	35	53	7	5611	8762
GOZ-8	784	0	3	28	0	0	6	2415	103	56	28	5915	9338
GOZ-9	1897	0	4	22	6	0	4	565	24	41	2	4916	7481
GOZ-10	499	0	0	24	0	0	6	2208	49	0	4	5385	8175
GOZ-11	3332	0	7	53	0	1	5	97	291	185	4	4849	8825
GOZ-12	377	0	0	5	0	2	0	2465	88	0	5	5825	8767
GOZ-13	855	0	2	0	0	0	2	1866	151	32	3	5061	7973
GOZ-14	1942	2	5	85	0	0	3	284	77	25	4	6088	8516
GOZ-15A	239	0	0	2	0	0	0	896	50	0	0	2943	4130
GOZ-15B	3594	0	106	117	23	4	2	0	100	94	3	1826	5870
GOZ-16	1275	0	3	26	0	0	2	2121	79	0	6	5278	8790
GOZ-17	2868	0	14	104	0	1	3	7	163	42	7	3743	6954
GOZ-18	823	0	4	7	0	0	2	2007	223	0	7	4116	7190
GOZ-19	4163	0	7	79	0	1	3	0	158	39	0	2122	6572
GOZ-20	1995	0	5	13	5	0	1	331	268	34	0	4059	6712
GOZ-21	1176	0	3	0	0	1	2	1231	175	28	1	4373	6990
GOZ-22	1073	1	2	8	0	0	0	1231	415	0	6	5409	8146
GOZ-23	1088	0	0	3	0	0	0	921	154	0	7	4847	7021
GOZ-24	1162	0	0	7	0	0	2	1143	219	30	4	5001	7568
GOZ-25	1271	0	0	7	0	0	5	1357	138	51	1	4416	7247
GOZ-26	926	0	0	7	1	0	3	1429	140	0	7	4857	7371
GOZ-27	880	0	0	0	0	0	0	2125	93	0	7	4024	7129
GOZ-28	6203	6	9	141	47	5	9	9	666	28	3	2248	9375
GOZ-29	1002	0	0	7	3	1	2	1677	59	7	3	4647	7409
GOZ-30	1890	0	3	6	0	0	0	496	312	14	0	3775	6496
GOZ-31	1041	1	3	7	0	0	2	2193	76	0	15	3556	6893
GOZ-32	726	1	3	2	3	0	0	1263	95	11	0	4205	6312
GOZ-33	693	0	0	5	0	0	0	1282	182	0	0	4347	6509
GOZ-34a	3715	3	14	0	1	17	4	3	387	11	3	1452	5612

Table A2: Continued.

GOZ-34b	804	0	2	15	0	0	1	27	70	0	2	2134	3056
GOZ-35	819	0	0	6	0	0	0	990	190	0	2	4132	6140
GOZ-36	1108	1	3	21	0	5	3	1412	237	0	3	4188	6982
GOZ-37	663	0	0	6	0	0	0	1234	76	0	3	3857	5839
GOZ-38	6979	4	15	50	6	10	8	2	509	0	0	2401	9984
GOZ-39	652	0	0	0	0	0	1	1551	239	0	5	5802	8250
GOZ-40	957	0	2	0	0	0	0	2135	29	0	1	4017	7141
GOZ-41a	2922	0	3	4	1	0	2	0	101	0	0	1557	4591
GOZ-41b	2129	0	3	69	2	11	3	0	220	0	1	1171	3610
GOZ-42	5464	0	63	45	5	27	6	2	636	0	9	2707	8965
GOZ-43	608	0	3	7	0	0	1	2003	65	0	6	4480	7174
GOZ-44	3438	0	4	22	0	0	2	116	380	0	0	3270	7231
GOZ-45(Lower)a	1015	0	1	6	2	1	0	0	123	0	0	1844	2991
GOZ-45(Middle)b	2517	0	5	8	3	2	0	16	244	0	0	1343	4138
GOZ-45(Upper)c	3728	0	6	7	6	2	0	0	446	0	0	3366	7561
GOZ-46	584	0	2	7	0	0	1	2052	120	0	10	4288	7064
GOZ-47	2413	0	0	36	0	0	1	363	73	51	6	4336	7280
GOZ-48	4605	0	3	31	0	0	2	5	497	0	0	2506	7649
GOZ-49(Lower)a	422	0	1	0	0	0	1	609	23	0	0	2294	3350
GOZ-49(Middle)b	1743	0	1	27	11	3	0	0	123	0	1	829	2739
GOZ-49(Upper)c	3235	0	0	14	5	0	0	2	143	0	0	3412	6810
GOZ-50	1948	0	0	7	0	0	0	8	346	0	5	4474	6789
GOZ-51	4545	0	6	38	2	2	0	0	429	0	0	2508	7529
GOZ-52	2819	0	4	0	5	0	0	0	376	0	0	4174	7379

APPENDIX B

GEOCHEMICAL DATA OF THE STUDIED SECTIONS

Table B1: Al-normalized major element of the red beds of Alagöz Section.

Sample	Type	Si/Al	Fe/Al	Mg/Al	Ca/Al	Na/Al	K/Al	Ti/Al	P/Al	Mn/Al	Cr/Al	D*
ZR0b	Packstone	24.71	0.66	0.28	6.53	0.12	0.42	0.04	0.01	0.05	0.016	0.59
ZR0	Packstone	19.71	0.43	0.31	10.13	0.13	0.37	0.04	0.01	0.07	0.005	0.67
ZR2	Silty Marl	3.41	0.87	0.41	0.96	0.17	0.29	0.10	0.01	0.01	0.006	0.53
ZR3	Silty Marl	3.31	0.94	0.45	0.72	0.18	0.27	0.10	0.01	0.01	0.007	0.51
ZR4	Silty Marl	3.24	0.95	0.52	1.27	0.17	0.22	0.11	0.01	0.01	0.007	0.51
ZR6	Silty Marl	3.12	0.99	0.59	1.18	0.18	0.20	0.12	0.01	0.01	0.006	0.50
ZR1	Siltstone	3.53	0.95	0.36	0.93	0.17	0.30	0.10	0.01	0.01	0.008	0.51
ZR4a	Siltstone	3.67	1.07	0.73	13.98	0.19	0.22	0.10	0.02	0.20	0.042	0.44
Mean		8.09	0.86	0.46	4.46	0.16	0.29	0.09	0.01	0.05	0.01	0.53
Standard Deviation		8.82	0.21	0.15	5.17	0.02	0.08	0.03	0.00	0.07	0.01	0.07
Minimum		3.12	0.43	0.28	0.72	0.12	0.2	0.04	0.01	0.01	0.01	0.44
Maximum		24.71	1.07	0.73	13.98	0.19	0.42	0.12	0.02	0.20	0.04	0.67

D* = Al/(Al+Fe+Mn)

Table B2: Al-normalized major element of the green-gray beds of Alagöz Section.

Sample	Type	Si/Al	Fe/Al	Mg/Al	Ca/Al	Na/Al	K/Al	Ti/Al	P/Al	Mn/Al	Cr/Al	D*
ZR5	Mudstone	2.92	0.86	0.64	1.30	0.18	0.18	0.12	0.01	0.01	0.007	0.53
ZR7	Mudstone	3.14	0.87	0.58	1.87	0.17	0.20	0.11	0.01	0.01	0.006	0.53
ZR8	Mudstone	3.16	0.91	0.58	3.84	0.17	0.23	0.10	0.01	0.03	0.005	0.52
ZR11	Mudstone	3.34	0.82	0.48	4.07	0.16	0.27	0.08	0.01	0.03	0.004	0.54
ZR17	Mudstone	3.02	0.73	0.42	3.74	0.17	0.26	0.09	0.01	0.02	0.004	0.57
ZR20	Mudstone	3.08	0.80	0.44	3.38	0.15	0.27	0.08	0.01	0.02	0.004	0.55
ZR21	Mudstone	2.96	0.79	0.47	2.58	0.16	0.26	0.08	0.01	0.02	0.003	0.55
ZR9	Claystone	3.18	0.83	0.53	3.35	0.17	0.26	0.08	0.01	0.02	0.004	
ZR10	Claystone	3.11	0.82	0.50	2.66	0.17	0.26	0.08	0.01	0.02	0.004	0.54
ZR12	Claystone	3.09	0.79	0.50	4.29	0.18	0.25	0.08	0.01	0.02	0.004	0.54
ZR13	Claystone	3.19	0.82	0.46	4.18	0.16	0.25	0.08	0.01	0.02	0.004	0.55
ZR14	Claystone	3.49	0.80	0.41	4.70	0.16	0.27	0.08	0.01	0.03	0.004	0.54
ZR15	Claystone	3.03	0.74	0.45	3.19	0.17	0.26	0.08	0.01	0.02	0.004	0.55
ZR16	Claystone	2.99	0.71	0.42	2.92	0.16	0.29	0.07	0.01	0.02	0.003	0.57
ZR18	Claystone	3.06	0.71	0.38	2.89	0.15	0.29	0.07	0.01	0.02	0.004	0.58
ZR19	Claystone	2.95	0.74	0.42	2.70	0.16	0.28	0.08	0.01	0.02	0.003	0.58
Mean		3.11	0.80	0.48	3.23	0.17	0.26	0.09	0.01	0.02	0.004	0.55
Standard Deviation		0.15	0.06	0.07	0.91	0.01	0.03	0.01	0.00	0.00	0.001	0.02
Minimum		2.92	0.71	0.38	1.3	0.15	0.18	0.07	0.01	0.01	0.003	0.52
Maximum		3.49	0.91	0.64	4.70	0.18	0.29	0.12	0.01	0.03	0.007	0.58

Table B3: Al-normalized major element of the red beds of Göynük Section.

Sample	Type	Si/Al	Fe/Al	Mg/Al	Ca/Al	Na/Al	K/Al	Ti/Al	P/Al	Mn/Al	Cr/Al	D*
GOZ1	Marl	3.07	0.64	0.26	7.09	0.12	0.36	0.05	0.01	0.03	0.00	0.60
GOZ2	Marl	2.98	0.62	0.23	6.00	0.11	0.37	0.05	0.01	0.02	0.00	0.61
GOZ3	Marl	2.87	0.59	0.22	5.25	0.11	0.37	0.05	0.01	0.02	0.00	0.62
GOZ4	Marl	2.88	0.58	0.23	5.74	0.11	0.37	0.05	0.01	0.02	0.00	0.63
GOZ5	Marl	2.83	0.61	0.24	5.63	0.11	0.38	0.05	0.01	0.02	0.00	0.61
GOZ6	Marl	2.79	0.62	0.23	5.21	0.12	0.38	0.05	0.01	0.02	0.00	0.61
GOZ7	Marl	2.88	0.61	0.22	4.40	0.11	0.39	0.05	0.01	0.02	0.00	0.62
GOZ8	Marl	2.91	0.64	0.25	5.48	0.11	0.39	0.05	0.01	0.02	0.00	0.60
Mean		2.90	0.61	0.24	5.60	0.11	0.38	0.05	0.01	0.02	0.00	0.61
Standard Deviation		0.09	0.02	0.01	0.77	0.00	0.01	0.00	0.00	0.00	0.00	0.01
Minimum		2.79	0.58	0.22	4.40	0.11	0.36	0.05	0.01	0.02	0.00	0.60
Maximum		3.07	0.64	0.26	7.09	0.12	0.39	0.05	0.01	0.03	0.00	0.63

Table B4: Al-normalized major element of the green-gray beds of Göynük Section.

Sample	Type	Si/Al	Fe/Al	Mg/Al	Ca/Al	Na/Al	K/Al	Ti/Al	P/Al	Mn/Al	Cr/Al	D*
GOZ11	Mudstone	2.84	0.57	0.22	3.56	0.12	0.40	0.05	0.01	0.01	0.001	0.63
GOZ13	Mudstone	2.93	0.59	0.24	3.79	0.14	0.38	0.05	0.01	0.02	0.001	0.62
GOZ16	Mudstone	3.01	0.57	0.25	4.16	0.12	0.37	0.05	0.01	0.02	0.001	0.63
GOZ17	Mudstone	2.87	0.57	0.21	2.32	0.13	0.38	0.05	0.01	0.01	0.001	0.63
GOZ18	Mudstone	3.07	0.58	0.25	4.26	0.14	0.36	0.05	0.01	0.02	0.001	0.62
GOZ20	Mudstone	3.02	0.63	0.25	2.95	0.13	0.38	0.05	0.01	0.01	0.001	0.61
GOZ21	Mudstone	3.00	0.65	0.25	3.35	0.13	0.37	0.05	0.01	0.02	0.001	0.60
GOZ25	Mudstone	2.97	0.54	0.22	1.39	0.11	0.36	0.06	0.00	0.01	0.001	0.65
GOZ27	Mudstone	3.63	0.65	0.26	3.69	0.12	0.33	0.05	0.02	0.02	0.001	0.60
GOZ29	Mudstone	3.67	0.59	0.25	3.76	0.13	0.32	0.05	0.01	0.02	0.001	0.62
GOZ30	Mudstone	3.83	0.62	0.26	3.12	0.14	0.32	0.05	0.01	0.02	0.001	0.61
GOZ31	Mudstone	3.29	0.58	0.24	4.28	0.15	0.31	0.05	0.02	0.03	0.001	0.62
GOZ36	Mudstone	3.22	0.66	0.25	4.29	0.12	0.36	0.05	0.01	0.03	0.001	0.59
GOZ40	Mudstone	3.10	0.66	0.26	5.17	0.12	0.35	0.05	0.01	0.03	0.001	0.59
GOZ43	Mudstone	3.01	0.60	0.23	3.73	0.10	0.36	0.05	0.01	0.02	0.001	0.62
GOZ44	Mudstone	3.07	0.66	0.24	3.69	0.11	0.38	0.05	0.02	0.02	0.001	0.59
GOZ46	Mudstone	3.22	0.70	0.25	4.11	0.11	0.39	0.05	0.02	0.03	0.001	0.58
GOZ47	Mudstone	3.02	0.66	0.25	1.42	0.12	0.37	0.05	0.01	0.01	0.002	0.60
GOZ52	Mudstone	3.19	0.61	0.23	3.75	0.12	0.38	0.05	0.01	0.02	0.004	0.61
GOZ0	Claystone	2.97	0.51	0.21	3.73	0.10	0.33	0.05	0.01	0.01	0.001	0.66
GOZ9	Claystone	2.87	0.59	0.22	2.29	0.11	0.42	0.05	0.01	0.01	0.002	0.62
GOZ10	Claystone	2.99	0.62	0.25	5.39	0.11	0.38	0.05	0.01	0.03	0.002	0.61
GOZ12	Claystone	3.03	0.56	0.25	6.04	0.13	0.38	0.05	0.01	0.03	0.001	0.63
GOZ14	Claystone	2.98	0.61	0.24	3.66	0.13	0.38	0.05	0.01	0.02	0.001	0.61
GOZ22	Claystone	3.23	0.67	0.26	5.01	0.12	0.34	0.05	0.01	0.03	0.001	0.59
GOZ23	Claystone	3.14	0.64	0.26	4.10	0.12	0.35	0.05	0.02	0.02	0.001	0.60
GOZ24	Claystone	3.14	0.59	0.24	3.79	0.12	0.33	0.05	0.01	0.02	0.001	0.62
GOZ26	Claystone	3.36	0.61	0.25	3.96	0.12	0.33	0.05	0.01	0.02	0.001	0.61
GOZ32	Claystone	3.21	0.58	0.24	4.18	0.14	0.33	0.05	0.01	0.03	0.001	0.62
GOZ33	Claystone	3.63	0.68	0.26	4.05	0.14	0.34	0.05	0.01	0.03	0.002	0.59
GOZ35	Claystone	3.44	0.67	0.25	3.16	0.12	0.34	0.05	0.01	0.02	0.001	0.59
GOZ37	Claystone	3.13	0.62	0.26	2.68	0.13	0.34	0.06	0.01	0.01	0.002	0.61
GOZ39	Claystone	3.11	0.68	0.26	4.55	0.12	0.35	0.05	0.01	0.03	0.001	0.59
GOZ50	Claystone	2.99	0.50	0.22	1.20	0.11	0.33	0.05	0.01	0.01	0.001	0.66
GOZ19	Siltstone	2.90	0.53	0.23	1.55	0.12	0.34	0.05	0.01	0.01	0.001	0.65
GOZ48	Siltstone	3.19	0.62	0.26	1.69	0.13	0.35	0.06	0.01	0.01	0.002	0.61
GOZ51	Siltstone	3.40	0.54	0.21	1.45	0.19	0.28	0.06	0.01	0.01	0.001	0.65
GOZ19	Siltstone	4.33	0.41	0.18	3.54	0.22	0.23	0.06	0.01	0.02	0.002	0.70
GOZ28	Sandstone	3.59	0.53	0.19	2.33	0.22	0.27	0.08	0.01	0.01	0.002	0.65
GOZ38	Sandstone	2.81	0.37	0.13	1.44	0.21	0.31	0.05	0.01	0.01	0.001	0.73

Table B4: Continued.

GOZ42	Sandstone	2.84	0.54	0.19	1.19	0.13	0.42	0.05	0.01	0.01	0.001	0.65
GOZ15	Mixed	3.38	0.54	0.21	1.58	0.18	0.27	0.06	0.01	0.01	0.001	0.65
GOZ34	Mixed	3.18	0.57	0.23	1.35	0.15	0.35	0.06	0.01	0.01	0.002	0.63
GOZ41	Mixed	3.35	0.60	0.23	1.55	0.19	0.33	0.07	0.01	0.01	0.002	0.62
GOZ45	Mixed	3.34	0.68	0.27	1.78	0.13	0.34	0.06	0.00	0.01	0.002	0.59
GOZ49	Mixed	3.07	0.64	0.26	7.09	0.12	0.36	0.05	0.01	0.03	0.001	0.63
Mean		3.19	0.59	0.24	3.20	0.13	0.35	0.05	0.01	0.02	0.001	0.62
Standard Deviation		0.30	0.07	0.03	1.28	0.03	0.04	0.01	0.00	0.01	0.001	0.03
Minimum		2.81	0.37	0.13	1.19	0.10	0.23	0.05	0.00	0.01	0.001	0.58
Maximum		4.33	0.70	0.27	6.04	0.22	0.42	0.08	0.02	0.03	0.004	0.73

Table B5: REE-normalization of the red beds of Alagöz Section by using PAAS (Taylor and McLennan, 1985).

Sample	Rock	La	Ce	Pr	Nd	Sm	Eu	Gd	Tb	Dy	Ho	Er	Tm	Yb	Lu
ZR0b	Packstone	0.18	0.10	0.16	0.17	0.21	0.30	0.27	0.26	0.23	0.25	0.25	0.25	0.24	0.25
ZR0	Packstone	0.20	0.12	0.19	0.22	0.26	0.35	0.32	0.30	0.29	0.31	0.30	0.30	0.30	0.30
ZR2	Silty Marl	0.54	0.47	0.55	0.57	0.71	0.92	0.77	0.81	0.83	0.71	0.68	0.74	0.69	0.67
ZR3	Silty Marl	0.55	0.52	0.60	0.57	0.72	0.97	0.87	0.87	0.82	0.70	0.69	0.74	0.71	0.79
ZR4	Silty Marl	0.64	0.52	0.65	0.69	0.85	1.08	0.92	0.87	0.80	0.75	0.73	0.77	0.70	0.72
ZR6	Silty Marl	0.54	0.51	0.60	0.60	0.70	0.95	0.79	0.83	0.74	0.66	0.66	0.67	0.62	0.67
ZR1	Siltstone	0.52	0.50	0.65	0.67	0.81	1.06	0.87	0.88	0.88	0.74	0.74	0.81	0.70	0.72
ZR4a	Siltstone	0.42	0.32	0.39	0.41	0.47	0.62	0.52	0.45	0.46	0.38	0.37	0.37	0.34	0.32
Mean		0.45	0.38	0.47	0.49	0.59	0.78	0.67	0.66	0.63	0.56	0.55	0.58	0.54	0.55
Standard Deviation		0.17	0.18	0.2	0.20	0.25	0.32	0.26	0.27	0.26	0.21	0.21	0.23	0.2	0.22
Minimum		0.18	0.10	0.16	0.17	0.21	0.3	0.27	0.26	0.23	0.25	0.25	0.25	0.24	0.25
Maximum		0.64	0.52	0.65	0.69	0.85	1.08	0.92	0.88	0.88	0.75	0.74	0.81	0.71	0.79

Table B6: REE normalization of the green-gray beds of Alagöz Section by using PAAS (Taylor and McLennan, 1985).

Sample	Type	La	Ce	Pr	Nd	Sm	Eu	Gd	Tb	Dy	Ho	Er	Tm	Yb	Lu
ZR5	Mudstone	0.60	0.57	0.68	0.69	0.78	1.07	0.81	0.83	0.79	0.73	0.66	0.69	0.63	0.65
ZR7	Mudstone	0.46	0.41	0.54	0.55	0.63	0.90	0.76	0.75	0.73	0.61	0.63	0.64	0.66	0.67
ZR8	Mudstone	0.45	0.38	0.44	0.45	0.53	0.70	0.56	0.59	0.65	0.53	0.53	0.57	0.52	0.53
ZR11	Mudstone	0.46	0.38	0.45	0.46	0.54	0.71	0.59	0.57	0.60	0.52	0.53	0.54	0.51	0.48
ZR17	Mudstone	0.40	0.35	0.41	0.43	0.51	0.67	0.56	0.56	0.52	0.49	0.51	0.54	0.54	0.53
ZR20	Mudstone	0.41	0.36	0.42	0.43	0.51	0.66	0.56	0.57	0.57	0.52	0.54	0.59	0.52	0.53
ZR21	Mudstone	0.48	0.43	0.49	0.48	0.56	0.71	0.69	0.68	0.62	0.53	0.53	0.62	0.63	0.67
ZR9	Claystone	0.42	0.36	0.43	0.42	0.49	0.63	0.60	0.57	0.56	0.47	0.51	0.49	0.52	0.55
ZR10	Claystone	0.50	0.40	0.48	0.48	0.62	0.76	0.67	0.62	0.62	0.57	0.58	0.64	0.60	0.62
ZR12	Claystone	0.43	0.35	0.40	0.41	0.44	0.58	0.53	0.56	0.51	0.48	0.50	0.49	0.50	0.55
ZR13	Claystone	0.38	0.31	0.36	0.36	0.43	0.57	0.52	0.50	0.47	0.44	0.44	0.49	0.48	0.51
ZR14	Claystone	0.38	0.29	0.37	0.40	0.47	0.59	0.53	0.49	0.48	0.43	0.46	0.49	0.47	0.46
ZR15	Claystone	0.42	0.34	0.42	0.44	0.56	0.62	0.55	0.58	0.59	0.53	0.54	0.57	0.52	0.53
ZR16	Claystone	0.49	0.38	0.43	0.42	0.49	0.59	0.55	0.61	0.57	0.54	0.52	0.57	0.53	0.58
ZR18	Claystone	0.46	0.40	0.42	0.41	0.47	0.61	0.59	0.66	0.58	0.62	0.60	0.62	0.54	0.58
ZR19	Claystone	0.45	0.42	0.47	0.47	0.60	0.72	0.66	0.62	0.60	0.54	0.57	0.62	0.65	0.62
Mean		0.45	0.38	0.45	0.46	0.54	0.69	0.61	0.61	0.59	0.54	0.54	0.57	0.55	0.57
Standard Deviation		0.05	0.06	0.07	0.08	0.09	0.13	0.09	0.09	0.08	0.07	0.06	0.06	0.06	0.06
Minimum		0.38	0.29	0.36	0.36	0.43	0.57	0.52	0.49	0.47	0.43	0.44	0.49	0.47	0.46
Maximum		0.60	0.57	0.68	0.69	0.78	1.07	0.81	0.83	0.79	0.73	0.66	0.69	0.66	0.67

Table B7: REE normalization of the red beds of Göynük Section by using PAAS (Taylor and McLennan, 1985).

Sample	Rock	La	Ce	Pr	Nd	Sm	Eu	Gd	Tb	Dy	Ho	Er	Tm	Yb	Lu
GOZ1	Marl	0.45	0.35	0.39	0.37	0.45	0.47	0.56	0.44	0.00	0.44	0.44	0.00	0.00	0.42
GOZ2	Marl	0.44	0.40	0.39	0.38	0.44	0.53	0.52	0.44	0.00	0.40	0.45	0.00	0.00	0.42
GOZ3	Marl	0.46	0.40	0.41	0.41	0.46	0.56	0.56	0.47	0.00	0.43	0.44	0.00	0.00	0.46
GOZ4	Marl	0.46	0.40	0.40	0.38	0.44	0.56	0.48	0.44	0.00	0.39	0.43	0.00	0.00	0.46
GOZ5	Marl	0.43	0.38	0.39	0.35	0.43	0.52	0.48	0.40	0.00	0.43	0.44	0.00	0.00	0.44
GOZ6	Marl	0.43	0.40	0.38	0.37	0.41	0.51	0.48	0.44	0.00	0.44	0.44	0.00	0.00	0.44
GOZ7	Marl	0.47	0.44	0.44	0.45	0.50	0.58	0.56	0.49	0.00	0.46	0.50	0.00	0.00	0.48
GOZ8	Marl	0.48	0.45	0.43	0.41	0.49	0.60	0.57	0.49	0.00	0.45	0.44	0.00	0.00	0.53
Mean		0.45	0.40	0.40	0.39	0.45	0.54	0.53	0.45	0.00	0.43	0.45	0.00	0.00	0.46
Standard Deviation		0.02	0.03	0.02	0.03	0.03	0.04	0.04	0.03	0.00	0.02	0.02	0.00	0.00	0.04
Minimum		0.43	0.35	0.38	0.35	0.41	0.47	0.48	0.40	0.00	0.39	0.43	0.00	0.00	0.42
Maximum		0.48	0.45	0.44	0.45	0.50	0.60	0.57	0.49	0.00	0.46	0.50	0.00	0.00	0.53

Table B8: REE normalization of the green-gray beds of Göynük Section by using PAAS (Taylor and McLennan, 1985).

Sample	Type	La	Ce	Pr	Nd	Sm	Eu	Gd	Tb	Dy	Ho	Er	Tm	Yb	Lu
GOZ11	Mudstone	0.53	0.47	0.49	0.50	0.59	0.73	0.63	0.53	0.00	0.45	0.51	0.00	0.00	0.55
GOZ13	Mudstone	0.53	0.47	0.47	0.45	0.58	0.66	0.64	0.49	0.00	0.44	0.48	0.00	0.00	0.48
GOZ16	Mudstone	0.51	0.48	0.46	0.45	0.53	0.62	0.60	0.49	0.00	0.46	0.47	0.00	0.00	0.51
GOZ17	Mudstone	0.60	0.53	0.55	0.54	0.63	0.77	0.68	0.59	0.00	0.58	0.53	0.00	0.00	0.58
GOZ18	Mudstone	0.47	0.43	0.43	0.42	0.52	0.56	0.52	0.45	0.00	0.44	0.46	0.00	0.00	0.44
GOZ20	Mudstone	0.53	0.48	0.48	0.50	0.57	0.67	0.62	0.53	0.00	0.50	0.51	0.00	0.00	0.48
GOZ21	Mudstone	0.53	0.48	0.47	0.46	0.59	0.63	0.58	0.50	0.00	0.46	0.48	0.00	0.00	0.55
GOZ25	Mudstone	0.43	0.38	0.40	0.42	0.50	0.60	0.53	0.47	0.00	0.44	0.41	0.00	0.00	0.46
GOZ27	Mudstone	0.77	0.64	0.65	0.61	0.69	0.71	0.74	0.61	0.00	0.54	0.63	0.00	0.00	0.62
GOZ29	Mudstone	0.69	0.54	0.52	0.57	0.59	0.70	0.65	0.54	0.00	0.52	0.51	0.00	0.00	0.53
GOZ30	Mudstone	0.78	0.72	0.69	0.69	0.74	0.78	0.81	0.67	0.00	0.61	0.64	0.00	0.00	0.62
GOZ31	Mudstone	1.13	1.04	0.98	0.93	0.96	0.88	1.09	0.85	0.00	0.83	0.80	0.00	0.00	0.83
GOZ36	Mudstone	0.68	0.60	0.62	0.58	0.66	0.68	0.68	0.61	0.00	0.54	0.69	0.00	0.00	0.62
GOZ40	Mudstone	0.52	0.47	0.48	0.45	0.50	0.62	0.61	0.52	0.00	0.46	0.50	0.00	0.00	0.46
GOZ43	Mudstone	0.84	0.72	0.74	0.72	0.84	0.86	0.92	0.78	0.00	0.76	0.71	0.00	0.00	0.69
GOZ44	Mudstone	0.73	0.64	0.66	0.61	0.74	0.77	0.79	0.68	0.00	0.53	0.62	0.00	0.00	0.65
GOZ46	Mudstone	0.57	0.51	0.54	0.51	0.56	0.60	0.61	0.56	0.00	0.50	0.57	0.00	0.00	0.53
GOZ47	Mudstone	0.57	0.52	0.57	0.55	0.66	0.74	0.70	0.63	0.00	0.61	0.66	0.00	0.00	0.67
GOZ52	Mudstone	0.58	0.57	0.55	0.50	0.66	0.69	0.66	0.65	0.00	0.51	0.52	0.00	0.00	0.53
GOZO	Claystone	0.50	0.44	0.44	0.43	0.52	0.56	0.66	0.58	0.00	0.53	0.57	0.00	0.00	0.53
GOZ9	Claystone	0.53	0.48	0.50	0.45	0.60	0.71	0.62	0.54	0.00	0.48	0.48	0.00	0.00	0.53
GOZ10	Claystone	0.50	0.46	0.45	0.43	0.54	0.55	0.53	0.48	0.00	0.40	0.47	0.00	0.00	0.42
GOZ12	Claystone	0.46	0.41	0.41	0.42	0.49	0.57	0.51	0.40	0.00	0.40	0.44	0.00	0.00	0.44
GOZ14	Claystone	0.61	0.56	0.56	0.52	0.63	0.69	0.73	0.61	0.00	0.57	0.57	0.00	0.00	0.58
GOZ22	Claystone	0.52	0.47	0.46	0.47	0.49	0.56	0.58	0.47	0.00	0.41	0.39	0.00	0.00	0.53
GOZ23	Claystone	0.65	0.55	0.55	0.53	0.62	0.65	0.65	0.56	0.00	0.50	0.50	0.00	0.00	0.53
GOZ24	Claystone	0.62	0.58	0.57	0.60	0.61	0.72	0.70	0.59	0.00	0.53	0.57	0.00	0.00	0.62
GOZ26	Claystone	0.53	0.46	0.47	0.46	0.55	0.62	0.58	0.49	0.00	0.48	0.48	0.00	0.00	0.46
GOZ32	Claystone	0.60	0.49	0.49	0.49	0.53	0.62	0.59	0.49	0.00	0.46	0.44	0.00	0.00	0.48
GOZ33	Claystone	0.62	0.50	0.51	0.51	0.53	0.62	0.62	0.52	0.00	0.50	0.49	0.00	0.00	0.48
GOZ35	Claystone	0.61	0.53	0.57	0.58	0.66	0.71	0.68	0.62	0.00	0.51	0.56	0.00	0.00	0.62
GOZ37	Claystone	0.51	0.47	0.51	0.47	0.59	0.67	0.65	0.61	0.00	0.55	0.60	0.00	0.00	0.58
GOZ39	Claystone	0.51	0.45	0.48	0.45	0.56	0.62	0.61	0.54	0.00	0.50	0.47	0.00	0.00	0.48
GOZ50	Claystone	0.60	0.52	0.54	0.54	0.55	0.69	0.58	0.53	0.00	0.45	0.47	0.00	0.00	0.55
GOZ19	Siltstone	0.62	0.59	0.60	0.61	0.67	0.84	0.76	0.65	0.00	0.63	0.59	0.00	0.00	0.65
GOZ48	Siltstone	0.48	0.42	0.46	0.46	0.53	0.66	0.56	0.54	0.00	0.50	0.53	0.00	0.00	0.51
GOZ51	Siltstone	0.67	0.59	0.62	0.63	0.69	0.88	0.70	0.63	0.00	0.55	0.54	0.00	0.00	0.55
GOZ28	Sandstone	0.74	0.59	0.58	0.58	0.66	0.80	0.69	0.62	0.00	0.55	0.62	0.00	0.00	0.48

Table B8: Continued.

GOZ38	Sandstone	0.64	0.58	0.62	0.62	0.74	1.00	0.79	0.71	0.00	0.62	0.60	0.00	0.00	0.53
GOZ42	Sandstone	0.64	0.57	0.61	0.57	0.66	1.00	0.75	0.68	0.00	0.62	0.60	0.00	0.00	0.46
GOZ15	Mixed	0.53	0.47	0.48	0.49	0.54	0.83	0.59	0.52	0.00	0.40	0.46	0.00	0.00	0.44
GOZ34	Mixed	0.57	0.50	0.55	0.53	0.63	0.81	0.66	0.58	0.00	0.49	0.55	0.00	0.00	0.51
GOZ41	Mixed	0.53	0.49	0.54	0.52	0.58	0.77	0.65	0.59	0.00	0.53	0.55	0.00	0.00	0.55
GOZ45	Mixed	0.56	0.52	0.55	0.54	0.66	0.86	0.70	0.65	0.00	0.52	0.64	0.00	0.00	0.53
GOZ49	Mixed	0.58	0.54	0.52	0.48	0.59	0.67	0.63	0.57	0.00	0.53	0.58	0.00	0.00	0.53
Mean		0.60	0.53	0.54	0.53	0.61	0.71	0.66	0.58	0.00	0.52	0.54	0.00	0.00	0.54
Standard Deviation		0.12	0.11	0.10	0.09	0.09	0.11	0.11	0.09	0.00	0.08	0.08	0.00	0.00	0.08
Minimum		0.43	0.38	0.40	0.42	0.49	0.55	0.51	0.40	0.00	0.40	0.39	0.00	0.00	0.42
Maximum		1.13	1.04	0.98	0.93	0.96	1.00	1.09	0.85	0.00	0.83	0.80	0.00	0.00	0.83

Table B9: Oxide ratios and log values in the red beds of Alagöz Section.

Sample	Type	SiO ₂ /Al ₂ O ₃	K ₂ O/NA ₂ O	Na ₂ O/K ₂ O	K ₂ O/Al ₂ O ₃	Al ₂ O ₃ /TiO ₂	Fe ₂ O ₃ /K ₂ O	Log (K ₂ O/Na ₂ O)	Log (Na ₂ O/K ₂ O)	Log (Fe ₂ O ₃ /K ₂ O)	Log (SiO ₂ /Al ₂ O ₃)	Rb/K ₂ O
ZR0b	Packstone	27.98	3.05	0.33	0.26	25.30	1.88	0.48	-0.48	0.27	1.45	31.19
ZR0	Packstone	22.32	2.44	0.41	0.23	26.00	1.38	0.39	-0.39	0.14	1.35	31.80
ZR2	Silty Marl	3.86	1.53	0.66	0.18	11.11	3.57	0.18	-0.18	0.55	0.59	35.82
ZR3	Silty Marl	3.75	1.34	0.75	0.17	11.08	4.19	0.13	-0.13	0.62	0.57	36.77
ZR4	Silty Marl	3.67	1.18	0.85	0.14	9.94	5.06	0.07	-0.07	0.70	0.57	36.71
ZR6	Silty Marl	3.53	0.99	1.01	0.13	9.14	5.99	-0.01	0.01	0.78	0.55	35.06
ZR1	Siltstone	4.00	1.55	0.65	0.19	11.21	3.72	0.19	-0.19	0.57	0.60	35.63
ZR4a	Siltstone	4.15	1.06	0.94	0.14	11.09	5.75	0.03	-0.03	0.76	0.62	36.98
Mean		9.16	1.64	0.70	0.18	14.36	3.94	0.18	-0.18	0.55	0.79	35.00
Standard Deviation		9.99	0.73	0.24	0.05	7.01	1.68	0.17	0.17	0.23	0.38	2.26
Minimum		3.53	0.99	0.33	0.13	9.14	1.38	-0.01	-0.48	0.14	0.55	31.19
Maximum		27.98	3.05	1.01	0.26	26.00	5.99	0.48	0.01	0.78	1.45	36.98

Table B10: Oxide ratios and log values in the green-gray beds of Alagöz Section.

Sample	Type	SiO ₂ /Al ₂ O ₃	K ₂ O/NA ₂ O	Na ₂ O/K ₂ O	K ₂ O/Al ₂ O ₃	Al ₂ O ₃ /TiO ₂	Fe ₂ O ₃ /K ₂ O	Log (K ₂ O/Na ₂ O)	Log (Na ₂ O/K ₂ O)	Log (Fe ₂ O ₃ /K ₂ O)	Log (SiO ₂ /Al ₂ O ₃)	Rb/K ₂ O
ZR5	Mudstone	3.31	0.90	1.11	0.12	9.24	5.54	-0.04	0.04	0.74	0.52	33.33
ZR7	Mudstone	3.56	1.01	0.99	0.13	10.44	5.29	0.01	-0.01	0.72	0.55	37.81
ZR8	Mudstone	3.58	1.20	0.83	0.15	11.85	4.73	0.08	-0.08	0.67	0.55	35.00
ZR11	Mudstone	3.79	1.46	0.69	0.17	13.77	3.66	0.16	-0.16	0.56	0.58	36.79
ZR17	Mudstone	3.42	1.39	0.72	0.17	13.19	3.32	0.14	-0.14	0.52	0.53	37.92
ZR20	Mudstone	3.48	1.59	0.63	0.17	14.32	3.46	0.20	-0.20	0.54	0.54	38.83
ZR21	Mudstone	3.35	1.46	0.69	0.17	13.53	3.58	0.16	-0.16	0.55	0.53	37.89
ZR9	Claystone	3.60	1.40	0.71	0.17	13.34	3.74	0.15	-0.15	0.57	0.56	37.45
ZR10	Claystone	3.52	1.40	0.72	0.17	13.73	3.70	0.15	-0.15	0.57	0.55	36.57
ZR12	Claystone	3.50	1.24	0.81	0.16	14.07	3.69	0.09	-0.09	0.57	0.54	35.15
ZR13	Claystone	3.62	1.35	0.74	0.16	13.34	3.93	0.13	-0.13	0.59	0.56	38.46
ZR14	Claystone	3.95	1.51	0.66	0.17	14.65	3.52	0.18	-0.18	0.55	0.60	37.94
ZR15	Claystone	3.43	1.37	0.73	0.16	13.67	3.43	0.14	-0.14	0.53	0.53	36.18
ZR16	Claystone	3.39	1.63	0.61	0.18	15.63	2.92	0.21	-0.21	0.47	0.53	36.23
ZR18	Claystone	3.47	1.69	0.59	0.18	15.46	2.93	0.23	-0.23	0.47	0.54	40.87
ZR19	Claystone	3.34	1.60	0.62	0.18	14.43	3.11	0.21	-0.21	0.49	0.52	38.12
Mean		3.52	1.39	0.74	0.16	13.42	3.78	0.14	-0.14	0.57	0.55	37.16
Standard Deviation		0.17	0.22	0.14	0.02	1.67	0.77	0.07	0.07	0.08	0.02	1.77
Minimum		3.31	0.90	0.59	0.12	9.24	2.92	-0.04	-0.23	0.47	0.52	33.33
Maximum		3.95	1.69	1.11	0.18	15.63	5.54	0.23	0.04	0.74	0.60	40.87

Table B11: Oxide ratios and log values in the red beds of Göynük Section.

Sample	Type	SiO ₂ /Al ₂ O ₃	K ₂ O/Na ₂ O	Na ₂ O/K ₂ O	K ₂ O/Al ₂ O ₃	Al ₂ O ₃ /TiO ₂	Fe ₂ O ₃ /K ₂ O	Log (K ₂ O/Na ₂ O)	Log (Na ₂ O/K ₂ O)	Log (Fe ₂ O ₃ /K ₂ O)	Log (SiO ₂ /Al ₂ O ₃)	Rb/K2O
GOZ1	Marl	3.48	2.65	0.38	0.23	21.20	2.10	0.42	-0.42	0.32	0.54	40.00
GOZ2	Marl	3.37	2.95	0.34	0.23	22.41	2.01	0.47	-0.47	0.30	0.53	38.69
GOZ3	Marl	3.25	2.97	0.34	0.24	22.03	1.88	0.47	-0.47	0.27	0.51	37.06
GOZ4	Marl	3.26	2.89	0.35	0.24	21.42	1.85	0.46	-0.46	0.27	0.51	36.21
GOZ5	Marl	3.20	3.00	0.33	0.24	21.19	1.90	0.48	-0.48	0.28	0.51	35.66
GOZ6	Marl	3.16	2.86	0.35	0.24	21.32	1.93	0.46	-0.46	0.29	0.50	37.61
GOZ7	Marl	3.26	3.28	0.30	0.25	22.05	1.85	0.52	-0.52	0.27	0.51	36.09
GOZ8	Marl	3.30	3.03	0.33	0.25	21.42	1.97	0.48	-0.48	0.29	0.52	37.28
Mean		3.29	2.95	0.34	0.24	21.63	1.94	0.47	-0.47	0.29	0.52	37.33
Standard Deviation		0.10	0.18	0.02	0.01	0.46	0.09	0.03	0.03	0.02	0.01	1.45
Minimum		3.16	2.65	0.30	0.23	21.19	1.85	0.42	-0.52	0.27	0.50	35.66
Maximum		3.48	3.28	0.38	0.25	22.41	2.10	0.52	-0.42	0.32	0.54	40.00

Table B12: Oxide ratios and log values in the green-gray beds of Göynük Section.

Sample	Type	SiO ₂ /Al ₂ O ₃	K ₂ O/Na ₂ O	Na ₂ O/K ₂ O	K ₂ O/Al ₂ O ₃	Al ₂ O ₃ /TiO ₂	Fe ₂ O ₃ /K ₂ O	Log (K ₂ O/Na ₂ O)	Log (Na ₂ O/K ₂ O)	Log (Fe ₂ O ₃ /K ₂ O)	Log (SiO ₂ /Al ₂ O ₃)	Rb/K2O
GOZ11	Mudstone	3.22	2.93	0.34	0.25	24.10	1.70	0.47	-0.47	0.23	0.51	32.06
GOZ13	Mudstone	3.32	2.50	0.40	0.24	23.30	1.85	0.40	-0.40	0.27	0.52	34.53
GOZ16	Mudstone	3.41	2.63	0.38	0.23	23.03	1.83	0.42	-0.42	0.26	0.53	36.95
GOZ17	Mudstone	3.25	2.62	0.38	0.24	23.34	1.79	0.42	-0.42	0.25	0.51	34.21
GOZ18	Mudstone	3.48	2.38	0.42	0.23	22.36	1.90	0.38	-0.38	0.28	0.54	41.45
GOZ20	Mudstone	3.42	2.58	0.39	0.24	22.24	1.98	0.41	-0.41	0.30	0.53	38.29
GOZ21	Mudstone	3.40	2.62	0.38	0.24	22.88	2.06	0.42	-0.42	0.31	0.53	39.17
GOZ25	Mudstone	3.36	3.07	0.33	0.23	20.21	1.76	0.49	-0.49	0.25	0.53	40.06
GOZ27	Mudstone	4.11	2.46	0.41	0.21	21.41	2.37	0.39	-0.39	0.38	0.61	46.70
GOZ29	Mudstone	4.16	2.22	0.45	0.20	21.68	2.20	0.35	-0.35	0.34	0.62	44.80
GOZ30	Mudstone	4.34	2.12	0.47	0.21	21.44	2.25	0.33	-0.33	0.35	0.64	43.30
GOZ31	Mudstone	3.73	1.89	0.53	0.20	25.06	2.23	0.28	-0.28	0.35	0.57	40.89
GOZ36	Mudstone	3.65	2.61	0.38	0.23	23.31	2.18	0.42	-0.42	0.34	0.56	44.46
GOZ40	Mudstone	3.51	2.61	0.38	0.23	21.50	2.21	0.42	-0.42	0.34	0.55	46.86
GOZ43	Mudstone	3.41	3.27	0.31	0.23	24.47	1.96	0.51	-0.51	0.29	0.53	43.75
GOZ44	Mudstone	3.48	3.15	0.32	0.24	22.44	2.06	0.50	-0.50	0.31	0.54	47.23
GOZ46	Mudstone	3.64	3.07	0.33	0.25	22.66	2.12	0.49	-0.49	0.33	0.56	46.88
GOZ47	Mudstone	3.42	2.72	0.37	0.24	21.28	2.10	0.43	-0.43	0.32	0.53	43.84
GOZ52	Mudstone	3.61	2.87	0.35	0.24	23.28	1.94	0.46	-0.46	0.29	0.56	41.33
GOZ0	Claystone	3.36	2.94	0.34	0.21	23.58	1.82	0.47	-0.47	0.26	0.53	39.75
GOZ9	Claystone	3.26	3.46	0.29	0.27	21.02	1.67	0.54	-0.54	0.22	0.51	31.45
GOZ10	Claystone	3.38	2.95	0.34	0.24	23.00	1.94	0.47	-0.47	0.29	0.53	37.43
GOZ12	Claystone	3.43	2.56	0.39	0.24	23.03	1.75	0.41	-0.41	0.24	0.53	34.94
GOZ14	Claystone	3.38	2.64	0.38	0.24	24.31	1.94	0.42	-0.42	0.29	0.53	33.26
GOZ22	Claystone	3.65	2.45	0.41	0.22	21.50	2.32	0.39	-0.39	0.37	0.56	43.20
GOZ23	Claystone	3.56	2.64	0.38	0.22	22.87	2.19	0.42	-0.42	0.34	0.55	43.21
GOZ24	Claystone	3.55	2.37	0.42	0.21	22.22	2.13	0.37	-0.37	0.33	0.55	42.76
GOZ26	Claystone	3.81	2.53	0.40	0.21	20.86	2.17	0.40	-0.40	0.34	0.58	46.74
GOZ32	Claystone	3.63	2.14	0.47	0.21	22.23	2.09	0.33	-0.33	0.32	0.56	44.78
GOZ33	Claystone	4.11	2.21	0.45	0.22	21.31	2.37	0.34	-0.34	0.38	0.61	44.25
GOZ35	Claystone	3.89	2.45	0.41	0.22	22.05	2.34	0.39	-0.39	0.37	0.59	44.66
GOZ37	Claystone	3.55	2.38	0.42	0.22	19.79	2.18	0.38	-0.38	0.34	0.55	44.91
GOZ39	Claystone	3.53	2.74	0.37	0.23	22.22	2.26	0.44	-0.44	0.35	0.55	48.66
GOZ50	Claystone	3.39	2.70	0.37	0.21	24.42	1.80	0.43	-0.43	0.25	0.53	41.85
GOZ19	Siltstone	3.28	2.64	0.38	0.22	23.39	1.83	0.42	-0.42	0.26	0.52	35.37
GOZ48	Siltstone	3.62	2.45	0.41	0.23	20.27	2.09	0.39	-0.39	0.32	0.56	45.22

Table B12: Continued.

GOZ51	Siltstone	3.85	1.31	0.76	0.18	18.41	2.30	0.12	-0.12	0.36	0.59	34.00
GOZ28	Sandstone	4.90	0.91	1.10	0.14	20.19	2.14	-0.04	0.04	0.33	0.69	36.16
GOZ38	Sandstone	4.06	1.12	0.89	0.18	15.06	2.30	0.05	-0.05	0.36	0.61	31.26
GOZ42	Sandstone	3.19	1.31	0.76	0.20	23.77	1.42	0.12	-0.12	0.15	0.50	24.50
GOZ15	Mixed	3.21	2.92	0.34	0.27	24.31	1.53	0.46	-0.46	0.19	0.51	29.40
GOZ34	Mixed	3.82	1.37	0.73	0.17	18.52	2.37	0.14	-0.14	0.38	0.58	34.21
GOZ41	Mixed	3.60	2.11	0.47	0.22	20.02	1.95	0.32	-0.32	0.29	0.56	39.90
GOZ45	Mixed	3.79	1.58	0.63	0.21	16.19	2.15	0.20	-0.20	0.33	0.58	32.28
GOZ49	Mixed	3.78	2.27	0.44	0.22	18.57	2.36	0.36	-0.36	0.37	0.58	48.94
Mean		3.61	2.43	0.45	0.22	21.85	2.04	0.37	-0.37	0.31	0.56	40.00
Standard Deviation		0.34	0.56	0.16	0.02	2.12	0.24	0.12	0.12	0.05	0.04	5.86
Minimum		3.19	0.91	0.29	0.14	15.06	1.42	-0.04	-0.54	0.15	0.50	24.50
Maximum		4.90	3.46	1.10	0.27	25.06	2.37	0.54	0.04	0.38	0.69	48.94

Table B13: Trace elements ratio in Red Beds of the Alagöz Section.

Sample	Type	Cu/Zn	Ni/Co	U/Th	(Cu+Mo)/Zn	V/Cr	V/(V+Ni)	Th/Sc	Th/Co	Th/U	La/Sc
ZR0b	Packstone	0.74	3.85	0.50	Na	1084.34	0.53	0.27	0.15	2.00	2.30
ZR0	Packstone	0.59	2.85	0.56	Na	2258.68	0.47	0.45	0.13	1.80	3.90
ZR2	Silty Marl	0.44	7.21	0.19	36.90	3905.32	0.39	0.39	0.19	5.15	1.22
ZR3	Silty Marl	0.35	7.40	0.19	31.20	3331.36	0.35	0.35	0.17	5.15	1.10
ZR4	Silty Marl	0.89	7.29	0.21	Na	3848.62	0.37	0.37	0.18	4.79	1.35
ZR6	Silty Marl	0.48	7.75	0.24	Na	4409.70	0.37	0.31	0.15	4.14	1.09
ZR1	Siltstone	0.24	6.85	0.20	20.10	2611.21	0.36	0.37	0.19	5.08	1.10
ZR4a	Siltstone	0.85	16.66	0.30	Na	629.75	0.17	0.25	0.12	3.33	2.03
Mean		0.57	7.48	0.30	11.03	2759.87	0.37	0.34	0.16	3.93	1.76
Standard Deviation		0.24	4.13	0.15	15.89	1371.34	0.10	0.07	0.03	1.40	0.98
Minimum		0.24	2.85	0.19	0.00	629.75	0.17	0.25	0.12	1.80	1.09
Maximum		0.89	16.66	0.56	36.90	4409.70	0.53	0.45	0.19	5.15	3.90

Table B14: Trace elements ratio of green-gray beds of the Alagöz Section

Sample	Type	Cu/Zn	Ni/Co	U/Th	(Cu+Mo)/Zn	V/Cr	V/(V+Ni)	Th/Sc	Th/Co	Th/U	La/Sc
ZR5	Mudstone	1.33	7.47	0.24	Na	3490.15	0.28	0.36	0.13	4.25	1.21
ZR7	Mudstone	0.70	7.77	0.22	Na	3924.40	0.35	0.34	0.16	4.58	1.09
ZR8	Mudstone	0.70	7.19	0.29	Na	4509.77	0.37	0.32	0.16	3.42	1.31
ZR11	Mudstone	0.41	6.21	0.25	Na	5034.06	0.39	0.40	0.18	4.00	1.60
ZR17	Mudstone	0.79	4.63	0.22	Na	6079.84	0.51	0.38	0.22	4.60	1.28
ZR20	Mudstone	0.53	6.33	0.24	Na	5677.37	0.42	0.42	0.23	4.17	1.29
ZR21	Mudstone	0.60	5.84	0.23	Na	6106.98	0.44	0.40	0.22	4.31	1.32
ZR9	Claystone	0.56	6.76	0.23	Na	5896.40	0.42	0.36	0.20	4.27	1.24
ZR10	Claystone	0.73	6.48	0.19	Na	5407.55	0.40	0.41	0.23	5.18	1.37
ZR12	Claystone	0.63	6.30	0.24	Na	5785.10	0.43	0.42	0.23	4.18	1.49
ZR13	Claystone	0.53	5.35	0.26	Na	5553.70	0.42	0.35	0.16	3.80	1.32
ZR14	Claystone	0.58	6.33	0.24	Na	5909.54	0.43	0.41	0.21	4.10	1.45
ZR15	Claystone	0.66	6.28	0.24	Na	5456.27	0.42	0.39	0.21	4.25	1.22
ZR16	Claystone	0.74	5.88	0.21	Na	7368.40	0.49	0.45	0.28	4.83	1.43
ZR18	Claystone	0.73	5.18	0.23	Na	6054.79	0.49	0.48	0.26	4.43	1.35
ZR19	Claystone	0.60	5.60	0.19	Na	6008.39	0.45	0.48	0.26	5.17	1.32
Mean		0.68	6.23	0.23	0.00	5516.42	0.42	0.40	0.21	4.35	1.33
Standard Deviation		0.20	0.83	0.02	0.00	928.37	0.06	0.05	0.04	0.46	0.12
Minimum		0.41	4.63	0.19	0.00	3490.15	0.28	0.32	0.13	3.42	1.09
Maximum		1.33	7.77	0.29	0.00	7368.40	0.51	0.48	0.28	5.18	1.60

Table B15: Trace elements ratio of the red beds of Göynük Section.

Sample	Type	Cu/Zn	Ni/Co	U/Th	(Cu+Mo)/Zn	V/Cr	V/(V+Ni)	Th/Sc	Th/Co	Th/U	La/Sc
GOZ1	Marl	0.69	2.13	0.19	0.70	14197.43	0.78	0.81	0.62	5.18	2.46
GOZ2	Marl	0.68	2.53	0.14	0.69	16285.29	0.76	0.79	0.66	7.00	2.11
GOZ3	Marl	0.66	2.13	0.13	0.66	15345.75	0.78	0.71	0.57	8.00	1.93
GOZ4	Marl	0.56	1.98	0.17	0.56	11854.39	0.75	0.74	0.47	5.90	2.18
GOZ5	Marl	0.65	2.22	0.19	0.66	14066.94	0.74	0.64	0.48	5.27	1.82
GOZ6	Marl	0.54	2.48	0.20	0.55	12568.90	0.73	0.60	0.42	4.91	1.82
GOZ7	Marl	0.81	2.35	0.14	0.82	15751.72	0.76	0.64	0.49	7.11	1.80
GOZ8	Marl	0.84	1.86	0.21	Na	15163.06	0.78	0.68	0.48	4.69	2.04
Mean		0.68	2.21	0.17	0.58	14404.18	0.76	0.70	0.52	6.01	2.02
Standard Deviation		0.11	0.23	0.03	0.25	1551.18	0.02	0.08	0.08	1.22	0.23
Minimum		0.54	1.86	0.13	0.00	11854.39	0.73	0.60	0.42	4.69	1.80
Maximum		0.84	2.53	0.21	0.82	16285.29	0.78	0.81	0.66	8.00	2.46

Table B16: Trace elements ratio of the green-gray beds of Göynük Section.

Sample	Type	Cu/Zn	Ni/Co	U/Th	(Cu+Mo)/Zn	V/Cr	V/(V+Ni)	Th/Sc	Th/Co	Th/U	La/Sc
GOZ11	Mudstone	0.83	2.29	0.18	Na	21087.36	0.80	0.72	0.65	5.54	2.04
GOZ13	Mudstone	0.89	1.91	0.20	0.89	19182.19	0.80	0.81	0.58	5.06	2.04
GOZ16	Mudstone	1.11	2.94	0.26	Na	20136.22	0.79	0.70	0.64	3.89	1.93
GOZ17	Mudstone	1.14	2.38	0.17	1.14	25471.86	0.79	1.02	0.90	5.81	1.91
GOZ18	Mudstone	1.16	2.56	0.28	Na	16624.56	0.72	0.68	0.49	3.58	1.79
GOZ20	Mudstone	0.98	2.45	0.23	0.99	16076.50	0.70	0.67	0.47	4.44	1.69
GOZ21	Mudstone	0.84	3.10	0.19	0.84	15264.56	0.74	0.81	0.77	5.40	2.02
GOZ25	Mudstone	0.82	3.07	0.21	0.83	14510.61	0.73	0.74	0.67	4.83	1.09
GOZ27	Mudstone	0.71	4.02	0.36	0.72	13445.80	0.69	0.67	0.65	2.79	2.95
GOZ29	Mudstone	0.87	4.05	0.25	Na	12715.05	0.68	0.70	0.61	3.94	2.92
GOZ30	Mudstone	0.70	3.40	0.25	0.70	12861.20	0.67	0.86	0.61	4.05	3.30
GOZ31	Mudstone	1.03	3.26	0.28	1.03	17538.00	0.77	1.03	1.24	3.57	5.40
GOZ36	Mudstone	1.09	3.32	0.28	Na	14797.69	0.74	0.85	0.77	3.58	3.26
GOZ40	Mudstone	0.93	3.64	0.26	Na	14432.31	0.74	0.73	0.74	3.87	2.49
GOZ43	Mudstone	0.84	4.27	0.26	Na	16989.94	0.75	0.91	1.12	3.90	3.56
GOZ44	Mudstone	0.86	3.82	0.31	Na	16259.19	0.73	0.98	1.01	3.26	3.09
GOZ46	Mudstone	0.81	3.53	0.33	0.81	16076.50	0.72	0.77	0.71	3.00	2.42
GOZ47	Mudstone	0.73	3.73	0.19	0.74	11874.69	0.66	0.73	0.53	5.28	1.68
GOZ52	Mudstone	0.80	4.74	0.24	Na	3253.02	0.68	0.87	1.11	4.11	2.47
GOZ0	Claystone	0.91	2.47	0.20	1.22	23566.69	0.84	0.91	0.90	5.06	1.90
GOZ9	Claystone	1.04	3.16	0.23	1.04	9886.62	0.69	0.71	0.58	4.38	1.55
GOZ10	Claystone	0.66	2.81	0.23	Na	12179.17	0.72	0.71	0.54	4.38	2.39
GOZ12	Claystone	1.23	2.10	0.39	Na	20461.00	0.83	0.71	0.58	2.59	2.18
GOZ14	Claystone	1.07	2.48	0.23	Na	17355.31	0.74	0.78	0.59	4.33	2.34
GOZ22	Claystone	0.71	2.78	0.25	0.72	13884.25	0.70	0.67	0.52	4.00	2.22
GOZ23	Claystone	0.76	3.61	0.43	0.76	15711.13	0.71	0.74	0.70	2.31	2.76
GOZ24	Claystone	0.97	3.56	0.22	Na	14615.00	0.73	0.72	0.69	4.50	2.38
GOZ26	Claystone	0.76	3.34	0.22	Na	13153.50	0.68	0.60	0.47	4.62	2.03
GOZ32	Claystone	0.83	3.02	0.29	Na	16807.25	0.75	0.76	0.66	3.40	2.56
GOZ33	Claystone	0.82	4.26	0.28	Na	12861.20	0.71	0.74	0.79	3.53	2.64
GOZ35	Claystone	0.75	3.90	0.21	0.75	12276.60	0.65	0.71	0.61	4.73	2.34
GOZ37	Claystone	0.80	4.78	0.17	0.80	10230.50	0.64	0.63	0.65	5.77	1.62
GOZ39	Claystone	0.64	4.73	0.27	0.65	12341.56	0.65	0.78	0.70	3.65	2.45
GOZ50	Claystone	0.78	2.66	0.20	0.78	15943.64	0.76	1.09	1.01	5.07	1.76
GOZ19	Siltstone	1.16	3.23	0.19	Na	18866.64	0.79	0.96	1.06	5.21	1.82
GOZ48	Siltstone	0.73	4.12	0.22	0.74	10778.56	0.64	0.57	0.45	4.63	1.42
GOZ51	Siltstone	0.66	1.97	0.47	0.67	12005.18	0.70	0.58	0.31	2.11	1.96
GOZ28	Sandstone	0.36	3.76	0.29	0.39	7532.35	0.74	0.88	1.13	3.50	3.55
GOZ38	Sandstone	0.64	2.43	0.25	0.65	11107.40	0.71	0.51	0.38	3.94	1.75
GOZ42	Sandstone	0.64	1.60	0.29	0.65	16953.40	0.81	0.94	0.73	3.49	1.88

Table B16: Continued.

GOZ15	Mixed	1.14	2.10	0.17	1.15	23221.61	0.78	0.95	0.73	5.72	1.34
GOZ34	Mixed	0.77	2.00	0.24	0.77	12840.32	0.76	0.64	0.45	4.24	1.55
GOZ41	Mixed	0.74	3.64	0.20	Na	10869.91	0.68	0.66	0.60	5.11	1.44
GOZ45	Mixed	0.72	2.33	0.28	0.72	10068.11	0.68	0.57	0.32	3.64	1.54
GOZ49	Mixed	0.62	3.73	0.19	0.62	10488.41	0.67	0.56	0.49	5.27	1.59
Mean		0.85	3.18	0.25	0.48	14768.94	0.73	0.76	0.69	4.20	2.24
Standard Deviation		0.18	0.82	0.07	0.42	4291.57	0.05	0.14	0.22	0.92	0.77
Minimum		0.36	1.60	0.17	0.00	3253.02	0.64	0.51	0.31	2.11	1.09
Maximum		1.23	4.78	0.47	1.22	25471.86	0.84	1.09	1.24	5.81	5.40

Table B17: Ratio of PAAS-normalized REE of the red beds of Alagöz Section.

Sample	Rock	La*/Lu*	La*/Sm*	Gd*/Yb*	Ce/Ce*	Log(Ce/Ce*)	Eu/Eu*	Log(Eu/Eu*)	Pr/Pr*	Gd/Gd*
ZR0b	Packstone	0.71	0.87	1.12	0.60	-0.22	1.24	0.09	1.26	4.19
ZR0	Packstone	0.68	0.79	1.05	0.58	-0.24	1.23	0.09	1.20	3.88
ZR2	Silty Marl	0.81	0.76	1.12	0.86	-0.07	1.24	0.09	1.07	3.84
ZR3	Silty Marl	0.70	0.76	1.23	0.90	-0.05	1.23	0.09	1.11	4.25
ZR4	Silty Marl	0.89	0.74	1.31	0.80	-0.10	1.22	0.09	1.08	3.83
ZR6	Silty Marl	0.81	0.78	1.27	0.89	-0.05	1.28	0.11	1.07	3.99
ZR1	Siltstone	0.72	0.64	1.26	0.86	-0.07	1.27	0.10	1.13	3.87
ZR4a	Siltstone	1.31	0.91	1.52	0.78	-0.11	1.25	0.10	1.07	3.69
Mean		0.83	0.78	1.23	0.78	-0.11	1.25	0.10	1.13	3.94
Standard Deviation		0.21	0.08	0.15	0.13	0.08	0.02	0.01	0.07	0.19
Minimum		0.68	0.64	1.05	0.58	-0.23	1.22	0.09	1.07	3.69
Maximum		1.31	0.91	1.52	0.90	-0.05	1.28	0.11	1.26	4.25

- $Ce/Ce^* = (Ce_{sample}/Ce^*) / [(La_{sample}/La^*)(Pr_{sample}/Pr^*)]^{0.5}$
- $Eu/Eu^* = (Eu_{sample}/Eu^*) / [(Sm_{sample}/Sm^*)(Gd_{sample}/Gd^*)]^{0.5}$
- $Pr/Pr^* = (Pr_{sample}/Pr^*) / [(Ce_{sample}/Ce^*)(Nd_{sample}/Nd^*)]^{0.5}$
- $Gd/Gd^* = (Gd_{sample}/Gd^*) / [0.33(Sm_{sample}/Sm^*) + 0.67(Tb_{sample}/Tb^*)]$
- [*PAAS-normalization (Taylor and McLennan, 1985)]

Table B18: Ratio of PAAS-normalized REE of the green-gray beds of Alagöz Section.

Sample	Type	La*/Lu*	La*/Sm*	Gd*/Yb*	Ce/Ce*	Log(Ce/Ce*)	Eu/Eu*	Log(Eu/Eu*)	Pr/Pr*	Gd/Gd*
ZR5	Mudstone	0.93	0.77	1.29	0.89	-0.05	1.35	0.13	1.08	3.71
ZR7	Mudstone	0.68	0.72	1.16	0.82	-0.08	1.29	0.11	1.14	4.15
ZR8	Mudstone	0.84	0.85	1.06	0.86	-0.07	1.30	0.11	1.07	3.61
ZR11	Mudstone	0.95	0.86	1.14	0.82	-0.09	1.27	0.10	1.09	3.70
ZR17	Mudstone	0.76	0.80	1.05	0.85	-0.07	1.25	0.10	1.06	3.74
ZR20	Mudstone	0.76	0.80	1.08	0.88	-0.05	1.23	0.09	1.06	3.72
ZR21	Mudstone	0.72	0.86	1.09	0.88	-0.05	1.15	0.06	1.07	4.18
ZR9	Claystone	0.76	0.86	1.15	0.84	-0.07	1.16	0.07	1.10	4.10
ZR10	Claystone	0.81	0.81	1.12	0.82	-0.09	1.18	0.07	1.09	3.66
ZR12	Claystone	0.77	0.98	1.06	0.86	-0.07	1.22	0.08	1.04	4.01
ZR13	Claystone	0.75	0.87	1.09	0.83	-0.08	1.20	0.08	1.09	3.99
ZR14	Claystone	0.82	0.80	1.12	0.78	-0.11	1.19	0.07	1.08	3.69
ZR15	Claystone	0.78	0.74	1.05	0.82	-0.09	1.12	0.05	1.08	3.33
ZR16	Claystone	0.84	0.99	1.04	0.82	-0.08	1.14	0.06	1.08	3.78
ZR18	Claystone	0.80	0.97	1.09	0.90	-0.04	1.16	0.06	1.03	4.22
ZR19	Claystone	0.72	0.75	1.02	0.92	-0.04	1.15	0.06	1.05	3.73
Mean		0.79	0.84	1.10	0.85	-0.07	1.21	0.08	1.08	3.83
Standard Deviation		0.07	0.08	0.07	0.04	0.02	0.07	0.02	0.03	0.25
Minimum		0.68	0.72	1.02	0.78	-0.11	1.12	0.05	1.03	3.33
Maximum		0.95	0.99	1.29	0.92	-0.04	1.35	0.13	1.14	4.22

Table B19: Ratio of PAAS-normalized REE of the red beds of Göynük Section.

Sample	Rock	La*/Lu*	La*/Sm*	Gd*/Yb*	Ce/Ce*	Log(Ce/Ce*)	Eu/Eu*	Log(Eu/Eu*)	Pr/Pr*	Gd/Gd*
GOZ1	Marl	1.08	1.01	Na	0.84	-0.08	0.94	-0.03	1.09	4.14
GOZ2	Marl	1.06	1.01	Na	0.95	-0.02	1.10	0.04	1.01	3.90
GOZ3	Marl	0.99	0.99	Na	0.92	-0.04	1.11	0.04	1.02	4.03
GOZ4	Marl	0.99	1.03	Na	0.93	-0.03	1.21	0.08	1.03	3.59
GOZ5	Marl	0.98	1.01	Na	0.93	-0.03	1.14	0.06	1.06	3.71
GOZ6	Marl	0.98	1.05	Na	0.97	-0.01	1.14	0.06	1.00	3.89
GOZ7	Marl	0.97	0.94	Na	0.96	-0.02	1.11	0.04	1.00	3.69
GOZ8	Marl	0.91	0.98	Na	0.99	-0.01	1.14	0.06	1.00	3.82
Mean		0.99	1.00	0.00	0.94	-0.03	1.11	0.05	1.02	3.85
Standard Deviation		0.06	0.03	0.00	0.05	0.02	0.08	0.03	0.03	0.18
Minimum		0.91	0.94	0.00	0.84	-0.08	0.94	-0.03	1.00	3.59
Maximum		1.08	1.05	0.00	0.99	-0.01	1.21	0.08	1.09	4.14

Table B20: Ratio of PAAS-normalized REE of the green-gray beds of Göynük Section.

Sample	Type	La*/Lu*	La*/Sm*	Gd*/Yb*	Ce/Ce*	Log(Ce/Ce*)	Eu/Eu*	Log(Eu/Eu*)	Pr/Pr*	Gd/Gd*
GOZ11	Mudstone	0.96	0.91	Na	0.92	-0.04	1.20	0.08	1.01	3.60
GOZ13	Mudstone	1.10	0.92	Na	0.93	-0.03	1.08	0.03	1.02	3.64
GOZ16	Mudstone	0.99	0.95	Na	0.99	0.00	1.10	0.04	0.99	3.74
GOZ17	Mudstone	1.04	0.95	Na	0.93	-0.03	1.17	0.07	1.02	3.69
GOZ18	Mudstone	1.07	0.91	Na	0.96	-0.02	1.09	0.04	1.02	3.33
GOZ20	Mudstone	1.10	0.94	Na	0.95	-0.02	1.13	0.05	0.98	3.64
GOZ21	Mudstone	0.95	0.89	Na	0.96	-0.02	1.08	0.03	1.00	3.31
GOZ25	Mudstone	0.93	0.86	Na	0.93	-0.03	1.17	0.07	0.99	3.51
GOZ27	Mudstone	1.24	1.11	Na	0.90	-0.05	0.99	0.00	1.04	3.65
GOZ29	Mudstone	1.30	1.17	Na	0.89	-0.05	1.13	0.05	0.95	3.73
GOZ30	Mudstone	1.25	1.06	Na	0.99	-0.01	1.01	0.00	0.98	3.79
GOZ31	Mudstone	1.36	1.17	Na	0.98	-0.01	0.86	-0.07	1.00	4.00
GOZ36	Mudstone	1.10	1.04	Na	0.92	-0.04	1.01	0.01	1.05	3.53
GOZ40	Mudstone	1.13	1.04	Na	0.94	-0.03	1.12	0.05	1.03	4.07
GOZ43	Mudstone	1.21	1.00	Na	0.92	-0.04	0.98	-0.01	1.03	3.86
GOZ44	Mudstone	1.13	0.99	Na	0.92	-0.04	1.01	0.00	1.06	3.68
GOZ46	Mudstone	1.07	1.01	Na	0.91	-0.04	1.02	0.01	1.06	3.67
GOZ47	Mudstone	0.86	0.87	Na	0.91	-0.04	1.09	0.04	1.07	3.64
GOZ52	Mudstone	1.09	0.89	Na	1.01	0.01	1.06	0.02	1.02	3.48
GOZ0	Claystone	0.94	0.95	Na	0.95	-0.02	0.95	-0.02	1.02	4.18
GOZ9	Claystone	1.00	0.88	Na	0.93	-0.03	1.17	0.07	1.07	3.51
GOZ10	Claystone	1.20	0.93	Na	0.96	-0.02	1.02	0.01	1.01	3.31
GOZ12	Claystone	1.04	0.93	Na	0.94	-0.02	1.15	0.06	0.98	3.39
GOZ14	Claystone	1.06	0.97	Na	0.96	-0.02	1.01	0.00	1.04	3.89
GOZ22	Claystone	0.99	1.08	Na	0.96	-0.02	1.07	0.03	0.98	3.89
GOZ23	Claystone	1.22	1.05	Na	0.91	-0.04	1.02	0.01	1.02	3.57
GOZ24	Claystone	1.00	1.01	Na	0.98	-0.01	1.10	0.04	0.97	3.84
GOZ26	Claystone	1.15	0.97	Na	0.92	-0.04	1.11	0.04	1.02	3.52
GOZ32	Claystone	1.24	1.13	Na	0.90	-0.04	1.11	0.04	0.99	3.71
GOZ33	Claystone	1.28	1.17	Na	0.90	-0.05	1.08	0.03	1.00	3.87
GOZ35	Claystone	0.98	0.93	Na	0.90	-0.05	1.06	0.03	1.03	3.56
GOZ37	Claystone	0.88	0.86	Na	0.92	-0.04	1.08	0.03	1.08	3.71
GOZ39	Claystone	1.06	0.91	Na	0.90	-0.05	1.06	0.03	1.08	3.64
GOZ50	Claystone	1.08	1.10	Na	0.91	-0.04	1.22	0.08	1.03	3.58
GOZ19	Siltstone	0.96	0.92	Na	0.98	-0.01	1.18	0.07	1.00	3.87
GOZ48	Siltstone	0.95	0.90	Na	0.89	-0.05	1.20	0.08	1.04	3.56
GOZ51	Siltstone	1.20	0.97	Na	0.91	-0.04	1.27	0.10	1.02	3.51
GOZ28	Sandstone	0.74	0.59	0.58	0.58	0.66	0.80	0.69	0.62	0.00
GOZ38	Sandstone	0.64	0.58	0.62	0.62	0.74	1.00	0.79	0.71	0.00
GOZ42	Sandstone	0.64	0.57	0.61	0.57	0.66	1.00	0.75	0.68	0.00

Table B20: Continued.

GOZ15	Mixed	0.53	0.47	0.48	0.49	0.54	0.83	0.59	0.52	0.00
GOZ34	Mixed	0.57	0.50	0.55	0.53	0.63	0.81	0.66	0.58	0.00
GOZ41	Mixed	0.53	0.49	0.54	0.52	0.58	0.77	0.65	0.59	0.00
GOZ45	Mixed	0.56	0.52	0.55	0.54	0.66	0.86	0.70	0.65	0.00
GOZ49	Mixed	0.58	0.54	0.52	0.48	0.59	0.67	0.63	0.57	0.00
Mean		1.10	0.98	0.00	0.93	-0.03	1.12	0.05	1.02	3.67
Standard Deviation		0.14	0.09	0.00	0.03	0.01	0.12	0.04	0.03	0.19
Minimum		0.86	0.86	0.00	0.89	-0.05	0.86	-0.07	0.95	3.31
Maximum		1.53	1.17	0.00	1.01	0.01	1.47	0.17	1.08	4.18

Table B21: Al-normalized trace element of the red beds of Alagöz Section.

Sample	Type	Sc/Al	Ba/Al	Co/Al	Nb/Al	Rb/Al	Sr/Al	Ta/Al	Th/Al	U/Al	V/Al	Zr/Al	Mo/Al	Cu/Al	Pb/Al	Zn/Al	Ni/Al	Cd/Al
ZR0b	Packstone	2.24	106.05	4.03	2.02	15.61	126.59	0.07	0.60	0.30	17.18	14.71	Na	10.01	4.78	13.44	15.53	Na
ZR0	Packstone	1.45	128.63	4.94	1.74	14.10	169.40	0.07	0.65	0.36	12.35	13.37	Na	8.14	5.60	13.81	14.10	Na
ZR2	Silty Marl	2.56	42.01	5.42	2.56	12.51	29.21	0.18	1.01	0.20	24.54	22.49	0.02	5.56	1.45	12.50	39.10	Na
ZR3	Silty Marl	2.72	42.00	5.49	2.59	11.76	27.63	0.17	0.96	0.19	22.22	22.48	0.01	4.47	1.49	12.90	40.66	Na
ZR4	Silty Marl	2.85	43.24	5.88	2.95	9.88	40.07	0.19	1.06	0.22	25.02	24.03	Na	11.17	1.38	12.51	42.86	Na
ZR6	Silty Marl	2.93	33.63	6.02	3.30	8.33	38.81	0.23	0.89	0.22	26.99	24.22	Na	6.40	1.16	13.27	46.60	Na
ZR1	Siltstone	2.73	47.69	5.21	2.52	12.99	31.05	0.15	1.00	0.20	20.35	21.81	0.02	3.05	1.82	12.61	35.66	Na
ZR4a	Siltstone	4.01	39.59	8.07	2.61	9.82	201.93	0.15	1.00	0.30	26.56	22.55	Na	12.38	3.31	14.53	134.42	0.05
Mean		2.69	60.36	5.63	2.54	11.87	83.08	0.15	0.90	0.25	21.90	20.71	0.01	7.65	2.62	13.20	46.12	0.01
Standard Deviation		0.71	35.90	1.16	0.49	2.43	71.68	0.06	0.18	0.06	5.08	4.21	0.01	3.33	1.73	0.72	37.72	0.02
Minimum		1.45	33.63	4.03	1.74	8.33	27.63	0.07	0.60	0.19	12.35	13.37	0.00	3.05	1.16	12.50	14.10	0.00
Maximum		4.01	128.63	8.07	3.30	15.61	201.93	0.23	1.06	0.36	26.99	24.22	0.02	12.38	5.60	14.53	134.42	0.05

Table B22: Al-normalized trace element of the Green-Gray Beds of Alagöz Section.

Sample	Type	Sc/Al	Ba/Al	Co/Al	Nb/Al	Rb/Al	Sr/Al	Ta/Al	Th/Al	U/Al	V/Al	Zr/Al	Mo/Al	Cu/Al	Pb/Al	Zn/Al	Ni/Al	Cd/Al
ZR5	Mudstone	2.88	31.67	8.20	3.05	7.42	40.74	0.18	1.03	0.24	24.24	23.03	Na	17.53	0.98	13.18	61.26	0.02
ZR7	Mudstone	2.76	35.17	6.02	3.03	8.93	57.15	0.21	0.95	0.21	25.00	22.39	Na	9.29	0.66	13.27	46.74	Na
ZR8	Mudstone	2.88	34.33	5.60	2.26	9.61	89.58	0.16	0.91	0.27	23.92	20.05	Na	9.13	1.17	13.07	40.29	Na
ZR11	Mudstone	2.52	41.86	5.47	2.04	11.78	103.21	0.11	1.01	0.25	21.27	18.71	Na	5.31	1.21	13.04	33.95	Na
ZR17	Mudstone	2.53	38.76	4.49	2.09	11.90	99.64	0.15	0.97	0.21	21.91	18.58	Na	8.93	0.88	11.37	20.79	Na
ZR20	Mudstone	2.44	41.61	4.40	1.89	12.77	82.68	0.12	1.01	0.24	20.50	17.82	Na	6.68	1.22	12.58	27.89	0.02
ZR21	Mudstone	2.54	39.17	4.70	2.12	12.02	79.71	0.15	1.02	0.24	21.22	20.91	Na	7.42	0.83	12.33	27.44	Na
ZR9	Claystone	2.71	37.08	4.87	2.25	11.94	88.12	0.15	0.98	0.23	24.37	19.85	Na	7.08	1.10	12.71	32.98	0.02
ZR10	Claystone	2.64	37.34	4.75	2.23	11.65	72.56	0.15	1.07	0.21	20.93	20.23	Na	8.81	1.32	12.07	30.81	0.02
ZR12	Claystone	2.50	52.36	4.48	2.05	10.72	111.32	0.11	1.05	0.25	21.63	18.76	Na	7.88	1.07	12.52	28.25	Na
ZR13	Claystone	2.51	43.64	5.55	2.06	11.42	115.61	0.14	0.87	0.23	21.71	19.17	Na	7.15	1.17	13.48	29.70	0.05
ZR14	Claystone	2.48	50.83	4.79	1.96	12.32	103.13	0.12	1.02	0.25	23.06	18.47	Na	7.17	1.19	12.40	30.28	0.02
ZR15	Claystone	2.57	38.70	4.78	2.03	11.21	89.20	0.14	1.01	0.24	22.11	18.66	Na	8.59	1.09	13.03	30.01	Na
ZR16	Claystone	2.46	43.84	3.97	1.81	12.53	73.12	0.11	1.10	0.23	22.86	17.76	Na	8.35	0.91	11.34	23.34	0.02
ZR18	Claystone	2.44	48.32	4.46	2.05	14.14	85.83	0.11	1.17	0.26	21.81	18.86	Na	8.42	1.05	11.47	23.07	0.02
ZR19	Claystone	2.36	43.65	4.35	2.05	12.89	69.43	0.15	1.13	0.22	20.19	20.31	Na	7.11	1.00	11.82	24.33	Na
Mean		2.58	41.14	5.05	2.19	11.45	85.07	0.14	1.02	0.24	22.30	19.60	0.00	8.43	1.05	12.48	31.94	0.01
Standard Deviation		0.16	5.83	1.00	0.35	1.64	19.76	0.03	0.08	0.02	1.46	1.52	0.00	2.65	0.17	0.70	10.17	0.01
Minimum		2.36	31.67	3.97	1.81	7.42	40.74	0.11	0.87	0.21	20.19	17.76	0.00	5.31	0.66	11.34	20.79	0.00
Maximum		2.88	52.36	8.20	3.05	14.14	115.61	0.21	1.17	0.27	25.00	23.03	0.00	17.53	1.32	13.48	61.26	0.05

Table B23: Al-normalized trace element of the red beds of Göynük Section.

Sample	Type	Sc/Al	Ba/Al	Co/Al	Nb/Al	Rb/Al	Sr/Al	Ta/Al	Th/Al	U/Al	V/Al	Zr/Al	Mo/Al	Cu/Al	Pb/Al	Zn/Al	Ni/Al	Cd/Al
GOZ1	Marl	2.08	186.57	2.73	1.46	17.35	170.29	0.12	1.69	0.33	20.20	17.26	0.09	6.54	2.64	9.51	5.82	Na
GOZ2	Marl	2.11	73.52	2.50	1.34	17.13	146.63	0.08	1.66	0.24	20.56	16.63	0.05	6.09	3.24	8.96	6.32	0.03
GOZ3	Marl	2.14	67.19	2.67	1.36	16.51	125.38	0.07	1.52	0.19	20.01	16.73	0.05	5.79	2.45	8.82	5.67	Na
GOZ4	Marl	1.96	52.45	3.06	1.42	16.15	132.31	0.07	1.45	0.25	17.89	15.93	0.05	4.93	2.13	8.82	6.08	0.02
GOZ5	Marl	2.17	99.78	2.92	1.37	16.24	128.82	0.07	1.40	0.27	18.56	15.81	0.05	5.52	2.34	8.44	6.48	Na
GOZ6	Marl	2.10	53.89	3.03	1.19	17.29	115.96	0.07	1.26	0.26	20.06	15.89	0.05	4.69	2.08	8.63	7.51	Na
GOZ7	Marl	2.14	47.77	2.81	1.16	17.01	103.15	0.06	1.37	0.19	20.78	15.40	0.04	6.45	1.93	7.93	6.60	Na
GOZ8	Marl	2.21	76.22	3.09	1.20	17.45	130.50	0.10	1.49	0.32	20.34	16.89	Na	7.65	2.01	9.07	5.73	Na
Mean		2.11	82.17	2.85	1.31	16.89	131.63	0.08	1.48	0.25	19.8	16.32	0.05	5.96	2.35	8.77	6.28	0.01
Standard Deviation		0.07	45.37	0.21	0.11	0.52	20.09	0.02	0.15	0.05	1.02	0.64	0.02	0.95	0.43	0.47	0.61	0.01
Minimum		1.96	47.77	2.5	1.16	16.15	103.15	0.06	1.26	0.19	17.89	15.4	0.00	4.69	1.93	7.93	5.67	0.00
Maximum		2.21	186.57	3.09	1.46	17.45	170.29	0.12	1.69	0.33	20.78	17.26	0.09	7.65	3.24	9.51	7.51	0.03

Table B24: Al-normalized trace element of the green-gray beds of Göynük Section.

Sample	Type	Sc/Al	Ba/Al	Co/Al	Nb/Al	Rb/Al	Sr/Al	Ta/Al	Th/Al	U/Al	V/Al	Zr/Al	Mo/Al	Cu/Al	Pb/Al	Zn/Al	Ni/Al	Cd/Al
GOZ11	Mudstone	1.960	76.834	2.156	1.117	15.269	95.083	0.078	1.411	0.3	19.797	15.465	Na	7.135	2.293	8.624	4.939	Na
GOZ13	Mudstone	2.027	103.801	2.818	1.298	15.753	100.902	0.081	1.642	0.3	21.287	17.374	0.020	7.055	2.859	7.907	5.393	Na
GOZ16	Mudstone	2.104	47.343	2.293	1.199	16.328	112.023	0.063	1.473	0.4	26.091	16.391	Na	8.879	2.420	7.996	6.733	0.042
GOZ17	Mudstone	1.943	130.338	2.202	1.263	15.511	85.165	0.081	1.975	0.3	19.753	18.296	0.032	8.112	2.493	7.124	5.230	Na
GOZ18	Mudstone	2.167	52.221	3.012	1.257	17.963	118.289	0.087	1.473	0.4	19.718	16.620	Na	9.816	2.535	8.451	7.714	0.043
GOZ20	Mudstone	2.216	48.761	3.140	1.201	17.325	85.720	0.092	1.478	0.3	18.285	15.774	0.055	7.979	2.493	8.127	7.702	Na
GOZ21	Mudstone	1.966	54.463	2.064	1.239	17.558	102.399	0.079	1.593	0.3	18.482	16.654	0.020	6.901	2.300	8.258	6.410	Na
GOZ25	Mudstone	2.125	65.580	2.351	1.360	17.592	62.818	0.085	1.572	0.3	19.688	16.133	0.014	6.062	2.819	7.365	7.224	0.014
GOZ27	Mudstone	2.152	44.978	2.217	1.399	18.292	109.432	0.086	1.442	0.5	19.799	17.281	0.043	6.887	2.475	9.684	8.909	Na
GOZ29	Mudstone	1.961	50.561	2.245	1.242	17.086	120.714	0.087	1.373	0.3	18.960	16.520	Na	8.543	2.637	9.807	9.088	Na
GOZ30	Mudstone	1.844	54.308	2.603	1.291	16.948	114.620	0.082	1.578	0.4	18.034	17.051	0.020	6.906	2.603	9.837	8.853	Na
GOZ31	Mudstone	1.774	60.766	1.464	1.153	15.236	154.198	0.089	1.819	0.5	15.968	16.766	0.044	7.984	2.639	7.762	4.768	Na
GOZ36	Mudstone	1.802	47.744	1.982	1.284	19.323	122.671	0.113	1.531	0.4	18.242	16.485	Na	9.369	2.387	8.558	6.576	Na
GOZ40	Mudstone	1.953	45.651	1.904	1.367	20.018	125.112	0.098	1.416	0.4	19.286	16.942	Na	7.934	2.466	8.544	6.933	0.024

Table B24: Continued.

GOZ43	Mudstone	1.829	59.326	1.483	1.544	19.200	129.705	0.102	1.666	0.4	18.895	19.525	Na	7.009	2.235	8.330	6.339	0.020
GOZ44	Mudstone	1.848	46.827	1.787	1.376	21.729	103.060	0.103	1.807	0.6	18.279	18.484	Na	6.901	2.896	8.010	6.819	Na
GOZ46	Mudstone	1.975	48.499	2.129	1.361	22.121	108.454	0.088	1.514	0.5	19.312	17.227	0.022	6.540	2.370	8.120	7.505	Na
GOZ47	Mudstone	1.892	60.557	2.620	1.485	19.594	48.140	0.102	1.383	0.3	18.924	17.498	0.029	6.842	2.067	9.316	9.768	Na
GOZ52	Mudstone	1.873	52.440	1.457	1.457	18.749	134.949	0.083	1.623	0.4	14.359	16.585	Na	6.305	2.664	7.908	6.909	0.021
GOZ0	Claystone	2.004	56.304	2.024	1.603	15.930	96.719	0.100	1.823	0.4	25.848	16.390	2.384	6.893	2.184	7.614	4.989	0.040
GOZ9	Claystone	2.125	67.832	2.615	1.373	15.986	64.890	0.082	1.504	0.3	18.797	16.983	0.016	9.186	2.730	8.826	8.271	Na
GOZ10	Claystone	1.992	54.768	2.614	1.319	17.053	136.348	0.075	1.419	0.3	18.671	17.028	Na	6.074	2.589	9.211	7.344	0.025
GOZ12	Claystone	2.117	56.632	2.593	1.217	16.090	152.854	0.079	1.508	0.6	25.934	17.122	Na	10.744	2.699	8.733	5.451	0.053
GOZ14	Claystone	1.993	104.441	2.631	1.176	15.048	98.043	0.080	1.555	0.4	18.935	16.125	Na	8.949	2.631	8.371	6.518	Na
GOZ22	Claystone	2.197	51.021	2.832	1.221	17.821	141.444	0.073	1.465	0.4	18.553	16.283	0.073	5.908	2.490	8.300	7.885	Na
GOZ23	Claystone	1.957	50.880	2.087	1.218	18.134	109.869	0.087	1.457	0.6	18.699	16.155	0.022	6.762	2.435	8.915	7.545	Na
GOZ24	Claystone	2.074	48.326	2.157	1.307	17.028	102.647	0.083	1.493	0.3	20.741	16.240	Na	8.836	2.385	9.126	7.674	Na
GOZ26	Claystone	2.157	46.159	2.739	1.251	18.852	104.656	0.086	1.294	0.3	19.413	15.638	Na	7.053	2.351	9.275	9.146	Na
GOZ32	Claystone	1.961	52.740	2.245	1.133	17.762	129.061	0.087	1.482	0.4	20.050	15.735	Na	6.843	2.375	8.282	6.778	0.022
GOZ33	Claystone	2.046	59.345	1.933	1.387	18.008	121.510	0.091	1.523	0.4	20.009	16.621	Na	7.071	2.456	8.640	8.231	Na
GOZ35	Claystone	1.993	50.626	2.312	1.475	18.337	100.833	0.100	1.415	0.3	16.742	16.284	0.020	6.577	2.511	8.770	9.009	Na
GOZ37	Claystone	2.161	42.689	2.089	1.495	18.445	64.394	0.108	1.351	0.2	17.652	16.734	0.018	7.169	2.324	9.006	9.979	Na
GOZ39	Claystone	1.839	46.893	2.023	1.425	20.803	113.669	0.069	1.425	0.4	17.470	16.229	0.023	5.770	2.575	8.965	9.562	Na
GOZ50	Claystone	1.765	66.920	1.900	1.385	16.587	101.181	0.095	1.928	0.4	16.289	19.696	0.014	6.353	2.525	8.144	5.063	0.027
GOZ19	Siltstone	1.875	82.215	1.702	1.370	14.539	78.566	0.087	1.803	0.3	20.482	18.563	Na	9.664	2.365	8.366	5.495	0.014
GOZ48	Siltstone	2.020	47.238	2.548	1.430	19.252	50.361	0.109	1.150	0.2	18.336	16.704	0.031	7.070	2.191	9.634	10.489	0.016
GOZ51	Siltstone	1.934	57.429	3.660	1.473	11.382	79.895	0.104	1.131	0.5	17.110	20.294	0.045	5.103	2.232	7.737	7.201	Na
GOZ28	Sandstone	1.741	383.777	1.350	1.393	9.839	208.955	0.109	1.524	0.4	14.585	25.752	0.152	2.286	2.133	6.313	5.072	Na
GOZ38	Sandstone	2.440	58.219	3.260	1.586	10.354	64.825	0.122	1.238	0.3	19.871	22.294	0.122	5.003	1.726	7.844	7.931	Na
GOZ42	Sandstone	1.723	74.069	2.213	1.405	9.090	70.320	0.080	1.617	0.5	15.370	18.882	0.040	4.174	2.544	6.493	3.551	0.013
GOZ15	Mixed	1.976	105.675	2.569	1.252	14.916	65.658	0.066	1.884	0.3	18.842	17.525	0.040	8.288	2.569	7.247	5.389	Na
GOZ34	Mixed	2.132	67.602	3.045	1.355	11.145	82.751	0.091	1.355	0.3	18.728	19.550	0.030	5.710	1.827	7.461	6.075	0.015
GOZ41	Mixed	2.033	47.637	2.237	1.394	16.746	47.114	0.102	1.336	0.3	17.283	18.924	Na	6.594	2.048	8.859	8.148	Na
GOZ45	Mixed	2.121	54.397	3.818	1.515	12.864	49.321	0.121	1.212	0.3	18.789	19.941	0.030	5.970	1.924	8.334	8.894	Na
GOZ49	Mixed	2.261	49.902	2.600	1.518	20.074	58.736	0.113	1.276	0.2	19.702	18.669	0.032	5.572	2.099	9.044	9.706	0.016
Mean		2.00	67.44	2.35	1.35	16.75	100.62	0.09	1.51	0.38	19.02	17.54	0.08	7.08	2.41	8.38	7.23	0.01
Standard Deviation		0.15	51.68	0.54	0.12	2.97	32.97	0.01	0.20	0.09	2.40	1.92	0.35	1.56	0.26	0.80	1.65	0.01
Minimum		1.72	42.69	1.35	1.12	9.09	47.11	0.06	1.13	0.23	14.36	15.46	0.00	2.29	1.73	6.31	3.55	0.00
Maximum		2.44	383.78	3.82	1.60	22.12	208.96	0.12	1.98	0.63	26.09	25.75	2.38	10.74	2.90	9.84	10.49	0.05

Table B25: Average major oxides, REE, normalization geochemical data of the lithofacies of the Alagöz and Göynük Section, and Comparison with PAAS (Taylor and McLennan, 1985).

Oxides	Average Red Bed of Alagöz Section			Average Greenish grayish Bed of Alagöz Section		Average Red Bed of Göynük Section	Average Greenish grayish Bed of Göynük Section				PAAS
Facies	Packstone	Silty Marl	Siltstone	Mudstone	Claystone	Marl	Mudstone	Claystone	Silt-stone	Sand-stone	Mixed
SiO ₂	64.42	46.23	32.69	34.31	32.58	25.25	35.45	32.82	45.26	44.00	46.40
Al ₂ O ₃	2.57	12.48	8.11	9.85	9.25	7.71	9.92	9.24	12.65	11.26	12.79
Fe ₂ O ₃	1.05	8.86	5.99	6.17	5.39	3.57	4.41	4.23	5.38	3.67	5.65
MgO	0.67	5.37	3.17	4.51	3.66	1.59	2.03	1.98	2.61	1.59	2.54
CaO	15.87	9.44	23.79	20.63	23.02	31.60	23.01	24.98	14.63	18.91	13.97
Na ₂ O	0.24	1.55	1.03	1.18	1.08	0.63	0.93	0.80	1.31	1.73	1.41
K ₂ O	0.64	1.95	1.47	1.48	1.59	1.85	2.21	2.07	2.61	1.98	2.81
TiO ₂	0.10	1.22	0.73	0.83	0.65	0.36	0.45	0.42	0.62	0.58	0.66
P ₂ O ₅	0.04	0.17	0.12	0.12	0.10	0.08	0.11	0.11	0.10	0.12	0.10
MnO	0.13	0.12	0.39	0.17	0.17	0.14	0.15	0.16	0.10	0.11	0.09
Cr ₂ O ₃	0.02	0.06	0.10	0.04	0.03	0.01	0.01	0.01	0.01	0.01	0.01
TOT/C	3.49	1.95	5.33	4.60	5.22	6.92	4.93	5.43	2.92	3.79	2.79
La	7.35	21.68	18.00	17.77	16.67	17.26	24.12	21.34	22.50	25.80	21.16
Ce	8.70	39.98	32.50	32.63	28.76	31.89	44.68	39.07	42.40	46.10	40.00
Pr	1.57	5.29	4.60	4.31	3.70	3.56	4.99	4.41	4.93	5.34	4.67
Nd	6.50	20.63	18.40	16.87	14.41	13.18	18.64	16.56	19.20	19.93	17.34
Sm	1.30	4.14	3.54	3.21	2.83	2.51	3.54	3.14	3.50	3.81	3.32
Eu	0.35	1.06	0.91	0.84	0.68	0.59	0.75	0.69	0.86	1.01	0.85
Gd	1.38	3.91	3.26	3.02	2.68	2.46	3.20	2.88	3.15	3.46	3.01
Tb	0.22	0.65	0.52	0.50	0.45	0.35	0.45	0.41	0.47	0.52	0.45
Dy	1.22	3.74	3.14	2.99	2.60	0.00	0.00	0.00	0.00	0.00	0.00
Ho	0.28	0.70	0.56	0.56	0.51	0.43	0.53	0.48	0.56	0.59	0.49
Er	0.78	1.97	1.58	1.60	1.50	1.27	1.60	1.43	1.58	1.73	1.58
Tm	0.11	0.30	0.24	0.24	0.22	0.00	0.00	0.00	0.00	0.00	0.405
Yb	0.77	1.93	1.47	1.62	1.50	0.00	0.00	0.00	0.00	0.00	2.82
Lu	0.12	0.31	0.23	0.25	0.24	0.20	0.25	0.23	0.25	0.21	0.22
ΣLREE	27.14	96.67	81.21	78.65	69.73	71.44	99.93	88.09	96.54	105.45	90.35
ΣHREE	3.50	9.58	7.72	7.76	7.02	2.25	2.84	2.55	2.86	3.05	2.75
ΣREE	30.64	106.25	88.92	86.42	76.74	73.69	102.77	90.64	99.39	108.50	93.10
ΣLREE/ΣHREE	7.78	10.10	11.01	10.10	9.94	31.78	34.96	34.72	33.69	34.54	33.08
Ce/Ce* (PAAS)	0.59	0.86	0.82	0.86	0.84	0.94	0.94	0.93	0.93	0.91	0.93

Table B25: Continued.

Eu/Eu* (PAAS)	1.24	1.24	1.26	1.26	1.17	1.11	1.07	1.08	1.21	1.30	1.27	
La*/Lu* (PAAS)	0.70	0.80	1.02	0.81	0.78	0.99	1.10	1.07	1.04	1.38	1.09	
La*/Sm* (PAAS)	0.83	0.76	0.77	0.81	0.86	1.00	0.98	0.99	0.93	0.99	0.93	
Gd*/Yb* (PAAS)	1.08	1.23	1.39	1.13	1.08	0.00	0.00	0.00	0.00	0.00	0.00	
Log(Ce/Ce*) (PAAS)	-0.23	-0.07	-0.09	-0.07	-0.07	-0.03	-0.03	-0.03	-0.03	-0.04	-0.03	
Log(Eu/Eu*) (PAAS)	0.09	0.09	0.10	0.10	0.07	0.05	0.03	0.03	0.08	0.11	0.10	
Pr/Pr* (PAAS)	1.23	1.08	1.10	1.08	1.07	1.02	1.02	1.02	1.02	1.04	1.04	
Gd/Gd* (PAAS)	4.04	3.98	3.78	3.83	3.83	3.85	3.66	3.68	3.65	3.73	3.66	

Table B26: Average trace element geochemical data of the lithofacies of the Alagöz and Göynük Section, and Comparison with PAAS (Taylor and McLennan, 1985) and NASC (Gromet et al., 1984).

Trace Element	Average Red Bed of Alagöz Section			Average Greenish grayish Bed of Alagöz Section		Average Red Bed of Göynük Section			Average Greenish grayish Bed of Göynük Section			PAAS
Facies	Pack-stone	Silty Marl	Silt-stone	Mudstone	Claystone	Marl	Mudstone	Claystone	Silt-stone	Sand-stone	Mixed	
LOI	14.20	12.30	22.30	20.50	22.27	27.08	21.97	23.01	14.53	15.77	13.38	6
Sc	2.50	18.25	13.00	13.86	12.33	8.63	10.00	9.87	13.00	11.67	14.20	16
Ba	159.50	265.75	196.50	193.71	214.11	322.75	314.05	282.33	420.00	885.33	448.40	650
Co	6.10	37.60	25.20	29.59	22.74	11.65	11.29	11.25	17.60	13.87	19.24	23
Nb	2.55	18.78	10.90	12.53	10.07	5.33	6.66	6.55	9.53	8.70	9.48	19
Rb	20.15	70.38	52.55	54.49	59.46	68.84	90.93	85.05	100.40	57.73	102.18	160
Sr	201.30	222.83	303.65	396.57	432.87	530.16	526.49	519.44	468.60	620.83	411.08	200
Ta	0.10	1.28	0.65	0.81	0.64	0.33	0.45	0.43	0.67	0.60	0.66	1.2
Th	0.85	6.48	4.30	5.14	5.13	6.00	7.96	7.46	9.17	8.77	9.66	14.6
U	0.45	1.35	0.95	1.23	1.14	1.03	1.93	1.85	2.53	2.43	2.02	3.1
V	20.00	162.75	93.50	118.29	107.89	80.75	97.00	94.80	125.00	99.00	126.20	150
Zr	19.05	153.73	94.30	106.50	93.77	66.36	86.22	81.81	124.20	129.57	127.78	210
Y	8.35	18.75	15.65	15.77	15.19	13.46	16.69	15.02	15.40	17.77	14.62	27
Mo	<0.05	0.05	0.05	<0.05	<0.05	0.19	0.08	0.85	0.17	0.57	0.18	1
Cu	12.30	45.03	22.40	50.03	38.57	24.23	37.90	35.89	48.93	23.57	43.94	50
Pb	7.05	9.05	9.30	5.10	5.37	9.50	12.70	12.15	15.17	12.97	14.26	20
Zn	18.50	84.50	56.00	66.29	60.11	35.63	42.47	42.33	57.33	41.00	55.20	85
Ni	20.10	279.00	251.50	199.01	136.66	25.69	35.86	36.77	51.33	31.87	51.14	55
Cd	<0.05	<0.05	0.05	0.03	0.08	0.03	0.04	0.05	0.07	0.03	0.04	

Table B27: Average Al-normalized major and trace element geochemical data of the lithofacies of the Alagöz and Göynük Section, and Comparison with PAAS (Taylor and McLennen, 1985)

Al-normalized Major Elements												
Major Element	Average Red Bed of Alagöz Section			Average Greenish grayish Bed of Alagöz Section			Average Red Bed of Göynük Section	Average Greenish grayish Bed of Göynük Section				
Facies	Packstone	Silty Marl	Silt-stone	Mudstone	Claystone	Marl	Mudstone	Claystone	Silt-stone	Sand-stone	Mixed	
Si/Al	22.21	3.27	3.60	3.09	3.12	2.90	3.19	3.15	3.16	3.58	3.22	2.93
Fe/Al	0.54	0.94	1.01	0.83	0.77	0.61	0.59	0.61	0.56	0.44	0.59	0.50
Mg/Al	0.30	0.49	0.55	0.51	0.45	0.24	0.24	0.25	0.24	0.17	0.23	0.13
Ca/Al	8.33	1.03	7.45	2.97	3.43	5.60	3.20	3.85	1.56	2.44	1.49	0.09
Na/Al	0.13	0.17	0.18	0.17	0.16	0.11	0.13	0.12	0.14	0.22	0.15	0.1
K/Al	0.39	0.24	0.26	0.24	0.27	0.38	0.35	0.35	0.32	0.27	0.34	0.31
Ti/Al	0.04	0.11	0.10	0.09	0.08	0.05	0.05	0.05	0.06	0.06	0.06	0.06
P/Al	0.01	0.01	0.01	0.01	0.01	0.01	0.01	0.01	0.01	0.01	0.01	0.01
Mn/Al	0.06	0.01	0.10	0.02	0.02	0.02	0.02	0.02	0.01	0.01	0.01	
Cr/Al	0.01	0.01	0.02	0.00	0.00	0.00	0.00	0.00	0.00	0.00	0.00	
Trace Elements												
Al-normalized Trace Elements												
Facies	Packstone	Silty Marl	Silt-stone	Mudstone	Claystone	Marl	Mudstone	Claystone	Silt-stone	Sand-stone	Mixed	
Sc/Al	1.85	2.77	3.37	2.65	2.52	2.11	1.97	2.03	1.94	1.97	2.10	1.60
Ba/Al	117.34	40.22	43.64	37.51	43.97	82.17	60.58	57.04	62.29	172.02	65.04	64.98
Co/Al	4.49	5.70	6.64	5.55	4.67	2.85	2.21	2.32	2.64	2.27	2.85	2.30
Nb/Al	1.88	2.85	2.56	2.35	2.05	1.31	1.31	1.33	1.42	1.46	1.41	0.12
Rb/Al	14.85	10.62	11.40	10.63	12.09	16.89	17.98	17.46	15.06	9.76	15.15	16
Sr/Al	147.99	33.93	116.49	78.96	89.81	131.63	107.02	109.21	69.61	114.70	60.72	19.99
Ta/Al	0.07	0.19	0.15	0.15	0.13	0.08	0.09	0.09	0.10	0.10	0.10	0.12
Th/Al	0.63	0.98	1.00	0.98	1.04	1.48	1.57	1.51	1.36	1.46	1.41	1.46
U/Al	0.33	0.20	0.25	0.24	0.23	0.25	0.39	0.38	0.38	0.40	0.30	0.31
V/Al	14.77	24.69	23.46	22.58	22.07	19.80	19.11	19.59	18.64	16.61	18.67	15
Zr/Al	14.04	23.30	22.18	20.21	19.12	16.32	17.00	16.62	18.52	22.31	18.92	20.99
Mo/Al	Na	0.01	0.01	Na	Na	0.05	0.02	0.17	0.03	0.10	0.03	10
Cu/Al	9.07	6.90	7.72	9.18	7.84	5.96	7.53	7.35	7.28	3.82	6.43	5
Pb/Al	5.19	1.37	2.57	0.99	1.10	2.35	2.51	2.48	2.26	2.13	2.09	2
Zn/Al	13.63	12.79	13.57	12.69	12.31	8.77	8.41	8.68	8.58	6.88	8.19	8.50
Ni/Al	14.82	42.30	85.04	36.91	28.09	6.28	7.04	7.56	7.73	5.52	7.64	5.50
Cd/Al	Na	Na	0.03	0.01	0.02	0.01	0.01	0.01	0.01	0.00	0.01	

Table B28: Average Major and trace element ratio concentration in the lithofacies of the Alagöz and Göynük Section, and Comparison with PAAS (Taylor and McLennen, 1985)

Trace Element	Average Red Bed of Alagöz Section			Average Greenish grayish Bed of Alagöz Section		Average Red Bed of Göynük Section	Average Greenish grayish Bed of Göynük Section				PAAS	
	Packstone	Silty Marl	Silt-stone	Mudstone	Claystone		Mudstone	Claystone	Silt-stone	Sand-stone		
SiO ₂ /Al ₂ O ₃	25.15	3.70	4.07	3.50	3.53	3.28	3.57	3.56	3.58	4.05	3.64	3.32
K ₂ O/Na ₂ O	2.74	1.26	1.30	1.29	1.47	2.95	2.65	2.61	2.13	1.11	2.05	2.85
Na ₂ O/K ₂ O	0.37	0.82	0.79	0.81	0.69	0.34	0.38	0.39	0.52	0.92	0.52	0.35
K ₂ O/Al ₂ O ₃	0.25	0.16	0.17	0.15	0.17	0.24	0.23	0.22	0.21	0.17	0.22	0.20
Al ₂ O ₃ /TiO ₂	25.65	10.32	11.15	12.33	14.26	21.63	22.63	22.29	20.69	19.67	19.52	18.90
Fe ₂ O ₃ /K ₂ O	1.63	4.70	4.74	4.23	3.44	1.94	2.03	2.06	2.08	1.95	2.07	1.94
Log (K ₂ O/Na ₂ O)	0.44	0.09	0.11	0.10	0.16	0.47	0.42	0.41	0.31	0.04	0.30	0.45
Log (Na ₂ O/K ₂ O)	-0.44	-0.09	-0.11	-0.10	-0.16	-0.47	-0.42	-0.41	-0.31	-0.04	-0.30	-0.45
Log (Fe ₂ O ₃ /K ₂ O)	0.21	0.66	0.67	0.62	0.53	0.29	0.30	0.31	0.32	0.28	0.31	0.29
Log (SiO ₂ /Al ₂ O ₃)	1.40	0.57	0.61	0.54	0.55	0.52	0.55	0.55	0.55	0.60	0.56	0.52
Rb/K ₂ O	31.50	36.09	36.30	36.79	37.44	37.33	41.41	41.46	38.20	30.64	36.94	43.24
Cu/Zn	0.67	0.54	0.55	0.72	0.64	0.68	0.90	0.85	0.85	0.55	0.80	0.59
Ni/Co	3.35	7.41	11.75	6.49	6.02	2.21	3.29	3.31	3.10	2.60	2.76	2.39
U/Th	0.53	0.21	0.25	0.24	0.23	0.17	0.25	0.26	0.29	0.28	0.21	0.21
(Cu+Mo)/Zn	Na	17.03	10.05	Na	Na	0.58	0.46	0.45	0.47	0.56	0.65	0.60
V/Cr	1671.51	3873.75	1620.48	4974.65	5937.79	14404.18	15715.64	14751.56	13883.46	11864.38	13497.67	Na
V/(V+Ni)	0.50	0.37	0.26	0.39	0.44	0.76	0.73	0.72	0.71	0.76	0.71	0.73
Th/Sc	0.36	0.36	0.31	0.37	0.41	0.70	0.80	0.75	0.71	0.77	0.68	0.91
Th/Co	0.14	0.17	0.16	0.18	0.23	0.52	0.75	0.67	0.61	0.75	0.52	0.63
Th/U	1.90	4.81	4.21	4.19	4.47	6.01	4.20	4.15	3.98	3.64	4.79	4.71
La/Sc	3.10	1.19	1.56	1.30	1.36	2.02	2.53	2.21	1.73	2.39	1.49	2.39

APPENDIX C

TOTAL AVERAGE VALUES IN THE RED AND GREEN-GRAY BEDS OF ALAGÖZ AND GÖYNÜK SECTIONS

Table C1: Total average oxides, REE geochemical data in the red beds and green-gray beds of Alagöz and Göynük Section, and Comparison with PAAS (Taylor and McLennan, 1985).

Oxides	Average Alagöz Red Bed	Average Alagöz Green-Gray Bed	Average Göynük Red Bed	Average Göynük Green-Gray Bed	PAAS
SiO ₂	47.39	33.34	25.25	36.43	62.80
Al ₂ O ₃	8.91	9.51	7.71	10.14	18.90
Fe ₂ O ₃	6.19	5.73	3.57	4.51	7.18
MgO	3.64	4.03	1.59	2.08	2.20
CaO	14.63	21.97	31.60	22.24	1.20
Na ₂ O	1.09	1.12	0.63	0.98	1.30
K ₂ O	1.50	1.54	1.85	2.24	3.70
TiO ₂	0.81	0.73	0.36	0.47	1.00
P ₂ O ₅	0.12	0.11	0.08	0.11	0.16
MnO	0.19	0.17	0.14	0.14	
Cr ₂ O ₃	0.06	0.03	0.01	0.01	
TOT/C	3.18	4.95	6.92	4.75	
La	17.18	17.15	17.26	22.87	38.20
Ce	30.29	30.45	31.89	42.24	79.60
Pr	4.19	3.97	3.56	4.78	8.83
Nd	16.54	15.49	13.18	17.93	33.90
Sm	3.28	3.00	2.51	3.39	5.55
Eu	0.85	0.75	0.59	0.77	1.08
Gd	3.11	2.83	2.46	3.09	4.66
Tb	0.51	0.47	0.35	0.45	0.77
Dy	2.96	2.77	0.00	0.00	4.68
Ho	0.56	0.53	0.43	0.52	0.99
Er	1.57	1.54	1.27	1.55	2.85
Tm	0.24	0.23	0.00	0.00	0.41
Yb	1.52	1.55	0.00	0.00	2.82
Lu	0.24	0.25	0.20	0.24	0.43
ΣLREE	75.42	73.63	71.44	95.06	171.82
ΣHREE	7.59	7.34	2.25	2.75	12.95
ΣREE	83.01	80.98	73.69	97.81	184.77
ΣLREE/ΣHREE	9.75	10.01	31.78	34.56	13.26

Table C2: Total Average REE-normalized ratio in the red beds and green-gray beds of Alagöz and Göynük Section (PAAS-Taylor and McLennan, 1985).

REE-Normalized Ratio	Average Alagöz Red Bed	Average Alagöz Green-Gray Bed	Average Göynük Red Bed	Average Göynük Green-Gray Bed
Ce/Ce*	0.78	0.85	0.94	0.93
Eu/Eu*	1.25	1.21	1.11	1.12
La*/Lu*	0.83	0.79	0.99	1.10
La*/Sm*	0.78	0.84	1.00	0.98
Gd*/Yb*	1.23	1.10	0.00	0.00
Log(Ce/Ce*)	-0.11	-0.07	-0.03	-0.03
Log(Eu/Eu*)	0.10	0.08	0.05	0.05
Pr/Pr*	1.13	1.08	1.02	1.02
Gd/Gd*	3.94	3.83	3.85	3.67

Table C3: Total average trace elements in the red beds and green-gray beds of Alagöz and Göynük Section (PAAS-Taylor and McLennan, 1985)

Trace Elements	Average Alagöz Red Bed	Average Alagöz Green-Gray Bed	Average Göynük Red Bed	Average Göynük Green-Gray Bed	PAAS
Ba	221.88	205.19	322.75	363.56	650
Co	26.63	25.74	11.65	12.75	23
Nb	12.75	11.14	5.33	7.26	19
Rb	53.36	57.28	68.84	88.64	160
Sr	237.65	416.99	530.16	513.75	200
Ta	0.83	0.72	0.33	0.49	1.2
Th	4.53	5.14	6.00	8.12	14.6
U	1.03	1.18	1.03	1.99	3.1
V	109.75	112.44	80.75	101.51	150
Zr	105.20	99.34	66.36	94.79	210
Y	15.38	15.44	13.46	15.89	27
Mo	0.04	0.00	0.19	0.39	1
Cu	31.19	43.58	24.23	37.68	50
Pb	8.61	5.25	9.50	12.87	20
Zn	60.88	62.81	35.63	44.73	85
Ni	207.40	163.94	25.69	38.62	55
Cd	0.01	0.06	0.03	0.05	

Table C4: Total average major and trace Al-normalized elements in the red beds and green-gray beds of Alagöz and Göynük Section (PAAS-Taylor and McLennan, 1985 and NASC-Gromet et al., 1984).

Al-normalized Major Elements	Average Alagöz Red Bed	Average Alagöz Green-Gray Bed	Average Göynük Red Bed	Average Göynük Green-Gray Bed	PAAS
Si/Al	8.09	3.11	2.90	3.19	2.93
Fe/Al	0.86	0.80	0.61	0.59	0.50
Mg/Al	0.46	0.48	0.24	0.24	0.13
Ca/Al	4.46	3.23	5.60	3.20	0.09
Na/Al	0.16	0.17	0.11	0.13	0.10
K/Al	0.29	0.26	0.38	0.35	0.31
Ti/Al	0.09	0.09	0.05	0.05	0.06
P/Al	0.01	0.01	0.01	0.01	0.01
Mn/Al	0.05	0.02	0.02	0.02	
Cr/Al	0.01	0.00	0.00	0.001	

Al-normalized Trace Elements	Average Alagöz Red Bed	Average Alagöz Green-Gray Bed	Average Göynük Red Bed	Average Göynük Green-Gray Bed	PAAS
Sc/Al	2.69	2.58	2.11	2.00	1.60
Ba/Al	60.36	41.14	82.17	67.44	64.98
Co/Al	5.63	5.05	2.85	2.35	2.30
Nb/Al	2.54	2.19	1.31	1.35	0.12
Rb/Al	11.88	11.45	16.89	16.75	16.00
Sr/Al	83.09	85.07	131.63	100.62	19.99
Ta/Al	0.15	0.14	0.08	0.09	0.12
Th/Al	0.90	1.02	1.48	1.51	1.46
U/Al	0.25	0.24	0.25	0.38	0.31
V/Al	21.90	22.30	19.80	19.02	15.00
Zr/Al	20.71	19.60	16.32	17.54	20.99
Mo/Al	0.01	na	5.00	0.08	10.00
Cu/Al	7.65	8.43	5.96	7.08	5.00
Pb/Al	2.62	1.05	2.35	2.41	2.00
Zn/Al	13.20	12.48	8.77	8.38	8.50
Ni/Al	46.12	31.94	6.28	7.23	5.50
Cd/Al	0.01	0.01	0.01	0.01	
D*	0.53	0.55	0.61	0.62	

Table C5: Total average oxides and trace elements ratio in the red beds and green-gray beds of Alagöz and Göynük Section (PAAS-Taylor and McLennan, 1985 and NASC-Gromet et al., 1984).

Element Ratio	Average Alagöz Red Bed	Average Alagöz Green-Gray Bed	Average Göynük Red Bed	Average Göynük Green-Gray Bed	PAAS
SiO ₂ /Al ₂ O ₃	9.16	3.52	3.29	3.61	3.32
K ₂ O/Na ₂ O	1.64	1.39	2.95	2.43	2.85
Na ₂ O/K ₂ O	0.70	0.74	0.34	0.45	0.35
K ₂ O/Al ₂ O ₃	0.18	0.16	0.24	0.22	0.20
Al ₂ O ₃ /TiO ₂	14.36	13.42	21.63	21.85	18.90
Fe ₂ O ₃ /K ₂ O	3.94	3.78	1.94	2.04	1.94
Log (K ₂ O/Na ₂ O)	0.18	0.14	0.47	0.37	0.45
Log (Na ₂ O/K ₂ O)	-0.18	-0.14	-0.47	-0.37	-0.45
Log (Fe ₂ O ₃ /K ₂ O)	0.55	0.57	0.29	0.31	0.29
Log (SiO ₂ /Al ₂ O ₃)	0.79	0.55	0.52	0.56	0.52
Rb/K ₂ O	35.00	37.16	37.33	40.00	43.24
Cu/Zn	0.57	0.68	0.68	0.85	0.59
Ni/Co	7.48	6.23	2.21	3.18	2.39
U/Th	0.30	0.23	0.17	0.25	0.21
(Cu+Mo)/Zn	11.03	Na	0.58	0.48	0.60
V/Cr	2759.87	5516.42	14404.18	14768.94	
V/(V+Ni)	0.38	0.42	0.76	0.73	0.73
Th/Sc	0.35	0.40	0.70	0.76	0.91
Th/Co	0.16	0.21	0.52	0.69	0.63
Th/U	3.93	4.35	6.01	4.20	4.71
La/Sc	1.76	1.33	2.02	2.24	2.39